วิธีการหาแรงจับยึดและความดันที่เหมาะสมในงานขึ้นรูปโลหะแผ่นด้วยน้ำผ่านการจำลองด้วยระเบียบวิธีไฟไนต์เอลิเมนต์

นายธนสาร อินทรกำธรชัย

ศูนย์วิทยทรัพยากร
จุฬาลงกรณ์มหาวิทยาลัย

วิทยานิพนธ์นี้เป็นส่วนหนึ่งของการศึกษาตามหลักสูตรปริญญาวิศวกรรมศาสตรดุษฎีบัณฑิต
สาขาวิชาวิศวกรรมอุตสาหการ ภาควิชาวิศวกรรมอุตสาหการ
คณะวิศวกรรมศาสตร์ จุฬาลงกรณ์มหาวิทยาลัย
ปีการศึกษา 2552
ลิขสิทธิ์ของจุฬาลงกรณ์มหาวิทยาลัย

STRATEGIES FOR BLANK HOLDER FORCE AND PRESSURE DESIGN THROUGH FEA SIMULATION IN SHEET HYDROFORMING

Mr. Thanasan Intarakumthornchai

ศูนย์วิทยทรัพยากร
จุฬาลงกรณ์มหาวิทยาลัย

A Dissertation Submitted in Partial Fulfillment of the Requirements
for the Degree of Doctor of Philosophy Program in Industrial Engineering
Department of Industrial Engineering
Faculty of Engineering
Chulalongkorn University
Academic Year 2009

Copyright of Chulalongkorn University

Thesis Title	STRATEGIES FOR BLANK HOLDER FORCE AND PRESSURE DESIGN THROUGH FEA SIMULATION IN SHEET HYDROFORMING
By	Mr. Thanasan Intarakumthornchai
Field of Study	Industrial Engineering
Thesis Advisor	Professor Sirichan Thongprasert, Ph.D.
Thesis Co-Advisor	Professor Pramote Dechaumphai, Ph.D.

Accepted by the Faculty of Engineering, Chulalongkorn University in Partial Fulfillment of the Requirements for the Doctoral Degree

..... Dean of the Faculty of Engineering
(Associate Professor Boonsom Lerdhirunwong, Dr.Ing.)

THESIS COMMITTEE

..... Chairman
(Assistant Professor Rein Boondiskulchok, Ph.D.)

..... Thesis Advisor
(Professor Sirichan Thongprasert, Ph.D.)

..... Thesis Co-Adviser
(Professor Pramote Dechaumphai, Ph.D.)

..... Examiner
(Associate Professor Parames Chutima, Ph.D.)

..... External Examiner
(Suwat Jirathearanat, Ph.D.)

ศูนย์วิทยทรัพยากร
จุฬาลงกรณ์มหาวิทยาลัย

ธนสาร อินทรกำธรชัย : วิธีการหาแรงจับยึดและความดันที่เหมาะสมในงานขึ้นรูปโลหะแผ่นด้วยน้ำผ่านการจำลองด้วยระเบียบวิธีไฟไนต์เอลิเมนต์ (STRATEGIES FOR BLANK HOLDER FORCE AND PRESSURE DESIGN THROUGH FEA SIMULATION IN SHEET HYDROFORMING). อ. ที่ปรึกษาวิทยานิพนธ์หลัก : ศ. ดร. ศิริจันทร์ ทองประเสริฐ, อ. ที่ปรึกษาวิทยานิพนธ์ร่วม : ศ. ดร. ปราโมทย์ เดชะอำไพ, 231 หน้า.

วิทยานิพนธ์ฉบับนี้ได้ศึกษาเกี่ยวกับการหาแรงจับยึดและความดันที่เหมาะสมในงานขึ้นรูปโลหะแผ่นด้วยน้ำ การขึ้นรูปโลหะแผ่นด้วยน้ำ เป็นการใช้แรงดันน้ำทดแทนแรงต้านของแม่พิมพ์ที่ทำจากเหล็ก การกำหนดค่าพารามิเตอร์ในการผลิตโดยเฉพาะแรงจับยึดและแรงดันจะมีความซับซ้อนกว่ากระบวนการดั้งเดิม แรงจับยึดที่มากเกินไปจะส่งผลให้ชิ้นงานบาง ในทางกลับกันแรงจับยึดที่น้อยเกินไปจะส่งผลให้ชิ้นงานบริเวณปีกย่น ในส่วนของแรงดันถ้าแรงดันมากเกินไปจะส่งผลให้ชิ้นงานบาง ในทางตรงกันข้ามถ้าแรงดันน้อยเกินไปชิ้นงานบริเวณผนังจะย่น ดังนั้นในการขึ้นรูปชิ้นงานด้วยกระบวนการขึ้นรูปโลหะแผ่นด้วยน้ำให้สำเร็จนั้น ขึ้นอยู่กับการควบคุมแรงจับยึดและแรงดันตลอดการขึ้นรูปเป็นสำคัญ การใช้ประสบการณ์และการลองผิดลองผิดถูกไม่เพียงพอต่อการหาแรงจับยึดและความดันเพื่อขึ้นรูปชิ้นงานให้สำเร็จ ระเบียบวิธีไฟไนต์เอลิเมนต์ได้ถูกนำมาจำลองควบคู่กับพื้นผิวตอบและตรรกศาสตร์คลุมเครือเพื่อทำการออกแบบแรงจับยึดและความดันที่เหมาะสม ในลักษณะคงที่และผันแปรตลอดการขึ้นรูป ตามลำดับ ชิ้นงานรูปทรงพาราโบลา ได้นำมาใช้เป็นตัวอย่างในการทดสอบวิธีการ โดยใช้ค่าเปอร์เซ็นต์การลดลงของความหนาที่ต่ำที่สุดเป็นวัตถุประสงค์ในการเปรียบเทียบคุณภาพของชิ้นงาน และในการขึ้นรูปชิ้นงานสุดท้ายจะต้องไม่เกิดการฉีกขาดและรอยย่น จากผลการออกแบบพบว่าลักษณะของแรงจับยึดและแรงดันแบบผันแปรให้ผลลัพธ์ของเปอร์เซ็นต์การลดลงของความหนาต่ำกว่าแบบคงที่ นอกจากนั้นวิธีการหาแรงจับยึดและแรงดันแบบคงที่ยังใช้จำนวนของการจำลองที่มากกว่า ส่วนวิธีการหาแรงจับยึดและแรงดันแบบผันแปรใช้การจำลองเพียงครั้งเดียว การออกแบบแรงจับยึดและแรงดันแบบผันแปรได้ใช้สมการเส้นตรงและเอ็กซ์โปเนนต์เชียลในการทำนายค่าล่วงหน้า พบว่า การทำนายค่าล่วงหน้าแบบเอ็กซ์โปเนนต์เชียลใช้จำนวนช่วงของการตรวจสอบที่น้อยกว่า

ภาควิชา วิศวกรรมอุตสาหการ	ลายมือชื่อนิสิต ธนสาร อินทรกำธรชัย
สาขาวิชา วิศวกรรมอุตสาหการ	ลายมือชื่อ อ.ที่ปรึกษาวิทยานิพนธ์หลัก
ปีการศึกษา 2552	ลายมือชื่อ อ.ที่ปรึกษาวิทยานิพนธ์ร่วม

487 18381 21 : MAJOR INDUSTRIAL ENGINEERING
KEYWORDS: BLANK HOLDER FORCE / PRESSURE / FEA / SHEET HYDROFORMING

THANASAN INTARAKUMTHORNCHAI : STRATEGIES FOR BLANK HOLDER FORCE AND PRESSURE DESIGN THROUGH FEA SIMULATION IN SHEET HYDROFORMING. THESIS ADVISOR: PROF. SIRICHAN THONGPRASERT, Ph.D., THESIS CO-ADVISOR: PROF. PRAMOTE DECHAUMPHAI, PhD., 231 pp.

To determine loading paths of blank holder force (BHF) and pressure in hydromechanical deep drawing (HMD) process of the parabolic cups is aim of this research. The process of HMD, the sheet is formed against a counter pressure in the pot rather than a female die in regular stamping operation. Successful HMD process requires the optimum relationship of the key process parameters. Excessive BHF leads to the part thinning. Conversely, insufficient BHF can lead to flange wrinkle. In case of pressure, excessive pressure leads to the part thinning. In opposition, insufficient pressure can lead to side wall wrinkle. Trial-and-error for the process design can be very time consuming. Finite element method coupled with optimization technique is applied to determine the proper constant BHF and proper linear counter pressure. The adaptive finite element method coupled with fuzzy logic control is applied to determine loading profiles of BHF and pressure just one simulation. The parabolic parts are used to investigate. The thinning is the index to compare the quality of part. The crack and wrinkles will be disappeared at the end of stroke.

ศูนย์วิทยทรัพยากร
จุฬาลงกรณ์มหาวิทยาลัย

Department : Industrial Engineering Student's Signature ธนสาร อินทร์เกิดชัย
Field of Study : Industrial Engineering Advisor's Signature
Academic Year : 2009 Co-Advisor's Signature

ACKNOWLEDGEMENTS

I express my sincere thank to my advisor, Professor Sirichan Thongprasert, Ph.D., for her useful advice, constant guidance, continuous encouragement, and endless patience during my graduate study program. I appreciate her commitment to assist me achieve my research goals.

I would like to express my gratitude to my co-advisor, Professor Pramote Dechaumphai, Ph.D., who gives me inspiration to study in Ph.D. program. His insight, wisdom, support, and trust were indispensable

In addition, I would like to appreciate to Suwat Jirathearanat, Ph.D. for taking the time to mentor and tutor me. His invaluable assistance in technical areas and their uplifting emotional support will always be remembered.

I am also grateful for the suggestions and beneficial comments that Assistant Professor Rein Boondiskulchok, D.Eng and Associate Professor Parames Chutima, Ph.D., as members of the examination committee provided me during my study.

I also would like to give special thank to Mr. Sedthawatt Sucharitpwatskul for suggestion of FORTRAN programming and to Mr. Atthapol Palasay for taking time in the experiment.

In closing, I would like to express my deepest gratitude to my entire family and my wife for their unyielding support, warmness, love, belief, and pride in my study that have driven me to become successful.

Finally, I would like to thank the National Metal and Materials Technology Center for their generous financial and technical support in the experiment.

ศูนย์วิทยทรัพยากร
จุฬาลงกรณ์มหาวิทยาลัย

CONTENTS

page

ABSTRACT (THAI) ..... **iv**

ABSTRACT (ENGLISH) ..... **v**

ACKNOWLEDGEMENTS ..... **vi**

CONTENTS ..... **vii**

LISTS OF TABLES ..... **x**

LISTS OF FIGURES ..... **xi**

CHAPTER I INTRODUCTION **1**

1.1 Introduction 1

1.2 Objective 2

1.3 Problem statement 2

1.4 Dissertation organization 4

1.5 Expected result 4

CHAPTER II LITERATURE REVIEW **5**

2.1 Mechanic of sheet metal forming 5

2.2 Sheet hydroforming 13

2.3 FEA of sheet metal forming and hydroforming 20

2.4 Effect of process parameters on hydroformability 23

2.5 Design of process parameters 27

CHAPTER III PROBLEM STATEMENT AND METHODOLOGY SETUP **39**

3.1 Parabolic parts 39

3.2 Material properties 41

3.3 FEA setup for HMD process 43

3.4 Experimental setup for HMD process 47

3.5 Investigation of parabolic parts with HMD 52

page

3.6 Optimization approach to find optimal BHF and P 53
3.7 Automatic approach to select loading paths in HMD 55

CHAPTER IV INVESTIGATION THE BEHAVIOR OF PARABOLIC PARTS WITH HYDROMECHANICAL DEEP DRAWING PROCESS 57
4.1 Defect criteria 57
4.1.1 Crack criterion 59
4.1.2 Wrinkles criteria 60
4.2 Process window of parabolic parts 64
4.2.1 Search space of parabolic part 64
4.2.2 Process windows 72
4.3 Effect of process parameters compared with punch stroke on quality of parabolic parts 80
4.4 Characteristics parabolic shape forming with HMD process 99

CHAPTER V OPTIMIZATION OF BLANK HOLDER FORCE AND PRESSURE FOR HYDROMECHANICAL DEEP DRAWING OF PARABOLIC PARTS USING 2-D INTERVAL HALVING AND RSM METHODS 102
5.1 Search space 103
5.2 Search method and neighborhood determination 105
5.3 Response surface method 116
5.4 Conclusion and discussion 123

CHAPTER VI AUTOMATIC APPROACH TO SELECT LOADING PATH IN HYDROMECHANICAL DEEP DRAWING OF PARABOLIC PARTS USING ADAPTIVE FEA SIMULATION COUPLED WITH FUZZY LOGIC 125
6.1 Adaptive FEA simulation 125
6.2 Fuzzy logic control 128

page

6.3 Fuzzy controller process 130
6.3.1 Fuzzy control for the blank holder force.....130
6.3.2 Fuzzy control for the pressure.....144
6.4 Calculation of ΔBHF and ΔP Conclusion and discussion 153
6.5 Modification of load function in linear form 155
6.6 Modification of load function in exponential form.....167
6.7 Validation of modification of load function in exponential form on other parabolic cup.....177
6.8 Effect of membership function shape of thinning, FAM and SW 183
6.9 Conclusion and discussion.....192

CHAPTER VII EXPERIMENTAL VALIDATIONS OF SIMULATION RESULTS 194
7.1 Comparison between FEA modeling and forming experiment of simple part using classical deep drawing process and sheet hydroforming process 194
7.1.1 Conical cup forming with deep drawing process (hard tooling).....194
7.1.2 Simple sheet hydroformed part and effect of process parameters using FEA modeling.....196
7.2 Comparison between FEA modeling and HMD experiment of parabolic part202

CHAPTER VIII CONCLUSION AND FUTURE RESEARCH.....219
8.1 Conclusion 219
8.2 Future Research 222

REFERENCES.....224
VITA.....231

ศูนย์วิทยทรัพยากร
จุฬาลงกรณ์มหาวิทยาลัย

LIST OF TABLES

page

Table 2.1 Summarize of optimization with FEM technique in metal forming.....36
Table 3.1 The properties of SPCC.....42
Table 4.1 Pressure and BHF calculation results of three parts.....71
Table 5.1 The solutions of combination between pressure and BHF searching by 2-D interval halving of Part1.....109
Table 5.2 The solutions of combination between pressure and BHF searching by 2-D interval halving of Part2.....111
Table 5.3 The solutions of combination between pressure and BHF searching by 2-D interval halving of Part3.....113
Table 5.4 The thinning comparison of FEM and Eq. 5.6 of Part1.....117
Table 5.5 The thinning comparison of FEM and Eq. 5.11 of Part3.....121
Table 6.1 The values of ΔBHF and ΔP.....155
Table 6.2 Results of Part 1 by adaptive simulation with fuzzy logic control.....157
Table 6.3 Results of Part 2 by adaptive simulation with fuzzy logic control.....158
Table 6.4 Results of Part 3 by adaptive simulation with fuzzy logic control.....161
Table 6.5 Results of Part1 obtained from different thinning membership function shapes.....186
Table 6.6 Results of Part1 obtained from different thinning membership function shapes.....189
Table 6.7 Results of Part1 obtained from different thinning membership function shapes.....192
Table 7.1 Effect of friction coefficient between punch and blank.....210

LIST OF FIGURES

page

Figure 1.1 Example parts after hydroforming 1
Figure 1.2 Sheet hydroforming process 2
Figure 1.3 The statement of problem 3
Figure 2.1 Boundary conditions for sheet metal stamping 6
Figure 2.2 Forming limit diagram (FLD) from distortion of printed circles localized neck and plot of the strains 12
Figure 2.3 Critical strains for diffuse and localized necking according to Eqs. (2.13-2.14) 13
Figure 2.4 Classification of the forming process using liquid media 16
Figure 2.5 Hydromechanical deep drawing process description 17
Figure 2.6 Combination of HMD with stretching and deep drawing to produce complex parts in less forming operations 18
Figure 2.7 High pressure sheet hydroforming process description 20
Figure 2.8 Wrinkle region in FLD 23
Figure 2.9 Pre-bulging method 24
Figure 2.10 A generic curve illustrating the optimum fluid pressure–punch stroke path for the stamp hydroforming process 27
Figure 2.11 Bizier curves representing a) forging die profile as design parameters, b) THF loading path as design parameters 30
Figure 2.12 General flow chart of the feedback control simulation method for process design in metal forming 34
Figure 3.1 Parabolic cup application 39
Figure 3.2 Parabolic cup dimensions 40
Figure 3.3 Problem statement to find proper process parameters of parabolic cups 41
Figure 3.4 Flow curve of SPCC 41

page

Figure 3.5 Forming limit diagram of SPCC steel with 0.8 mm. of thickness..... 43
Figure 3.6 Finite element quarter model of blank and tool components 43
Figure 3.7 Comparison of solutions between the Balat-Lian's three-parameter model and Hill's transversely anisotropic model 44
Figure 3.8 Two hundred ton of hydraulic press machine and blank holder force control system 49
Figure 3.9 Pressure intensifier system built by BT Engineering Company..... 50
Figure 3.10 Hydromechanical deep drawing die of parabolic part..... 51
Figure 3.11 Typical BHF and Pressure curves for tapered punch 53
Figure 3.12 Normal procedure of optimization with FEM 54
Figure 3.13 Procedure of control loading path with simulation 55
Figure 4.1 The schematic to form tapered shape such as a parabolic cup in conventional process..... 58
Figure 4.2 Schematic of the HMD process of parabolic cup 58
Figure 4.3 Comparison between part formability and thinning in SPCC parabolic cup of HMD process 59
Figure 4.4 Measurement of flange wrinkling amplitude (FAM) 61
Figure 4.5 Flange wrinkling amplitude (FAM) results by varying gap 62
Figure 4.6 Sidewall wrinkles 63
Figure 4.7 Measurement of sidewall wrinkle (SW)..... 64
Figure 4.8 Measurement of the minimum radius of parts..... 65
Figure 4.9 The reaction forces of punch and blank holder from fixed gap method 67
Figure 4.10 Forming a bulge with hydromechanical deep drawing components with tapered shaped walls (Koç 2008)..... 67
Figure 4.11 Determining the true stresses of the outer edge of the blank and of the inner edge of the draw ring (Koç 2008)..... 69
Figure 4.12 Forces acting on the sheet metal when hydromechanical deep drawing (Koç 2008) 69

page

Figure 4.13 Process window of Part1 73
Figure 4.14 The solutions of Part1 are conducted with BHF as 76,250 N (for quarter) and pressure as 28.75 MPa 74
Figure 4.15 Process window of Part2 75
Figure 4.16 The solutions of Part2 are conducted with BHF as 84,000 N (for quarter) and pressure as 26.5 MPa 76
Figure 4.17 Process window of Part3 77
Figure 4.18 The solutions of Part3 are conducted with BHF as 210,625 N (for quarter) and pressure as 23.75 MPa..... 78
Figure 4.19 General process window of relationship between constant BHF and linear pressure affected on part quality 79
Figure 4.20 Generic curve illustrating the optimum fluid pressure-punch stroke path for the stamp hydroforming process..... 80
Figure 4.21 Illustration of the BHF working window for successful part drawing, Doege and Sommer (1983)..... 81
Figure 4.22 Visual inspection and zebra lines are criteria used to detect side wall wrinkle82
Figure 4.23 The effect of fluid pressure and punch stroke on part quality at 50,000 N of BHF for Part1..... 83
Figure 4.24 The effect of fluid pressure and punch stroke on part quality at 76,250 N of BHF for Part1..... 83
Figure 4.25 The effect of fluid pressure and punch stroke on part quality at 102,500 N of BHF for Part1..... 84
Figure 4.26 The effect of fluid pressure and punch stroke on part quality at 128,750 N of BHF for Part1..... 84
Figure 4.27 The effect of fluid pressure and punch stroke on part quality at 155,000 N of BHF for Part1..... 85
Figure 4.28 The effect of fluid pressure and punch stroke on part quality at 181,250 N of BHF for Part1..... 85

page

Figure 4.29 The effect of fluid pressure and punch stroke on part quality at 207,500 N of BHF for Part1 86
Figure 4.30 The effect of fluid pressure and punch stroke on part quality at 233,750 N of BHF for Part1 86
Figure 4.31 The effect of fluid pressure and punch stroke on part quality at 260,000 N of BHF for Part1 87
Figure 4.32 The effect of fluid pressure and punch stroke on part quality at 56,000 N of BHF for Part2 87
Figure 4.33 The effect of fluid pressure and punch stroke on part quality at 84,000 N of BHF for Part2 88
Figure 4.34 The effect of fluid pressure and punch stroke on part quality at 112,000 N of BHF for Part2 88
Figure 4.35 The effect of fluid pressure and punch stroke on part quality at 140,000 N of BHF for Part2 89
Figure 4.36 The effect of fluid pressure and punch stroke on part quality at 168,000 N of BHF for Part2 89
Figure 4.37 The effect of fluid pressure and punch stroke on part quality at 196,000 N of BHF for Part2 90
Figure 4.38 The effect of fluid pressure and punch stroke on part quality at 224,000 N of BHF for Part2 90
Figure 4.39 The effect of fluid pressure and punch stroke on part quality at 252,000 N of BHF for Part2 91
Figure 4.40 The effect of fluid pressure and punch stroke on part quality at 280,000 N of BHF for Part2 91
Figure 4.41 The effect of fluid pressure and punch stroke on part quality at 79,000 N of BHF for Part3 92

page

Figure 4.42 The effect of fluid pressure and punch stroke on part quality at 122,875 N of BHF for Part3..... 92
Figure 4.43 The effect of fluid pressure and punch stroke on part quality at 166,750 N of BHF for Part3..... 93
Figure 4.44 The effect of fluid pressure and punch stroke on part quality at 210,625 N of BHF for Part3..... 93
Figure 4.45 The effect of fluid pressure and punch stroke on part quality at 254,500 N of BHF for Part3..... 94
Figure 4.46 The effect of fluid pressure and punch stroke on part quality at 298,375 N of BHF for Part3..... 94
Figure 4.47 The effect of fluid pressure and punch stroke on part quality at 342,250 N of BHF for Part3..... 95
Figure 4.48 The effect of fluid pressure and punch stroke on part quality at 386,125 N of BHF for Part3..... 95
Figure 4.49 The effect of fluid pressure and punch stroke on part quality at 430,000 N of BHF for Part3..... 96
Figure 4.50 General process window of relationship between pressure and punch stroke and their effects on part quality in HMD process of parabolic part..... 97
Figure 4.51 General process window of relationship between pressure and punch stroke and their effects on part quality in HMD process of parabolic part with various BHF levels 97
Figure 4.52 General process window of relationship between BHF and punch stroke and their effects on part quality in HMD process of parabolic part 98
Figure 4.53 Forming stages of parabolic cup in HMD 100
Figure 4.54 The good forming of parabolic cup in HMD..... 101
Figure 5.1 Flow chart for determination of the optimal BHF and P..... 104
Figure 5.2 Schematic of search algorithm 105

page

Figure 5.3 General process window of relationship between constant BHF and linear pressure affected on part quality with limit lines 106
Figure 5.4 Schematic to determine the centers of the next search 107
Figure 5.5 The results of 2-D interval halving method on the general process window of relation between pressure and BHF of Part1 110
Figure 5.6 The feasible region with bound of Part1 110
Figure 5.7 The results of 2-D interval halving method on the general process window of relation between pressure and BHF of Part2 112
Figure 5.8 The feasible region with bound of Part2 113
Figure 5.9 The results of 2-D interval halving method on the general process window of relation between pressure and BHF of Part3 115
Figure 5.10 The feasible region with bound of Part3 115
Figure 5.11 Part thinning response surface of two variables; BHF and P with constraints of Part1 118
Figure 5.12 The solutions of Part1 are conducted with optimal BHF as 63,125 N (for quarter) and optimal pressure as 27.625 MPa 119
Figure 5.13 Part thinning response surface of two variables; BHF and P with constraints of Part2 119
Figure 5.14 The solutions of Part2 are conducted with optimal BHF as 70,000N (for quarter) and optimal pressure as 27.375 MPa 120
Figure 5.15 Part thinning response surface of two variables; BHF and P with constraints of Part3 122
Figure 5.16 The solutions of Part3 are conducted with optimal BHF as 276,437.5 N (for quarter) and optimal pressure as 21.3125 MPa 123
Figure 6.1 A general conceptual flow chart of the adaptive simulation interfacing with LS-DYNA 127
Figure 6.2 A general scheme of fuzzy controller 129
Figure 6.3 The fuzzy controlling schematic of the blank holder force 131

page

Figure 6.4 The full triangular membership function 133
Figure 6.5 The half triangular membership function 133
Figure 6.6 The thinning membership function 134
Figure 6.7 The FAM membership function 135
Figure 6.8 The β output membership function 136
Figure 6.9 The draw-in speed depend on time 136
Figure 6.10 The draw-in speed membership function 137
Figure 6.11 The μ membership function 137
Figure 6.12 The expected BHF controlled trajectory on process window of BHF and punch stroke 138
Figure 6.13 The rule matrix to control the BHF concerning thinning and FAM 140
Figure 6.14 The probabilistic graphical calculation based on nine rules of BHF control 142
Figure 6.15 The implication and graphical aggregation to control the BHF 143
Figure 6.16 The fuzzy controlling schematic of the pressure 145
Figure 6.17 The dome height related with the side wall wrinkle 146
Figure 6.18 The SW membership function 147
Figure 6.19 The α output membership function 147
Figure 6.20 The expected pressure controlled trajectory on process window of pressure and punch stroke 148
Figure 6.21 The rule matrix to control the pressure concerned with thinning and SW .. 150
Figure 6.22 The probabilistic graphical calculation based on nine rules of pressure control 152
Figure 6.23 The implication and graphical aggregation to control the BHF 152
Figure 6.24 The surface of β weight factor 153
Figure 6.25 The area for generating the loading profiles 155
Figure 6.26 BHF profiles varying by number of monitoring steps of Part1 156
Figure 6.27 Pressure profiles varying by number of monitoring steps of Part1 156

page

Figure 6.28 The thinning distribution and zebra lines on the Part1 at 100 monitoring steps..... 157
Figure 6.29 The thickness distribution on curvilinear of the Part1..... 158
Figure 6.30 BHF profiles varying by number of monitoring steps of Part2..... 159
Figure 6.31 Pressure profiles varying by number of monitoring steps of Part2..... 159
Figure 6.32 The thinning distribution and zebra lines on the Part2 at 100 monitoring steps..... 160
Figure 6.33 The thickness distribution on curvilinear of the Part2..... 161
Figure 6.34 BHF profiles varying by number of monitoring steps of Part3..... 162
Figure 6.35 Pressure profiles varying by number of monitoring steps of Part3..... 162
Figure 6.36 The thinning distribution and zebra lines on the Part3 at 100 monitoring steps..... 163
Figure 6.37 The thickness distribution on curvilinear of the Part3..... 164
Figure 6.38 BHF profiles using 100 monitoring steps of three parabolic parts..... 165
Figure 6.39 Pressure profiles using 100 monitoring steps of three parabolic parts..... 165
Figure 6.40 The thickness distribution on curvilinear of three parabolic parts..... 166
Figure 6.41 The β output membership function of load function in exponential form.. 168
Figure 6.42 The μ output membership function of load function in exponential form.. 169
Figure 6.43 The α output membership function of load function in exponential form.. 169
Figure 6.44 BHF profiles varying by monitoring steps of Part1 with 10 monitoring steps of load function in exponential form..... 170
Figure 6.45 Pressure profiles varying by monitoring steps of Part1 with 10 monitoring steps of load function in exponential form..... 171
Figure 6.46 The thinning distribution and zebra lines on the Part1 at 10 monitoring steps of load function in exponential form..... 172
Figure 6.47 BHF profiles varying by monitoring steps of Part2 with 10 monitoring steps of load function in exponential form..... 172

page

Figure 6.48 Pressure profiles varying by monitoring steps of Part2 with 10 monitoring steps of load function in exponential form 173
Figure 6.49 The thinning distribution and zebra lines on the Part2 at 10 monitoring steps of load function in exponential form 174
Figure 6.50 BHF profiles varying by monitoring steps of Part3 with 10 monitoring steps of load function in exponential form 174
Figure 6.51 Pressure profiles varying by monitoring steps of Part3 with 10 monitoring steps of load function in exponential form 175
Figure 6.52 The thinning distribution and zebra lines on the Part3 at 10 monitoring steps of load function in exponential form 176
Figure 6.53 The new parabolic part (Part51) 178
Figure 6.54 The new parabolic part 179
Figure 6.55 BHF profiles of Part51 with 10 monitoring steps using load function in exponential form 179
Figure 6.56 Pressure profiles of Part51 with 10 monitoring steps using load function in exponential form 180
Figure 6.57 The thinning distribution and zebra lines on the Part51 using 10 monitoring steps of load function in exponential form 180
Figure 6.58 BHF profiles of Part51 with 10 monitoring steps of load function in exponential form with limit 181
Figure 6.59 Pressure profiles of Part51 with 10 monitoring steps of load function in exponential form with limit 182
Figure 6.60 The thinning distribution and zebra lines on the Part51 using 10 monitoring steps of load function in exponential form with limit 182
Figure 6.61 The thinning membership function skewed to the left 184
Figure 6.62 The thinning membership function skewed to the right 184
Figure 6.63 BHF profiles of Part1 obtained from different thinning membership function shapes 185

page

Figure 6.64 Pressure profiles of Part1 obtained from different thinning membership function shapes..... 186
Figure 6.65 The FAM membership function skewed to the left..... 187
Figure 6.66 The FAM membership function skewed to the right..... 187
Figure 6.67 BHF profiles of Part1 obtained from different FAM membership function shapes..... 188
Figure 6.68 Pressure profiles of Part1 obtained from different FAM membership function shapes..... 188
Figure 6.69 The SW membership function skewed to the left..... 190
Figure 6.70 The SW membership function skewed to the right..... 190
Figure 6.71 BHF profiles of Part1 obtained from different SW membership function shapes..... 191
Figure 6.72 Pressure profiles of Part1 obtained from different SW membership function shapes..... 191
Figure 7.1 Shapes and dimensions of conical cup tool components..... 195
Figure 7.2 Quarter finite element model of conical cup drawing..... 195
Figure 7.3 Tooling components of conical cup drawing..... 196
Figure 7.4 Conical cup obtained from experiments..... 197
Figure 7.5 Comparison of the results from FEA and experiment..... 198
Figure 7.6 Comparison of major and minor strains from the FEA and experiment of conical cup drawing..... 199
Figure 7.7 Comparison of hemispherical cups formed using fluid punch (left) and solid punch (right)..... 200
Figure 7.8 FE model and pressure curve to simulate the hemispherical dome..... 201
Figure 7.9 The limited dome height from simulation and experiment..... 201
Figure 7.10 Thickness distributions from simulation and experiment along curvilinear of the part..... 202
Figure 7.11 Die set drawing of Part1..... 203

page

Figure 7.12 Die installed in press machine 203
Figure 7.13 Blank position 204
Figure 7.14 Final stroke and ram up 204
Figure 7.15 Top view of part with no pressure condition 205
Figure 7.16 Front view of part with no pressure condition 205
Figure 7.17 Pre-bulge stage of part 206
Figure 7.18 Loading profiles of constant BHF and pressure 207
Figure 7.19 Top view of part with constant BHF of 63,125 N (full as 25.25 tons) and constant pressure of 4 MPa 207
Figure7.20 Front view of part with constant BHF of 63,125 N (full as 25.25 tons) and constant pressure of 4 MPa 208
Figure7.21 Top view of part with constant BHF of 63,125 N (full as 25.25 tons) and constant pressure of 6 MPa 208
Figure7.22 Front view of part with constant BHF of 63,125 N (full as 25.25 tons) and constant pressure of 6 MPa 208
Figure7.23 Top and bottom view of part with constant BHF of 63,125 N (full as 25.25 tons) and constant pressure of 8 MPa 209
Figure7.24 Front and back view of part with constant BHF of 63,125 N (full as 25.25 tons) and constant pressure of 8 MPa 209
Figure7.25 Top view of part with constant BHF of 63,125 N (full as 25.25 tons) and no pressure 212
Figure7.26 Front view of part with constant BHF of 63,125 N (full as 25.25 tons) and no pressure 213
Figure7.27 Top view of part with constant BHF of 63,125 N (full as 25.25 tons) and constant pressure of 3 MPa 213
Figure7.28 Front view of part with constant BHF of 63,125 N (full as 25.25 tons) and constant pressure of 3 MPa 214

page

Figure7.29 Parabolic part with constant BHF of 63,125 N (full as 25.25 tons) and constant pressure of 3 MPa 214
Figure7.30 Parabolic part with constant BHF of 63,125 N (full as 25.25 tons) and constant pressure of 3 MPa in half-section 215
Figure7.31 Thickness distributions from simulation and experiment along curvilinear of the part with constant BHF of 63,125 N (full as 25.25 tons) and constant pressure of 3 MPa 215
Figure7.32 Top view of part with constant BHF of 63,125 N (full as 25.25 tons) and linear pressure of 27.625 MPa at height of 66 mm 216
Figure7.33 Front view of part with constant BHF of 63,125 N (full as 25.25 tons) and linear pressure of 27.625 MPa at height of 66 mm 217
Figure7.34 Parabolic part with constant BHF of 63,125 N (full as 25.25 tons) and linear pressure of 27.625 MPa in half-section view at height of 66 mm 217
Figure7.35 Thickness distributions from simulation and experiment along curvilinear of the part with constant BHF of 63,125 N (full as 25.25 tons) and linear pressure of 27.625 MPa at height of 66 mm 218

ศูนย์วิทยทรัพยากร
จุฬาลงกรณ์มหาวิทยาลัย

CHAPTER I

INTRODUCTION

1.1 Introduction

Sheet hydroforming, one of the new manufacturing methods offers benefits such as; a) low tooling cost, b) better properties (dimension accuracy and rigidity) of part after forming, c) ability to form complex shape with hard-to-form materials (high strength steels and aluminum alloys), example parts of sheet hydroforming as shown in figure 1.1. Sheet hydroforming is classified into hydromechanical deep drawing and high pressure sheet hydroforming depending on the male or the female die that has the shape to be formed. High pressure sheet hydroforming is further classified into hydroforming of single blank and double blank depending on number of blanks being used in the forming process.

Figure 1.1 Example parts after hydroforming

In figure 1.2a shows the process of hydromechanical deep drawing, the sheet is formed against a counter pressure in the pot rather than a female die in regular stamping operation and figure 1.2b shows the process of high pressure sheet hydroforming, the sheet is pressurized and formed against a female die. The working fluid in the pressure pot can be either passive or active.

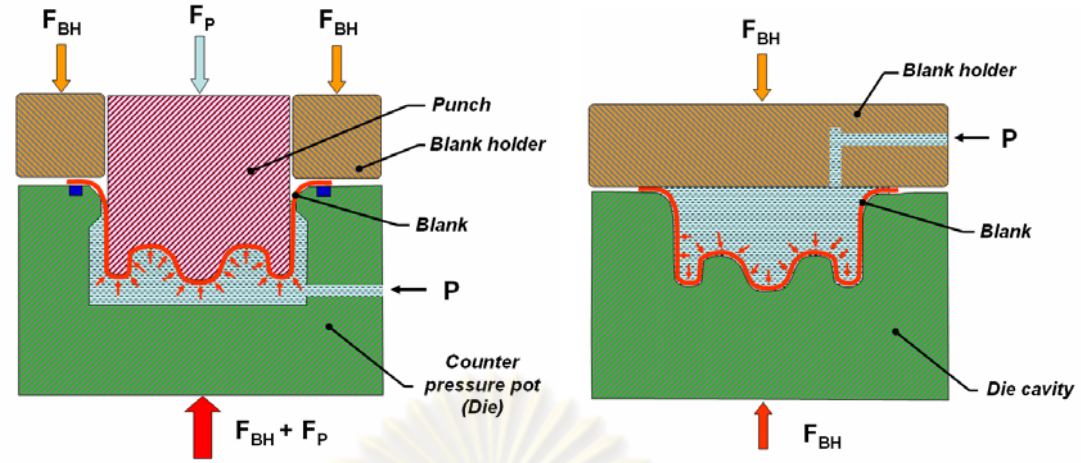

2a) Hydromechanical process

2b) High pressure sheet hydroforming process

Figure 1.2 – Sheet hydroforming process

Successful sheet hydroforming process requires optimum relationship of key process parameters; 1) blank holding force versus time, 2) pressure versus time to effectively form the part. FE simulation coupled with optimization techniques, has been used to determine loading paths of blank holding force and counter pressure that would result in good parts with no fracture and wrinkle. This research leads to design the process parameters. This information is necessary to set up the press operation for successful sheet hydroforming of any given part.

1.2 Objective

To develop and implement methodology to determine

1) The proper constant blank holder force and proper linear counter pressure in hydromechanical deep drawing process of the parabolic cups.

2) The feasible loading paths of blank holder force and pressure in hydromechanical deep drawing process of the parabolic cups.

1.3 Problem Statement

Many of the problems related to improvement of the product quality and production efficiency can be directly associated with the optimization procedures. Efficiency of optimization procedure integrated with the finite element method, has

been developed and applied to the area of sheet hydroforming. More powerful design tools are needed to help engineers design better products and processes and to reduce lead times and cost.

Successful sheet hydroforming process is affected by a large number of parameters such as material properties, blank geometry, complex die interface, lubrication, and process parameters, i.e. loading paths. However, the proper blank holder force and proper counter pressure are very important in carrying out the forming process successfully. In this research, the parabolic cups are the shape of interest, so we have two problems to determine 1) the proper constant blank holder force and proper linear counter pressure of the parabolic cups and 2) the feasible profile of blank holder force and pressure as shown in figure 1.3. The methodologies will utilize systematic FEA simulations and FEA enhanced with numerical optimization methods. These tools will enable the engineers to select loading paths (i.e. counter pressure profile and blank holder profile) optimized for sheet hydroformed part.

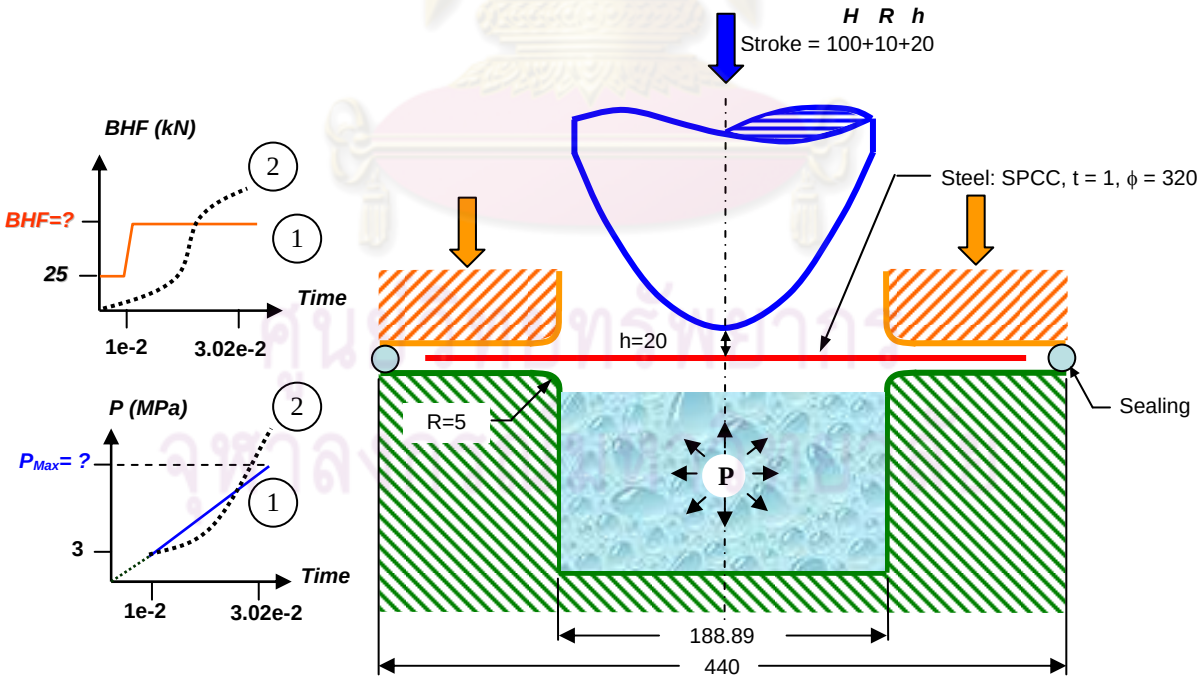

Figure 1.3 – The statement of problem

1.4 Dissertation Organization

The outline of this dissertation by chapters is:

Chapter 1: Introduction

Chapter 2: Literature review

Chapter 3: Problem statement and methodology setup

Chapter 4: Investigation on forming of parabolic parts with hydromechanical deep drawing process

Chapter 5: Optimization of blank holder force and pressure for hydromechanical deep drawing of parabolic cups using 2-D internal halving and RSM methods

Chapter 6: Automatic approach to select loading path in hydromechanical deep drawing of parabolic parts using adaptive FEA simulation coupled with fuzzy logic

Chapter 7: Validation of simulation with experiment

Chapter 8: Conclusion and future work

1.5 Expected Result

1) Process windows of hydromechanical deep drawing of parabolic cups
2) Understanding of forming behavior of parabolic cups with hydromechanical deep drawing
3) Methodology to find optimum constant blank holder force and linear pressure in hydromechanical deep drawing of parabolic cups
4) Methodology to find feasible variable blank holder force and pressure in hydromechanical deep drawing of parabolic cups

ศูนย์วิทยทรัพยากร
จุฬาลงกรณ์มหาวิทยาลัย

CHAPTER II

LITERATURE REVIEW

Literature is available on the mechanics of sheet metal forming, sheet hydroforming technology, FEA of sheet hydroforming, effects of process parameters on hydroformability and design of process parameters.

2.1 Mechanics of sheet metal forming

In sheet metal forming, a part of material is plastically deformed among tools. Thus, the mechanics of deformation provides the means for determining, how the desired geometry can be obtained by plastic deformation.

2.1.1 Plastic deformation

The theory of plasticity describes the mechanics of deformation in plastically deforming solids and as applies to metals and alloys, it is based on experimental studies of the relations between stresses and strains under simple loading condition.

In the late 1960s, the rigid-plastic finite difference method was used to analyze a sheet metal forming process. In the 1970s-1980s, the quasi-static rigid-plastic (also known as ‘flow formulation’) and elastic–plastic (also known as ‘solid formulation’) finite element formulations were developed by Kobayashi et al. 1989. The utilization of dynamic formulations for the numerical simulation of sheet metal forming processes takes its roots in the investigations reported by Silva et al. 2004.

The analysis of sheet metal forming process based on the dynamic formulation is governed by the equilibrium equation, strain-displacement relations and constitutive equations as follows.

2.1.1.1 Equilibrium equation

The equilibrium equation can be written in tensor form as (Fung, 1965)

$$\sigma_{ij,j} + \rho b_j = \rho \ddot{u}_j \qquad (2.1)$$

where σ_{ij}, is the stress components, ρ is density, b_j is the body force, and $\ddot{u}_j$ is acceleration.

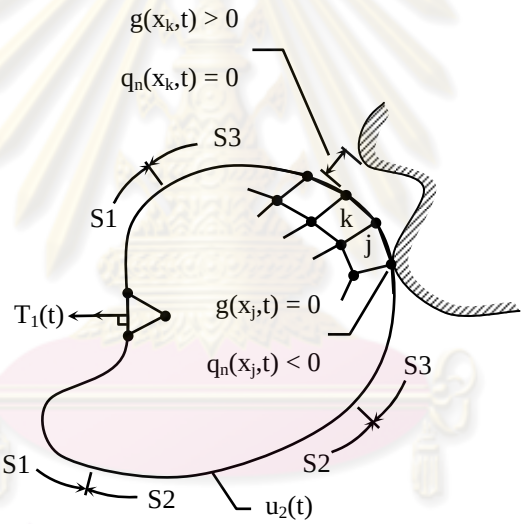

Figure 2.1 Boundary conditions for sheet metal stamping

ศูนย์วิทยทรัพยากร
จุฬาลงกรณ์มหาวิทยาลัย

Boundary conditions may consist of specifying the surface traction (Zhong, 1993) as depicted in figure 2.1 as,

$$\sigma_{ij} n_i = T_1(t) \qquad (2.2a)$$

where n_i and $T_1(t)$ are the outward unit normal vector and surface traction on the boundary S_1 at time t, respectively. The boundary condition may include the prescribed displacement on the boundary S_2 as,

$$u_i(x,t) = u_2(t) \qquad (2.2b)$$

Also along the contact boundary S_3, the normal contact stress should be compressive and the boundary should not penetrate into the other as follows,

$$q_n(x,t) = q_c(x,t)\, n_i \leq 0 \qquad (2.2c)$$

$$g(x,t) = g(x) - u(x,t)\, n_i \geq 0 \qquad (2.2d)$$

where $q_c(x,t)$ is the contact traction, $q_n(x,t)$ is the normal component of contact traction, and $g(x,t)$ is the gap between the two boundary surfaces.

2.1.1.2 Strain-displacement relations

Large strain behavior is normally considered in the analysis. The strain-displacement relations are in the form,

$$\varepsilon_{ij} = \frac{1}{2}\left(u_{i,j} + u_{j,i} + u_{k,i}u_{k,j}\right) \qquad (2.3)$$

where ε_{ij}, is the strain components; u_i, u_j, and u_k are the displacement components.

2.1.1.3 Constitutive equations

The total incremental strain at a point on the metal sheet during stamping process may consist of the elastic and plastic parts as,

$$d\varepsilon = d\varepsilon^e + d\varepsilon^p \qquad (2.3a)$$

where $d\varepsilon$ is the total incremental strain, $d\varepsilon^e$ is the incremental elastic strain, and $d\varepsilon^p$ is the incremental plastic strain. The incremental elastic strain is related to the incremental stress, $d\sigma$, by

$$d\varepsilon^e = C^{-1}d\sigma \qquad (2.3b)$$

where C is the elasticity matrix (Dechaumphai, 1999).

The incremental plastic strain $d\varepsilon^p$ can be derived from yield function, strain-hardening rule, and associated flow rule as described in the following sections.

2.1.1.4 Yield function

A yield criterion is a law defining the limit of elasticity under any possible combination of stresses. It is expressed by

$$f(\sigma_{ij}) = C \text{ (constant)} \qquad (2.4)$$

A function of stresses $f(\sigma_{ij})$ is called yield function. Several yield functions have been developed by many researchers such as von Mises criterion, Tresca criterion for isotropic materials; and Hill criterion, Barlat criterion for anisotropic materials (Bathe,1996 and Zienkiewicz, 1991).

The yield function, F, depends on the stress state, σ, and hardening parameter, κ, as,

$$F(\sigma,\kappa) = 0 \qquad (2.5)$$

Several yield surface functions have been developed by many researchers such as Von Mises criterion, Tresca criterion for isotropic materials; and Hill criterion, Barlat criterion for anisotropic materials.

ศูนย์วิทยทรัพยากร
จุฬาลงกรณ์มหาวิทยาลัย

2.1.1.5 Strain-hardening rule

The yield surface function changes as a result of the hardening that develops during the plastic deformation history. There are two basic models for hardening; the isotropic and the kinematics hardening models. The isotropic hardening model assumes the yield surface center remains fixed and the surface expands without changing shape. The general expression of the isotropic hardening rule can be written as,

$$F(\sigma) = k(\kappa) \qquad (2.6a)$$

where the function $k(\kappa)$ defines the yield surface size that depends on the deformation history.

The second model, kinematics hardening model, assumes the yield surface translates in the six dimensional stress spaces but fixes surface size or shape. The model has the general form as,

$$F(\sigma - \alpha) = k(\kappa) \qquad (2.6b)$$

where α is the back stress parameter that represents the translation of the yield surface center.

ศูนย์วิทยทรัพยากร
จุฬาลงกรณ์มหาวิทยาลัย

2.1.1.6 Associated flow rule

The direction of yield surface expansion depends on the incremental plastic strain, $d\varepsilon^p$, as,

$$d\varepsilon^p = \lambda \frac{\partial F}{\partial \sigma} \qquad (2.7)$$

where λ is the proportional constant that depends on the slope of stress-strain curve and the current stress or strain increment.

2.1.2 Finite element formulation

The governing equations are the equilibrium equation, the strain-displacement relations and the constitutive equations. The boundary conditions are prescribed in terms of velocity and traction. Along the tool-workpiece interface, the velocity component is prescribed in the direction normal to the interface and the traction is specified by the frictional stress in the tangential direction. Since it is difficult to obtain a complete solution that satisfies all of the governing equations, various approximate methods have been devised, depending upon the assumptions and approximations. The methods most well known are the slab method, the slip-line field method, the viscoplasticity method, upper- (and lower-) bound techniques, Hill's general method and the finite element method (FEM). In this study, the FEM has assumed to simulation of sheet metal forming.

The weak form of virtual work principle is applied to the equilibrium equation (2.1) by using the weighting function, δu, and written in the tensor form as,

$$\int_V \sigma_{ij,j}\, \delta u_i \, dV + \int_V \rho b_j \, \delta u_i \, dV = \int_V \rho \ddot{u}_j \, \delta u_i \, dV \qquad (2.8)$$

where u_i is the components of the displacement and V is the volume of the computational domain. The first term of Eq. 2.8 is then integrated by parts to give,

$$\int_V \frac{\partial}{\partial x_i}\left(\sigma_{ij}\delta u_i\right) dV - \int_V \sigma_{ij} \frac{\partial(\delta u_i)}{\partial x_i} dV \qquad (2.9)$$

The divergence theorem is then applied to the first term of Eq. 2.9 to yield the boundary terms. Then substitute these into Eq. 2.8 to obtain,

$$\int_V \rho \ddot{u}_j \, \delta u_i \, dV + \int_V \sigma_{ij} \frac{\partial(\delta u_i)}{\partial x_i} dV = \int_V \rho b_j \, \delta u_i \, dV + \int_S \delta u_i T_j \, dS + \int_S \delta u_i q_n \, dS \qquad (2.10)$$

Eq. 2.10 is then used to derive the corresponding finite element equations. The equations can be written in matrix form as,

$$MA + KU = F + F_c \qquad (2.11)$$

where **M** is the mass matrix, **A** is the acceleration vector, **K** is the stiffness matrix, **U** is the displacement vector, **F** is the external load vector, and $\mathbf{F_c}$ is the load vector of contact force.

2.1.3 Sheet metal formability

2.1.3.1 Formability parameters

The strain hardening exponent *n*, the plastic strain ratio *r* (the ratio of true width strain to true thickness strain) and the planar anisotropy Δr are the conventional indicators of formability of sheet metals. The stain hardening exponent *n* was determined from the regression of the load–elongation data obtained from the tensile tests, using the Hollomon equation, $\sigma = K\varepsilon^n$. The *r* value was then evaluated from the slope (*S*) of the plot of ε_2 versus ε_1 using the relation $r = -S/(1+S)$. This procedure gives a strain independent value for *r* and also normalizes any experimental scatter. The *r* value was evaluated in the three directions as in tensile tests specified above. The normal anisotropy, $\bar{r}$ and the planar anisotropy Δr were calculated using the standard formulae (Kumar, 2002):

$$\bar{r} = \frac{1}{4}(r_0 + 2r_{45} + r_{90}), \quad \Delta r = \frac{1}{4}(r_0 - 2r_{45} + r_{90}) \qquad (2.12)$$

where the subscripts indicate the orientation of the specimen axis with respect to rolling direction.

ศูนย์วิทยทรัพยากร
จุฬาลงกรณ์มหาวิทยาลัย

2.1.3.2 Forming limit diagram (FLD)

The FLD provides information on how much a particular metal can be deformed before necking occurs. The FLD is produced by data from experiment and theory as follows.

The experiment: Sheets are pre-marked with circle grids. During deforming, these circles are distorted into ellipses. Measurements of the major, d_1, and minor, d_2, diameters after deformation are made to determine the principal strains. These may be expressed as true strains, $\varepsilon_1 = \ln(d_1 / d_0)$ and $\varepsilon_2 = \ln(d_2 / d_0)$, or engineering strains, $e_1 = (d_1 - d_0)/d_0$ and $e_2 = (d_2 - d_0)/d_0$. The values for the whole or partial circles in the neck are considered "fail," while the strains in circles, one or more diameters away from it, are considered "safe". By plotting these strains, it is possible to construct a forming limit diagram as shown in figure 2.2.

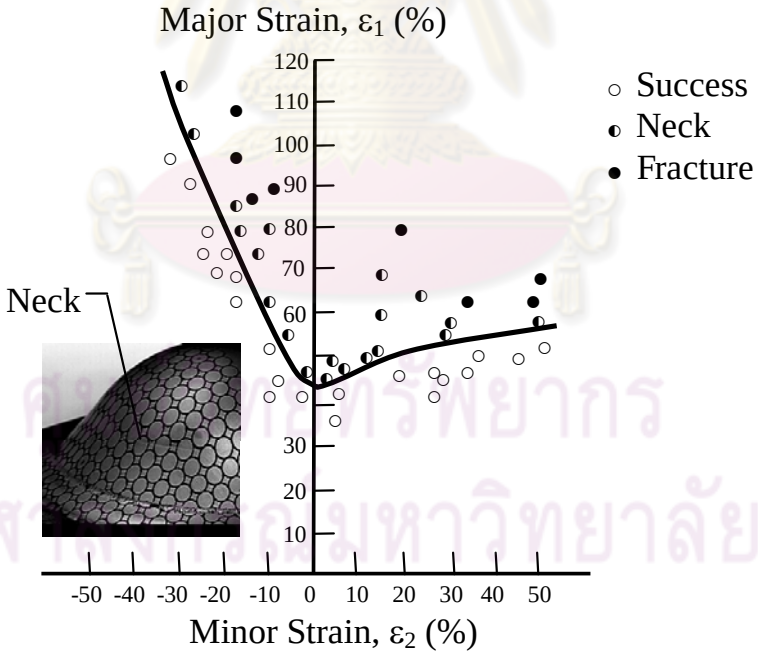

Figure 2.2 Forming limit diagram (FLD) from distortion of printed circles localized neck and plot of the strains

The theory: The FLD with the theoretical conditions for local and diffuse necking as expressed by Eqs. 2.13-2.14 are (Hosford and Caddell, 1993),

$$\varepsilon_1^* = \frac{n}{1+\gamma} \tag{2.13}$$

$$\varepsilon_1^* = \frac{2n(1+\gamma+\gamma^2)}{(\gamma+1)(2\gamma^2-\gamma+2)} \tag{2.14}$$

where ε_1^* is the critical strain in loading axis, n is hardening exponent, and γ is a constant strain ratio ($\varepsilon_2/\varepsilon_1$). The criteria for local and diffuse necking given by Eqs. 2.13-2.14 is plotted in figure 2.3.

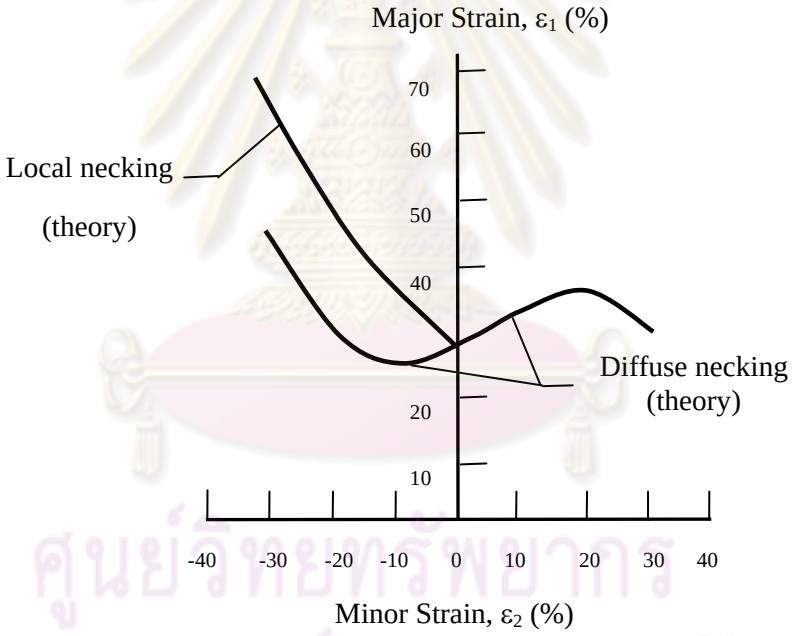

Figure 2.3 Critical strains for diffuse and localized necking according to Eqs. (2.13-2.14)

2.2 Sheet Hydroforming

Sheet hydroforming has gained increasing interest around the world in the automotive and aerospace industries recently. Sheet hydroforming has many virtues that meet the needs in reality very well, such as improvement of the sheet formability,

good surface quality, higher dimensional accuracy, reduction of springback amount compared with the conventional sheet metal forming processes.

Numerous studies have been conducted on traditional sheet metal stamping methods such as mechanical stretch forming and deep drawing where both methods requiring a male and a female die for the proper forming of a finished part. Much less literature is available on the sheet metal stamp hydroforming process, which uses a punch and hydrostatic fluid pressure to form a finished part. In this section a review of the literature focusing on the technology of sheet hydroforming processes will be presented.

Klaus Siegert and HaÈussermann et al. 2000 show an overview about possibilities of hydroforming sheet metal as well as hydroforming tubes and extrusions. Coming from the deep drawing process with rigid dies, specially designed dies for presses with multipoint cushion systems required for hydroforming sheet metal are discussed. Further special press systems for presses with high ram forces are shown.

Yossifon and Tirosh, 1985 published a series of articles dealing with simple analysis of the hydroforming deep drawing process as applied to the formation of cups from metallic materials such as copper, aluminum, steel and stainless steel. The goal of the studies was to establish a hydroforming fluid pressure path, relative to the punch stroke, that would prevent part failure due to rupture or to wrinkling. Their earlier studies demonstrated the effect that excessive and insufficient fluid pressures have on the premature failure of hydroformed parts. The purpose of the later investigations was to determine a predetermined path that can be followed to produce parts that are free from these types of defects.

Zhang, Wang et al. 2004 described development of sheet hydroforming technology such as varied sheet hydroforming application including innovation of tooling.

The process of stamp hydroforming, unlike conventional stamping, involves supporting the bottom of the sheet with a bed of viscous fluid during the stamping

process. This external support provides a through-thickness compressive stress that delays the onset of tensile instabilities as well as reduces the formation of wrinkles due to tensile frictional forces. The advantages of the stamp hydroforming process are numerous and the process is receiving significant attention from both the automotive and aerospace industries. Advantages of sheet hydroforming include improved formability of the blank due to the applied pressure by the fluid, low wear rate of dies and punch, a better distribution of plastic deformation when compared to conventional stamping, significant economic savings associated with the decreased tooling, and the potential for reducing the amount of finishing work required (Zampaloni, Abedrabbo et al. 2003). A schematic of the hydroforming process is shown in the next title.

2.2.1 Classification of sheet hydroforming process

The metal forming using liquid media is classified into sheet and tube hydroforming depending on the input pre-form. Further, sheet hydroforming is classified into hydromechanical deep drawing and high pressure sheet hydroforming depending on the male or the female die that has the shape/impression to be formed. High pressure sheet hydroforming is further classified into hydroforming of single blank and double blank depending on number of blanks being used in the forming process. The classification of hydroforming is shown in figure2.4. (Schmoeckel, Hielscher et al. 1999; Altan, Palaniswamy et al. 2004).

ศูนย์วิทยทรัพยากร
จุฬาลงกรณ์มหาวิทยาลัย

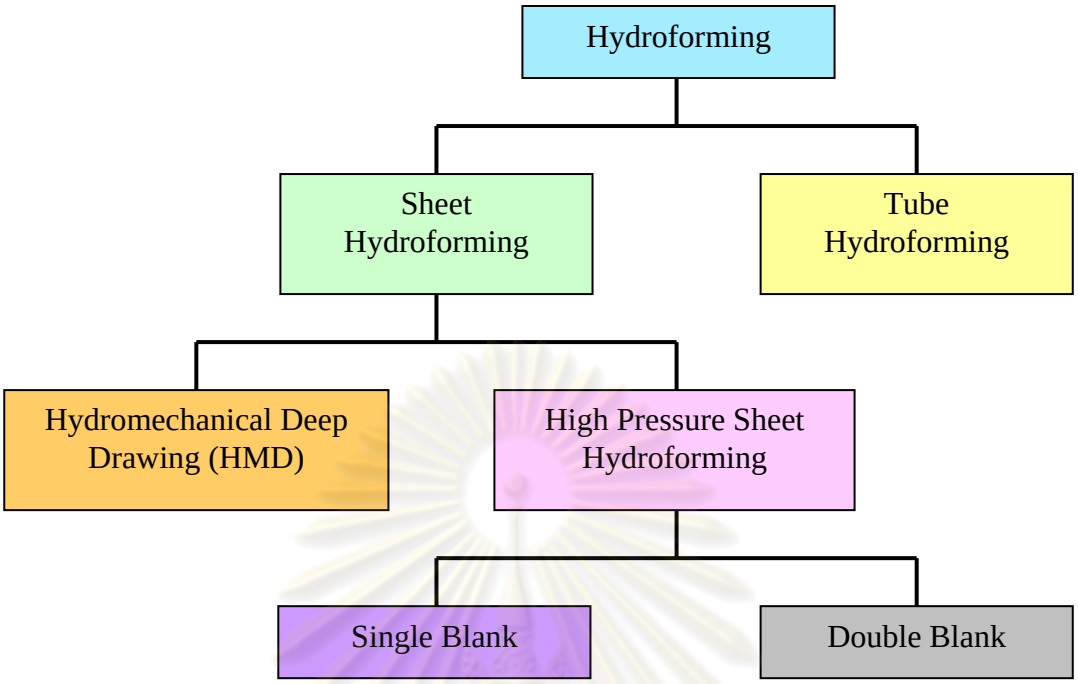

Figure 2.4 Classification of the forming process using liquid media [Schmoeckel et al]

2.2.2 Sheet hydroforming as a system

In this study, we are interested in sheet hydroforming. The hydromechanical deep drawing and high pressure sheet hydroforming are described as follows:

ศูนย์วิทยทรัพยากร
จุฬาลงกรณ์มหาวิทยาลัย

2.2.2.1 Hydromechanical deep drawing

In HMD, the sheet is deep drawn against a counter pressure in the pot rather than a female die in regular stamping operation as shown in figure 2.5 (Altan, Palaniswamy et al. 2004; Aust, 2001). The medium in the pressure pot can be either “passive” (pressure generated due to the incompressibility of the medium during forward stroke of the punch) or “active”(pressure generated by external pump).

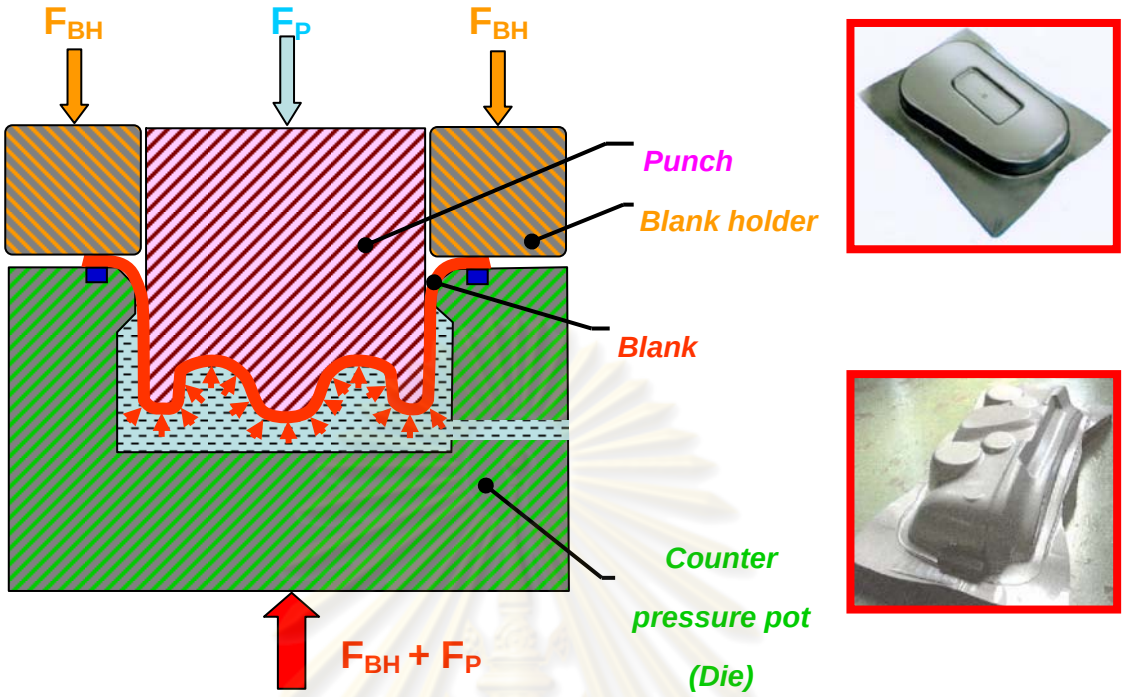

Figure 2.5 Hydromechanical deep drawing process description [Aust]

HMD results in higher LDR (deep drawability) compared to conventional stamping because during HMD the sheet metal is forced to form against the punch surface due to the fluid pressure. Due to the friction between the sheet and the punch surface, the sheet attached to the punch surface is not stretched during the forming process resulting in uniform wall thickness and higher LDR. HMD can be combined with regular stamping operations resulting in reduction of forming stages. figure 2.6 shows the combination of HMD with regular stamping, to form complex parts.

HMD is advantageous compared to conventional stamping because a) Elimination of female die results in lower tool cost and lower die development time. b) Elimination of sidewall wrinkles during forming process due to external fluid pressure allows more freedom in designing auto body panels c) Ability to form complicated shapes and features in the sheet metal resulting in less forming operations compared to the conventional stamping thereby reduces the manufacturing cost. d) Better surface quality as the outer surface of the sheet is in contact with fluid only thereby reducing the chance of tool marks (Altan, Palaniswamy et al. 2004).

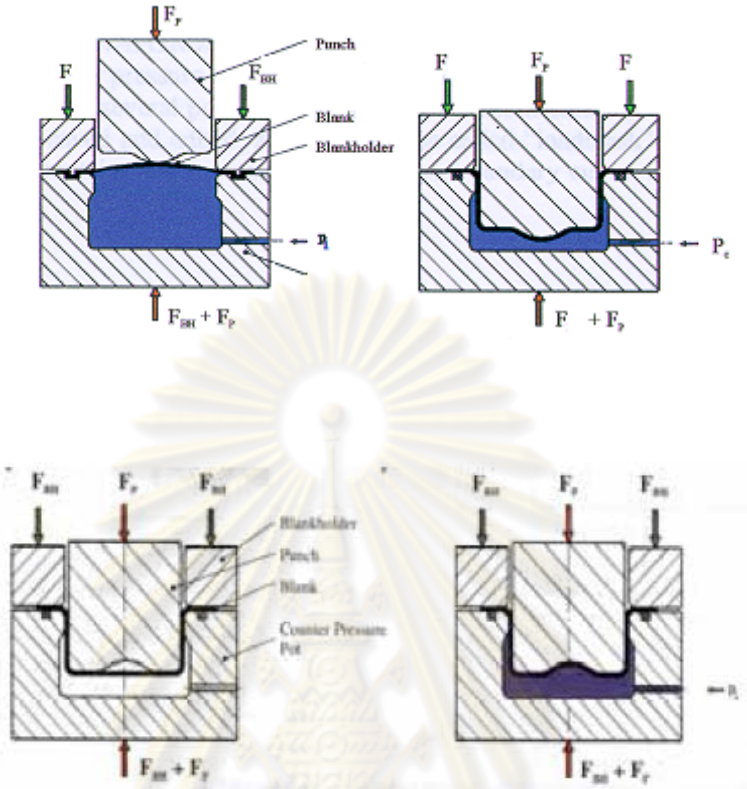

Figure 2.6 Combination of HMD with stretching and deep drawing to produce complex parts in less forming operations

Successful application of HMD requires careful consideration of all components of HMD system namely: a) Quality of incoming sheet, b) Tool-workpiece interface issue (friction and lubrication), c) Tool design for efficient application of blank holder force and avoid leakage d) Relationship between the internal fluid pressure and blank holder force (loading path), e) Press and Tooling, and d) Dimensions and properties of the HMD part.

2.2.2.2 High pressure sheet hydroforming

In high-pressure sheet hydroforming, the sheet is formed against female die by the hydraulic pressure of the fluid as shown in figure2.7 (Altan, Palaniswamy et al. 2004). During the forming process, the intermediate plate acts as a

blank holder to control the material movement from the flange and also seals the fluid medium to avoid leakage. Viscous pressure forming is similar to sheet hydroforming in which the pressure acting on the sheet is generated by compressing the viscous medium rather than hydraulic fluid/water in sheet hydroforming.

The forming operation in high pressure sheet hydroforming can be divided into two phases. Phase I involves the free forming where the sheet bulges freely in the die cavity until it initiates contact with the die. This introduces uniform strain distribution throughout the sheet thereby a) The formability of the material is effectively used compared to conventional stamping process where deformation is localized in the sheet at the punch corner radius, and b) Improves the dent resistance of the hydroformed part compared to stamped part. Phase II involves calibrating the sheet against the die cavity to obtain the desired shape. High fluid pressure is required in phase II depending on the material, sheet thickness, and the smallest corner radius in the die geometry. Thus, sheet hydroforming offers a viable alternative process for fabricating automotive parts from low formability advanced high strength steels and aluminum alloys.

Successful application of high pressure sheet hydroforming requires careful consideration of all components of high pressure sheet hydroforming system namely: a) Quality of incoming sheet, b) Die-workpiece interface issue (friction and lubrication), c) Tool design for efficient application of BHF and avoid leakage d) Relationship between the internal fluid pressure and blank holder force (loading path), e) Press and tooling, and d) Dimensions and properties of the hydroformed part.

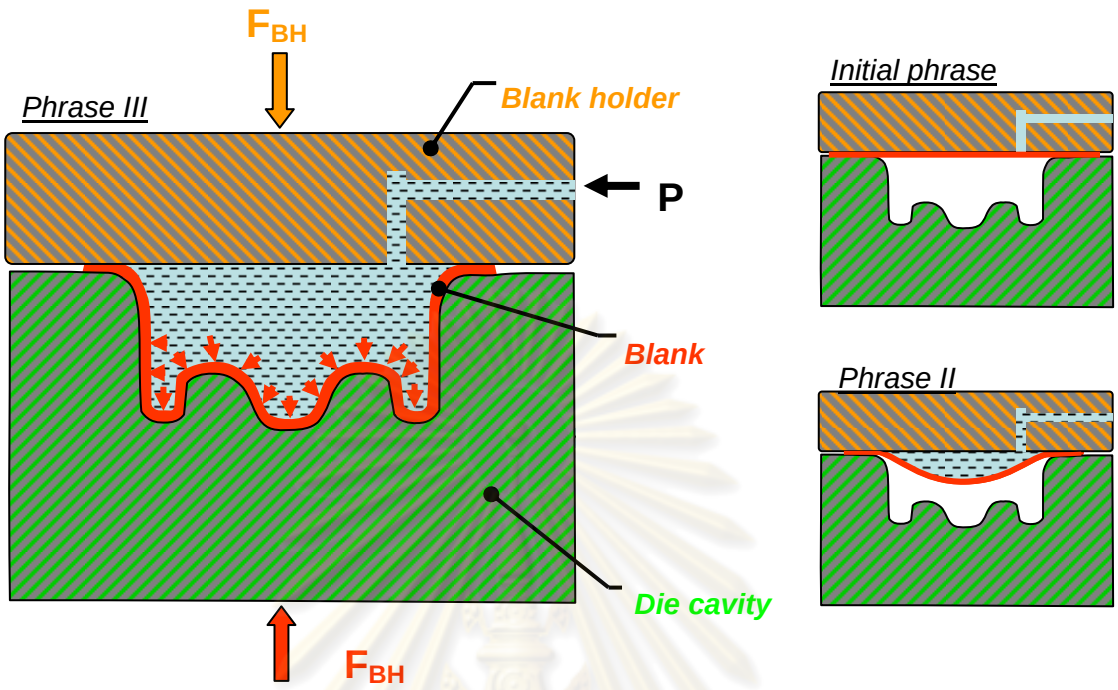

Figure 2.7 High pressure sheet hydroforming process description

2.3 FEA of sheet metal forming and hydroforming

2.3.1 Sheet hydroforming applications with FEA

In this section a review of the literature focusing on the most recent experimental and numerical studies conducted on sheet hydroforming processes will be presented.

Kumar, Dixit et al. (2007) used an explicit FEA to design die without blank holder in hydromechanical deep drawing process. They applied the concept of tractrix die. The cup can form successfully.

Lang, Danckert et al. 2004; Lang, Danckert et al. 2005 investigated a complex square round cup and round cup in hydromechanical deep drawing process with uniform

pressure both experiment and FEA simulation and they proved that the simulated results kept reasonable agreement with the experiment.

Qin and Balendra, 2004 conducted the FEA simulation to examine the deformation of the sheet during the forming of these component-forms and to qualify the influence of counter pressure paths on the product quality, with a view to developing a reference for process, tool and component design considerations for the hydromechanical deep drawing process of such component forms.

Zhang, Lang et al. 2000; Zhang, Nielsen et al. 2000; Zhang, Jensen et al. 2003 studied the effect of anisotropy, pre-bulging, counter pressure and blank holder force on the quality of parts such as round cup, parabolic workpiece and rectangular box in hydromechanical deep drawing process both explicit FEA simulation and experiment. The numerical results are compared with those obtained in the experiment.

Many researchers show that the FEA simulation can be used instead of experiment to design and predict the behavior of sheet deformation during the process in sheet hydroforming process.

2.3.2 Defect criterion

There are two main defects in sheet hydroformed parts. Necking or cracks is a defect that is avoided throughout the forming stroke, while wrinkles can take place during the process; however, it has to disappear at the end of the stroke.

2.3.2.1 Necking or crack

The Forming Limit Diagram (FLD) proposed by Keeler and Backofen, 1963 is widely used for measuring acceptable strain states of material deformation without failure. A typical FLD has a forming limit curve (FLC); a curve constituted by limiting surface strains by which the parts neck. FLC can be produced

by experimental data or theoretical modeling. Experimental determination of the forming limits in all sheet metal forming processes is very time consuming and costly.

2.3.2.2 Wrinkle

Wrinkles that form during the sheet forming are due to internal compressive instabilities. There are two types of wrinkles occur on parts.

(i) Wrinkles of first order in the flange and

(ii) Wrinkles of second order in the free-forming (unsupported) zone between the punch radius and the die radius. (Abedrabbo, 2002)

The wrinkling is a problem of equilibrium state, the prediction of wrinkles is more difficult for implicit codes than for explicit codes.

The flange wrinkle amplitude (FAM) (Sheng, Suwat Jirathearanat et al. 2004) is measured from the gap distance between blank holder surface and die addendum surface. The flange wrinkle can be easily visualized on the parts if it is over 5% of nominal sheet thickness. This critical wrinkle amplitude, however, would be different for different parts depending on the part functionality. Abedrabbo et al. 2002 defined the wrinkle criterion by using the area under a pure shear line in FLD as shown in figure 2.8.

Wang and Cao, 2000 presented the model to predict the onset of side wall wrinkle in term of stress base method.

ศูนย์วิทยทรัพยากร
จุฬาลงกรณ์มหาวิทยาลัย

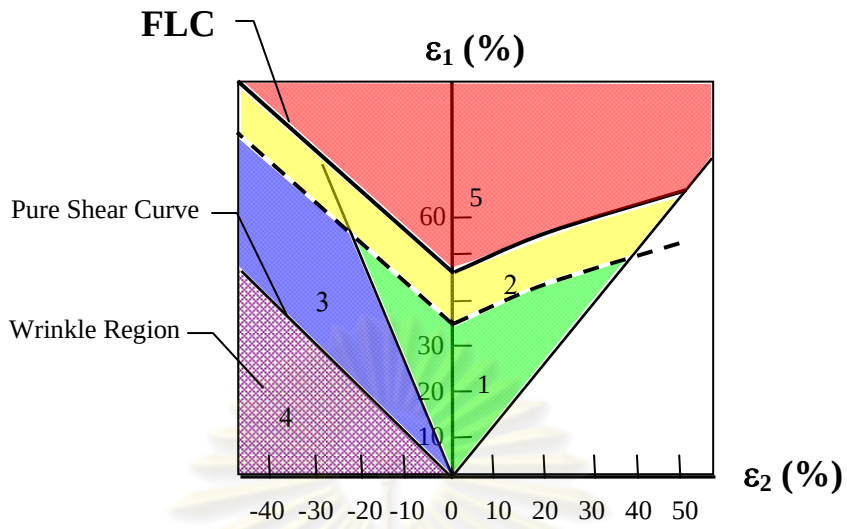

Figure 2.8 Wrinkle region in FLD

2.4 Effect of process parameters on hydroformability

The influence of process parameters and material properties on the hydroforming process has been studied by means of analytical models and experiments. Amino et al. 1990 found that limiting drawing ratio (LDR) improved significantly in case of hydro mechanical deep drawing when compared with conventional deep drawing. Elsebaie and Mellor 1983 determined that high chamber pressure is required to achieve maximum possible LDR, but when the chamber pressure is too high blank may be ruptured at the die profile. Pre-bulging means that at the primary stage of sheet hydroforming, one pre-bulging unit is used to increase the pressure in the die cavity actively, meanwhile, the punch is fixed at a certain position. When the pre-bulging pressure has reached the pre-setting value, the punch will go down as illustrated in figure 2.9 (Lang et al. 2004). Generally, pre-bulging has two functions: the first is to build the pressure at the beginning stage of hydroforming, and the second is to change the stress state of sheet around the punch nose to avoid the defects of fracture and wrinkling at the beginning of forming.

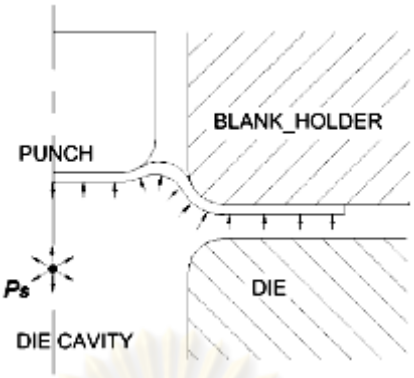

Figure 2.9 Pre-bulging method [Lihui Lang]

Zhang and Dackert 1998 using finite element simulation showed that pre-bulging pressure has greater influence on the thickness distribution along the cup wall. Sharma and Rout 2009 used FEM to study the main effect parameters in hydromechanical deep drawing process in circular cup. They concluded from ANOVA analysis for maximum thinning in the cup with DRAWING MODE of deformation lower thinning is possible with higher friction between blank and punch and better lubrication between blank-die and blank holder. Thinning in this case is not affected by the material properties, i.e. strain hardening exponent and anisotropy ratio. The friction is the main parameter affected on successfully forming. However, it is not uniform along the part geometry and varied with normal pressures. Therefore in practice, to determine the friction coefficients on all the contacting areas between blank and tools are very difficult. In hydromechanical deep drawing simulation, the values of the friction coefficients are assumed to be just one value, i.e. uniform friction condition, for the whole areas between blank and tools during the process. Kim et al. 2004 performed hydro mechanical forming and concluded that the hydro mechanical forming process could produce part with more uniform and sound thickness distribution compared to stamping operation. Sheng et al. 2004 established the variation of blank holder force can improve formability of the deep drawing process. Lang et al. 2009 conducted the FEM and experimental for aluminum part and concluded that the blank shape and the pressure in the die cavity will affect the forming process significantly and only by using both the optimized blank shape and

the pressure the part can be formed successfully in hydromechanical deep drawing. Lin et al. 2009 established the formulas for passive chamber pressure and blank holder pressure to form round cup with drawing ratio as 2.63 with no crack and no wrinkle in HMD process.

The challenges that are present during the sheet hydromechanical deep drawing process can be classified into two broad categories: effect of blank holder force and effect of fluid pressure with the other shape i.e. parabolic.

2.4.1 Effect of blank holder force

The quality of the formed part is affected by the amount of metal drawn into the die cavity. Excessive metal flow will cause wrinkles in the part, while insufficient metal flow will result in tears or splits. The blank holder plays a key role in regulating the metal flow by exerting a predefined blank holder force (BHF) profile. When selected properly, this BHF profile can eliminate wrinkles and delay fracture in the drawn part (Hsu et al. 2002, Sheng, Suwat Jirathearanat et al. 2004).

Design of blank holder plays a dominant role in HMD because the applied blank holder force controls the material flow during draw-in and also applies the necessary force to avoid leakage of the pressure medium during forming process. Usually, a constant BHF is applied over the punch stroke. During the drawing process, the state of stress in the deforming material changes significantly. Consequently, the process conditions that reduce wrinkling and fracture also change. To take into account these changes, it is reasonable that the BHF should also be modified to increase the formability of the drawn part (Sheng, Suwat Jirathearanat et al. 2004). To further improve the formability when drawing complex or asymmetric parts, an elastic or segmented blank holder can be used to obtain a non-uniform BHF over the part flange area. Thus, it is possible to account for variations of the metal flow over different locations of the blank holder surface.

2.4.2 Effect of counter pressure

This fluid pressure serves two main purposes. First, it delays the onset of material fracture as described earlier (Zampaloni, Abedrabbo et al. 2003) and secondly, it forces the material to conform much more closely to the shape of the punch than the parts formed without the resisting fluid. The fluid pressure needs to be high enough to stretch and bend the work piece through its radius of curvature to conform to the shape of the punch, yet the material needs to be ductile enough to form without rupturing.

The variable fluid pressure during the process investigated by Yossifon and Tirosh, 1984 fluid pressures within the upper fluid chamber that are too high will cause the material to bend to the radius of curvature of the punch much faster than the ductility of the material may allow. This will lead to premature rupturing of the sheet metal. On the other hand, if the fluid pressure is too low the sheet may not stretch enough during the process and wrinkle. Therefore, there is the need to establish an upper and lower limit on the fluid pressure, as it relates to the punch stroke, to determine an optimum fluid pressure path to ensure limited rupturing and wrinkling failures of the finished part. A generic curve is shown in figure 2.10 to help illustrate this idea. In the stamp hydroforming of sheet metals the difficulty lies in finding this appropriate fluid pressure path while avoiding rupture and wrinkling instabilities. Lo et al. 1993 and Hsu and Hsieh 1996 performed a series of experiments and analyses that established this fluid pressure path for the stamp hydroforming of metallic hemispherical cups.

ศูนย์วิทยทรัพยากร
จุฬาลงกรณ์มหาวิทยาลัย

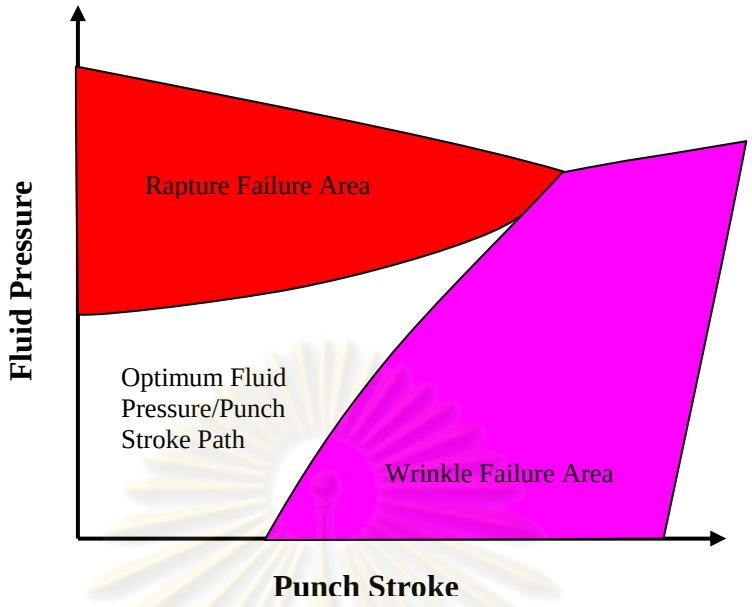

Figure 2.10 A generic curve illustrating the optimum fluid pressure–punch stroke path for the stamp hydroforming process

2.5 Design of process parameters

In previous title, the main process parameters in sheet hydroforming are blank holder force and pressure. In this research, we are focusing on the effects of pressure and blank holder force loading path on the quality of parts by blocking the other parameters.

These are also often referred to as “loading paths” or “part program” when presented in time domain. The success of sheet hydroforming processes is largely dependent on the choice of the loading paths. Part geometry, sheet material, and lubrication conditions need to be taken into account in designing of loading paths. The selection of proper loading paths can be done using empirical methods, analytical methods, or numerical methods.

Empirical methods are most suitable to roughly estimate the process parameters for simple to moderate complex sheet hydroforming part geometries. Usually these methods are quick but not accurate. Analytic methods are developed based on

plasticity theory. Most of the analytical models available for sheet hydroforming are often not applicable for even part geometries with moderate complexity. However, for simple part geometries the available analytical models can predict proper process parameters rather accurately. For general cases, numerical methods (FEA simulations) are very practical and widely applied in the industry.

2.5.1 Empirical and analytical method

Most empirical rules for sheet hydroforming part and process designs are developed through prototyping. Ahmetoglu and Hua et al. 2004 showed the equations for blank holder force and pressure of sheet metal using a viscous medium. They should be only used to get some conceptual ideas during initial design stage.

Analytical equations enable the engineer to estimate accurately the necessary process parameters. Analytical models for sheet hydroforming are normally developed based on plasticity and thin-walled or thick-walled theories. E.Siebel and H. Beisswanger 1955 developed equations to determine the variable blank holder force for a simple part. However, most analytical to predict the blank holder force profile have not correlated well with experiment. Analytical equations to determine process limits are difficult to be developed, particularly for complex sheet hydroformed parts.

It is noted here that even though the empirical rules and analytical equations provides guidelines on sheet hydroforming part and process design, many more design iterations are often necessary. FEA simulations are normally used in the design improvement stage. The process parameters are modified till successful sheet hydroforming process is obtained. (Suwat Jirathearanat, 2004).

2.5.2 Numerical method

Trial-and-error simulation method for the process design can be very time consuming, i.e. pressure and blank holder force curves versus time are selected

to conduct a simulation. If the results are not satisfactory, the input curves are modified by “intuition” and the simulation is run again until satisfactory results are obtained. Fortunately, this iterative FEA method can be done systematically and automatically with kinds of optimization. For example, determination of the loading paths can be treated as a classical optimization problem. By this way the resultant loading paths are optimized to maximize the part formability. Alternative approaches, aimed at efficient process FEA modeling are under development in several research institutes and companies. Five main different strategies can be followed: a) Optimization Simulation Method, b) Response Surface Simulation Method c) Feedback Control Simulation Method d) Fuzzy Logic Simulation Method and e) Adaptive Simulation Method

2.5.2.1 Optimization simulation method

Optimization can be broadly divided into two main groups: a) static optimization and b) dynamic optimization. In static optimization problems, design variables are time invariant (Suwat Jirathearanat, 2004), such as optimizing dimensions of a mechanical component to minimize its weight. There are two main methods to solve static optimization problems; gradient-based methods and non-gradient-based methods. The gradient-based methods include steepest descent method, Newton method, and Quasi-Newton method used for linear and non-linear static optimization problems. For highly complex problems (optimizing a very large number of design variables), non-gradient-based methods are normally applied, such as response surface methods and genetic algorithms. In dynamic optimization problems, the design variables are time variant, such as an optimization of flight trajectory control. One of the most powerful methods to solve the problems is dynamic programming.

In metal forming, FEA simulations integrated with an optimization solver are used to optimize either geometric parameters or process parameters in order to maximize formability of that specific process. To understand the applications of optimization,

the literature review in various metal forming processes was conducted. In forging, the die shapes are optimized to achieve the most uniform deformations (constant strain rates), which improves metallurgy properties of the forged components (Fourment and Vieilledent et al. 2001; Suwat Jirathearanat, 2004). The die profile was represented by a Bezier curve with a finite number of control points, see Figure2.11a. Fourment and Vieilledent et al. 2001 applied Direct Differentiation Method (DDM) to determine the objective function (i.e. strain rates) sensitivity to the change of design variables (positions of the control points representing the die profile), and then Broyden-Fletcher-Goldfarb-Shannon (BFGS) algorithm was used for the optimization through iterative FEA simulations. To avoid complexity in calculating the derivatives of the objective functions, non-gradient methods such as genetic algorithm were applied by Jo, Lee et al. 2001; Kusiak, 1996; Chung and Hwang, 1997; Suwat Jirathearanat, 2004 on the similar problem of forging die design.

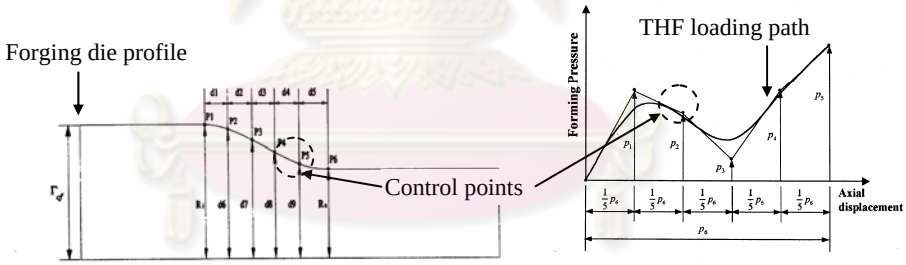

a) b)

Figure 2.11 Bizier curves representing a) forging die profile as design parameters, b) THF loading path as design parameters

A few researchers applied static optimization methods through iterative FEA simulations to determine metal forming process parameters in time domain. In forging, ram speeds at which a workpiece is being formed are optimized so that the deformation is uniform. In sheet metal forming the blank holder force is also optimized so that final stamping part has the highest obtainable drawn depth with no

wrinkles and fracture. In tube hydroforming, pressure and axial feed curves versus time (loading paths) are also optimized (Yang, Joen et al. 2001). The loading path is often described by a Bezier curve representation whose control points are the design variables in the optimization problem, see figure 2.11b. The objective function can be strain rate variations, part thickness variations, or maximum thinning, which are minimized. The problem is then reduced to determination of the positions of control points so to minimize the objective function value. Ghouati, Lenoir et al. 2000 and Yang, Joen et al. 2001 applied this optimization method to determine the loading path for a simple axisymmetric bulging.

Design parameters are the control points (pi) describing a B-spline function of loading path (figure2.11).

Objective function takes into account of element thickness variations after each forming simulation run:

$$f(p) = \left(\frac{1}{N} \sum_{i=0}^{N} \left| \frac{h_i - h_0}{h_0} \right|^2 \right)^{\frac{1}{2}}$$

where N is the total number of elements considered, h_0 is the initial thickness and h_i is the final thickness of element ith, which is an implicit function of design parameters (p_i).

ศูนย์วิทยทรัพยากร
จุฬาลงกรณ์มหาวิทยาลัย

Constraint function represents the distance from the desired shape to the final part at simulation end:

$$g(p) = \left(\sum_{i=0}^{M} |d_i|^2 \right)^{\frac{1}{2}}$$

where M is the total number of nodes considered, and d_i is the distance of node i to the tool (final

desired part shape), which is an implicit function of design parameters (p_i).

This optimization method may be called “global optimization of process parameters in time domain”. This method tends to generate very complex and non-linear objective functions as the number of control points (design variables) increases, which may lead to non-convergent solutions.

2.5.2.2 Response surface simulation method

The response surface methodology (RSM) is a method for constructing global approximations of the objective and constraint functions based on functional evaluations at various points in the design space. The strength of the method is in applications where gradient based methods fail, i.e. when design sensitivities are difficult or impossible to evaluate. Two important issues when applying RSM to a particular problem concern the design of experiments and construction of accurate function approximations so that rapid convergence may be achieved. RSM is well established for physical processes as documented by Myers and Montgomery, 2002 while the applications to simulation models in computational mechanics form a relatively young research field. Among other recent works, Roux, Stander et al. 1998 discuss experimental design techniques and the regression equations for structural optimization.

RSM combined with stochastic finite elements are used by Kleiber, Knabel et al. 2002 for reliability assessment in metal forming. Huang, Lo et al. 2006 fined the optimal radius of punch and radius of punch nose of round cup for minimization of the thickness variation by using RSM coupled with FEM. Wang and Lee, 2005 using RSM and FEM to control strain path forming process with space variant blank holder force.

2.5.2.3 Feedback control simulation method

Control theories have been applied in many industrial applications for many years, such as control of temperatures in chemical processes. A controller regulates some quantities to stabilize a process by automatically adjusting a variable(s) (controlled variable) in real time. The simplest and most widely used control schemes are PID controllers. For highly non-linear processes, non-mathematics based controllers, such as fuzzy logic controller, and neural network controller are preferred. A few researchers have applied feedback control schemes in conjunction with metal forming process FEA simulations (Suwat Jirathearanat, 2004). With the help of a feedback controller integrated into a process FEA code, the process parameters can be adjusted at every simulation time step to achieve high process formability predicted through the simulation.

The main difference in determination of process parameters through FEA using optimization methods mentioned above and feedback controllers is apparent in the time duration where corrective actions, i.e. adjusting process parameters, take place. The optimization simulation method requires many simulation runs. After the end of a simulation, a parameter correction is done and applied into the next simulation run with the attempt to minimize the objective function value. A feedback controller adjusts process parameters at every time step in one simulation run in order to maintain the controlled quantities, i.e. formability, see figure 2.12. The advantage of the feedback control simulation method is that it requires less total computation time in predicting the process parameters than the optimization simulation method does.

Cao and Boyce, 1994 controlled wrinkles and maximum strains in a conical cup drawing simulation by automatically adjusting the binder force by using a PI controller. Thomas, 1998 further developed Cao's work by introducing the control of stresses as well. Grandhi, Kumar et al. 1993 and Feng and Luo, 2000 implemented

optimal feedback controllers in simulation of forging processes. The controller tried to regulate the ram speed to track the predefined strain rate of the part being forged.

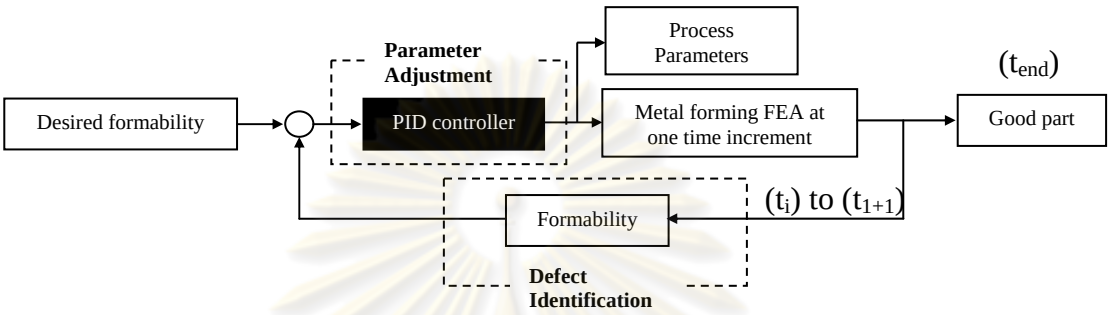

Figure 2.12 General flow chart of the feedback control simulation method for process design in metal forming

2.5.2.4 Fuzzy logic simulation method

The basic fuzzy rules incorporate a simple logical term, based on "IF 'X'AND 'Y ' THEN 'Z"' approach to solve any basic control problem rather than attempting to model the system mathematically, where 'X' and 'Y ' are two different input conditions and 'Z' is the outcome or result due to the inputs. Ray and Mac Donald, 2004 applied fuzzy logic to find loading path; pressure and axial feed in tube hydroforming process of T-branch and X-branch shape. They fuzzified the input variables and conditions into 27 fuzzy rules, which judge whether the incremental axial feed (Δd) and internal pressure (Δp) have to be high, medium or low (fuzzy inference). Finally, a defuzzification computes the output (Δd and Δp) as the weight center of the output set. Ho Choi and Koc et al. 2007 also used fuzzy logic algorithm to determine the pressure profile and blank holder force profile in warm hydroforming of a round cup.

2.5.2.5 Adaptive simulation method

This method makes use of both optimization method and feedback control method in design of process parameters. The adjustments of process parameters are carried out at each time step (or certain interval of simulation time step) during a single simulation run similar to the feedback control method. However, the adjustments of process parameters are done with the help of optimization methods. By this way, the automatic design of the process parameters can be done quickly and in an optimized manner (Suwat Jirathearanat, 2004).

Sheng, Suwat Jirathearanat et al. 2004 proposed an adaptive simulation strategy to adjust the magnitude of the BHF continuously during the simulation process. Thus, a BHF profile is predicted in a single process simulation run and the computation time is reduced. The proposed strategy has been applied successfully to two conical cup drawing operations. The predictions have been compared with experiments and the results indicate that the adaptive simulation strategy can also be used to improve the drawing process for forming non-symmetric parts. Aydemir, Vree et al. 2005 proposed an adaptive method is presented to obtain a more efficient process control for tube hydroforming processes. This method avoids the onset of wrinkling and bursting via dedicated stability criteria. The wrinkling criterion uses an energy-based indicator inspired on the plastic bifurcation theory. For necking, followed by bursting, a criterion based on the forming limit curve is employed. Applying these two criteria, the process parameters are adjusted during the simulation via a fuzzy knowledge based controller (FKBC). A case study is carried out for the hydroforming of a T-shape part using the designed adaptive system in combination with the finite element method. For the simulations ABAQUS/Explicit is used.

Table 2.1 showed the researches about the optimization coupled with FEM in metal forming.

Table 2.1 Summarize of optimization with FEM technique in metal forming

Author	Process	Objective	Parameters (Design Variables)	Technique
Heung-Kyu Kim (2007)	Multi-Stage Deep Drawing (Round Cup)	Max. Thickness of the bottom	Clearance, Punch Dia., Stroke	Simulated Annealing (SA)
Ho Choi (2007)	Warm Sheet Hydrofroming (Round Cup)	Thickness, Strain, Stress Distribution	Pressure, BHF Profile	Fuzzy Logic
H. Naceur (2007)	Deep Drawing (Round Cup)	Springback	Die, Punch Radius	Response Surface Method
Lin Zhong-Qin (2007)	Sheet Metal Forming (Pan Cup)	Drawing Limit	BHF Profile	PID Close-loop
Qiang Liu (2007)	Deep Drawing (Pan Cup)	Max. Reduced Thickness Min. Increase Thickness	Constant BHF	Divergence Marginal Method (Gradient)
S.K. Singh (2007)	HMD (Round Cup; Tractrix)	Max. Limit Drawing Ratio (LDR)	Die Lip Dia. Draft Angle	Gradient Optimization
Benny Endelt (2006)	Sheet Metal Forming (Pan Cup)	Flange Draw-in	BHF Profile	On-line Feedback Control
Ken-ichi Manabe (2006)	Tube Hydroforming (T-Branch)	Successful	Pressure, Axial Feed, Counter Punch Distance Profile	Fuzzy Logic

Author	Process	Objective	Parameters (Design Variables)	Technique
Lihui Lang (2006)	Sheet Hydroforming	Min. Error of Punch Force	n, K, μ	Non-Linear Least Square Method
Y. Huang (2006)	Deep Drawing (Round Cup)	Uniform Thickness Distribution	Punch Radius Punch Nose Radius	RSM
A. Aydemir (2005)	Tube Hydroforming (T-Branch)	Successful	Pressure, Axial Feed Profile	Adaptive Simulation
Lin Wang (2005)	Deep Drawing (Rectangular Cup)	Min. Major-Minor Strain	Constant BHF in each segments	RSM
M. Imaninejad (2005)	Tube Hydroforming (T-Joint)	Min. Thickness Variation Max. Effective Stress	Pressure, Axial Feed Profile	Conjugate Gradient Optimization
T. Jansson (2005)	Deep Drawing (Automotive Part)	Draw-in Target	Drawbead Restraining Force	Surrogate Model and Response Surface
Hiroshi Koyama (2004)	Sheet Metal Forming (Non-Symmetric)	No Defects	BHF Profile	Database
Jun Zhao (2004)	Deep Drawing	No Defects	n, K, r, μ	Neural Network
P. Ray (2004)	Tube Hydroforming (T-X Shape)	No Defects Max. Thickness	Pressure, Axial Feed Profile	Fuzzy Logic
Z.Q. Sheng (2004)	Deep Drawing	Height	BHF Profile	Adaptive Simulation

ศูนย์วิทยทรัพยากร
จุฬาลงกรณ์มหาวิทยาลัย

Author	Process	Objective	Parameters (Design Variables)	Technique
Kuang-Jau Faan (2003)	Tube Hydroforming (T-Shape)	Thickness Uniform and Accuracy Shape	Pressure, Axial Feed Profile	Conjugate Gradient Optimization
Jae- Bong Yang (2001)	Hydrofroming	Uniform Thickness	Pressure, Axial Feed Profile	Sensitivity Analysis
S.H. Park (1999)	Deep Drawing	Min. Shape Error	Blank Size	Gradient

ศูนย์วิทยทรัพยากร
จุฬาลงกรณ์มหาวิทยาลัย

CHAPTER III

PROBLEM STATEMENT AND METHODOLOGY SETUP

3.1 Parabolic parts

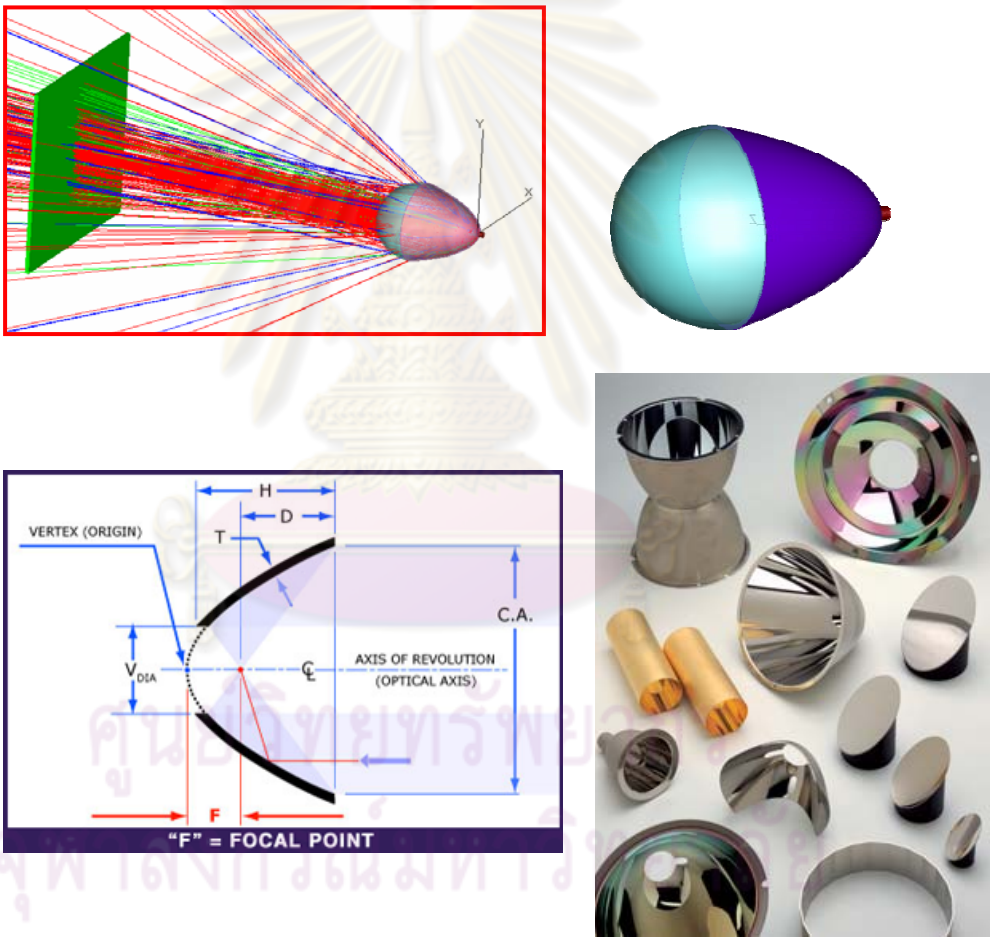

Figure 3.1 Parabolic cup application

Parabolic cups are mostly used in application of light reflector as shown in figure 3.1. To form a parabolic shape using conventional deep drawing process is typically necessary to use six steps, while hydromechanical deep drawing process can form the part in one step (Zhang, Lang et al. 2000). Furthermore, dimensional

accuracy of the products is remarkably improved. This research focuses on a family of parabolic cups as shown in figure 3.2. During forming process, this shape is very much prone to fracture and wrinkle, if the process parameters are not proper. The key process parameters affecting the parts are blank holder force and counter pressure. Excessive blank holder force and high counter pressure can lead to fracture. On the other hand, insufficient blank holder force and low counter pressure can lead to wrinkle. Therefore, proper blank holder force and proper counter pressure are very important in carrying out the forming process successfully. In this research, we have two problems to determine 1) the proper constant blank holder force and proper linear counter pressure of the parabolic cups and 2) the feasible profile of blank holder force and pressure as shown in figure 3.3.

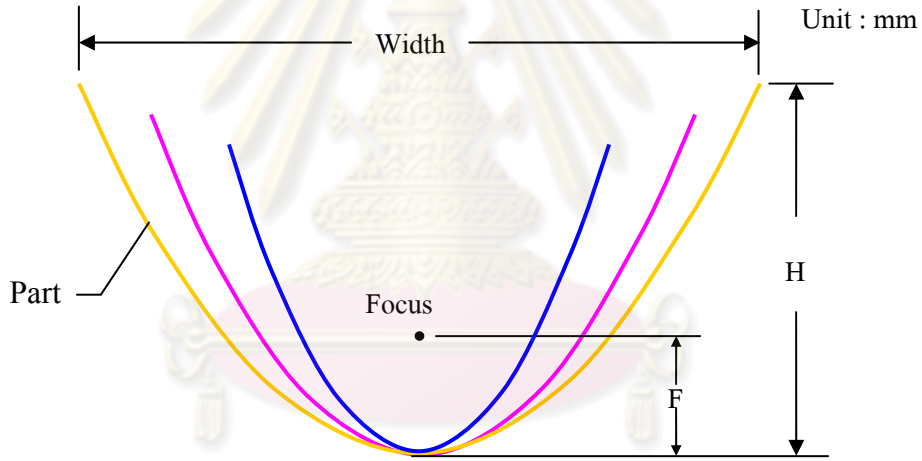

	Focus (mm)	Width (mm)	Height (mm)	Blank Dia. ϕ (mm)
Part #1	**20.0**	**178.89**	**100.00**	**320.00**
Part #2	**25.0**	**219.09**	**120.00**	**380.00**
Part #3	**39.5**	**297.46**	**140.00**	**480.00**

Figure 3.2 Parabolic cup dimensions

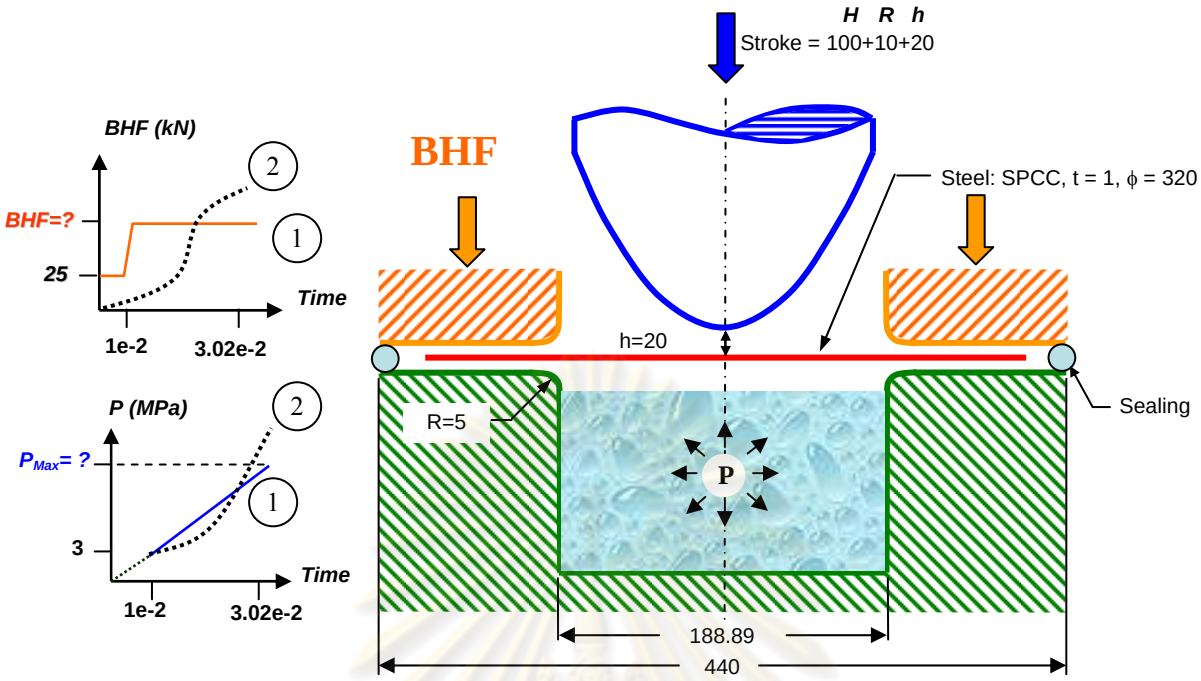

Figure 3.3 Problem statement to find proper process parameters of parabolic cups

3.2 Material properties

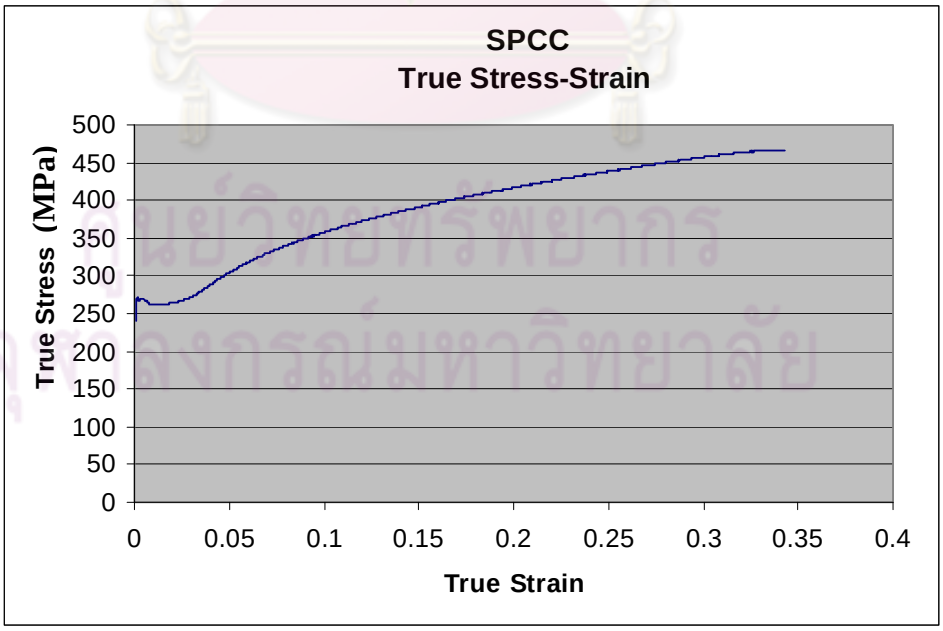

Figure 3.4 Flow curve of SPCC

SPCC, low carbon sheet steel in Japanese steel grade, is used in this research because this material is widely used in Thailand automotive industries. It is not a deep draw quality grade. To improve formability of this material, it is necessary to change the forming process to hydromechanical deep drawing and process parameters should be properly designed. In this study, uniaxial tensile test was used to find mechanical properties of SPCC material with 0.8 mm thickness as shown in table 3.1 and a flow curve is shown in figure 3.4. Experimental forming limit curve (FLC) of this particular material is shown in figure 3.5.

Table 3.1 The properties of SPCC

Material:	SPCC
Blank thickness:	1.0 mm
Young's modulus	207,000 MPa
Poisson's ratio	0.28
Yield strength	267 MPa
Ultimate strength	471 MPa
Strain hardening component (n):	0.216
Strength coefficient (K):	589.4 MPa
Anisotropy	
r_{00}:	1.20
r_{45}:	1.09
r_{90}:	1.86

ศูนย์วิทยทรัพยากร
จุฬาลงกรณ์มหาวิทยาลัย

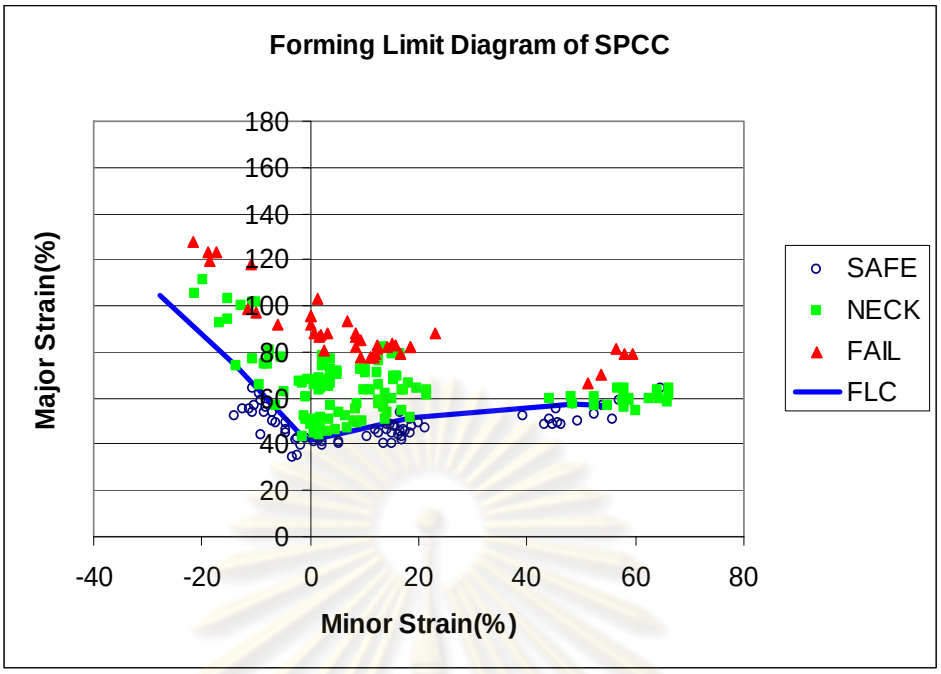

Figure 3.5 Forming limit diagram of SPCC steel with 0.8 mm. of thickness

3.3 FEA setup for HMD process

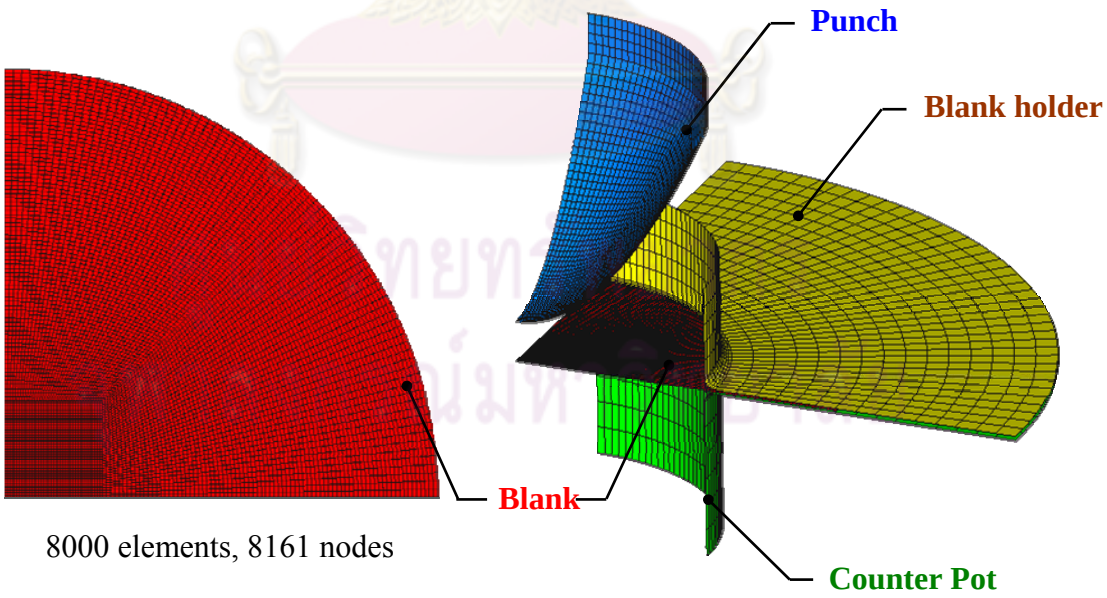

Figure 3.6 – Finite element quarter model of blank and tool components

Finite element simulation used in this research is solved an incremental dynamic explicit finite element code; LS-DYNA. FE quarter models of the blank and tool components are used in the analysis to take advantage of the symmetry and to reduce calculation time as shown in figure 3.6. The blank model is a structured mesh model with 8,000 quadrilateral elements and 8,161 nodes. Belytchko-Tsay thin-shell elements are used. The tool components are modeled with a rigid material model (material type 20).

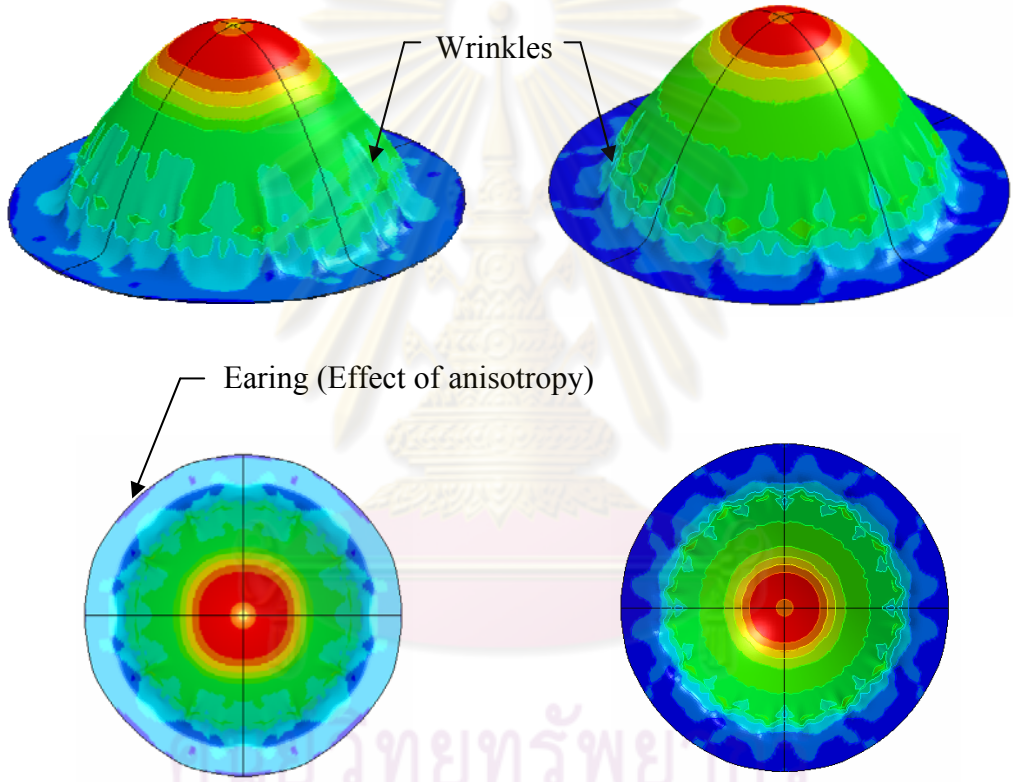

a) Balat-Lian's three-parameter model b) Hill's transversely anisotropic model

Figure 3.7 Comparison of solutions between the Balat-Lian's three-parameter model and Hill's transversely anisotropic model

There are many constitutive material models for the steel blank such as von Mises isotropic material model (material type 18), Balat-Lian's three-parameter model (material type 36) and Hill's transversely anisotropic model (Hill 1948 model;

material type 37). It has been shown that experimental results compared with the simulation ones are in very good agreements when using either Hill's transversely anisotropic model or Balat-Lian's three-parameter model (Zhang, Lang et al. 2000). The comparison of solutions between the Balat-Lian's three-parameter model and Hill's transversely anisotropic model are shown in figure 3.7. In this research, Balat-Lian's three-parameter model was used for the blank material model. Barlat recommends M = 8 for face centered cubic (FCC) materials, M = 6 for body centered (BCC) materials. SPCC sheet steel is indicated to have BCC structure (Lee, Kumai et al. 2007), so in this research M = 6 was applied. The mechanical properties of SPCC used in this research are given in Table 3.1.

The friction coefficient (μ_s) is dependent on material, contact surface and lubricant. Moreover, it is not uniform along the part geometry and varied with normal pressures. Therefore in practice, to determine the friction coefficients on all the contacting areas between blank and tools are very difficult. In hydromechanical deep drawing simulation, the values of the friction coefficients are assumed to be just one value, i.e. uniform friction condition, for the whole areas between blank and tools during the process. In papers based on the works by (a) Khandeparkar and Liewald 2007, (b) Lang et al. 2004 and (c) Zhang et al.2000, these researchers have used a lower friction coefficient in the range of 0.03 – 0.08 at the flange contacting interfaces whereas a higher friction coefficient in range of 0.1 – 0.2 was considered at the punch wall contact interface. In this research work, the coulomb friction coefficient of 0.06 was used between the blank and the blank holder, and between the blank and the counter pot ring. The friction coefficient of 0.12 was assumed for the contact model between the blank and the punch. The fluid was not modeled; instead, a uniformly distributed pressure was applied directly to the blank surface. After the pre-bulging stage, the internal pressure was increased linearly up to the end of the forming stroke, while the blank holder force remained constant throughout the process.

The time step has to be less than (Tekkaya, 2000)

$$\Delta t = \left(\frac{L}{C}\right) = \left(\frac{L}{\sqrt{E/\rho}}\right) \qquad (3.1)$$

where L is a characteristic length of the element, C the speed of sound in the workpiece material, E is the Young's modulus of the material and ρ is the density of the material. Consider a process operation for which C is 5000 m/s for steel, L is in the order of mm's, around 2 mm (this corresponds to the smallest element in the mesh!). The minimum time step is given by the above equation as 4×10^{-7} s. The punch speed is about 6.25 mm/s (forming after pre-bulge is set for 20 second) and the punch traveling distance is roughly 125 mm. The time for forming can found as 20 s. Dividing the total process time by the minimum time step yields the number of time increments as 5×10^{7}. This is an unacceptable high number of increments, which would make the dynamic explicit methods unfeasible. For this reason, two different numerical tricks are applied:

1. The punch speed is increased as compared to the real process speed. In order to reduce the undesired effects of the artificial mass forces numerical damping is introduced. The damping matrix is taken proportional to the mass matrix usually. This precaution, however, does not work if the material is strain rate sensitive. Also, if a thermo-mechanical phenomenon is involved, increasing the process speed is not allowed. In such cases the second treatment is used.

2. Increasing the density of the material leads to a reduction of the speed of sound in the material and hence an increase in the allowable time increment.

In this case, the material is formed in room temperature (it is not thermo-mechanical phenomena) and the material was tested by tensile test with cross head speed as punch speed. Time scaling technique was used to guarantee a reasonable calculation time, taken as 1,000, i.e. the artificial punch speed is 6,250 mm/s while a typical punch speed is 6.25 mm/s, however, increasing the density is not possible (no mass scaling).

Generally, pre-bulging has two functions: the first is to build the pressure at the beginning stage of hydroforming, and the second is to change the stress state of sheet around the punch nose to avoid the defects of fracture and wrinkling at the beginning of forming. In the simulation, the pre-bulging stage takes place for 0.01 seconds; pressure, blank holder force and dome height are set up to produce a plastic strain (pre-strain) of 2-8%. The dome height is around 20% of final part height.

To improve the analysis accuracy, the development and application of new constitutive equations, failure criteria and friction models are expected (Tekkaya, 2000).

3.4 Experimental setup for HMD process

3.4.1 Equipments

- Press machine
- Blank holder force control system
- Pressure intensifier
- Pressure control system
- Force transducer
- Pressure transducer
- Die
- Blank material

ศูนย์วิทยทรัพยากร
จุฬาลงกรณ์มหาวิทยาลัย

3.4.2 Press machine and blank holder force control system

A press machine and blank holder force control system are used in the experimental is specified follows:

Equipment: Hydraulic Press 200 tons

Main Press:

- Hydraulic Press Single action and programmable active cushion force

- Pressing Capacity 200 tons
- Lifting Capacity 20 tons
- Table Size 1,200 x 1,000 mm
- Max. Day Light 1,050 mm
- Stroke 700 mm
- Down Speed 160-200 mm/sec
- Pressing Speed 8-12 mm/sec

Cushion Press: Programmable active cushion force with respect to ram position

- Cushion Capacity 100 tons
- Cushion Stroke 350 mm

Control:

- Control Panel Touch Screen shows:
  - Ram Force
  - Cushion Force
  - Ram Displacement

- Programmable ram down positioning

- Programmable active cushion force/stroke

- Allow using signals from force sensors/transducers in the control unit

- Allow sending signals from the control unit to outside data acquisition system

ศูนย์วิทยทรัพยากร
จุฬาลงกรณ์มหาวิทยาลัย

The machine and blank holder force control system were built by National Metal and Materials Technology (MTEC) as shown in figure 3.8.

Figure 3.8 Two hundred ton of hydraulic press machine and blank holder force control system

3.4.3 Press intensifier and pressure control system

Pressure intensifier and pressure control system is used to intensifier the pressure from a normal hydraulic pump to a much larger pressure using fluid media such as treated water or hydraulic oil. The controller regulates the fluid pressure during the forming according to the design pressure profile. These systems were created by BT Engineering Company. The hydraulic bulge test die and pressure intensifier were built and integrated with the common hydraulic press machine as shown in figure 3.9.

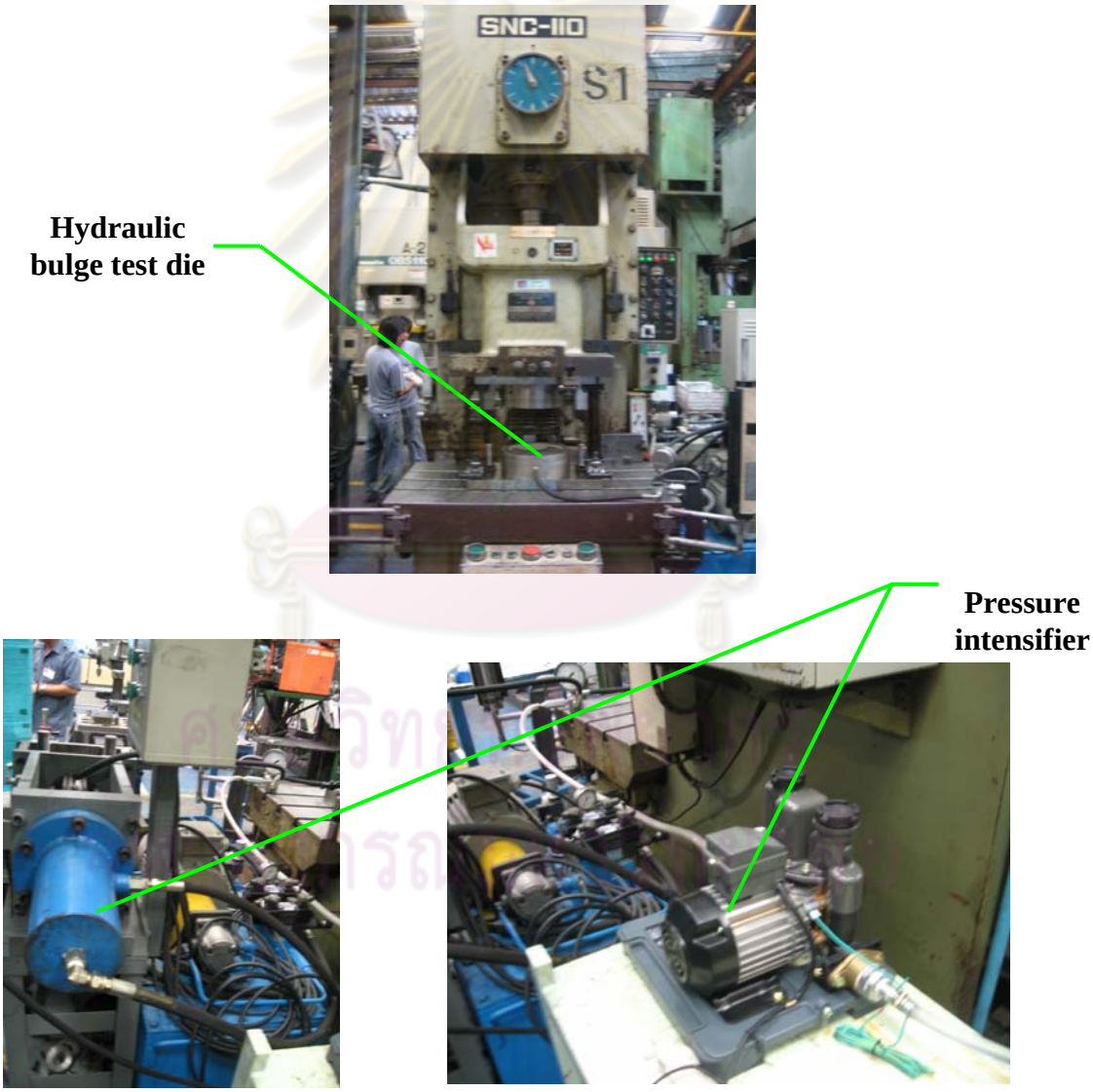

Figure 3.9 Pressure intensifier system built by BT Engineering Company

3.4.4 Die

The die was designed by modifying from the hydraulic bulge die [MTEC] as shown in figure 3.10

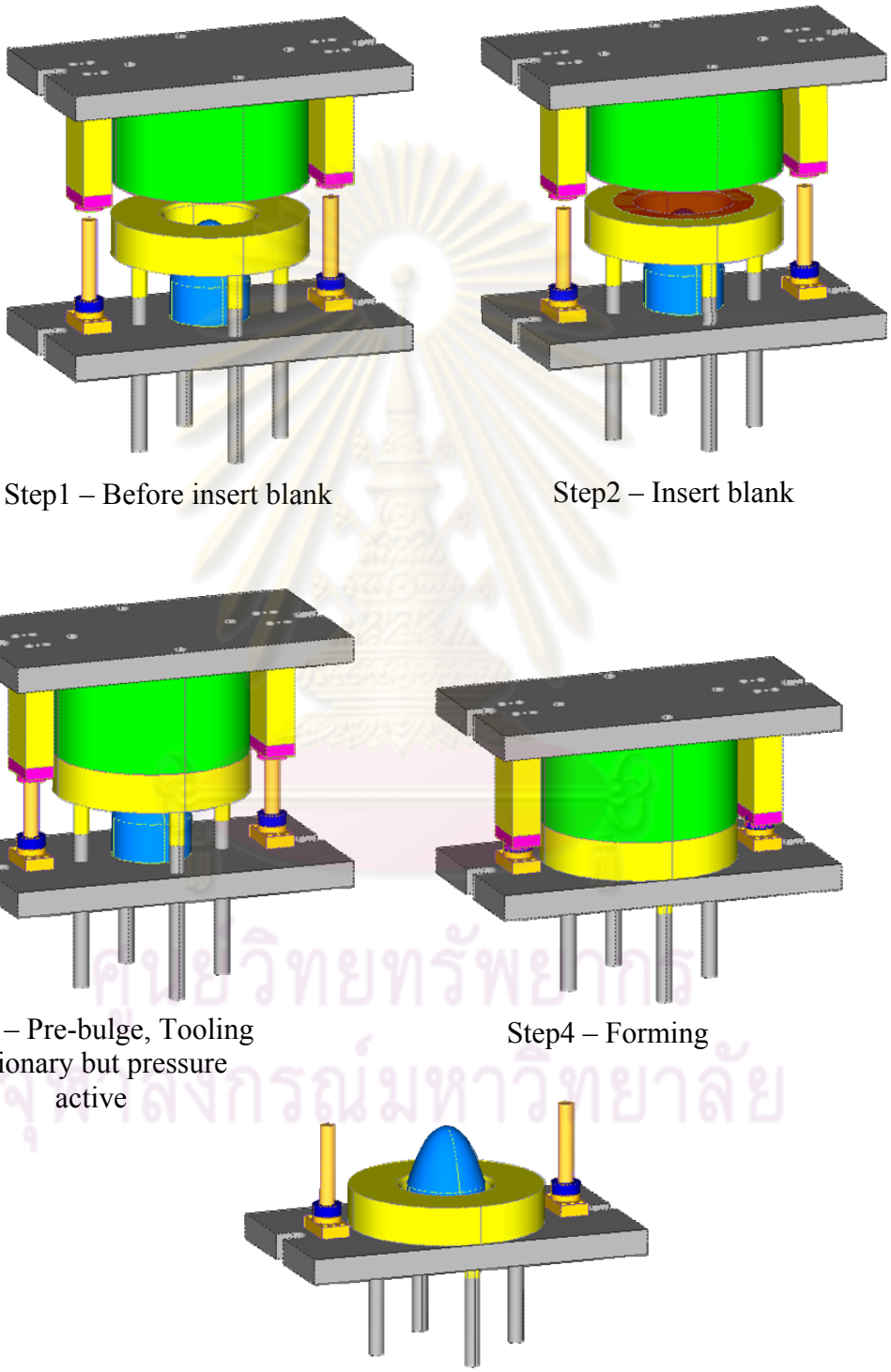

Figure 3.10 Hydromechanical deep drawing die of parabolic part

ศูนย์วิทยทรัพยากร
จุฬาลงกรณ์มหาวิทยาลัย

3.5 Investigation of the parabolic parts with HMD

The main defects of HMD process of parabolic parts are cracks and wrinkles. The thinnest area often occurs in surface contacted with punch head, while severe side wall wrinkling is taken place in the unsupported area and flange wrinkling happens in the flange area.

Generally, fracture can be predicted by: (1) strain based criteria, e.g. forming limit diagrams (FLDs) and maximum part thinning; (2) stress based criteria, e.g. forming limit stress diagrams (FLSDs); and (3) ductile damage criteria, e.g. the Cockcroft and Latham 1968 criterion.

Two types of wrinkle can occur in the parabolic parts: a) flange wrinkle and b) sidewall wrinkle. In FE simulations, both types of wrinkles can be indicated by certain geometry based rules or stress based rules. During cup forming, the flange under influence of circumferential compressive stress, the blank has a tendency to buckle and the blank's thickness increases toward the outside edge of the flange. The distance between blank holder and die is determined by the greatest (local) flange thickness. Thus there will be a small gap between blank holder and sheet for areas of smaller thickness. The parabolic shape makes this part family very susceptible to sidewall wrinkle formation. During the hydromechanical drawing of this part, large hydraulic pressures are needed to suppress these potential sidewall wrinkles. The defect criteria are defined in the next chapter.

After defects criteria were defined, the process windows of all parts have been created. The process window in terms of blank holder force and counter pressure can show the influence of two process parameters on part quality. The crack, flange wrinkle, side wall wrinkle and good part are plotted on the process window. The good process parameters are bounded to be a feasible region, so a surface of thickness as a function of internal pressure and blank holder force is constructed by using these collected data, which in terms is used to find the optimal solution.

3.6 Optimization approach to find optimal BHF and P

The parabolic cup can be formed with HMD in one step using a linear pressure and stepped constant BHF profile (Maki, T.) as shown in figure 3.11.

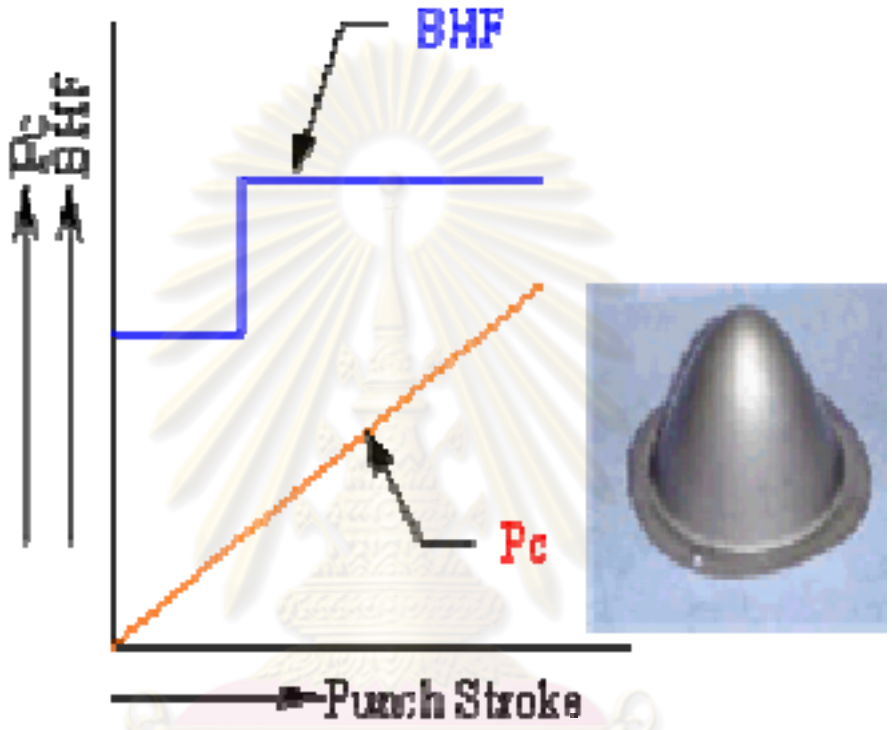

Figure 3.11 Typical BHF and Pressure curves for tapered punch (Maki, T.)

Determining of optimal process parameters in hydroforming process is key, however, it is difficult to do in a shop floor. FEM simulation coupled with optimization technique can be used to find them. However, this technique is time consuming due to the CPU-time of non-linear finite element problem and numerous samplings to identify the optimal constant BHF and linear pressure. This procedure is shown in figure 3.12.

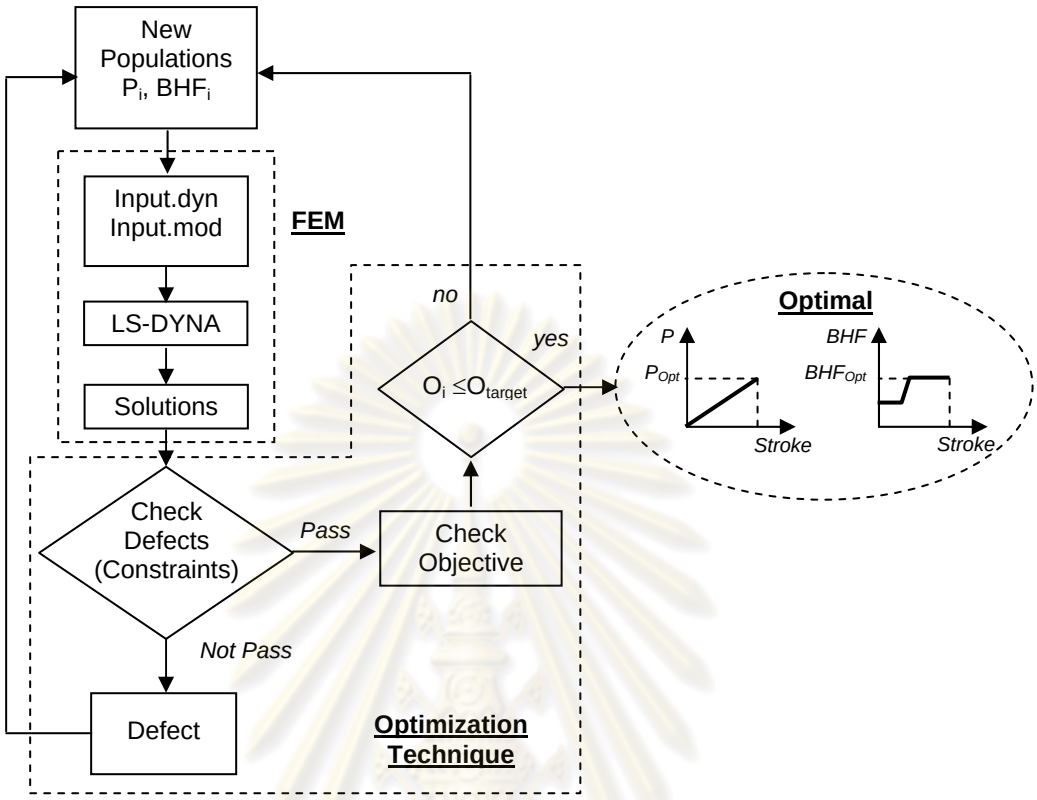

Figure 3.12 Normal procedure of optimization with FEM

Response surface methodology (RSM) is a method for constructing global approximations of valued objective and constraint functions based on functional evaluations at various points in the design space. Many researchers have applied RSM to simulation models in computational mechanics field. Roux, Stander et al. 1998 discussed experimental design techniques and the regression equations for structural optimization.

RSM combined with stochastic finite elements were used by Kleiber, Rojek et al. 2002 for reliability assessment in metal forming. Huang, Lo et al. 2006 found optimal punch nose radius for forming of a round cup to minimize part thickness variation. Wang and Lee 2005 used RSM and FEA to control strain path during forming process with space-variant blank holder force.

The feasible region data from process window or search technique are use for RSM to find the minimum thinning of the parts without crack and wrinkle.

3.7 Automatic approach to select loading paths in HMD

Many researchers discretized the time to monitor and control process parameters such as pressure, axial feed and blank holder force. The result in each monitoring step should be close to the successful target results. This method requires a computer program to manage and adjust the commercial code of non-linear finite element software. The procedure of loading paths control is shown in figure 3.13.

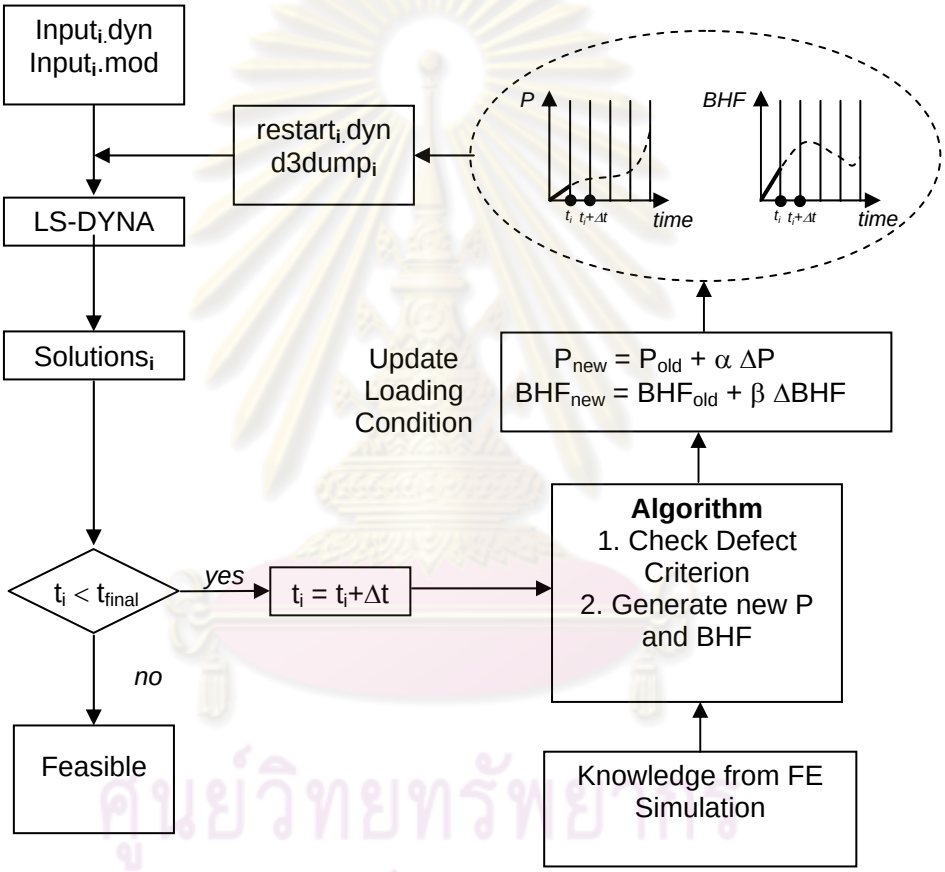

Figure 3.13 Procedure of control loading path with simulation

However, controlling the process parameters to get the required solutions needs knowledge of effect of that parameters on the part quality. This can be done by producing the process window related in terms of blank holder force and punch stroke and in terms of pressure and punch stroke.

Determination of feasible loading paths needs "a part quality trajectory" to trace by adjusting loading paths incrementally. The favorable techniques to determine loading paths are a feedback control, adaptive simulation and fuzzy logic.

Due to the optimization process in this study is a repeated calculation process, if the modification of the design variables, the start of the finite element simulation and the calculation of cost function gradient were manipulated by hand, it would waste a lot of time and would be inefficient. Conveniently, LS-DYNA can be run as a command in the DOS operation system, so that the LS-DYNA process simulation and the related calculation programs generated with Compaq Visual FORTRAN 6.0 could be integrated in this study as a batch or a script file for DOS to fulfill the optimization process. The optimization process could then be executed by setting the related parameters in the input file and by launching the batch file. This methodology was used in by Fann and Hsiao 2003. However, they applied Visual C++ instead of Compaq Visual FORTRAN 6.0.

Methodologies of optimum loading paths for general parts without process windows are challenge. Therefore, this research aims to determine feasible loading paths of pressure and blank holder force in hydromechanical deep drawing process of parabolic cups family.

Choi and Koc et al. 2007 and Ray, Mac Donald 2004 applied fuzzy logic to determine loading paths of round cup and T-branch in warm hydroforming and tube hydroforming. The fuzzy logic starts by checking the defects are occurring during the process or not? And then, what types of defects are on the part. The next information that fuzzy logic ask is what parameters make that defects on and they need to be increased or reduced or maintained these values. If they need to be increased or reduced, how much of the value are for eliminating the defects. Choi and Koc et al. 2007 and Ray, Mac Donald 2004 adjusted the parameters according the level of defects by using linear extrapolation for pressure and BHF. This method is appropriate for unknown profiles but a lot of monitoring steps need to capture the feasible profiles.

CHAPTER IV

INVESTIGATION ON FORMING OF PARABOLIC PARTS WITH HYDROMECHANICAL DEEP DRAWING PROCESS

Parabolic shaped cups are commonly used in spot lights and car headlamps as light reflectors. Due to their particularly pointy and tapered shape, if poorly designed, the cupping process can easily form part wrinkles or fractures. Therefore, these parabolic cups often require at least six forming steps using conventional deep drawing process to produce good cups, see in figure 4.1. Interestingly, hydromechanical deep drawing (HMD), a relatively new forming process where the solid die cavity is replaced by highly-pressurized water, can potentially form these cups using just a single step with improved part dimensional accuracy (Zhang, Lang et al. 2000).

When applying HMD, the key process parameters affecting part quality are blank holder force and counter pressure. Excessive blank holder force and counter pressure can lead to fracture. On the other hand, insufficient blank holder force and counter pressure can lead to wrinkle. Therefore, proper blank holder force and proper counter pressure are very important in carrying out the forming process successfully. Investigation of these two proper process parameters is the goal of this chapter.

ศูนย์วิทยทรัพยากร
จุฬาลงกรณ์มหาวิทยาลัย

4.1 Defect Criteria

In the HMD process of parabolic cup, a large area of blank surface is unsupported. The blank is initially bulged, and becomes in contact with punch. As the punch is descending downwards, both pressure and blank holder force will keep the blank stretching for successfully forming, figure 4.2

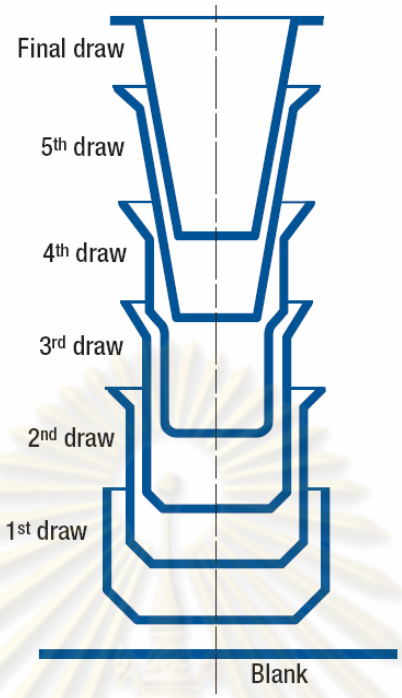

Figure 4.1 The schematic to form tapered shape such as a parabolic cup in conventional process

The main defects of the HMD process of parabolic parts are cracks and wrinkles. The thinnest area often occurs in surface contacted with punch head, while severe side wall wrinkling is taken place in the unsupported area and flange wrinkling happens in the flange area. This following section are aimmed to define the defects on the parabolic cups.

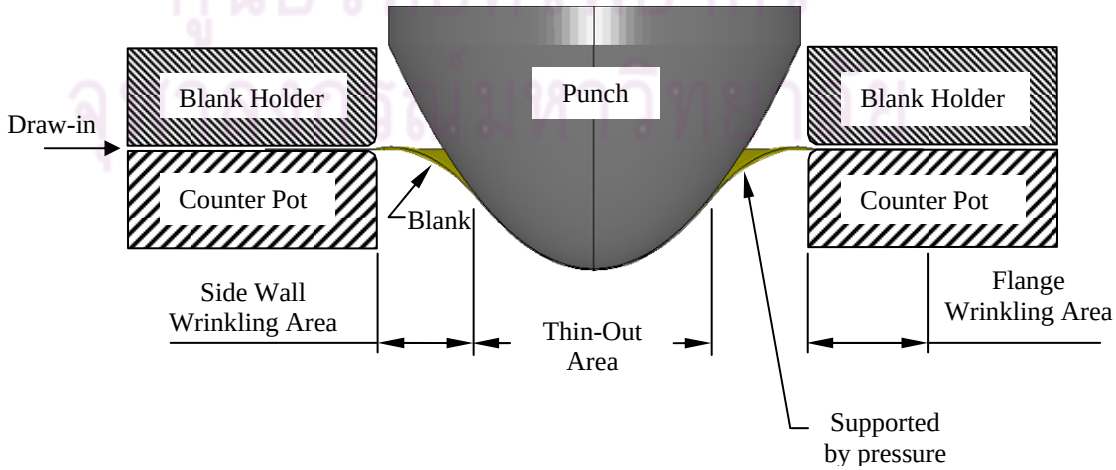

Figure 4.2 Schematic of the HMD process of parabolic cup

4.1.1 Crack criterion

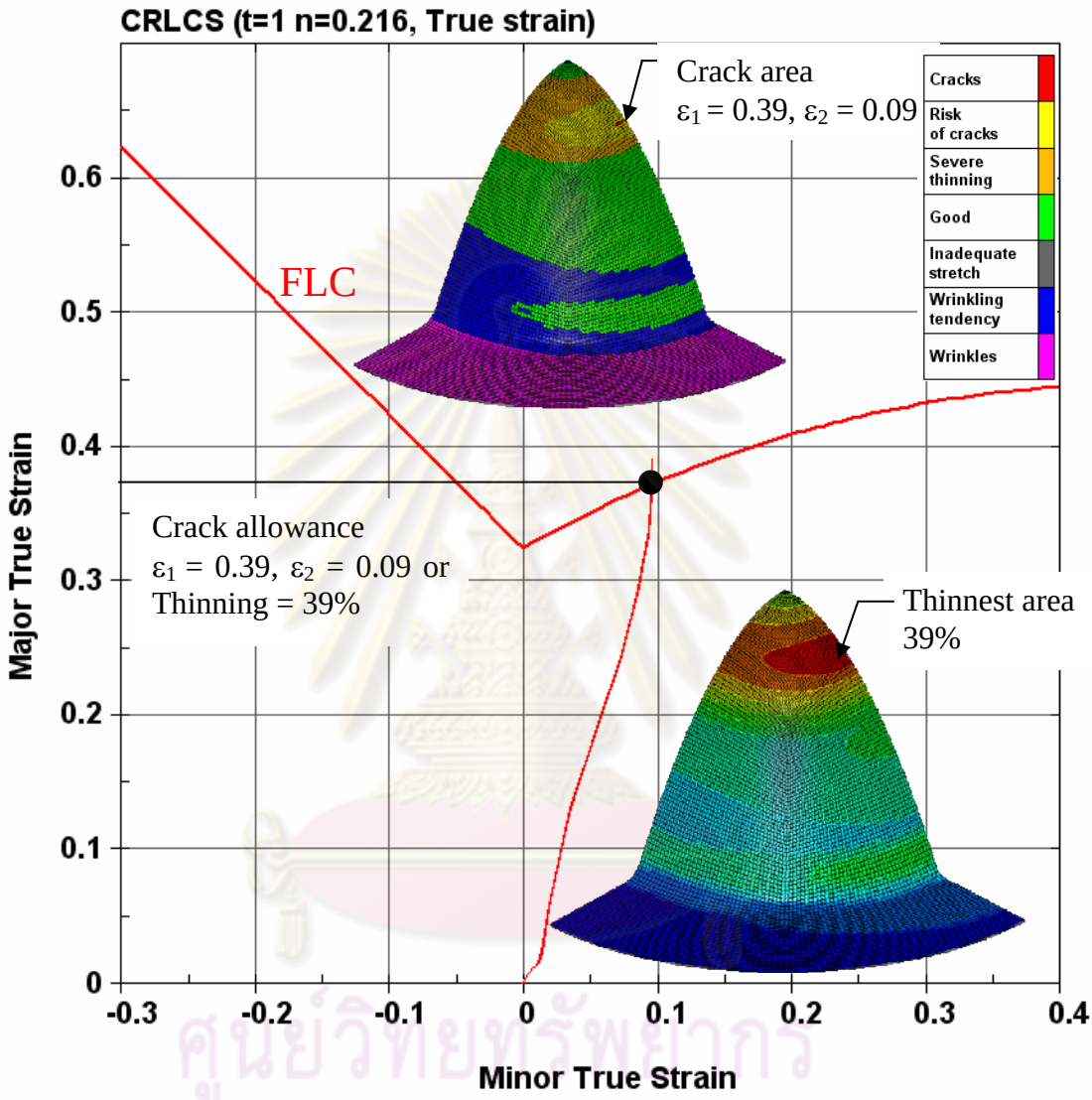

Figure 4.3 Comparison between part formability and thinning in SPCC parabolic cup of HMD process

Generally, fracture can be predicted by: (1) strain based criteria, e.g. forming limit diagrams (FLDs) (Obermeyer and Majlessi 1998) and maximum part thinning (Thomas 1999); (2) stress based criteria, e.g. forming limit stress diagrams (FLSDs) (Haddad, Arrieux et al. 2000); and (3) ductile damage criteria, e.g. the Cockcroft and Latham 1968 criterion. Thinning of the part wall is commonly used in industry to

indicate probability of fracture (Sheng, Suwat Jirathearanat et al. 2004). Therefore, in the present study, we also selected wall thinning as a fracture criterion. However, this is an approximate criterion because the critical maximum thinning is known to be affected by strain paths. From many hydromechanical deep drawing simulations of SPCC parabolic parts, the minimum major and minor strains at the crack site of the parts are around 0.39 and 0.09, respectively, which corresponds to part thinning of 39%. The location of crack site is in the punch nose area and it is found to be the same location as the thinnest area of parts as well, 39% as shown in figure 4.3. For this SPCC parabolic part, therefore, the thinning criterion limit ($Thin_{Lim}$) was chosen to be around 40% as it corresponded with the fracture of the part predicted by the forming limit curve.

4.1.2 Wrinkles criteria

Two types of wrinkle can occur in the parabolic parts: a) flange wrinkle and b) sidewall wrinkle. In FE simulations, both types of wrinkles can be indicated by certain geometry based rules or stress based rules. Owning to its simplicity, a geometry based method was used to indicate and quantify the wrinkles in this work.

4.1.2.1 Flange wrinkle

During cup forming, the flange under the influence of the compressive stress, the blank has a tendency to buckle and the blank's thickness increases toward the outside edge of the flange. The distance between blank holder and die is determined by the greatest (local) flange thickness. Thus there will be a small gap between blank holder and sheet for areas of smaller thickness.

The flange wrinkle amplitude (FAM) is measured from the gap distance between blank holder surface and counter pot addendum surface as shown in figure 4.4 (Sheng, Suwat Jirathearanat et al. 2004). To determine the critical FAM value, several

forming simulations were conducted with various fixed gap distance. The gaps were varied from 1.00, 1.01, 1.02, 1.03, 1.04, 1.05, 1.06, 1.07 and 1.08 mm respectively. The results were shown in figure 4.5; flange wrinkle can be easily visualized on the parts if FAM is over 1.05, which agrees with Sheng, Suwat Jirathearanat et al. 2004. They used 5% of nominal sheet thickness to be flange wrinkle criteria. This critical wrinkle amplitude, however, would be different for different parts depending on the part functionality. In this parabolic part with HMD process, the flange wrinkle limit (FAM_{Lim}) was chosen to be 1.05 mm.

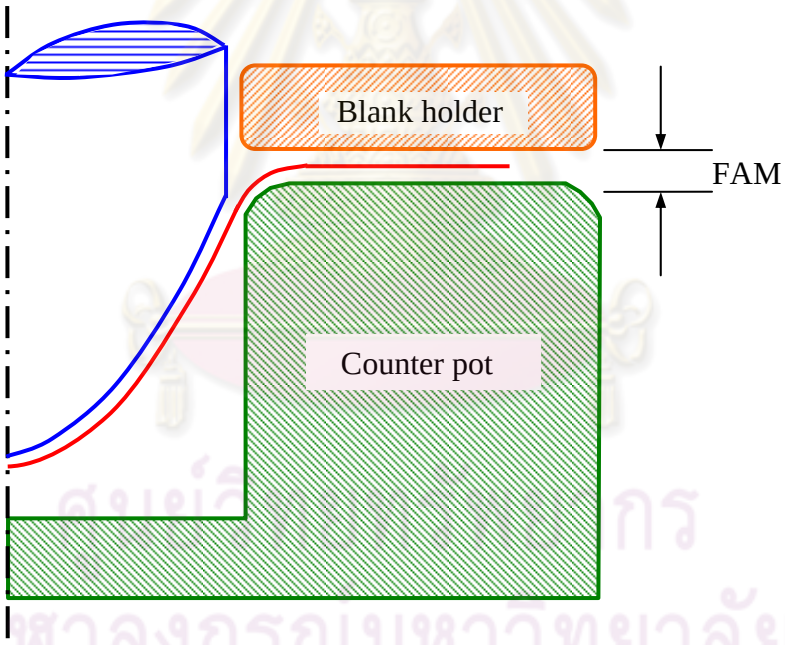

Figure 4.4 Measurement of flange wrinkling amplitude (FAM)

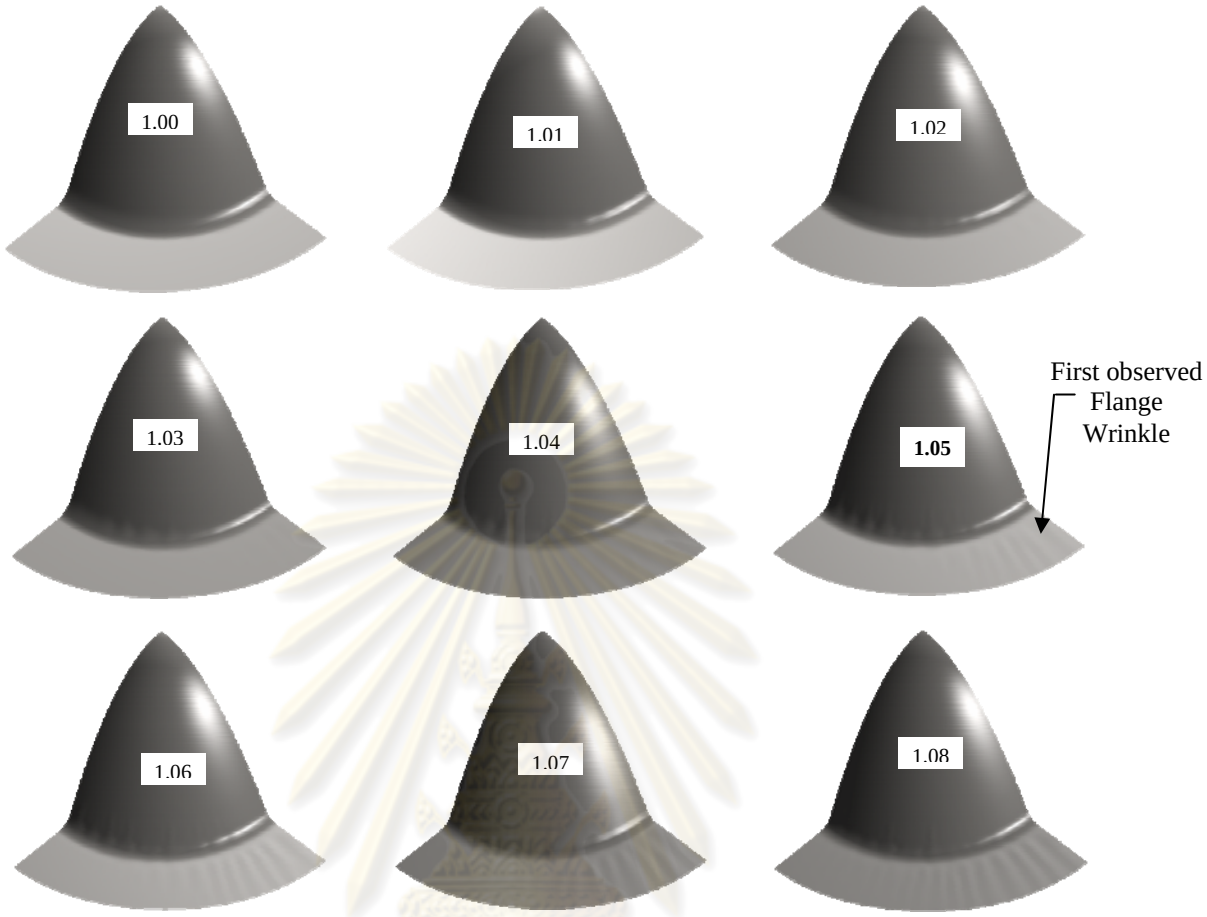

Figure 4.5 Flange wrinkling amplitude (FAM) results by varying gap

4.1.2.2 Sidewall wrinkle

The parabolic shape makes this part family very susceptible to sidewall wrinkle formation. During the hydromechanical drawing of this part, large hydraulic pressures are needed to suppress these potential sidewall wrinkles. The severity of these wrinkles can be quantified by normal distances from part wrinkle-affected nodes to the corresponding punch surfaces, which are referred to as a sidewall wrinkle parameter (SW), see figure 4.6. The part is found to be defective when SW becomes larger than 5% of initial part thickness, which is referred to as sidewall limit (SW_{Lim}). Due to the middle surface simulation model, SW_{Lim} in this study is 0.525.

Upon completion of the forming simulation, normal distances between the punch and formed part mesh are measured at every node as shown in figure 4.7. The largest distance is chosen to be the SW.

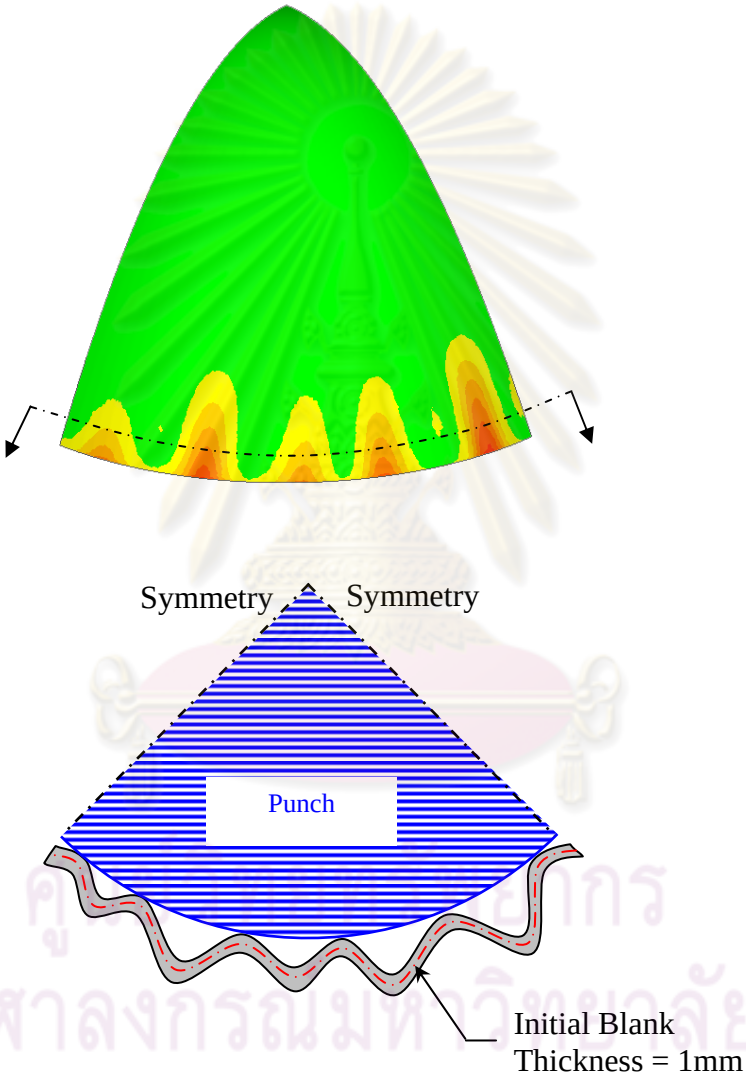

Figure 4.6 Sidewall wrinkles

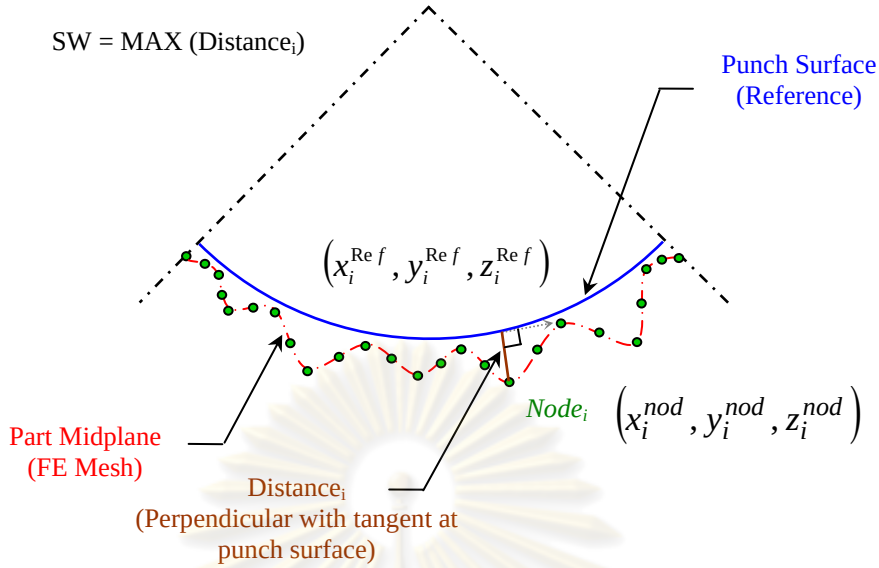

Figure 4.7 Measurement of sidewall wrinkle (SW)

4.2 Process windows of parabolic parts

The key process parameters affecting part quality are blank holder force and counter pressure. The process window represented in terms of blank holder force and counter pressure can show the influence of the two process parameters on quality of part. Process windows of parabolic parts are investigated in this section.

4.2.1 Search space of parabolic parts

The possible region of pressure (P) and blank holder force (BHF) is defined by L_i and U_i which are, respectively, the lower and upper bounds on design variables; P and BHF.

4.2.1.1 Pressure

The minimum pressure required to begin forming as shown in Eq. 4.1 (Koç 2008)

$$p_{\min} = \frac{\sigma_{yield} \times t}{r_{\min}} \tag{4.1}$$

where $p_{\min}$ = minimum pressure to begin forming (MPa), σ_{yield} = the yield strength of the blank material (MPa), t = the wall thickness of the blank (mm) and $r_{\min}$ = the minimum radius of the part (mm).

A simple formula for the maximum pressure can provide an reasonable estimate of the pressure required to burst a blank, see Eq. (4.2) (Koç 2008)

$$p_{\max} = \frac{\sigma_{UTS} \times t}{r_{\min}} \tag{4.2}$$

where $p_{\max}$ = maximum pressure to burst a blank (MPa), σ_{UTS} = the ultimate strength of the blank material (MPa).

The counter pressure radius is the minimum radius of the tooling, actually chosen to be. However, the HMD process cannot form the blank with this radius due to the pressure. Thus, the $r_{\min}$ used for the calculation can be taken from the simulation results by measuring it near the counter pressure radius as shown in figure 4.8. Therefore, the $r_{\min}$ of Part 1 is around 12 mm, Part 2 is around 16mm and Part 3 is around 18 mm.

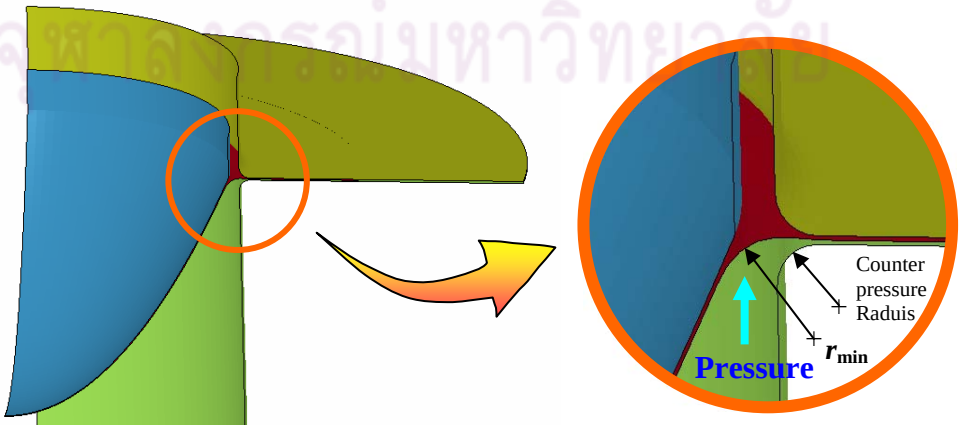

Figure 4.8 Measurement of the minimum radius of parts

4.2.1.2 Blank holder force

The minimum BHF can becalculated from the Eq. 4.3

$$MinF_{BH} = p_n \frac{\pi}{4}(D_0^2 - D_s^2) + F_{BH/pressure} + F_{BH/bulge} \quad (4.3)$$

where p_n = the blank holder pressure, D_0 = outgoing blank diameter, D_s = sealing diameter, $F_{BH/pressure}$ = the vertical force from pressure acting on the blank holder and $F_{BH/bulge}$ = the bulge force acting on the blank holder (Koç 2008).

The blank holder pressure p_n, which is the normal pressure between the sheet and the blank holder and between the sheet and the draw ring, should be high enough at least to avoid wrinkles of type A (Flange wrinkle) in the sheet guided between blank holder and draw ring. For axisymmetric components, one finds in Eq. 4.4 (Koç 2008).

$$p_n = 0.002...0.0025\left[(\beta_0 - 1)^3 + 0.5\frac{D_{punch}}{100t_0}\right]\sigma_{UTS} \quad (4.4)$$

where $\beta_0 = \frac{D_0}{D_{punch}}$, D_{punch} = punch diameter, t_0 = outgoing blank thickness, σ_{UTS} = ultimate tensile strength, σ_{yield} = yield tensile strength.

$F_{BH/pressure}$ is the vertical force acting on the blank holder in the gap between the draw ring and sheet metal. It can determine in Eq. 4.5.

$$F_{BH/pressure} = \frac{\pi}{4} p_c (D_s^2 - D_{BH}^2) \quad (4.5)$$

where p_c = working pressure, D_{BH} = inner blank holder diameter.

$F_{BH/bulge}$ is the bulge force acting on the blank holder in the area between the inner diameter of the blank holder and the contact line. It can compute in Eq. 4.6.

$$F_{BH/bulge} = \sigma D_{BH} \pi t \quad (4.6)$$

where $\sigma = \frac{p_c}{4t}(D_{BH} - D_{contact})$ and $D_{contact}$ = contact line diameter

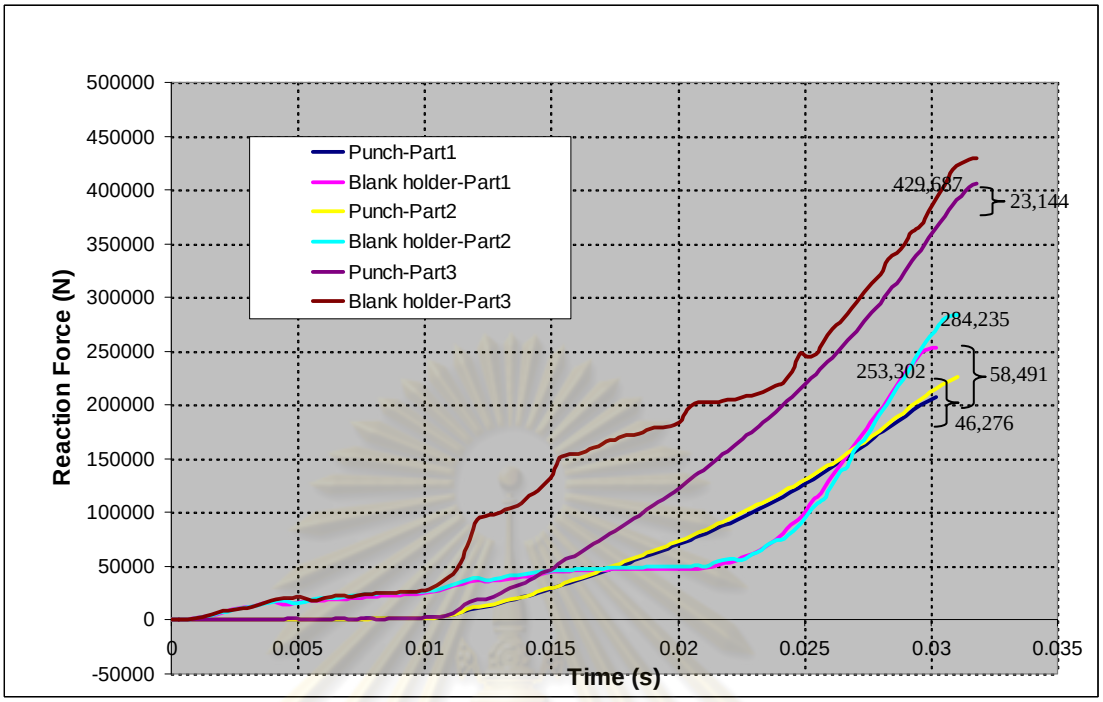

Figure 4.9 The reaction forces of punch and blank holder from fixed gap method

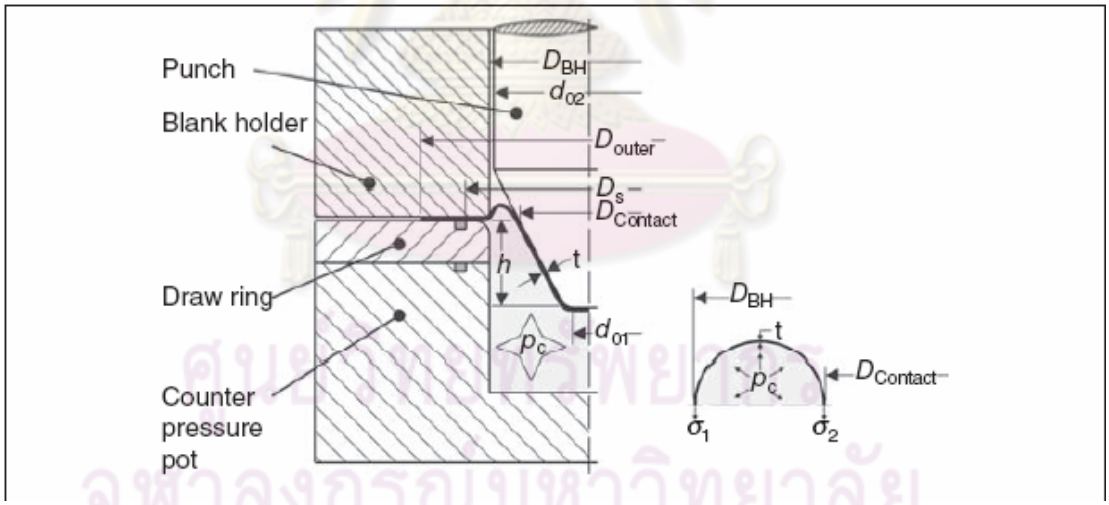

Figure 4.10 Forming a bulge with hydromechanical deep drawing components with tapered shaped walls (Koç 2008)

It is difficult to estimate the maximum blank holder force. However, in this work, it was assumed from the punch force. From a simulation of parabolic by fixed gap method, it showed that in case of a good part, the reaction forces of punch are close to

blank holder forces as shown in figure 4.9. Therefore, the maximum BHF estimated by the corresponding punch force.

The punch force F_{Punch} acting on the sheet metal for hydromechanical deep drawing may be obtained from Eq. 4.7. Figure 4.10 shows the forces acting on the sheet metal for hydromechanical deep drawing. For the hydromechanical deep drawing process, the situation regarding the stresses and strains in the sheet metal between the outer blank diameter D_{outer} and the seal (diameter D_s) is the same as with conventional deep drawing for the same blank form and size. The differences between conventional and hydromechanical deep drawing are the different stresses, strains and forces inside the sealing (diameter D_s). Here the hydraulic pressure p (counter pressure) has to be taken into account (Koç 2008).

$$F_{Punch} = F_{id} + F_{Friction/Sheet/BH} + F_{Friction/Sheet/DrawRing} + 0 + F_{Drawbead} + 0 + F_{Punch/Bulge} + F_{Counter\,Pressure} \tag{4.7}$$

The ideal force F_{id} is the punch force for the ideal condition where there are no frictions or bending forces. This force cannot be reached in reality. For axisymmetric parts, the ideal force F_{id} is needed to plastically form the sheet metal between the outer edge of the blank D_{outer} and the inner edge of the draw ring D_{DR}. This force can be calculated with the Eq. 4.8

$$F_{id} = D_{Punch}\pi t k_{fm} \ln\left(\frac{D_{Outer}}{D_{Punch}}\right) \tag{4.8}$$

The medium true stress (medium flow stress) $k_{fm} = 0.5(k_{fo} + k_{fi})$, which is the average of the flow stress at the outer edge of the blank k_{outer} and at the inner edge of the draw ring opening k_{inner} can be determined with the Eq. 4.9 (Koç 2008).

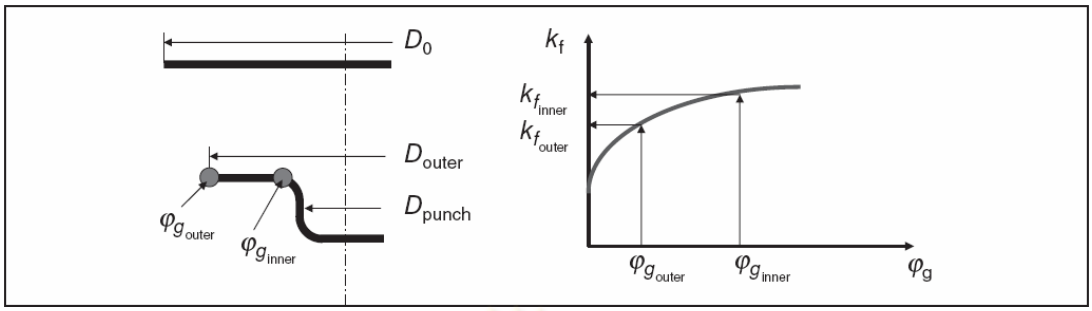

Figure 4.11 Determining the true stresses of the outer edge of the blank and of the inner edge of the draw ring (Koç 2008)

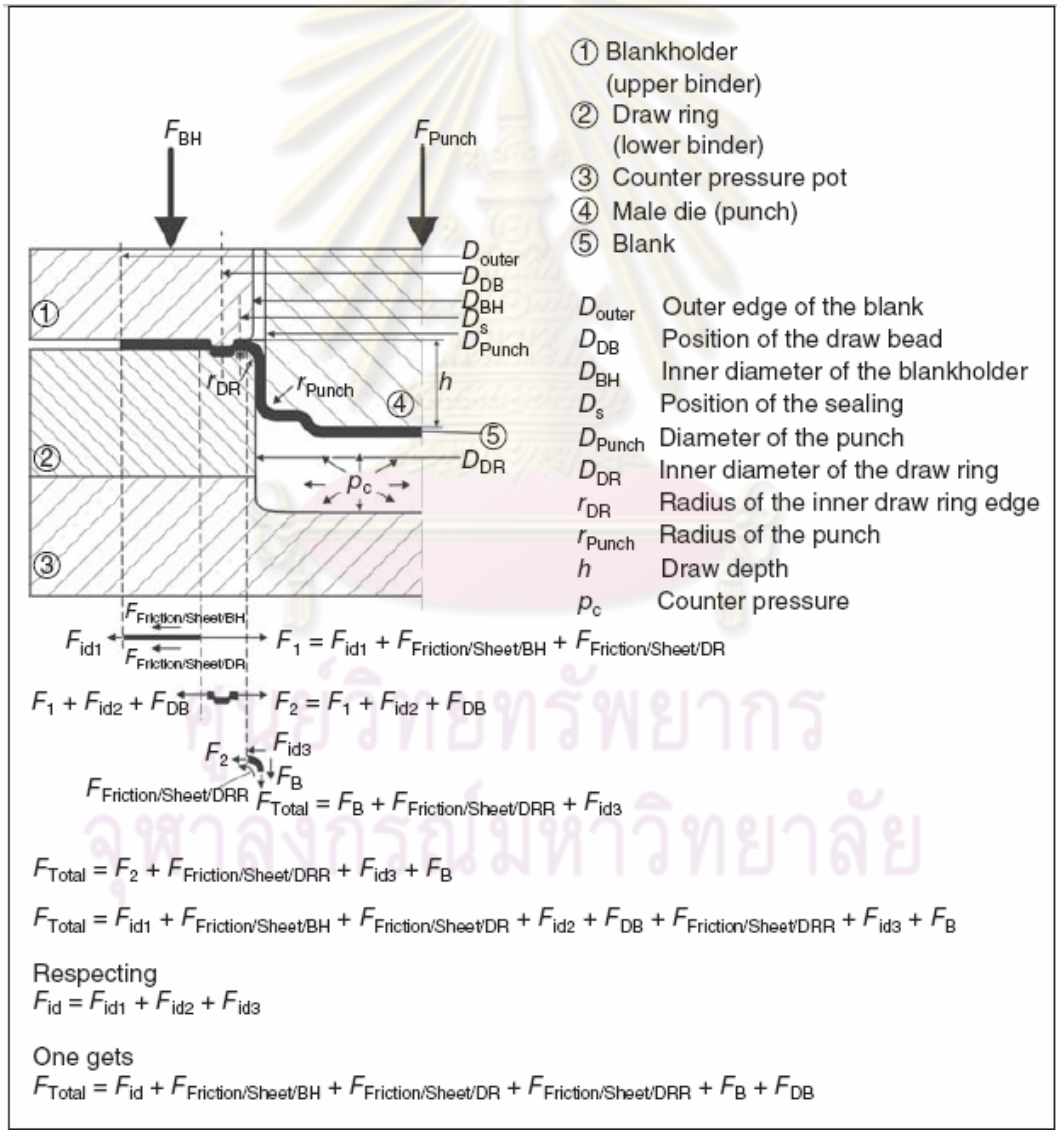

Figure 4.12 Forces acting on the sheet metal when hydromechanical deep drawing (Koç 2008)

$$\varphi_{outer} = \ln\left(\frac{D_0}{D_{outer}}\right) \tag{4.9}$$

and

$$\varphi_{ginner} = \ln\sqrt{\frac{D_0^2 + D_{punch}^2 - D_{outer}^2}{D_{Punch}^2}} \tag{4.10}$$

out of the flow curve $k_f = f(\varphi_g)$ of a sheet metal (see figure 4.11).

The friction force can calculate by Eq. 4.11

$$F_{Friction/Sheet} = \mu F_{BH} \tag{4.11}$$

μ = friction coefficient and F_{BH} = blank holder force

There is no contact between the sheet metal and the inner round draw ring edge, the friction force is zero that shown in Eq. 4.12.

$$F_{Drawbead} = 0 \tag{4.12}$$

The sheet metal is pressed by the counter pressure p_c against the punch. The outer contour of this area is the contact line $D_{contact} = f(h)$ where the sheet metal comes in contact with the punch (see figure 4.12). The vertical force acting on the punch in this area is shown in Eq. 4.13.

$$F_{Punch/Pressure} = \frac{\pi}{4} p_c D_{contact}^2 \tag{4.13}$$

The sheet metal is made to bulge upwards by the counter pressure against the travel direction of the punch. The bulge force acting on the punch is calculated in Eq. 4.14.

$$F_{Punch/Bulge} = \sigma D_{Contact} \pi t \tag{4.14}$$

The table 4.1 shows the information of parts and forces acting on the sheet metal for hydromechanical deep drawing.

ศูนย์วิทยทรัพยากร
จุฬาลงกรณ์มหาวิทยาลัย

Table 4.1 Pressure and BHF calculation results of three parts

		Part1	Part2	Part3
r_{min}		12	16	18
K	**MPa**	589.4	589.4	589.4
n		0.216	0.216	0.216
Yield Strength	**MPa**	267	267	267
Utimate Strength	**MPa**	471	471	471
Thickness	**mm**	1	1	1
Min Pressure	**MPa**	**22.25**	**16.69**	**14.83**
AVG Pressure	**MPa**	30.75	23.06	20.50
Max Pressure	**MPa**	**39.25**	**29.44**	**26.17**
Curve length	**mm**	280.868	340.112	426.85
Blank Diameter	**mm**	320	380	480
BH Diameter (cavity)	**mm**	188.886	229.09	307.46
Punch Diameter	**mm**	178.886	219.09	297.46
Contact Diameter	**mm**	178.886	219.09	297.46
Flange Outer Diameter	**mm**	285	325	440
Flange Inner Diameter	**mm**	198	240	318
Strain Outer Diameter		0.115831816	0.15634607	0.087011377
Strain Inner Diameter		0.253924979	0.296056783	0.173883278
Stress Outer	**MPa**	369.9959327	394.7597971	347.8232082
Stress Inner	**MPa**	438.3555436	453.1345061	403.929731
Stress AVG	**MPa**	404.1757382	423.9471516	375.8764696
Seal Diameter	**mm**	198.886	239.09	317.46
β		1.789	1.734	1.614
Pn	**MPa**	1.305	1.405	1.619
σ	**MPa**	76.88	57.66	51.23
Min BHF				
$F_{BH/contact\ pressure}$	**N**	93,603.31	84,750.94	00,561.92
$F_{BH/Bulge}$	**N**	45,594.72	41,474.60	9,457.57
$F_{BH/Pn}$	**N**	64,377.77	96,222.51	64,710.53
Min F_{BH}	**N**	203,575.80	222,448.05	314,730.02
Min F_{BH} Quarter	**N**	**50,893.95**	**55,612.01**	**78,682.50**
Max BHF (F_{Punch})				
F_{id}	**N**	168,456.86	170,607.61	203,307.61
$F_{friction/Sheet/BH}$	**N**	15000	15000	15000
$F_{friction/Sheet/DrawRing}$	**N**	15000	15000	15000
$F_{drawbead}$	**N**	-	-	-
$F_{Punch/Bulge}$	**N**	43,180.84	39,664.19	47,849.60
$F_{Counter\ Pressure}$	**N**	772,444.85	869,002.75	1,423,903.85
Max F_{BH}	**N**	1,014,082.56	1,109,274.55	1,705,061.07
Max F_{BH} Quarter	**N**	**253,520.64**	**277,318.64**	**426,265.27**

ศูนย์วิทยทรัพยากร
จุฬาลงกรณ์มหาวิทยาลัย

The ranges of the optimal search space of the three parts were bounded as follows:

Part1

$L_i \le P \le U_i$; 22.00 MPa ≤ P ≤ 40.00 MPa

$L_i \le BHF \le U_i$; 50,000 N ≤ BHF ≤ 260,000 N

Part2

$L_i \le P \le U_i$; 16.00 MPa ≤ P ≤ 30.00 MPa

$L_i \le BHF \le U_i$; 56,000 N ≤ BHF ≤ 280,000 N

Part3

$L_i \le P \le U_i$; 14.00 MPa ≤ P ≤ 27.00 MPa

$L_i \le BHF \le U_i$; 79,000 N ≤ BHF ≤ 430,000 N

4.2.2 Process windows

A process window (a diagram showing feasible and defective regions of all forming process conditions) was generated by separating the range of pressure and blank holder force into nine points and conducting FE analyses to investigate them. In this case, the total number of combinations between P and BHF is 81 simulations. A crack was determined by the crack criterion and plotted on to the process window with ♦ symbol. The flange wrinkle (FW) was determined by the FW criterion and plotted on to the process window with ■ symbol. The side wrinkle (SW) was determined by SW criterion and plotted on to the process window with ● symbol. All the good part forming conditions were plotted on to process window with ▲ symbol.

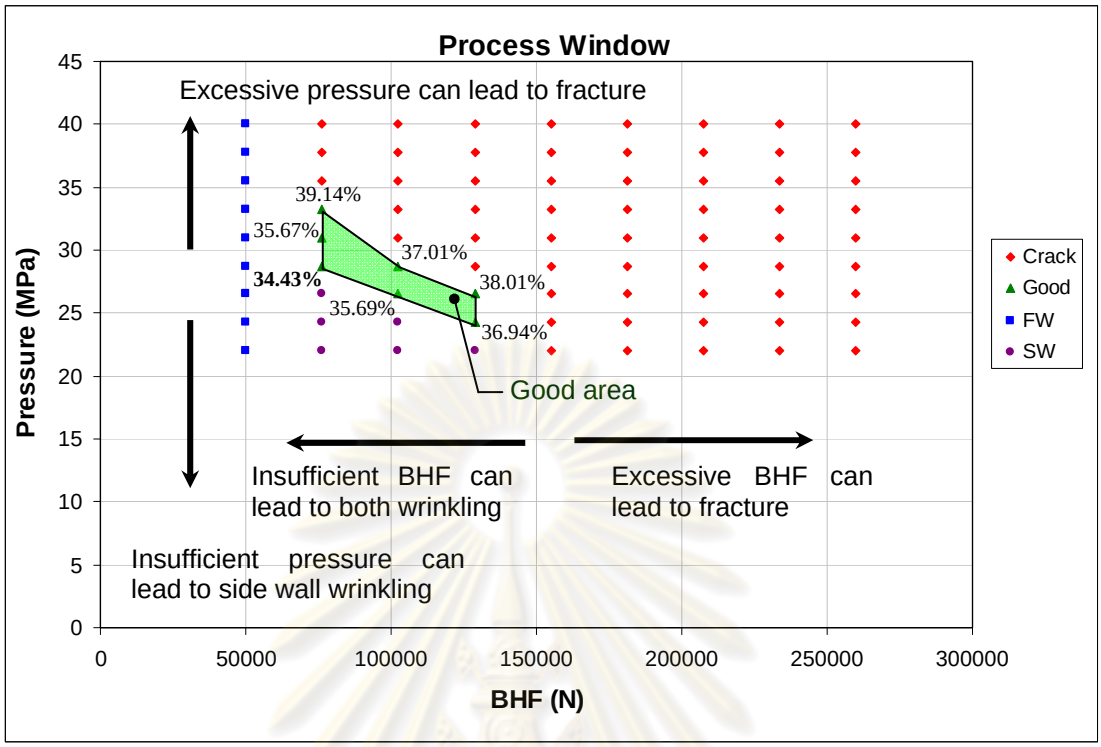

Figure 4.13 Process window of Part1

The process window was constructed in a diagram as shown in figure 4.13. The left boundary shows a flange wrinkle limit caused by insufficient blank holder force. The right boundary shows a crack limit caused by excessive blank holder force. The upper boundary is another crack limit caused by excessive pressure. The lower boundary is a sidewall wrinkle limit affected by insufficient pressure. The region bounded by all the defective limits mentioned is the successful forming area so called "feasible region". For this part, there are three ways to enter the feasible region; 1) from crack boundary, 2) from flange wrinkle boundary and 3) from side wall wrinkle boundary. Solutions accessed from the crack boundary will have thinning near the thin limit (39%). The solutions accessed from the flange wrinkle boundary will have FAM near the FAM limit (1.05). The solutions accessed from the side wall wrinkle boundary will have SW near the SW limit (0.525) and the maximum thinning less than that accessed from the thinning boundary. For example, from the process window, BHF as 76,250 N (for quarter) and pressure as 28.75 MPa would form a part with maximum thinning less than 34.43%, FAM of 1.040 mm (no flange wrinkle), SW of 0.487 mm (no side wall wrinkle). The strain paths of thinnest elements (near

the punch nose area) is in the biaxial stage which have the major strain (ε_1) as 0.324 and the minor strain (ε_2) as 0.0998. Therefore, the part will be thinned before crack. The solutions were shown in figure 4.14.

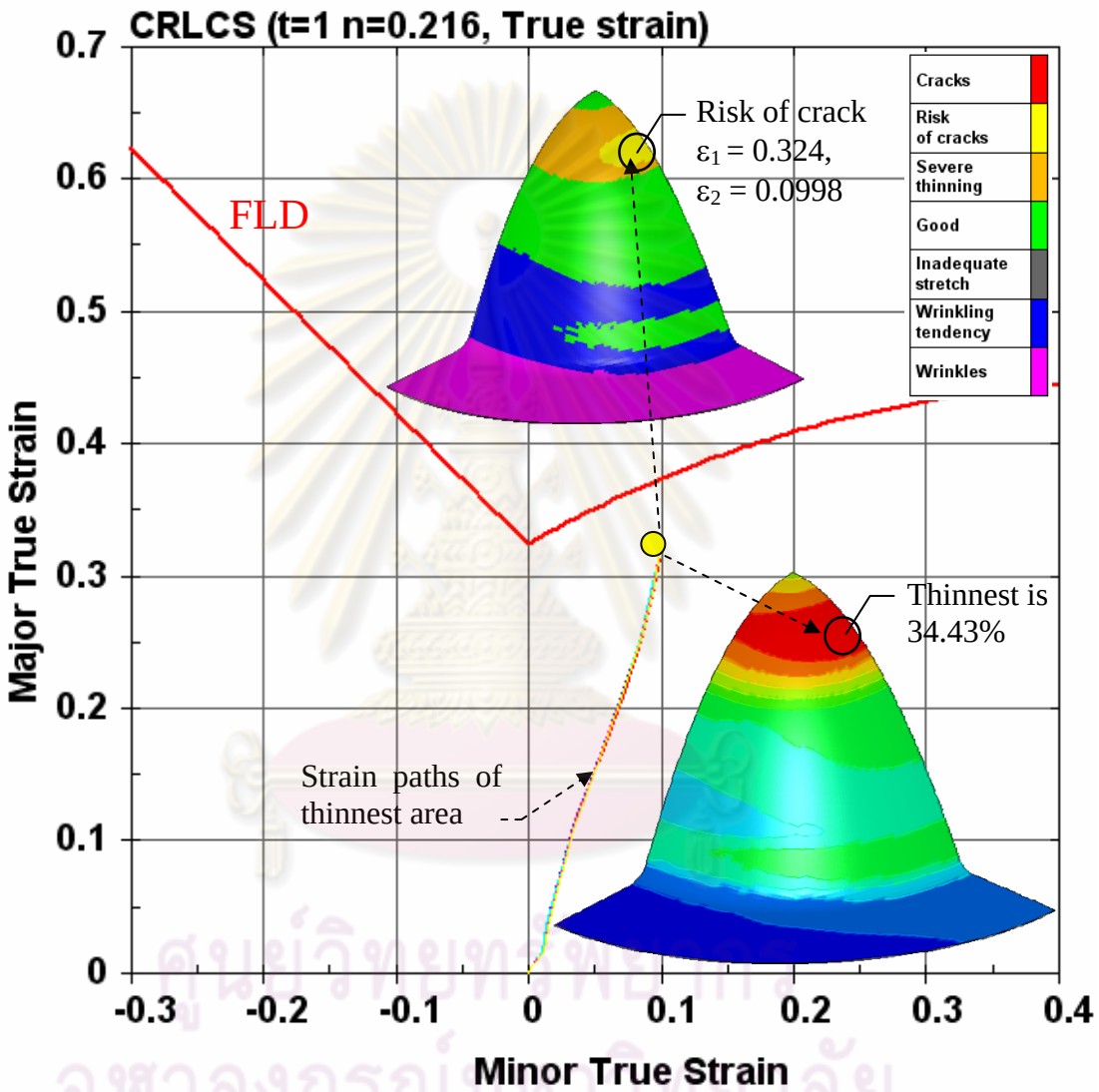

Figure 4.14 The solutions of Part1 are conducted with BHF as 76,250 N (for quarter) and pressure as 28.75 MPa

ศูนย์วิทยทรัพยากร
จุฬาลงกรณ์มหาวิทยาลัย

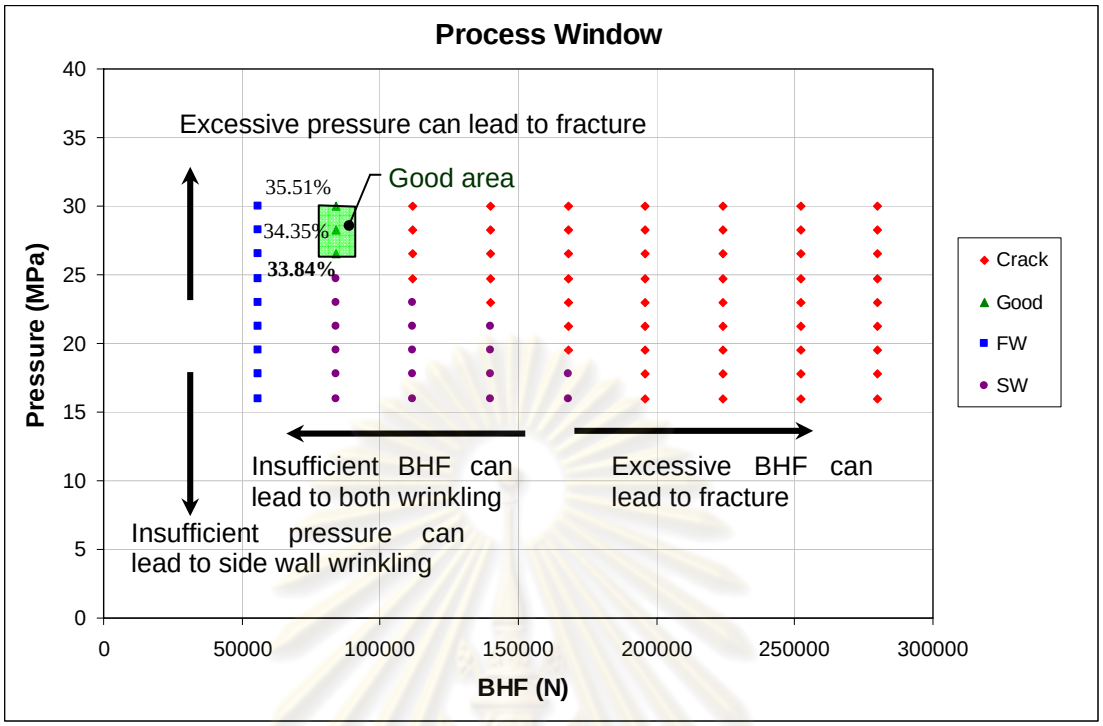

Figure 4.15 Process window of Part2

In the same procedure followed to chart the process window for HMD of Part1, Part2 and Part3 were studied as well to make their process windows, see figure 4.15 for Part2. From process window of Part 2, BHF as 84,000 N (for quarter) and pressure as 26.5 MPa conduct the maximum thinning less than the other as 33.84%. This condition gives FAM as 1.045 mm (no flange wrinkle), SW as 0.496 (no side wall wrinkle). The strain paths of thinnest elements (near the punch nose area) is in the biaxial stage which have the major strain (ε_1) as 0.33 and the minor strain (ε_2) as 0.0846. Therefore, the part will be thinned before crack. The solutions were shown in figure 4.16.

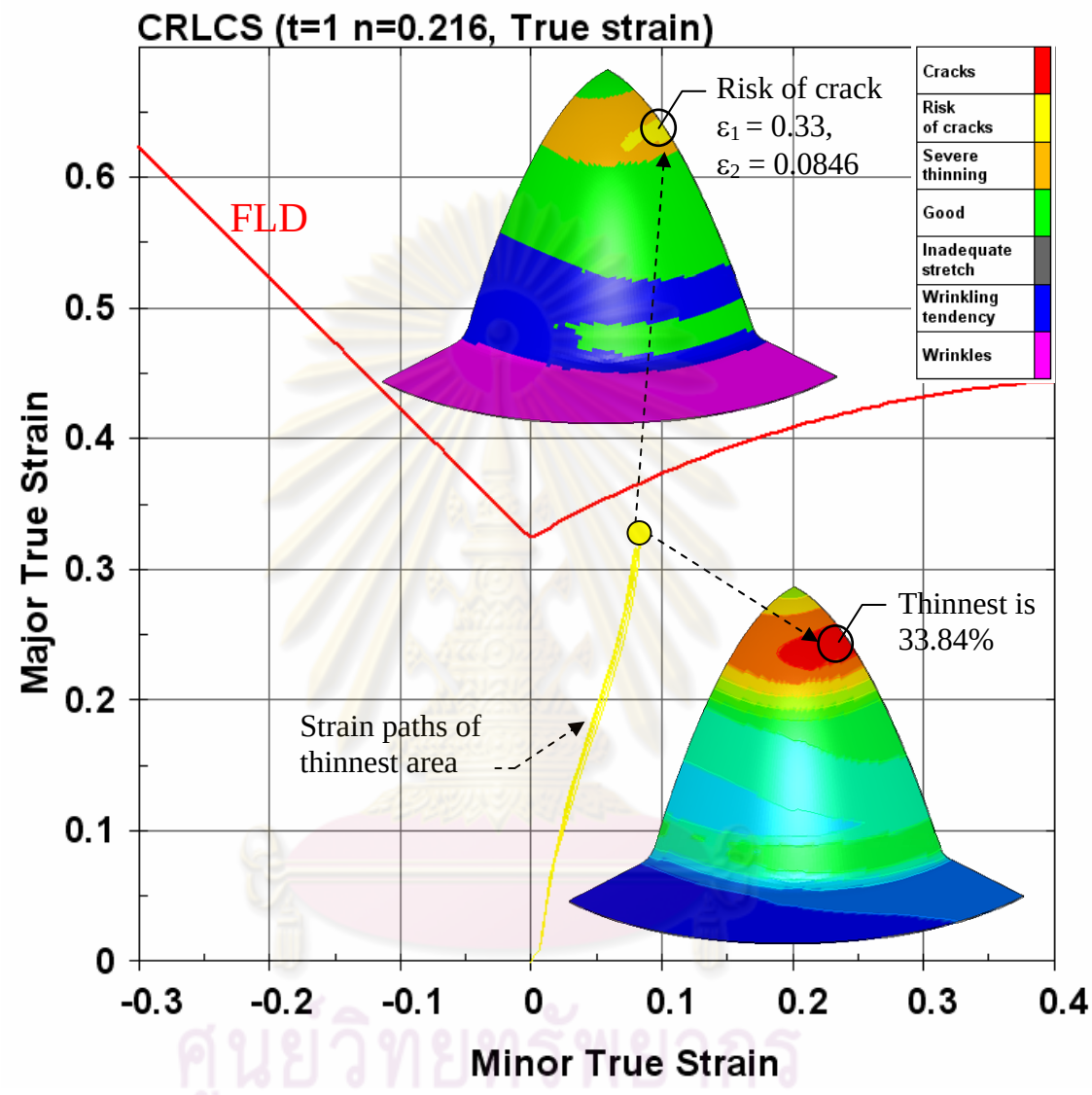

Figure 4.16 The solutions of Part2 are conducted with BHF as 84,000 N (for quarter) and pressure as 26.5 MPa

The process window for Part3 is shown in figure 4.17. From process window of Part 3, BHF as 210,625 N (for quarter) and pressure as 23.75 MPa conduct the maximum thinning less than the other as 25.64%. This condition gives FAM as 1.021 mm (no

flange wrinkle), SW as 0.491 (no side wall wrinkle). The strain paths of thinnest elements (near the punch nose area) is in the biaxial stage which have the major strain (ε_1) as 0.214 and the minor strain (ε_2) as 0.0832. Therefore, the part will be thinned before crack. The solutions were shown in figure 4.18.

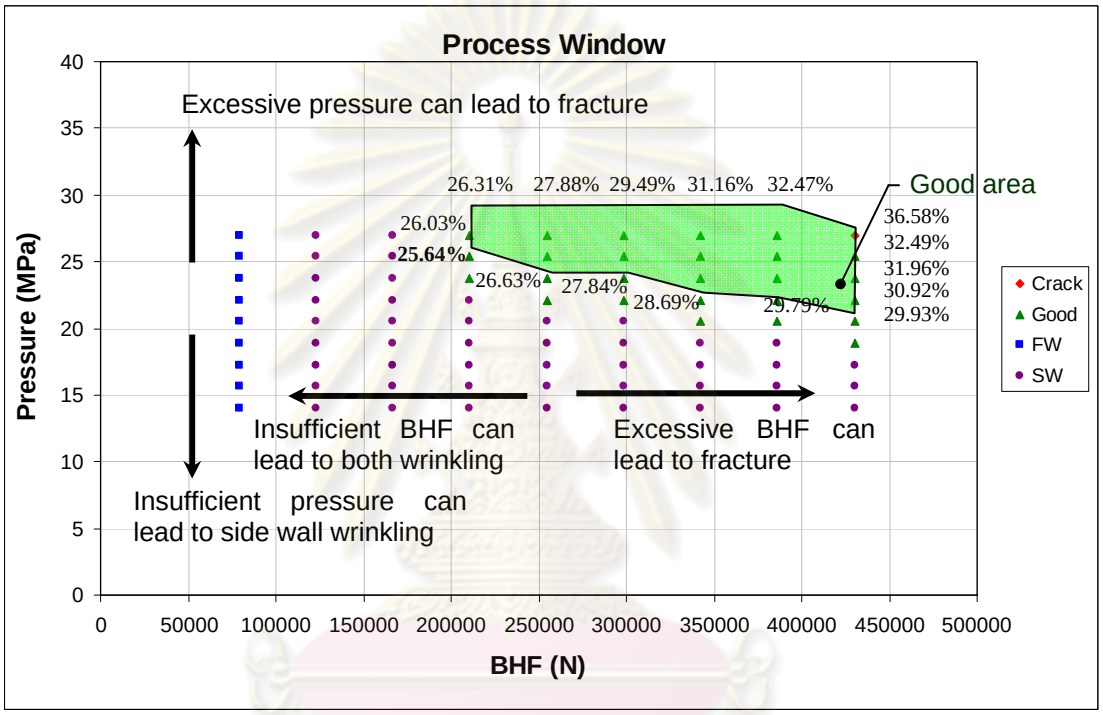

Figure 4.17 Process window of Part3

It can be seen that each part has its unique process window. However, the process windows of the three parts strongly indicate that good parts with minimum thinning can be formed using the process conditions near the sidewall wrinkling limit.

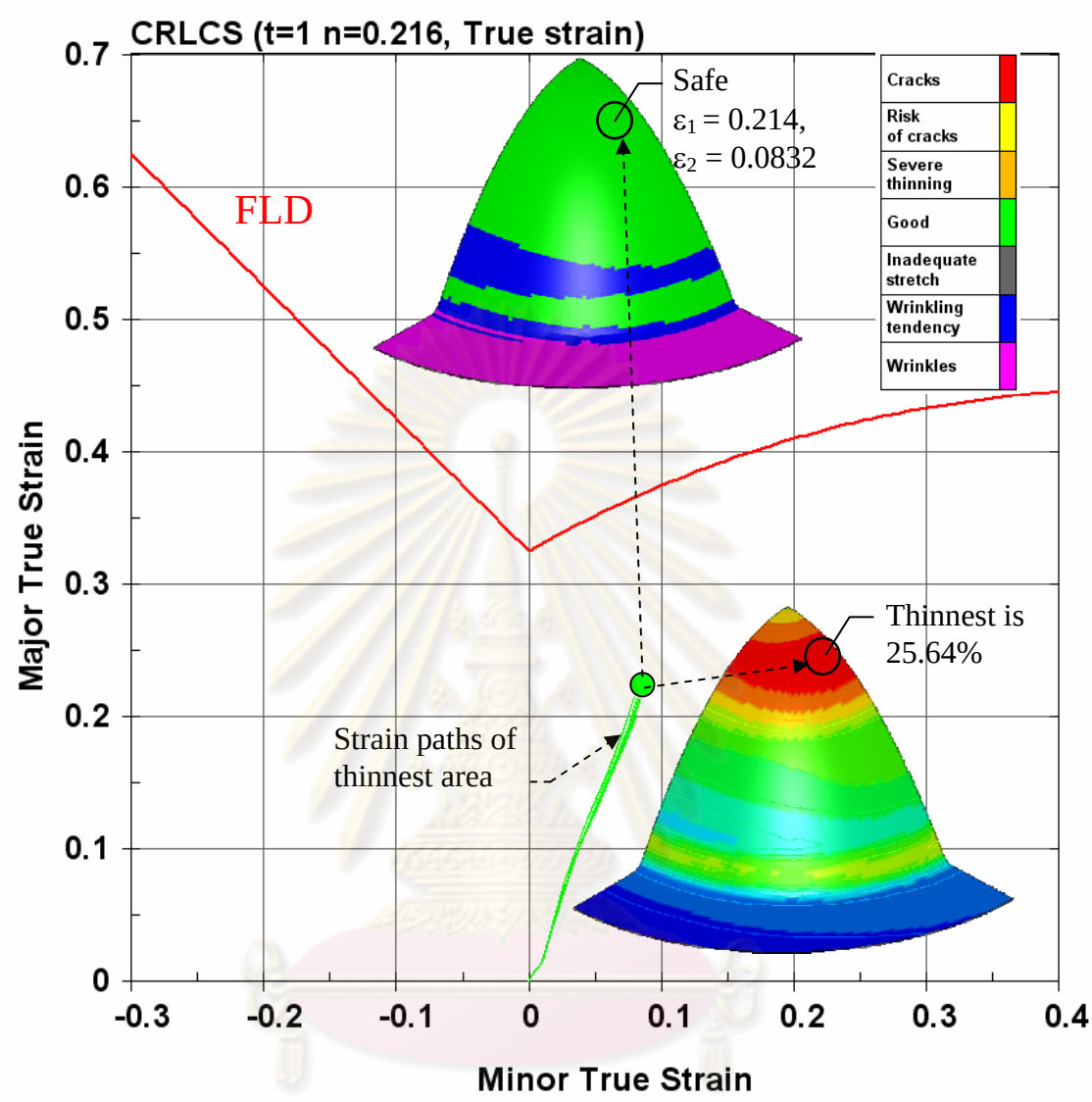

Figure 4.18 The solutions of Part3 are conducted with BHF as 210,625 N (for quarter) and pressure as 23.75 MPa

From the process windows of the three parts, the general process window of constant BHF and linear pressure can be sketched as shown in figure 4.19 and it can be concluded that;

- The constant BHF and linear pressure profile can form parabolic cups in HMD process

- Excessive BHF and pressure can lead to fracture

- Insufficient BHF and pressure can lead to wrinkle

- In general, there are three ways to access the feasible zone (shown as “Safe”); 1) Access from crack boundary, 2) Access from flange wrinkle and 3) Access from side wall wrinkle. The parts using process conditions near the side wall wrinkle boundary have thinning less than the other boundaries.

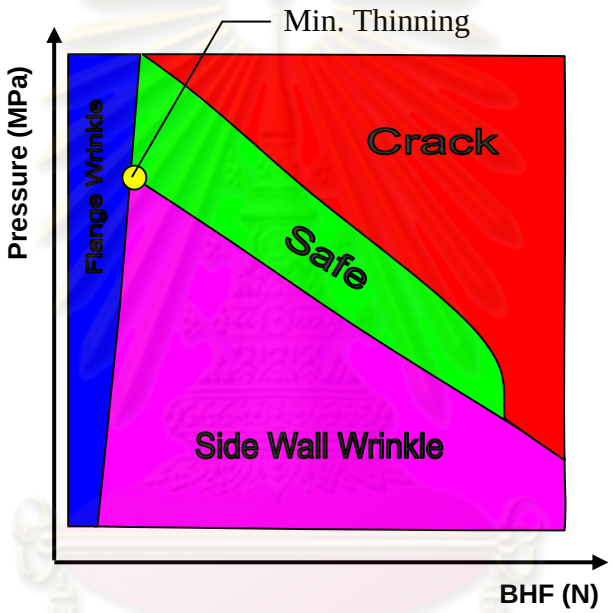

Figure 4.19 General process window of relationship between constant BHF and linear pressure and resultant part quality

The determination of process windows is expensive, time consuming and trial-and-error based iterative procedures. However, the knowledge obtained is very useful for generating a procedure to find the optimal process parameters by optimization techniques, see details in the next chapter.

4.3 Effect of process parameters compared with punch stroke on quality of parabolic parts

The relation of part quality variation on punch stroke is important for designing loading trajectory. This section aims to investigate the effect of pressure and blank holder force over the punch stroke on quality of parabolic parts.

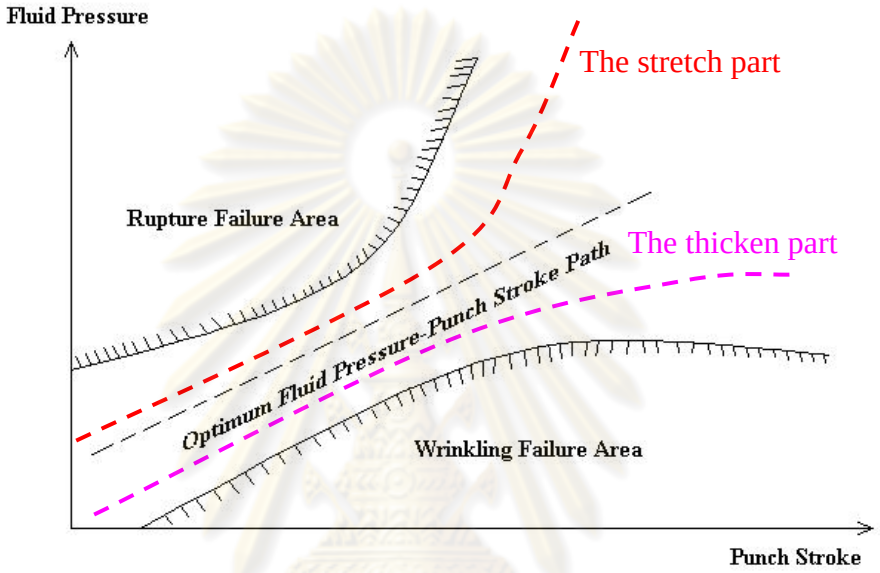

Figure 4.20 Generic curve illustrating the optimum fluid pressure-punch stroke path for the stamp hydroforming process

From literature, Lo et al. (1993) and Hsu et al. (1996) performed a series of experiments and analyses that established this fluid pressure-punch stroke path for the stamp hydroforming of metallic hemispherical cups. A generalized curve is illustrated in figure 4.20 to help demonstrate one of the goals of the numerical and experimental research; determination of the optimum fluid pressure-punch stroke path for the stamp hydroforming of sheet metals. From figure 4.20, if the red line is followed the part will be more stretched. However, if the maximum thickness is require on the parts, the pink line should be selected. Selection of only pressure profile cannot guarantee that it can form the part successfully. The blank holder parameter is another important parameter. Doege and Sommer (1983) examined the possibility of controlling the blank holder force (BHF) with respect to the punch displacement as a means of safely avoiding the onset of wrinkling or tearing, see figure 4.21. The constant BHF in

acceptable zone can form the part successfully. The use of lower BHF in the beginning of stroke and higher through the stroke increases the limit drawing ratio.

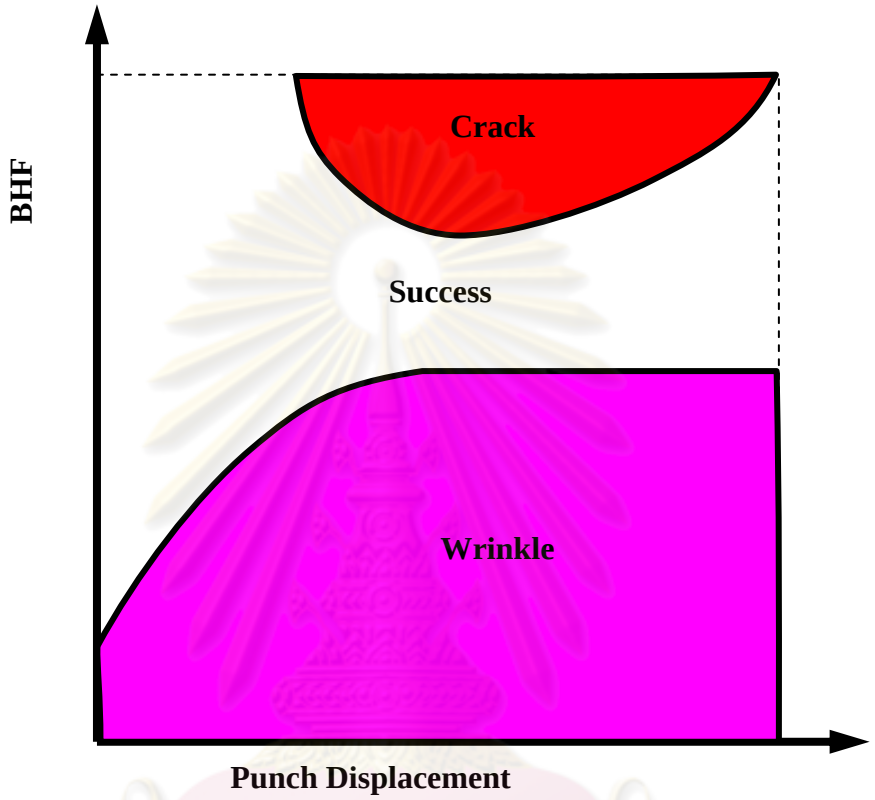

Figure 4.21 Illustration of the BHF working window for successful part drawing, Doege and Sommer (1983)

ศูนย์วิทยทรัพยากร
จุฬาลงกรณ์มหาวิทยาลัย

Due to the difficulty to indicate side wall wrinkle presence during the forming, simple visual inspection is not adequate. A specialized inspection technique, zebra lines can help to inspect this defect more effectively. In the case of side wall wrinkle onset, the zebra lines will change from straight lines to curly line as shown in figure 4.22. Clearly, as side wall wrinkles are happening to the part, the zebra lines become coiled.

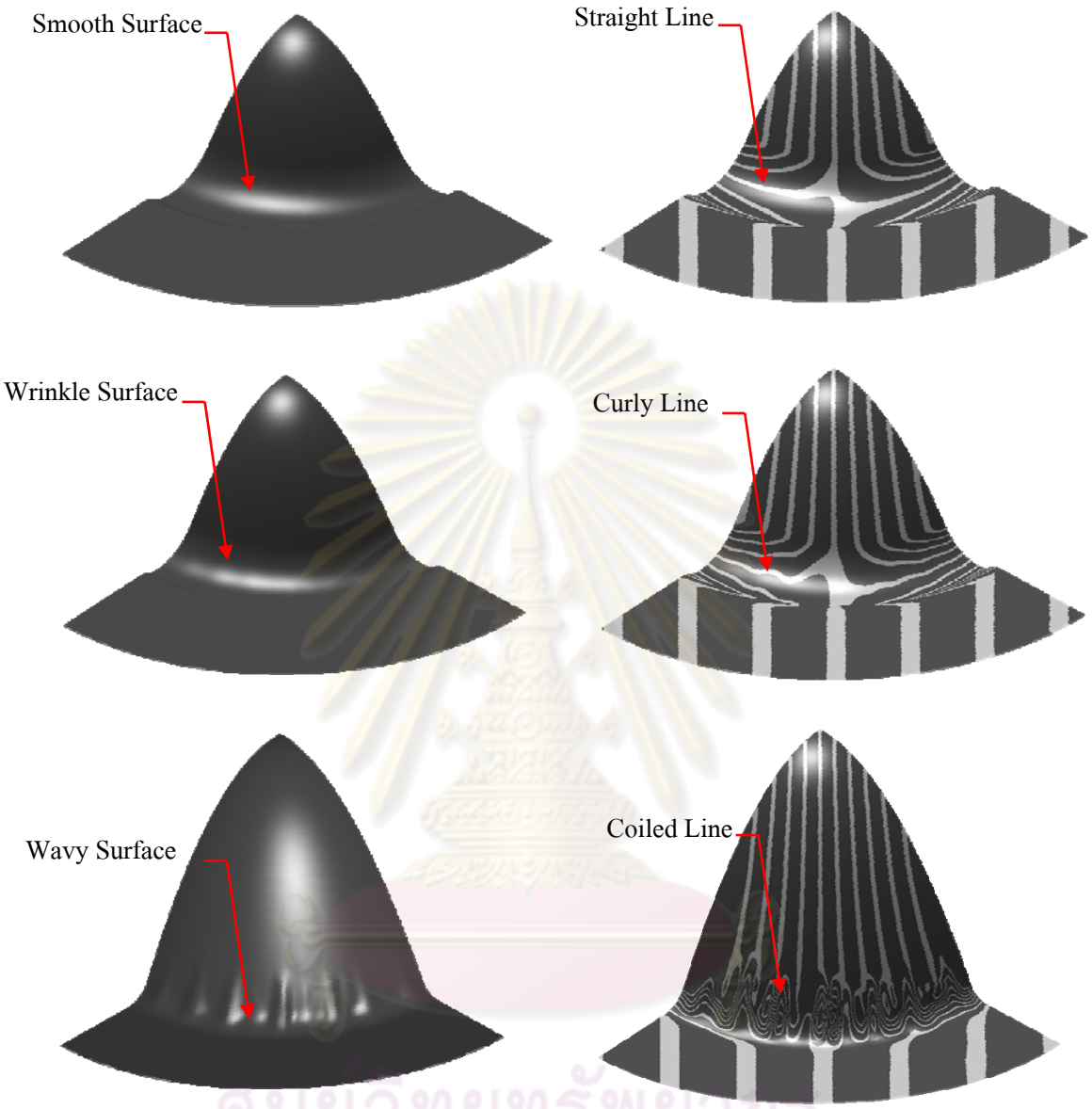

Figure 4.22 Visual inspection and zebra lines are criteria used to detect side wall wrinkle

The windows of relationship between pressure and punch stroke affecting on part quality for Part 1 are shown in figure 4.23 - 4.31, for Part 2 are shown in figure 4.32 - 4.40 and for Part 3 are shown in figure 4.41 – 4.49.

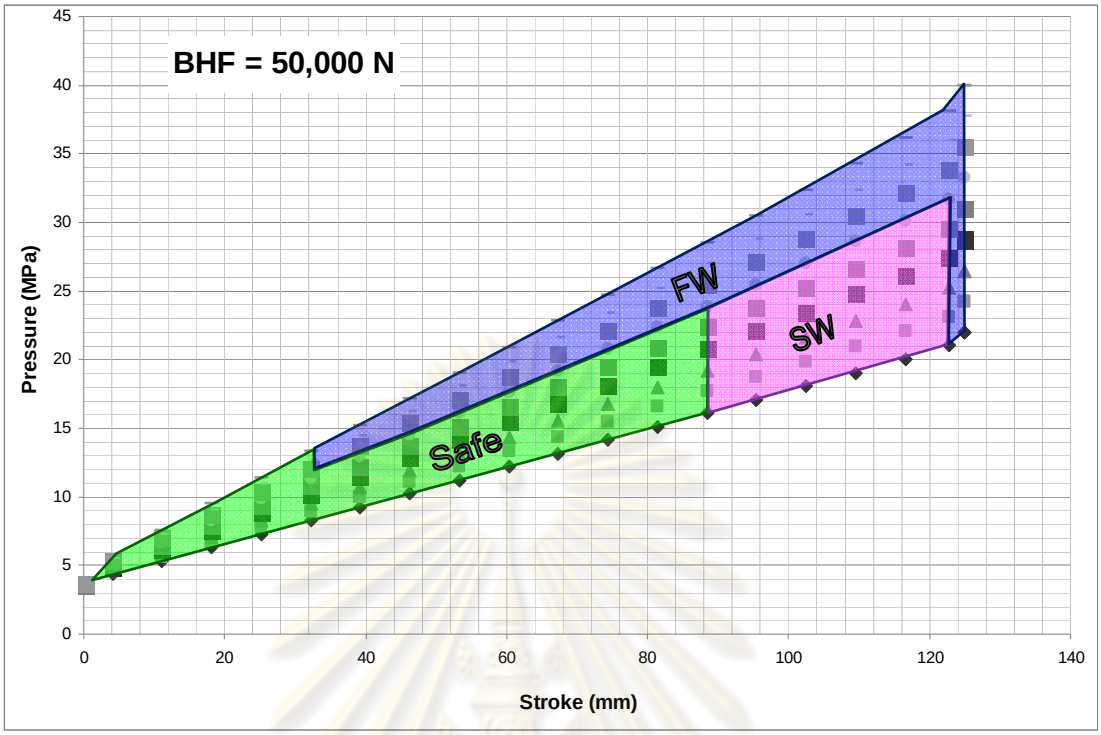

Figure 4.23 The effect of fluid pressure and punch stroke on part quality at 50,000 N of BHF for Part1

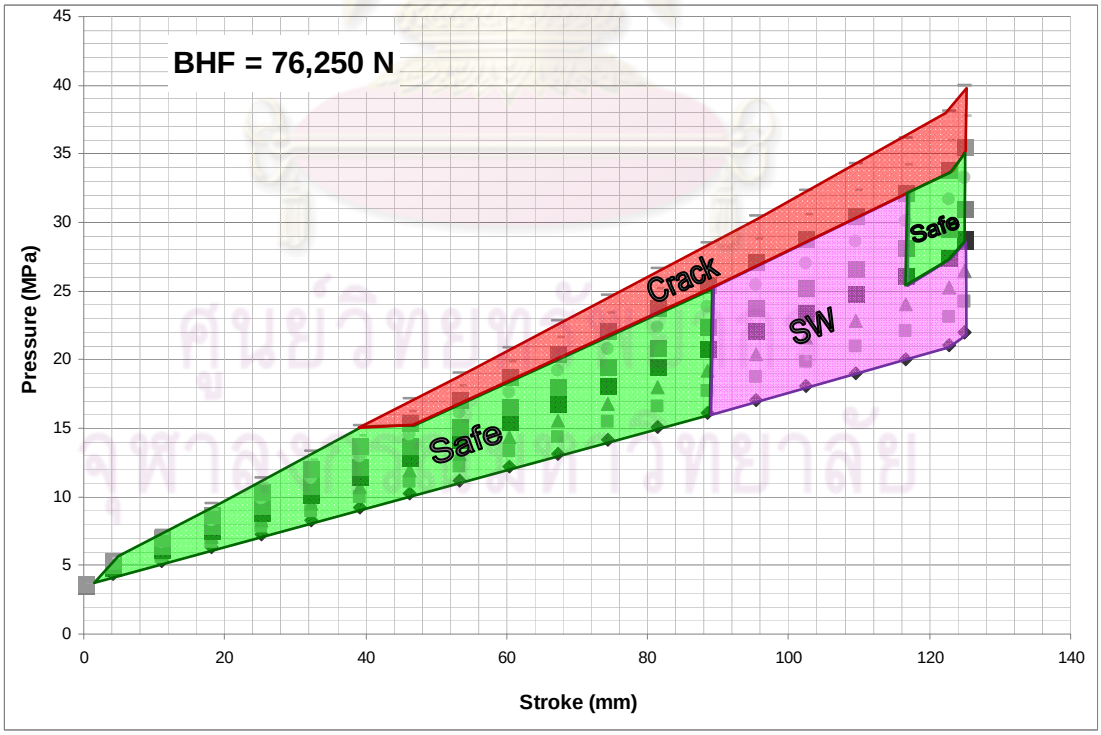

Figure 4.24 The effect of fluid pressure and punch stroke on part quality at 76,250 N of BHF for Part1

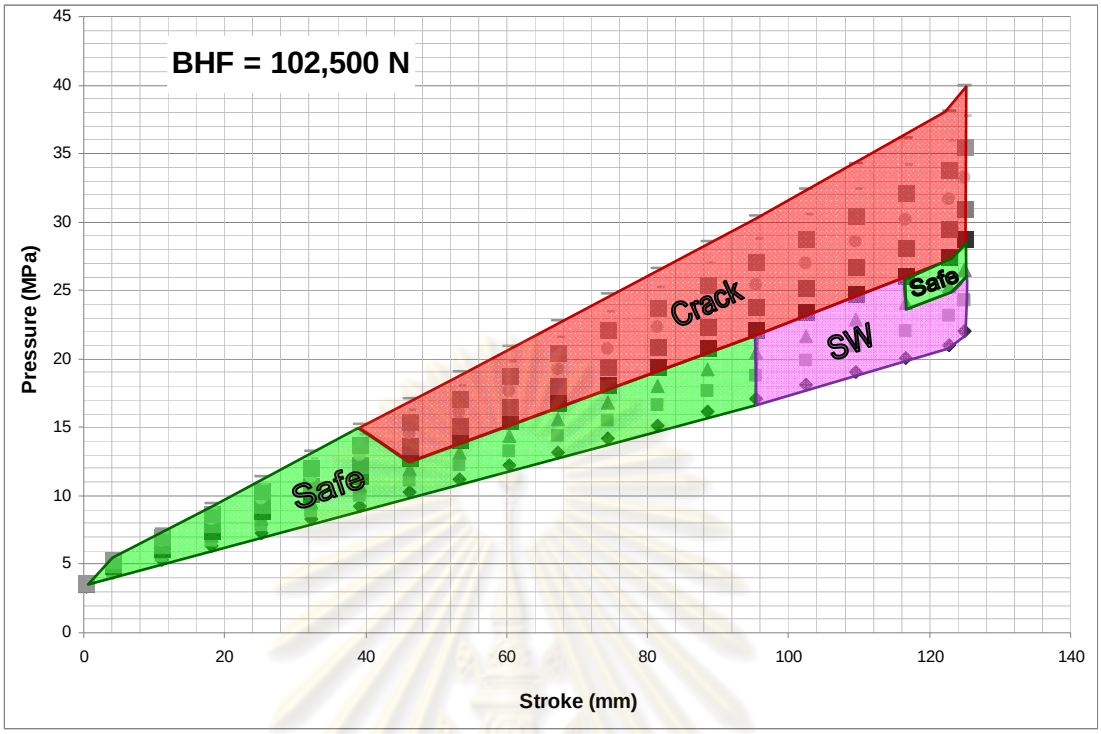

Figure 4.25 The effect of fluid pressure and punch stroke on part quality at 102,500 N of BHF for Part1

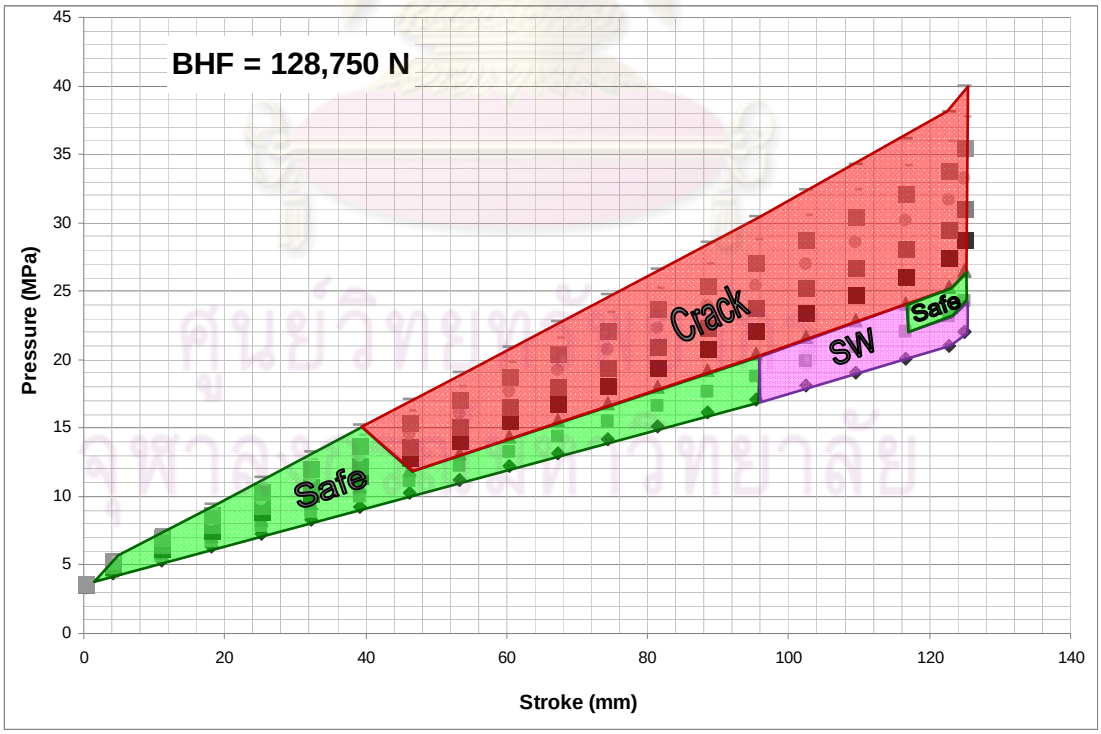

Figure 4.26 The effect of fluid pressure and punch stroke on part quality at 128,750 N of BHF for Part1

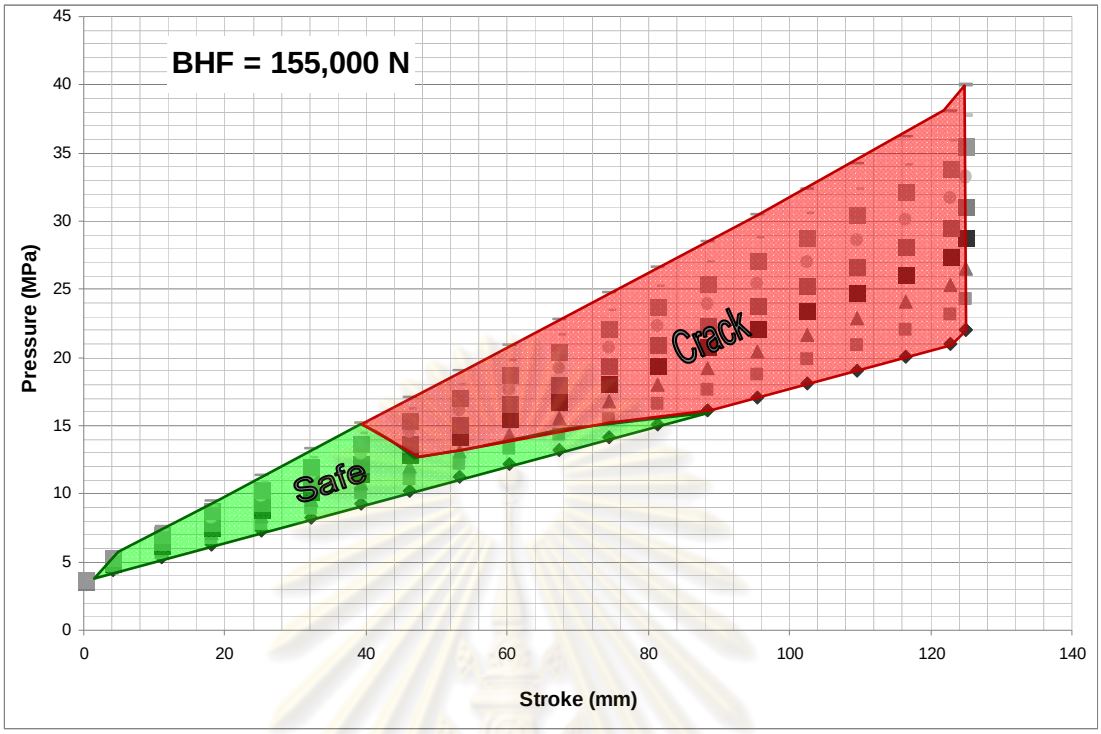

Figure 4.27 The effect of fluid pressure and punch stroke on part quality at 155,000 N of BHF for Part1

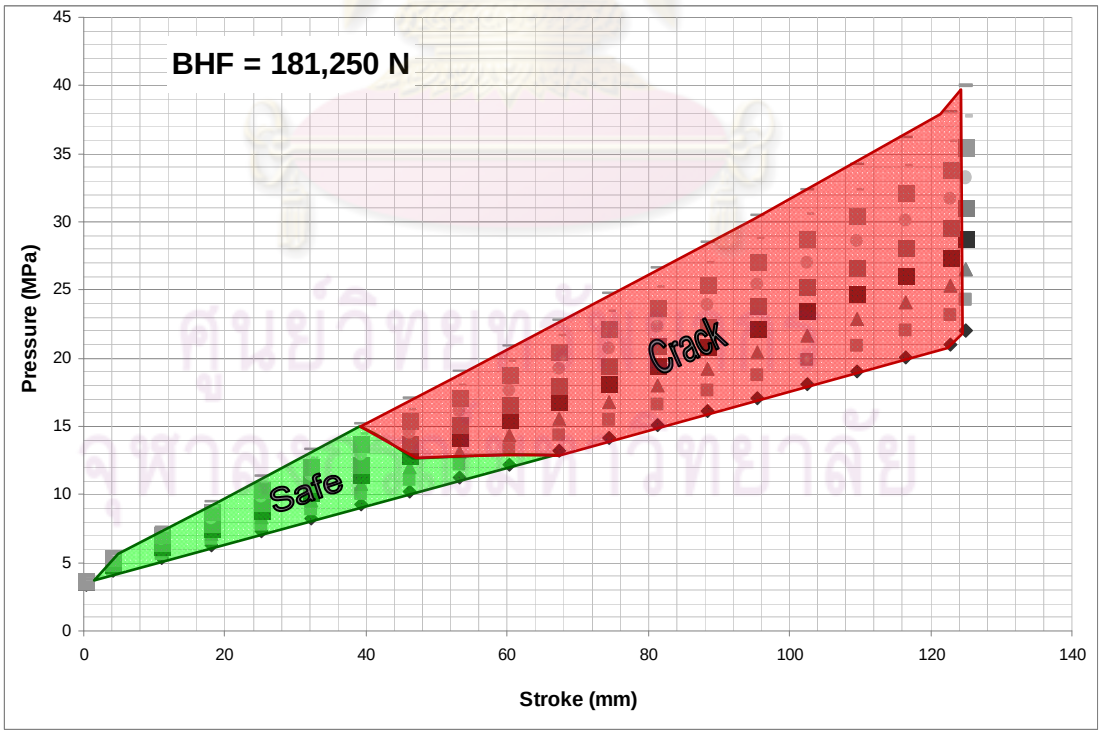

Figure 4.28 The effect of fluid pressure and punch stroke on part quality at 181,250 N of BHF for Part1

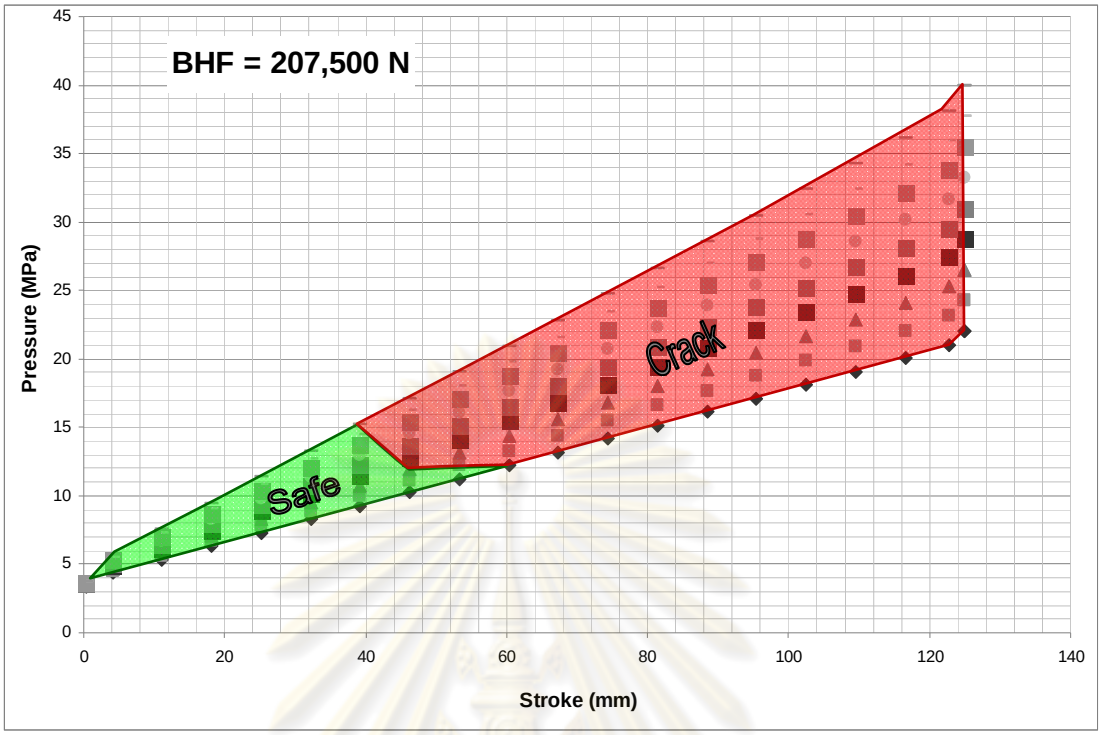

Figure 4.29 The effect of fluid pressure and punch stroke on part quality at 207,500 N of BHF for Part1

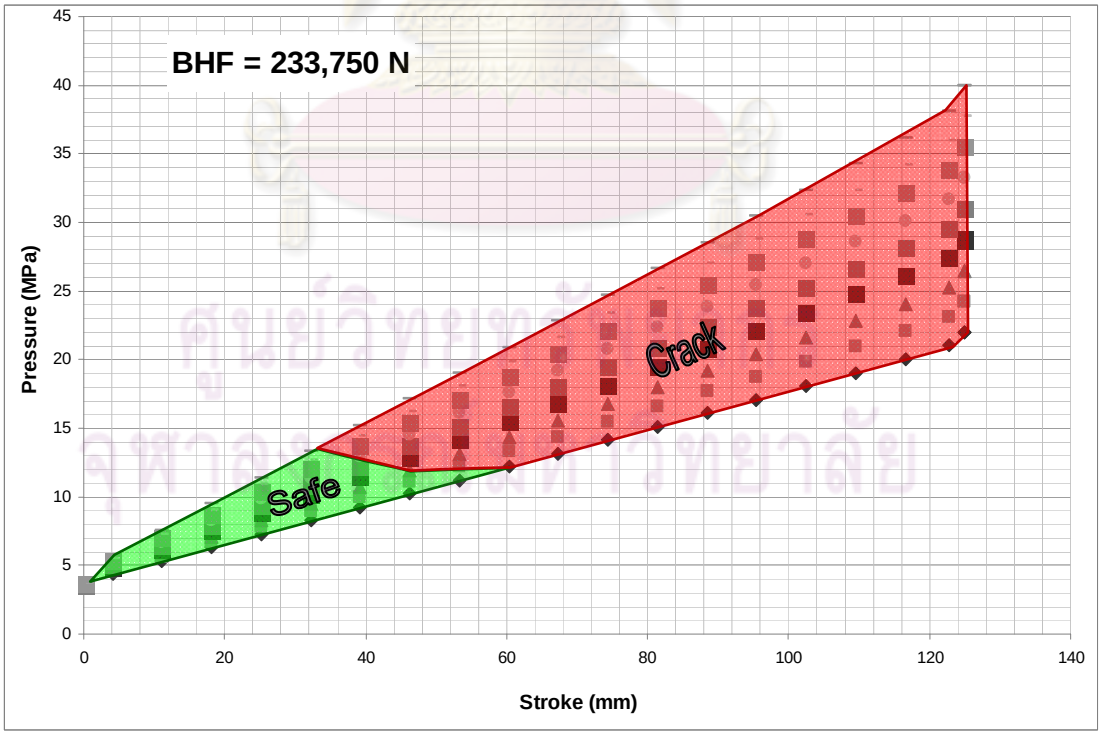

Figure 4.30 The effect of fluid pressure and punch stroke on part quality at 233,750 N of BHF for Part1

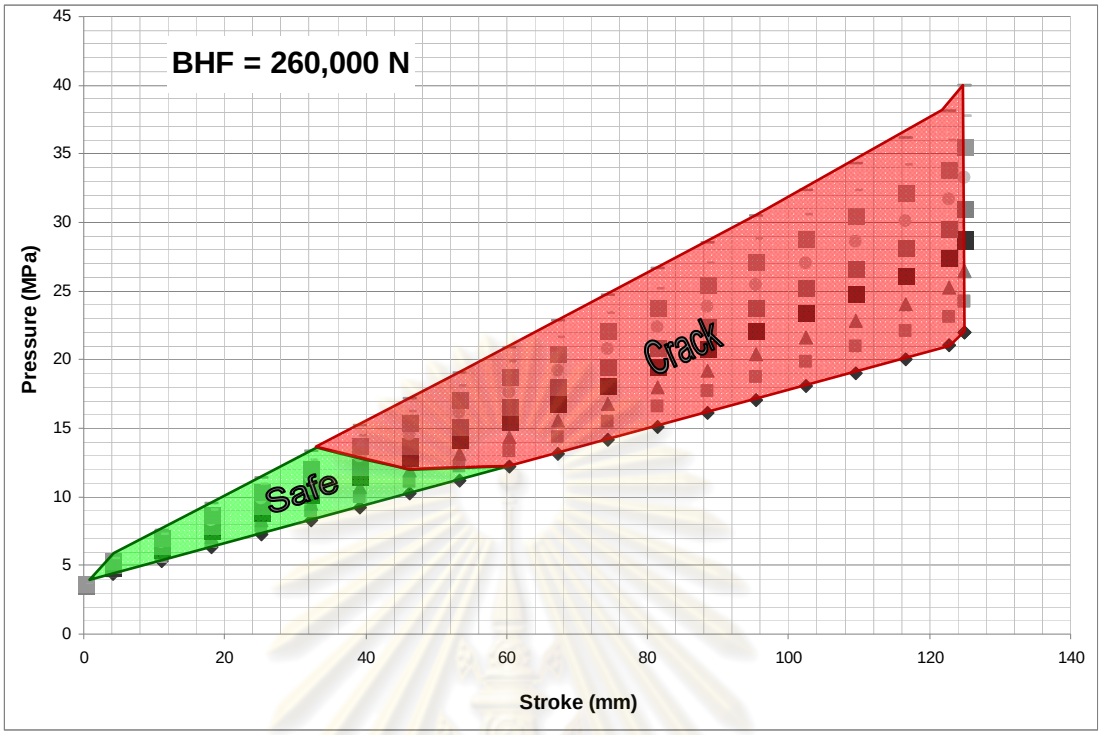

Figure 4.31 The effect of fluid pressure and punch stroke on part quality at 260,000 N of BHF for Part1

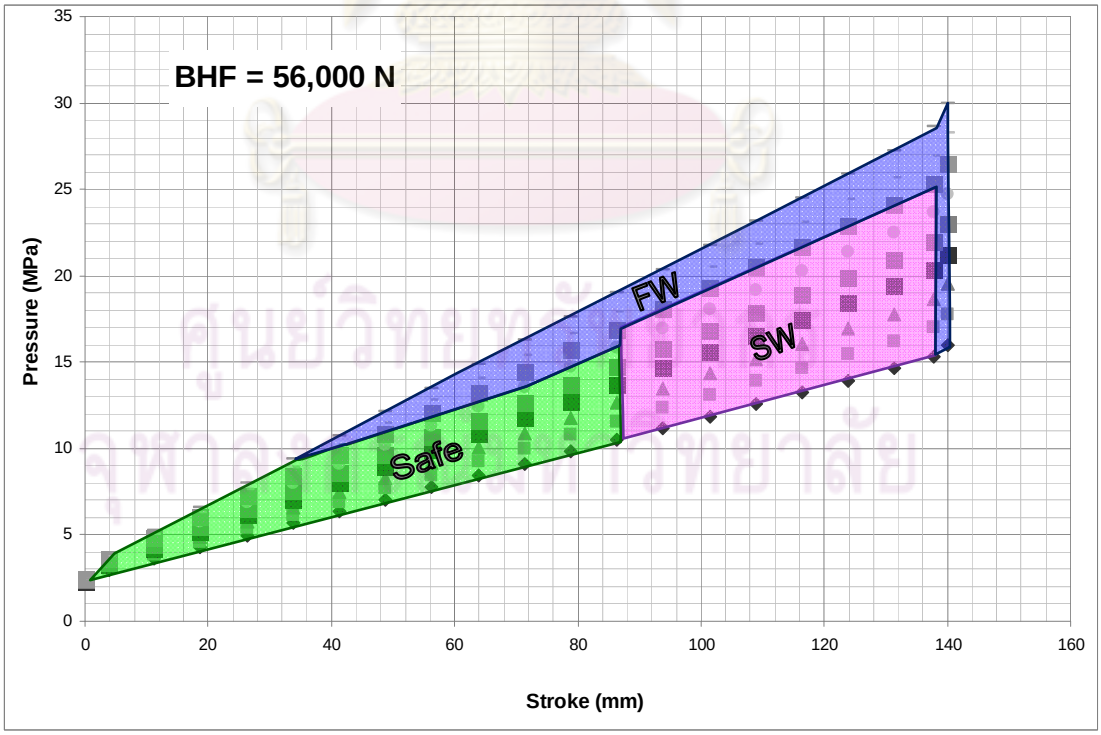

Figure 4.32 The effect of fluid pressure and punch stroke on part quality at 56,000 N of BHF for Part2

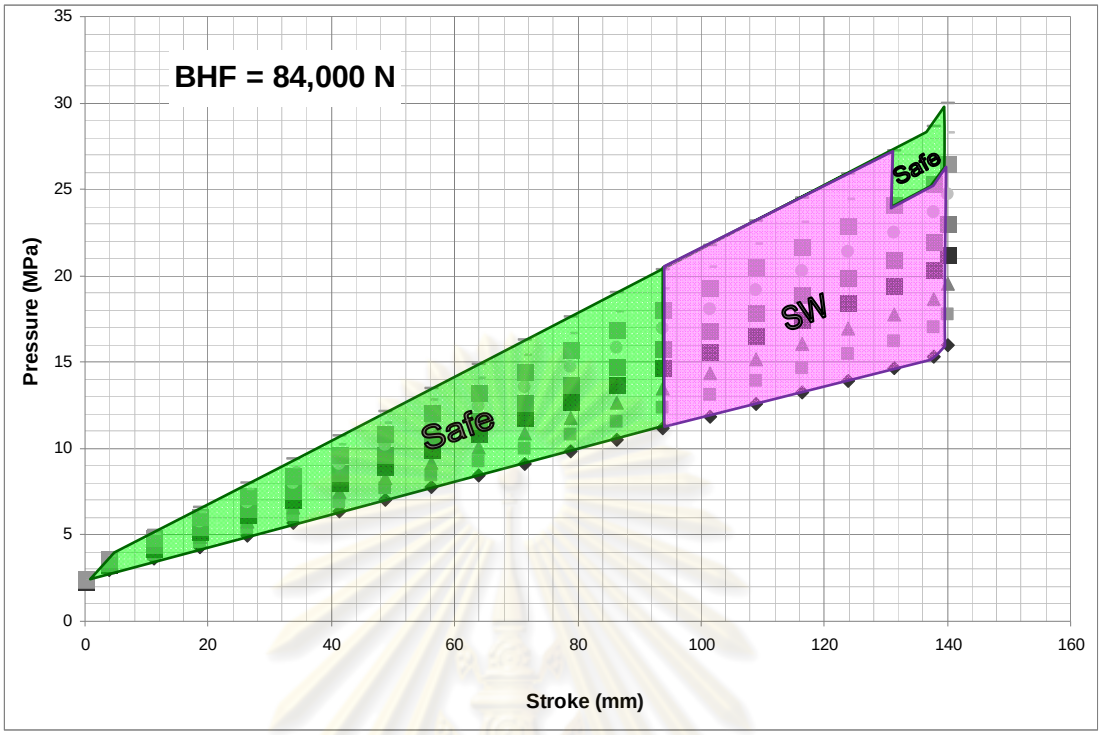

Figure 4.33 The effect of fluid pressure and punch stroke on part quality at 84,000 N of BHF for Part2

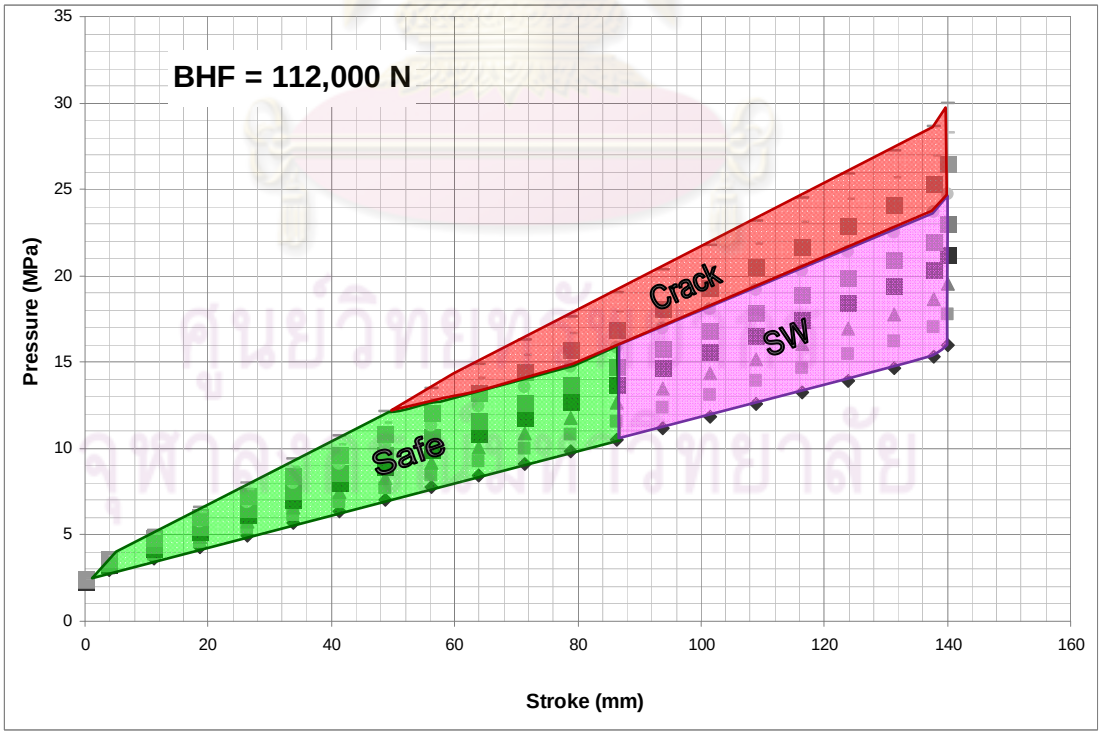

Figure 4.34 The effect of fluid pressure and punch stroke on part quality at 112,000 N of BHF for Part2

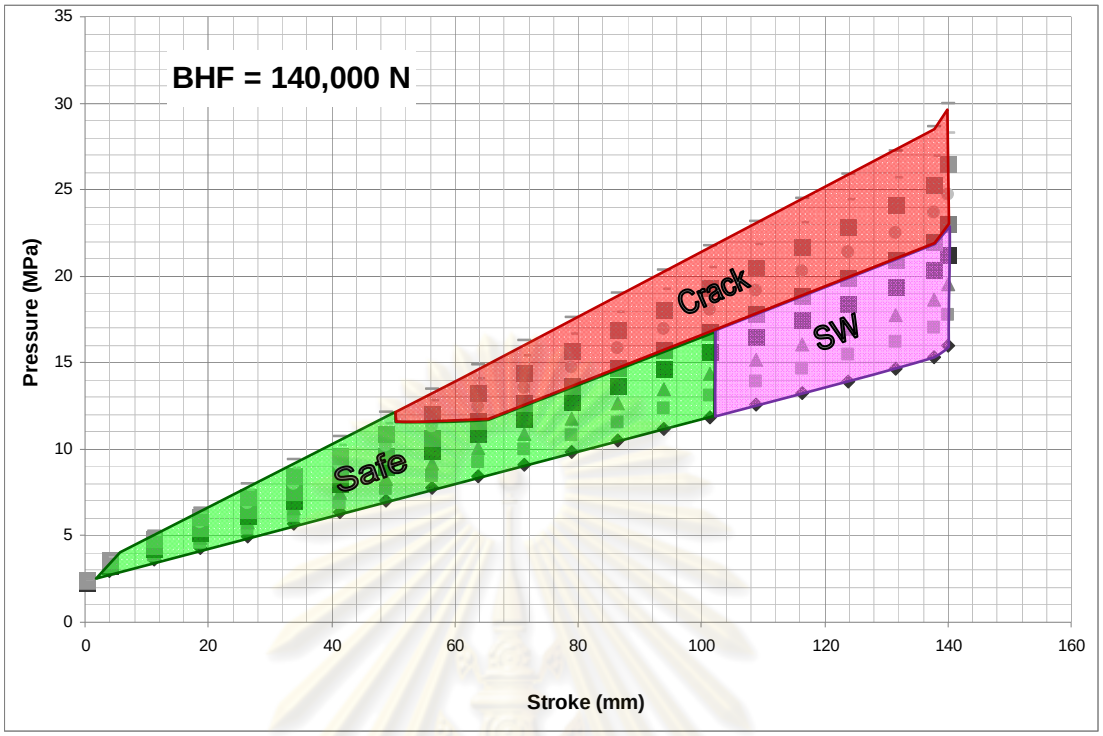

Figure 4.35 The effect of fluid pressure and punch stroke on part quality at 140,000 N of BHF for Part2

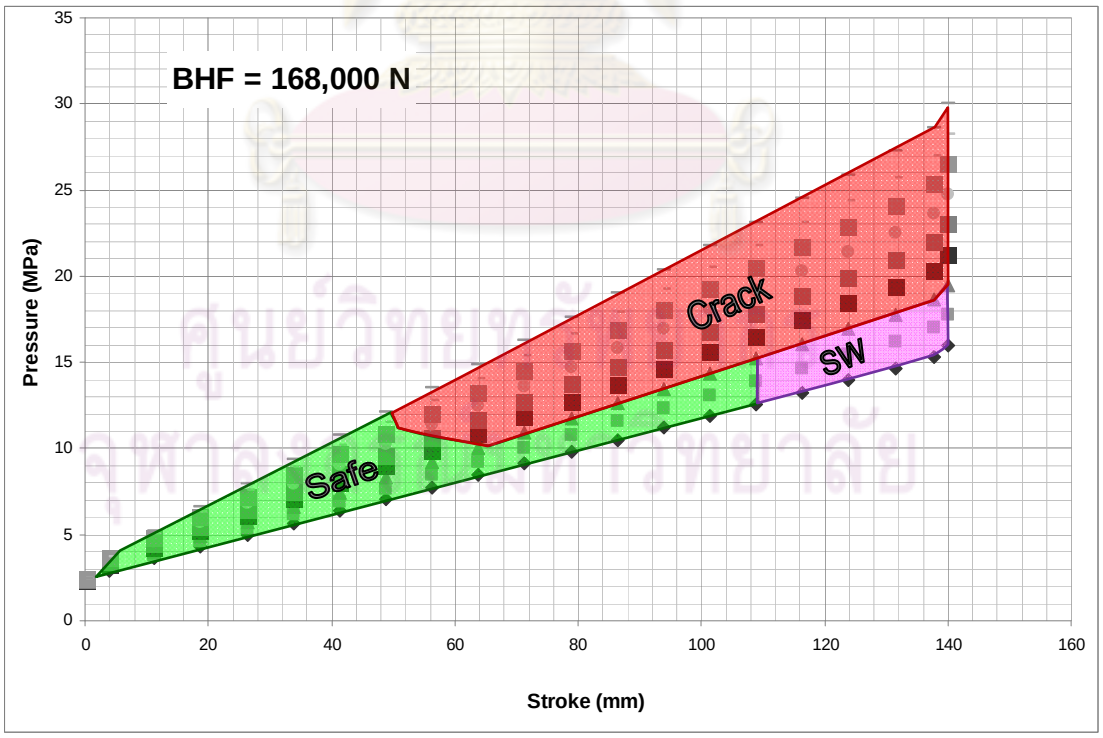

Figure 4.36 The effect of fluid pressure and punch stroke on part quality at 168,000 N of BHF for Part2

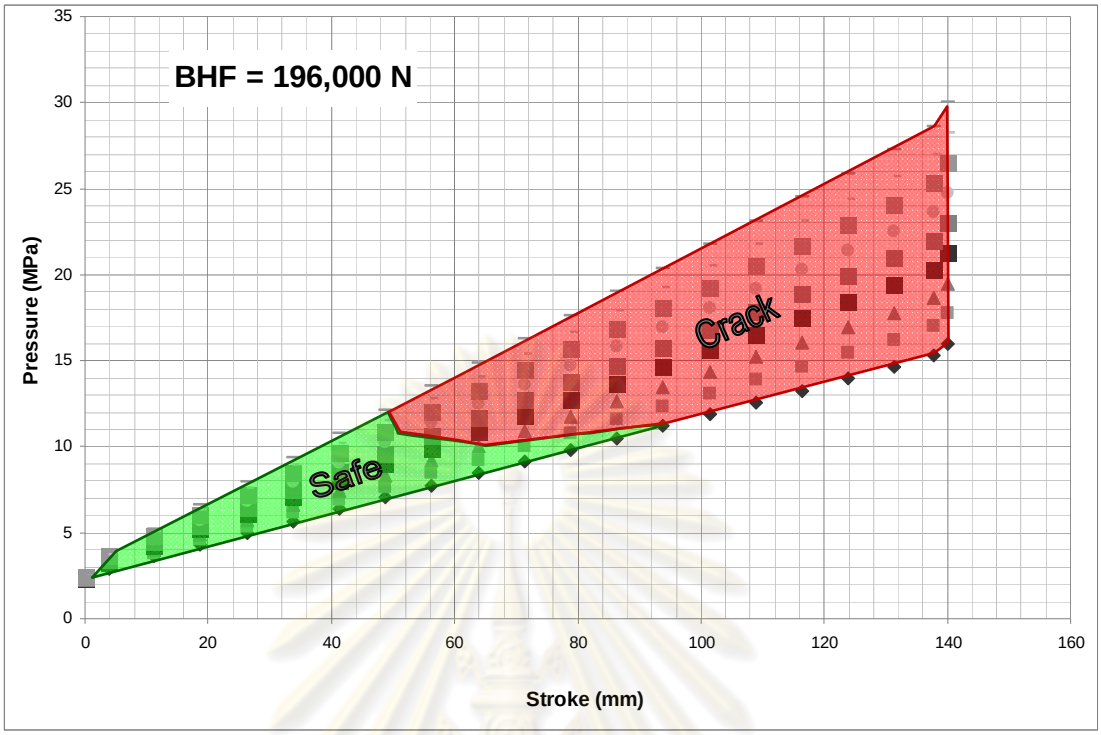

Figure 4.37 The effect of fluid pressure and punch stroke on part quality at 196,000 N of BHF for Part2

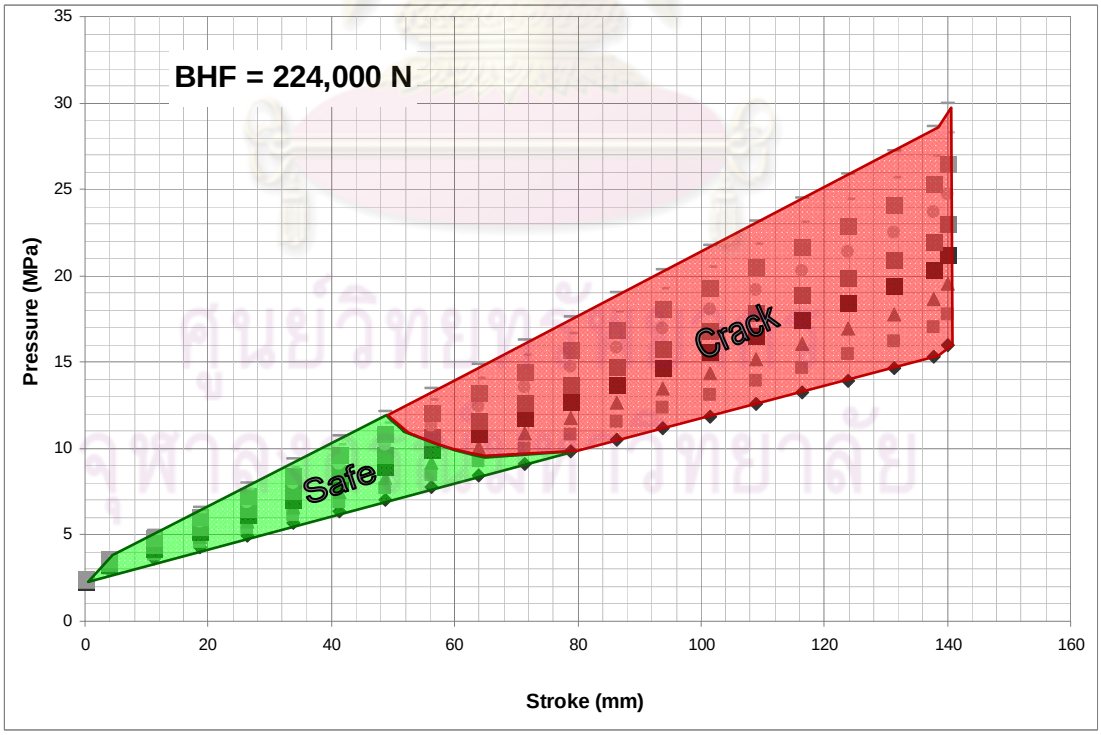

Figure 4.38 The effect of fluid pressure and punch stroke on part quality at 224,000 N of BHF for Part2

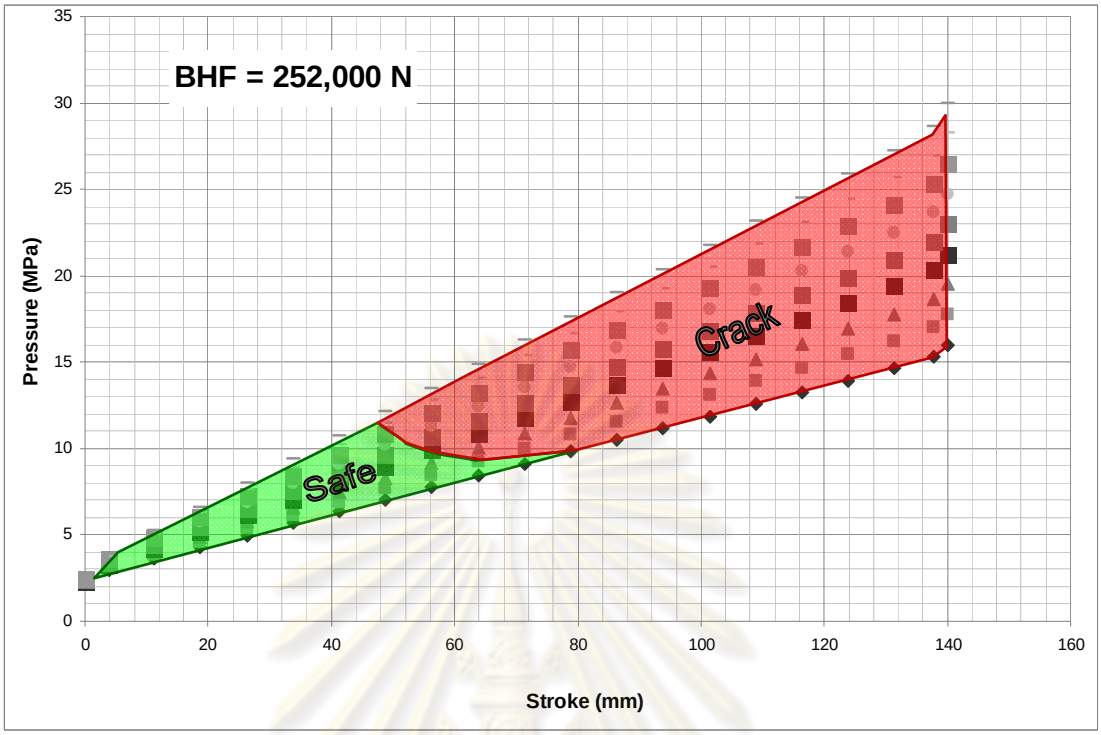

Figure 4.39 The effect of fluid pressure and punch stroke on part quality at 252,000 N of BHF for Part2

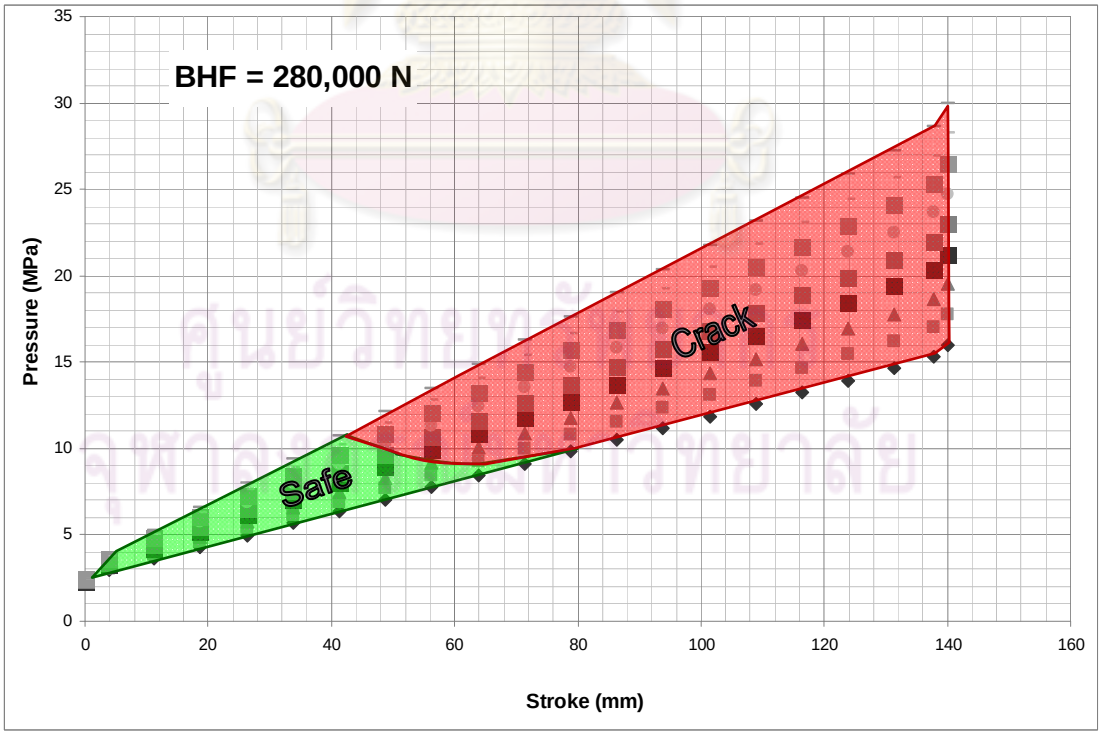

Figure 4.40 The effect of fluid pressure and punch stroke on part quality at 280,000 N of BHF for Part2

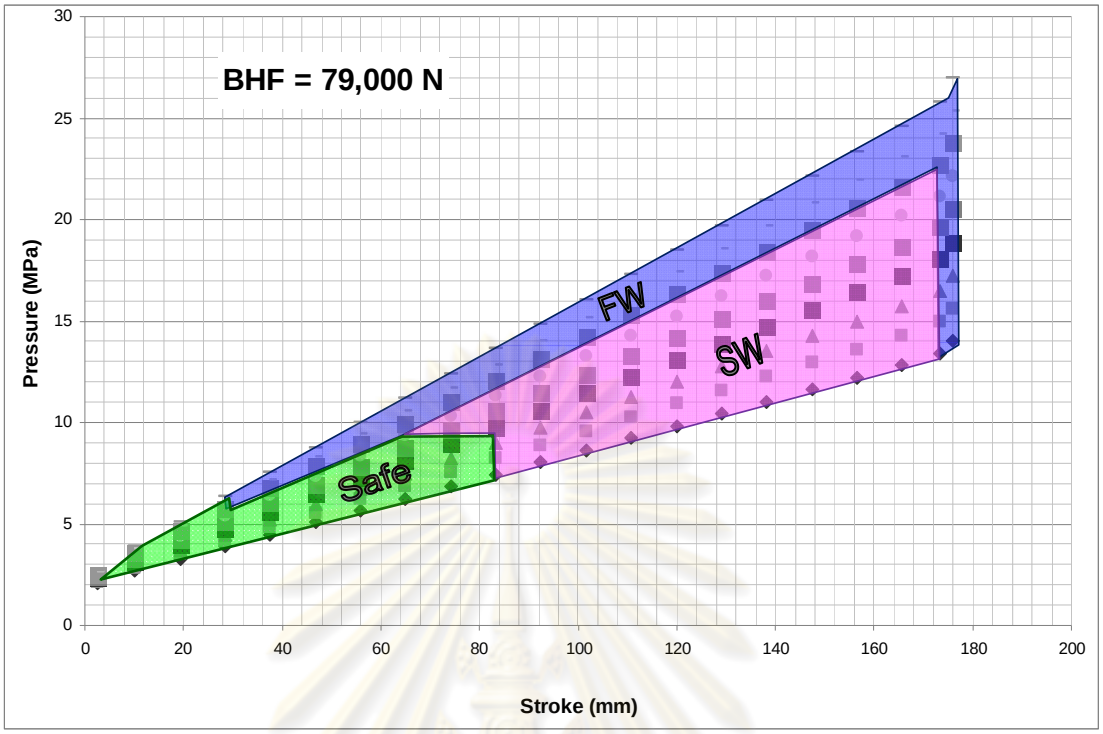

Figure 4.41 The effect of fluid pressure and punch stroke on part quality at 79,000 N of BHF for Part3

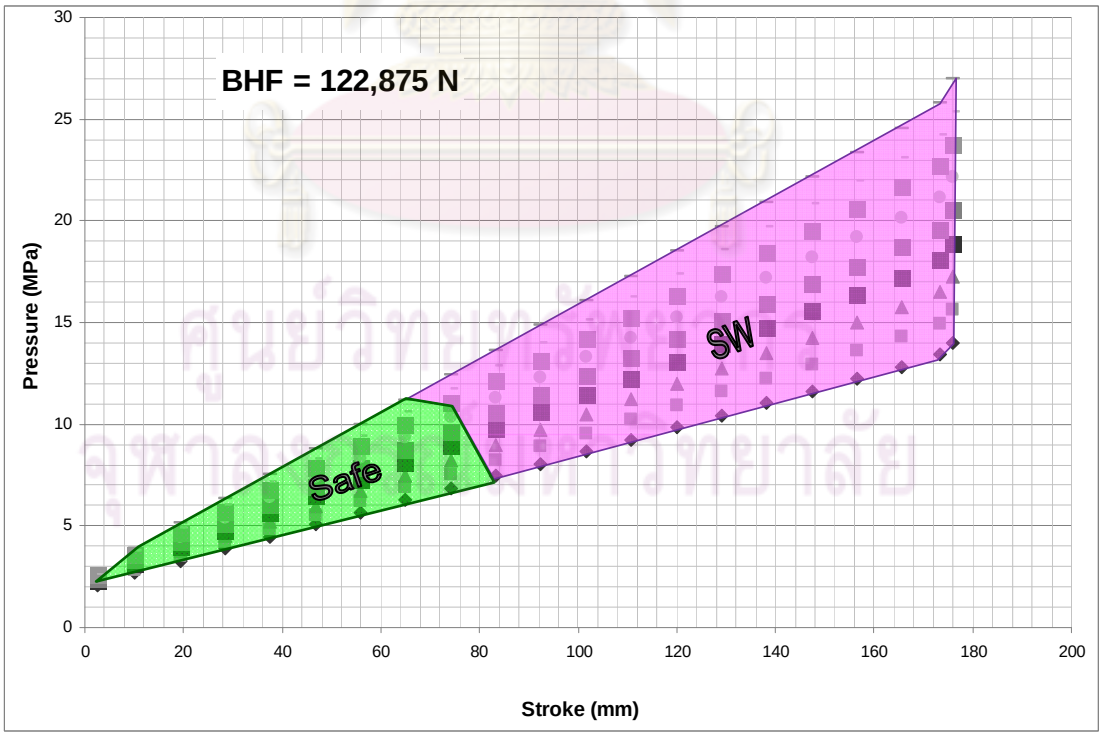

Figure 4.42 The effect of fluid pressure and punch stroke on part quality at 122,875 N of BHF for Part3

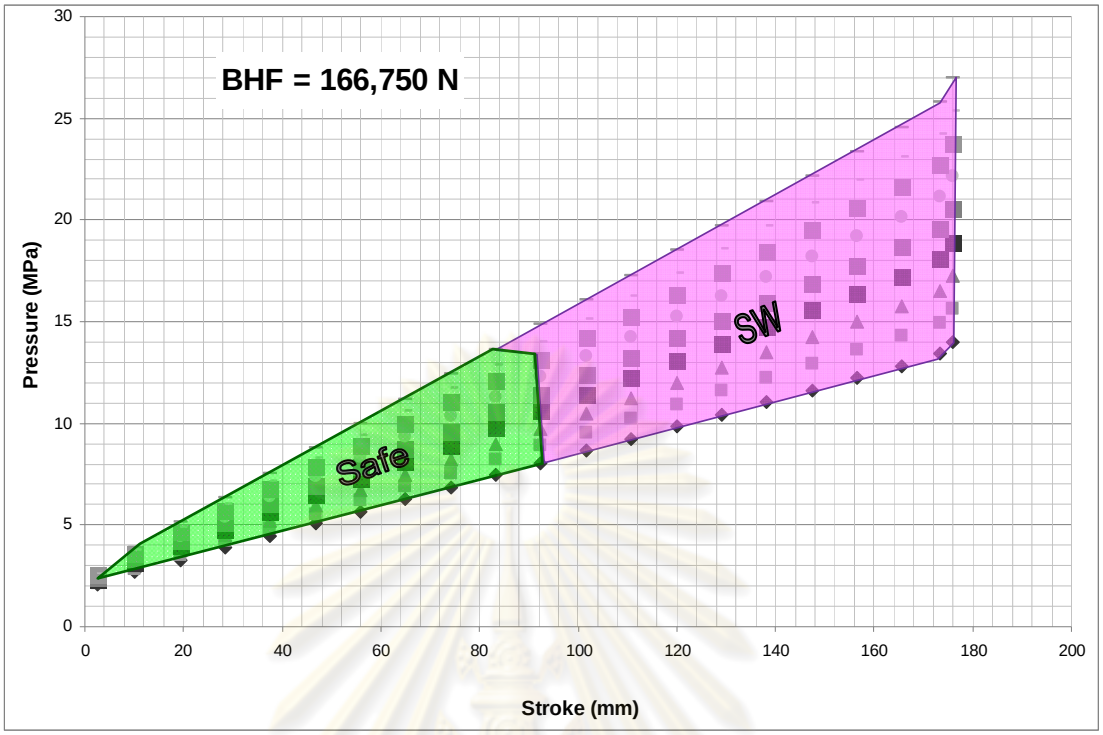

Figure 4.43 The effect of fluid pressure and punch stroke on part quality at 166,750 N of BHF for Part3

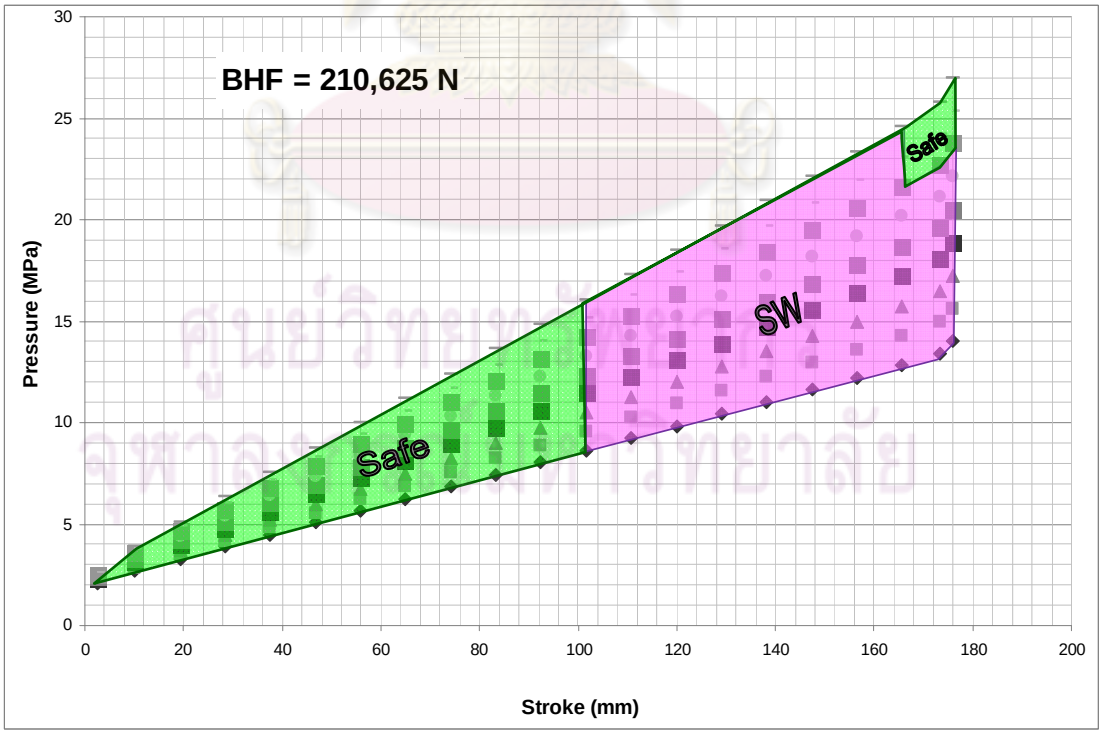

Figure 4.44 The effect of fluid pressure and punch stroke on part quality at 210,625 N of BHF for Part3

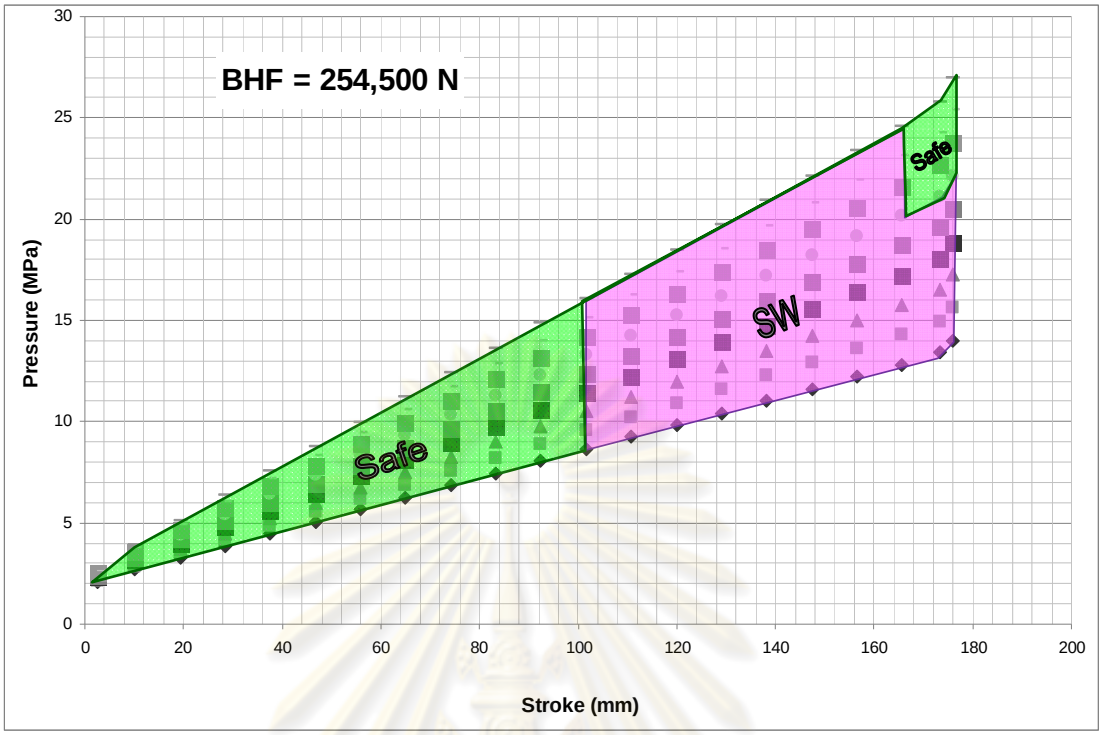

Figure 4.45 The effect of fluid pressure and punch stroke on part quality at 254,500 N of BHF for Part3

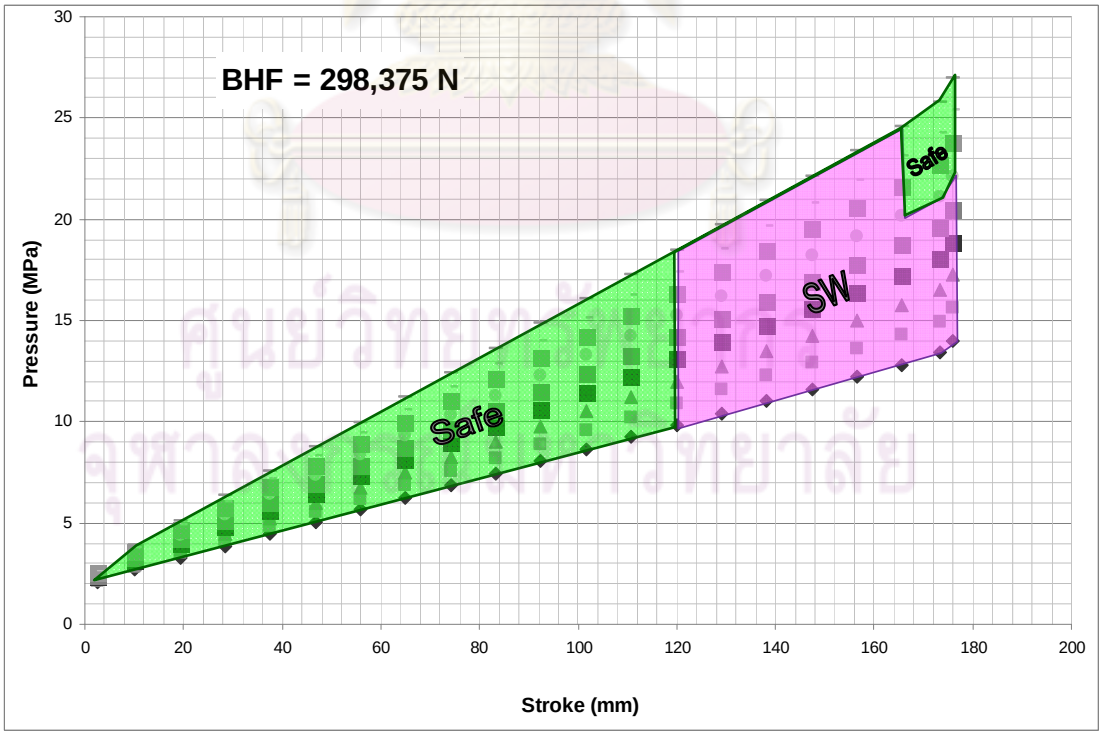

Figure 4.46 The effect of fluid pressure and punch stroke on part quality at 298,375 N of BHF for Part3

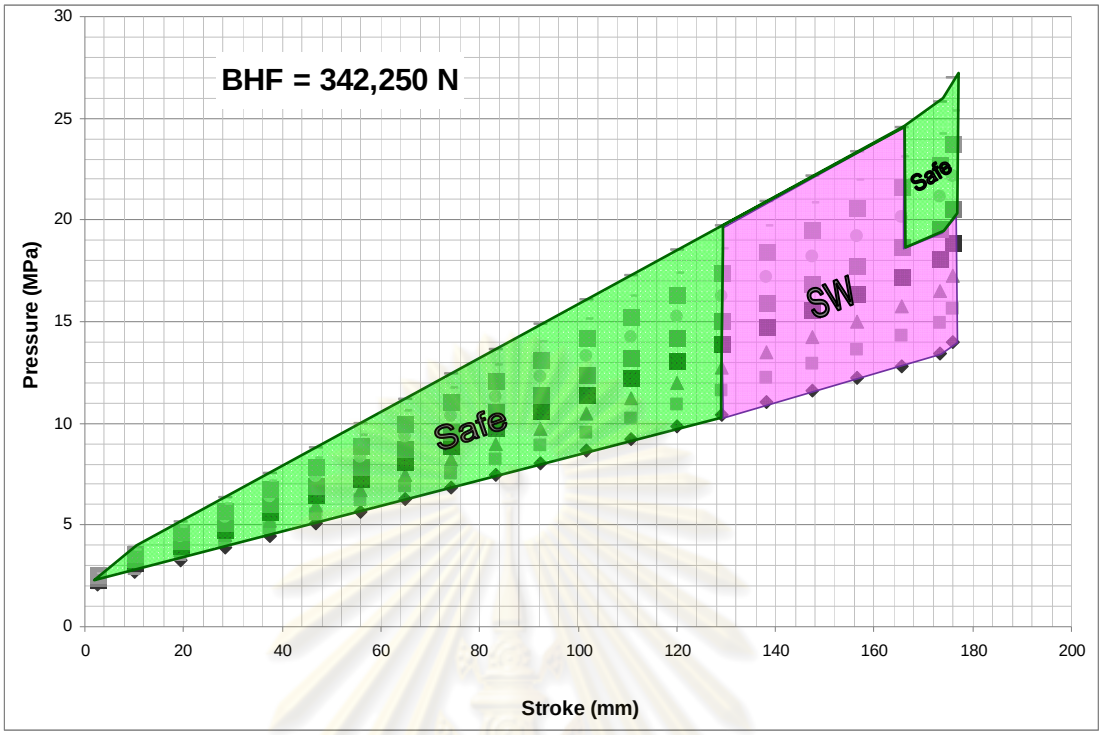

Figure 4.47 The effect of fluid pressure and punch stroke on part quality at 342,250 N of BHF for Part3

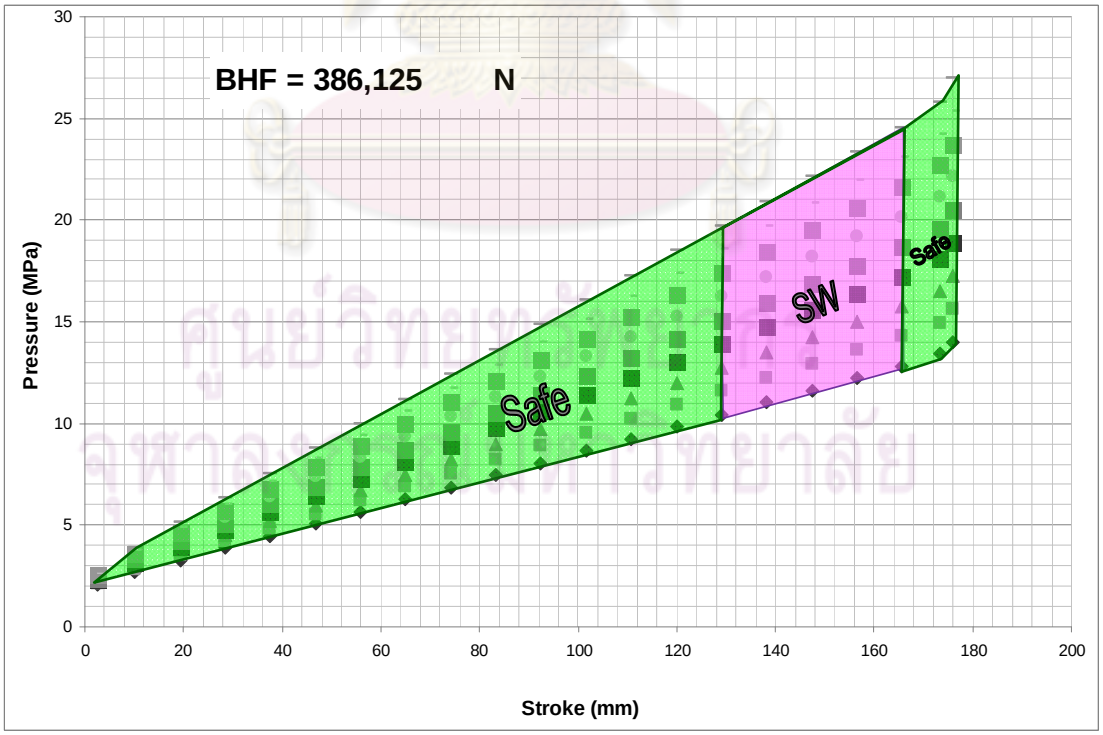

Figure 4.48 The effect of fluid pressure and punch stroke on part quality at 386,125 N of BHF for Part3

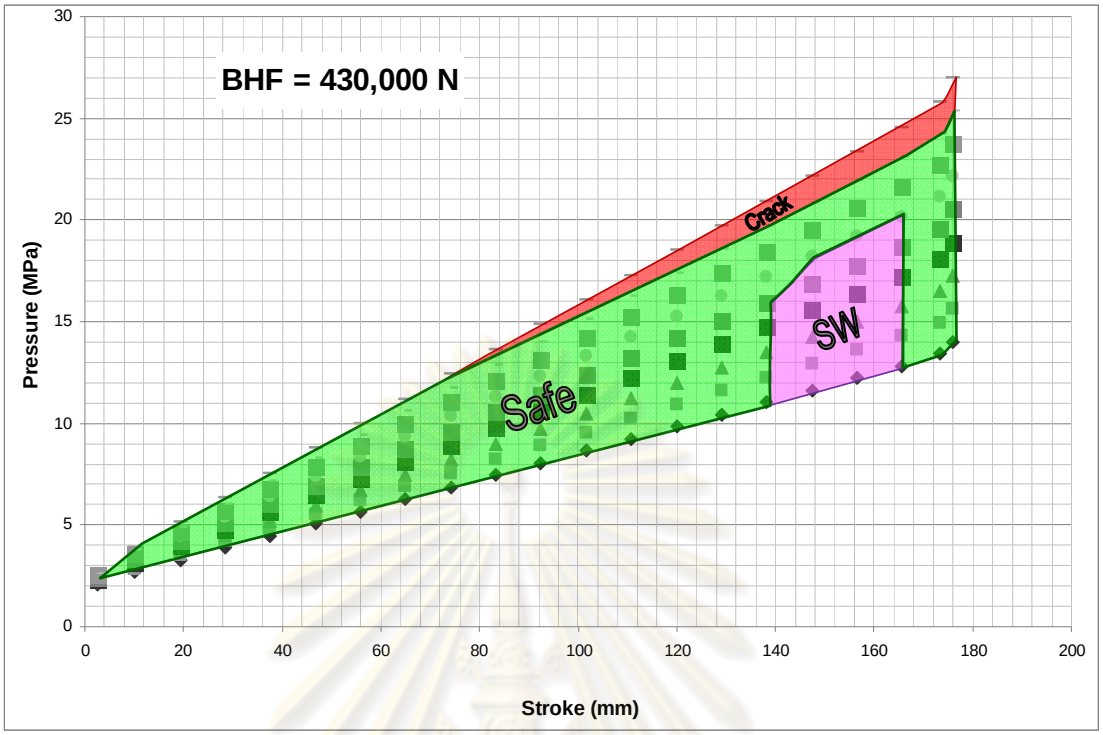

Figure 4.49 The effect of fluid pressure and punch stroke on part quality at 430,000 N of BHF for Part3

From figure 4.23 - 4.49, the general process window of relationship between pressure and punch stroke and their effects on part quality for parabolic part is shown in figure 4.50. In the beginning of stroke, the pressure does not really affect the part quality. After one-third of stroke, higher pressures lead parts to the crack. Conversely, after a half of stroke, low pressures lead parts to the side wall wrinkle. The onset of crack and side wall wrinkle changes depending on the punch distance and the blank holder force level. From the figure 4.50, a linear pressure can form the parabolic part successfully. However, a constant BHF cannot form parabolic part successfully. Clearly, a low pressure that increases with the stroke will form parts with minimum thinning. BHF is another important process parameter as it can be seen in figure 4.51. The general window of relationship between pressure and punch stroke and their effects on part quality for parabolic part with various BHF levels is shown in figure 4.51

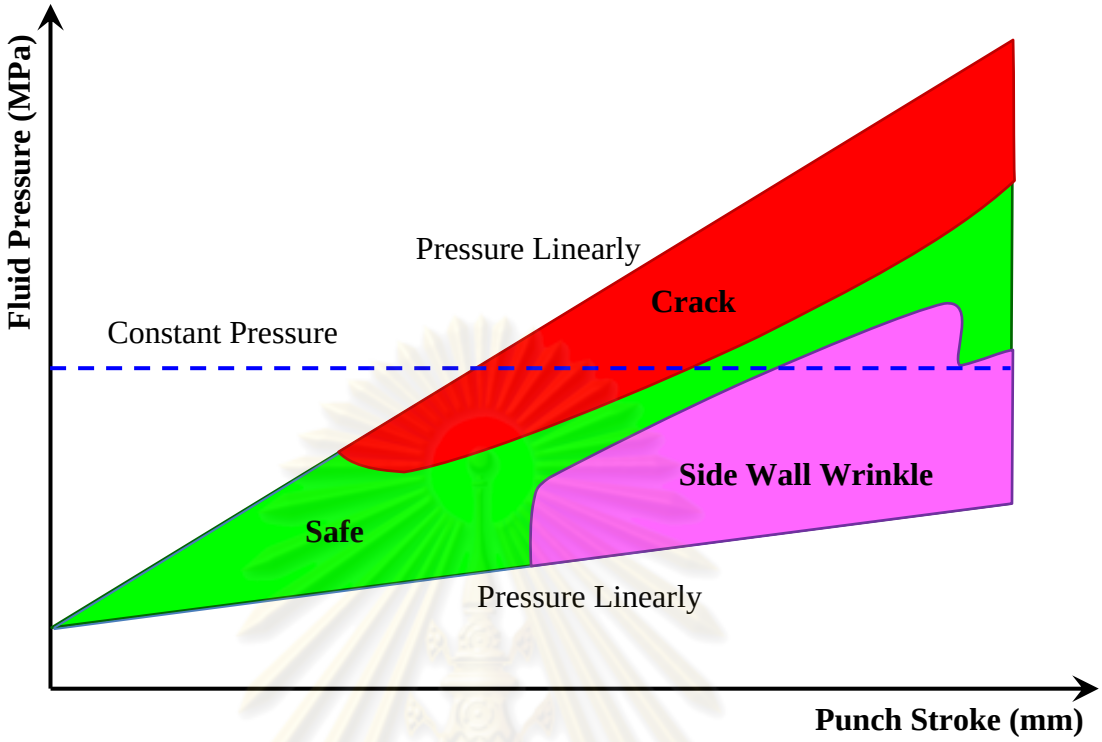

Figure 4.50 General process window of relationship between pressure and punch stroke and their effects on part quality in HMD process of parabolic part

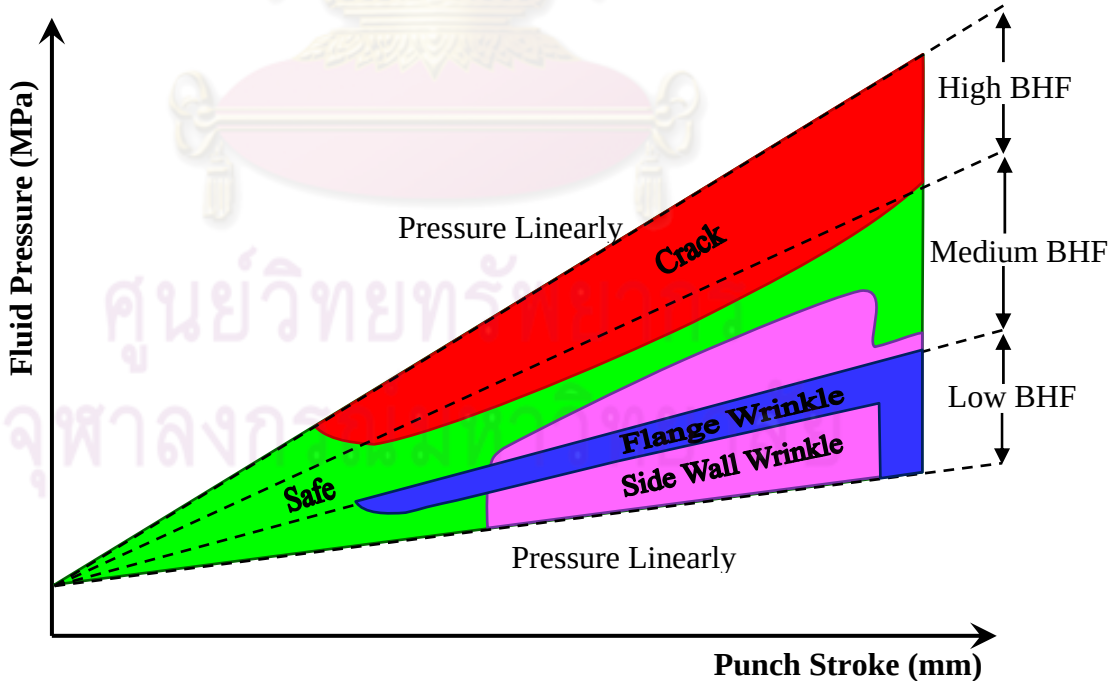

Figure 4.51 General process window of relationship between pressure and punch stroke and their effects on part quality in HMD process of parabolic part with various BHF levels

A general process window of relationship between BHF and punch stroke and their effects on part quality for parabolic part is shown in figure 4.52. This process window is plotted with the medium ranged constant pressure profile. In the beginning of stroke, the level of blank holder force does not at all affect part quality. However, after one-fourth of stroke the higher BHF lead parts to crack. Conversely, the low BHF lead parts to wrinkle in the flange area. The blank holder force is directly effect on the flange wrinkle. The side wall wrinkle starts to appear after one-third of stroke and can disappear when applying more blank holder force and pressure. From figure, it is evident now that constant BHF can form the parabolic part successfully. Also, in the same way as pressure, an application of a low BHF that increases with the stroke will form parts with minimum thinning.

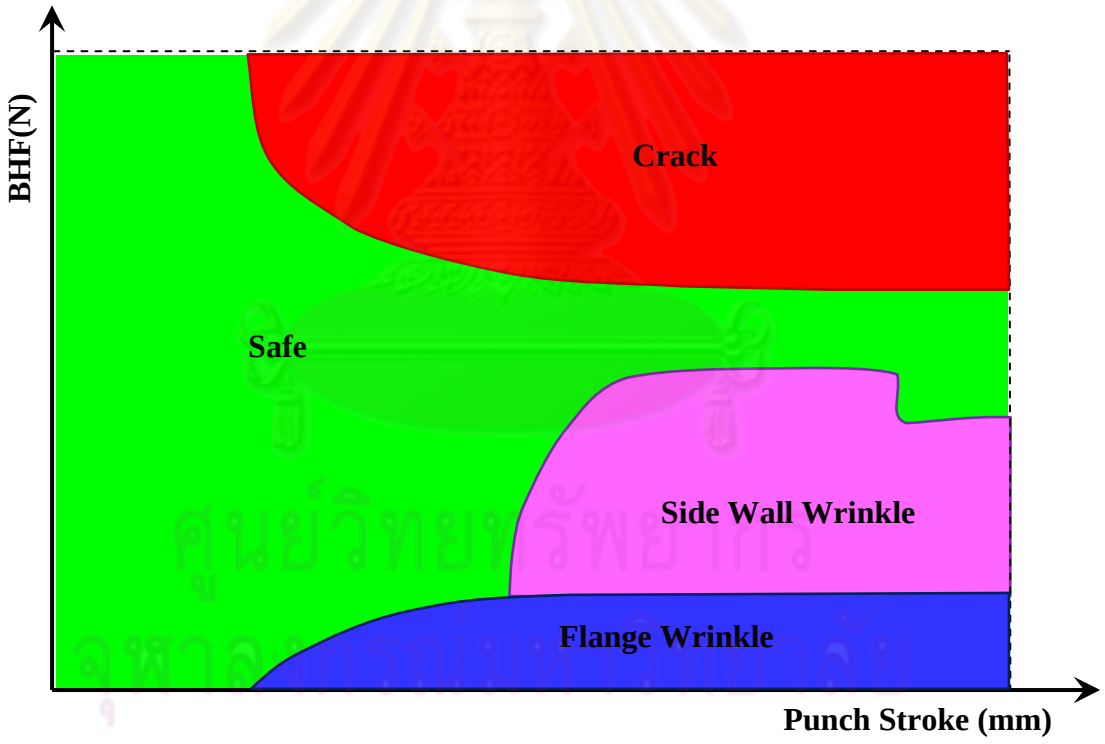

Figure 4.52 General process window of relationship between BHF and punch stroke and their effects on part quality in HMD process of parabolic part

4.4 Characteristics parabolic shape forming with HMD process

In the HMD of a parabolic part, metal flow must be closely controlled to obtain a good balance between excessive thinning in one area and wrinkling in others. In the top illustration in figure 4.53, the blank is first bulged upward and then reversely formed downward by the punch movement. Then, the punch moves to stretch the blank, which is restrained by the blank holder in the flange area and pressure in the forming area. At this stage, the blank around the punch nose is subjected to biaxial tension, which results in metal thinning before crack. With proper pressure and blank holder force, part thinning falls in the range of 20 to 40% (depend on part geometry). More than 40% part thinning is likely to result in fracture near the punch nose. In figure 4.53, the portion of the blank under the blank holder has not begun to move.

As the drawing operation continues, the metal begins to move from the blank holder, and a forming mechanics develops (the third illustration, figure 4.53). Here the metal has been drawn into a partial parabolic shape with unsupported metal in a tangential slope between the punch and the clamped surface. Unlike the drawing of straight-sided shapes, the wide gap (side wall wrinkle area, figure 4.53) prevents the use of the draw ring bore as the means of forcing the metal against the punch surface; therefore, the probability of wrinkling increases. Because the metal is not confined between the punch and die, wrinkling is likely to occur in this area. To prevent wrinkles, the bulge height between the punch and blank holder must be high enough and metal must flow slowly from the flange area (slow draw-in speed) simultaneously. This is to maintain the sheet metal in tensile state of stress at all time. If the high hydraulic pressure and BHF are kept properly during this last forming stage, a good part without any side wall wrinkle will result as shown in figure 4.51.

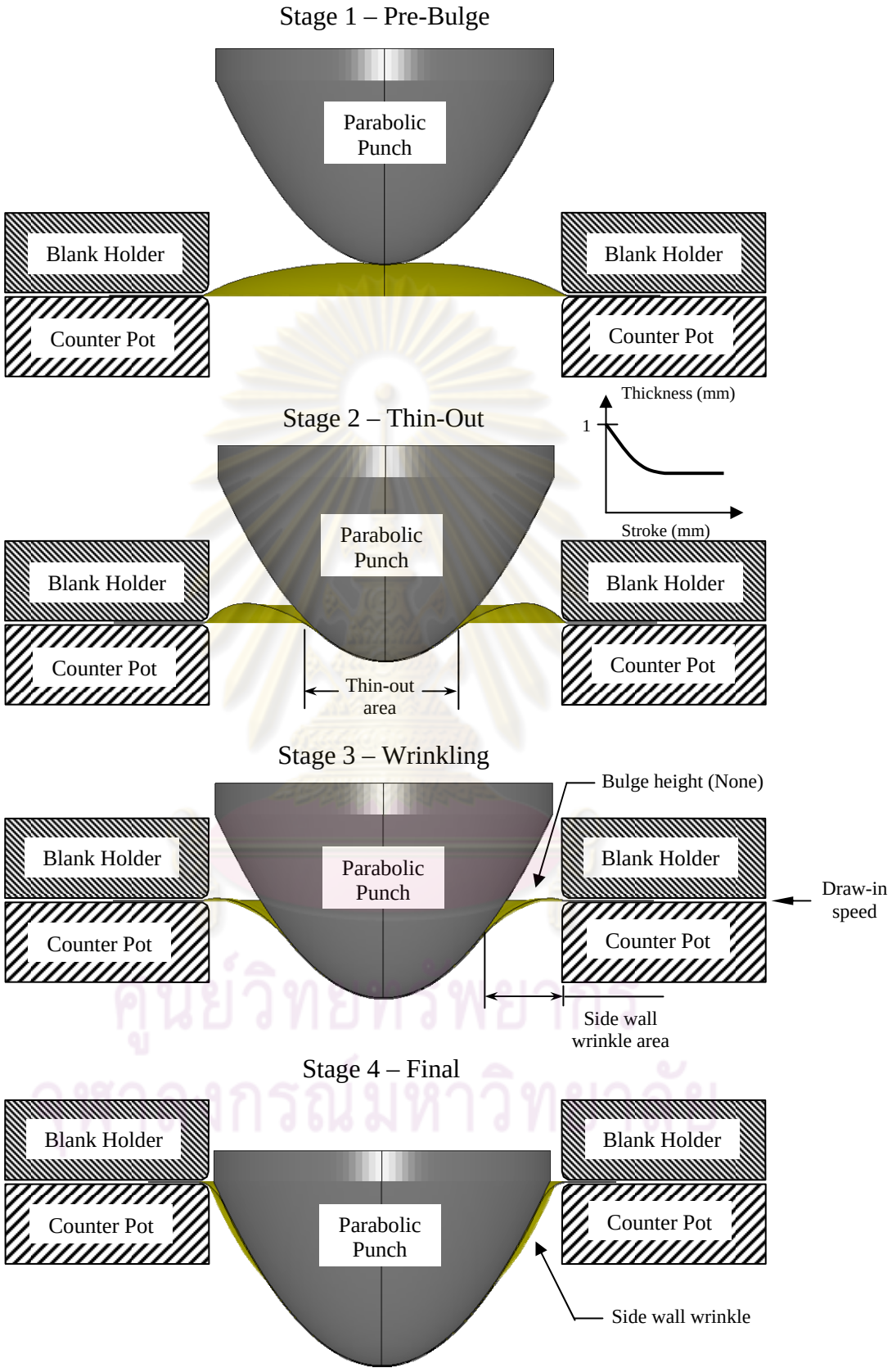

Figure 4.53 Forming stages of parabolic cup in HMD

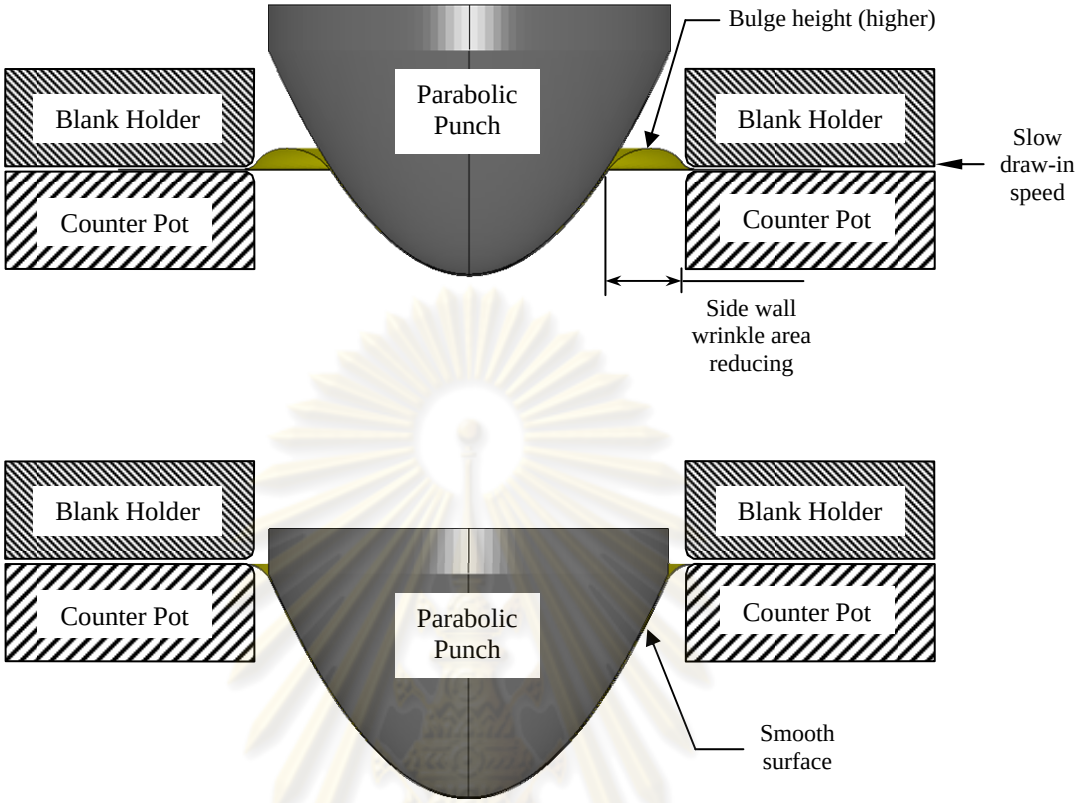

Figure 4.54 The good forming of parabolic cup in HMD

ศูนย์วิทยทรัพยากร
จุฬาลงกรณ์มหาวิทยาลัย

CHAPTER V

OPTIMIZATION OF BLANK HOLDER FORCE AND PRESSURE FOR HYDROMECHANICAL DEEP DRAWING OF PARABOLIC PARTS USING 2-D INTERVAL HALVING AND RSM METHODS

The key process parameters affecting part quality are blank holder force and counter pressure. Excessive blank holder force and counter pressure can lead to fracture. On the other hand, insufficient blank holder force and counter pressure can lead to wrinkle. Therefore, proper blank holder force and proper counter pressure are very important in carrying out the forming process successfully. In previous chapter, numerous of simulations were used to find the feasible region of the parts, thus requiring expensive and time consuming. The aim of this chapter is to reduce a number of simulations and find the minimum thinning of the parts.

Zhang, Lang et al. 2000; Zhang, Nielsen et al. 2000; Zhang, Jensen et al. 2003 studied the effect of anisotropy, pre-bulging, counter pressure and blank holder force on the quality of parts such as round cups, parabolic workpieces and rectangular boxes in HMD process using both FEA simulations and experiments. Lang, Danckert et al. 2004; Lang, Danckert et al. 2005 investigated forming of a complex square cup and a round cup using HMD process with uniform pressure by both experiment and FEA simulation. They showed that the simulated results reasonably agreed with the experiment.

Response surface methodology (RSM) is a method for constructing global approximations of valued objective and constraint functions based on functional evaluations at various points in the design space. Many researchers have applied RSM to simulation models in computational mechanics field. Roux, Stander et al. 1998 discussed experimental design techniques and the regression equations for structural optimization.

RSM combined with stochastic finite elements were used by Kleiber, Rojek et al. 2002 for reliability assessment in metal forming. Huang, Lo et al. 2006 found optimal punch nose radius for forming of a round cup to minimize part thickness variation. Wang and Lee 2005 used RSM and FEA to control strain path during forming process with space-variant blank holder force.

In this research, RSM is applied to determine optimal constant BHF and linear pressure from the feasible region. Normally, sampling is a good method to obtain feasible data points for RSM but it needs a large number of samplings. In this research, we use the 2-D interval halving method, an efficient wide space search method, combined with RSM to determine optimal process parameters that form a parabolic cup with minimum part thinning.

5.1 Search space

The procedure for determining the optimal P and BHF profiles is shown in figure 5.1. The region of interest is defined by L_i and U_i which are respectively the lower and upper bounds on design variables; BHF and P. The ranges of the optimal search were restricted as follows:

Part1 :	$Li \le P \le Ui$;	22.00 MPa ≤ P ≤ 40.00 MPa
	$L_i \le BHF \le U_i$;	50,000 N ≤ BHF ≤ 260,000 N
Part2 :	$L_i \le P \le U_i$;	16.00 MPa ≤ P ≤ 30.00 MPa
	$L_i \le BHF \le U_i$;	56,000 N ≤ BHF ≤ 280,000 N
Part3 :	$Li \le P \le Ui$;	14.00 MPa ≤ P ≤ 27.00 MPa
	$L_i \le BHF \le U_i$;	79,000 N ≤ BHF ≤ 430,000 N

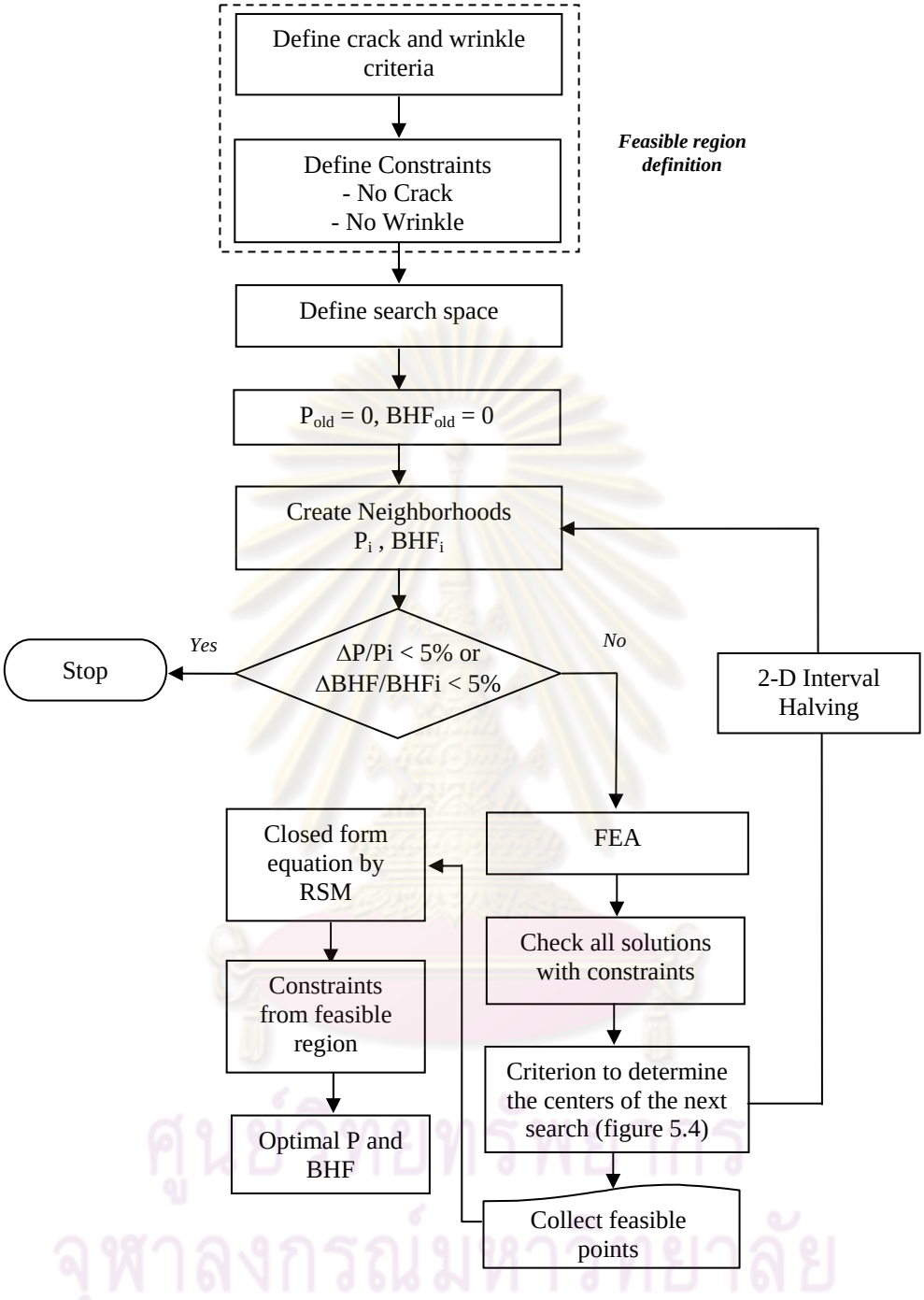

Figure 5.1 Flow chart for determination of the optimal BHF and P

ศูนย์วิทยทรัพยากร
จุฬาลงกรณ์มหาวิทยาลัย

5.2 Search method and neighborhood determination

After a search space has been established, the neighborhoods are created by separation of the search space into four areas equally, figure 5.2. Then, the center points of the four areas are evaluated through simulation runs. Center points that are found to form a good part (i.e. acceptable wrinkles and thinning) are to be labeled as feasible points.

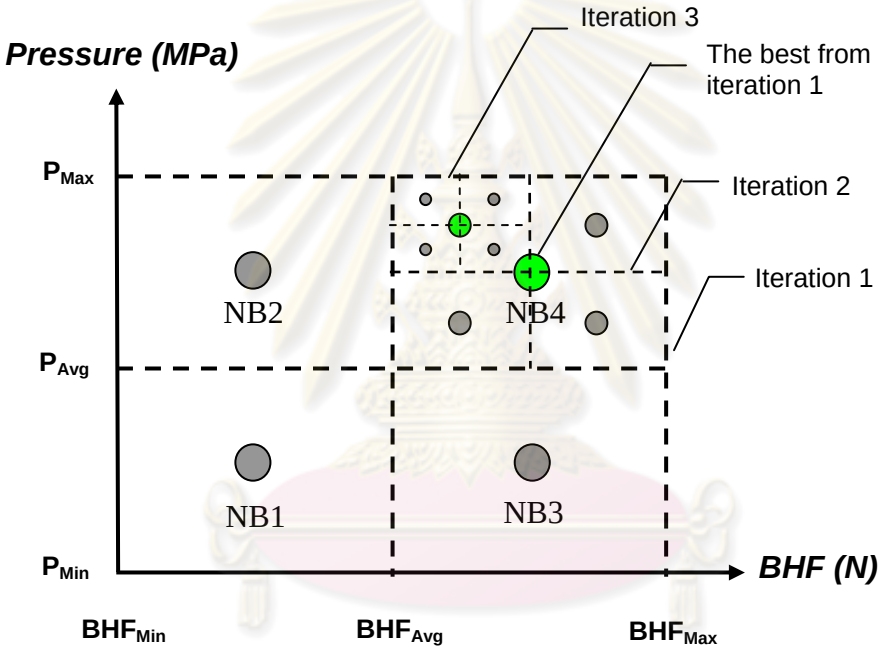

Figure 5.2 Schematic of search algorithm

In each search iteration, all the center points of the current neighborhoods are evaluated through FEA simulations. A center point in the process parameter space is said to be a feasible point if it forms a part with the defect parameters; SW, FAM, and %thinning, under their limits; SW_{Lim}, FAM_{Lim} and $Thin_{Lim}$, respectively. All the center points in each iteration are also compared to determine the one with the best quality to be the center of the next search.

In assessment of part quality from each neighborhood with different combinations of BHF and pressure parameters, levels of difficulty in adjusting the parameters to result in a good part for the next iteration are considered. During the early search iterations, the three part defects (i.e. crack, flange wrinkle, and sidewall wrinkle) are most likely to occur in the chosen neighborhoods.

2-D interval halving method was applied as the search method in this study. In each iteration, the method searches for center point(s) in the current neighborhoods that is either of (a) feasible forming parameters or (b) able to be the best quality for the center point. Then, these points determined are to be center points of new neighborhoods, which are split into four regions, to be evaluated in the next iteration. These search iterations keep progressing until the forming parameters (blank holder force and pressure) of newly found points are only 5% different from the previous point.

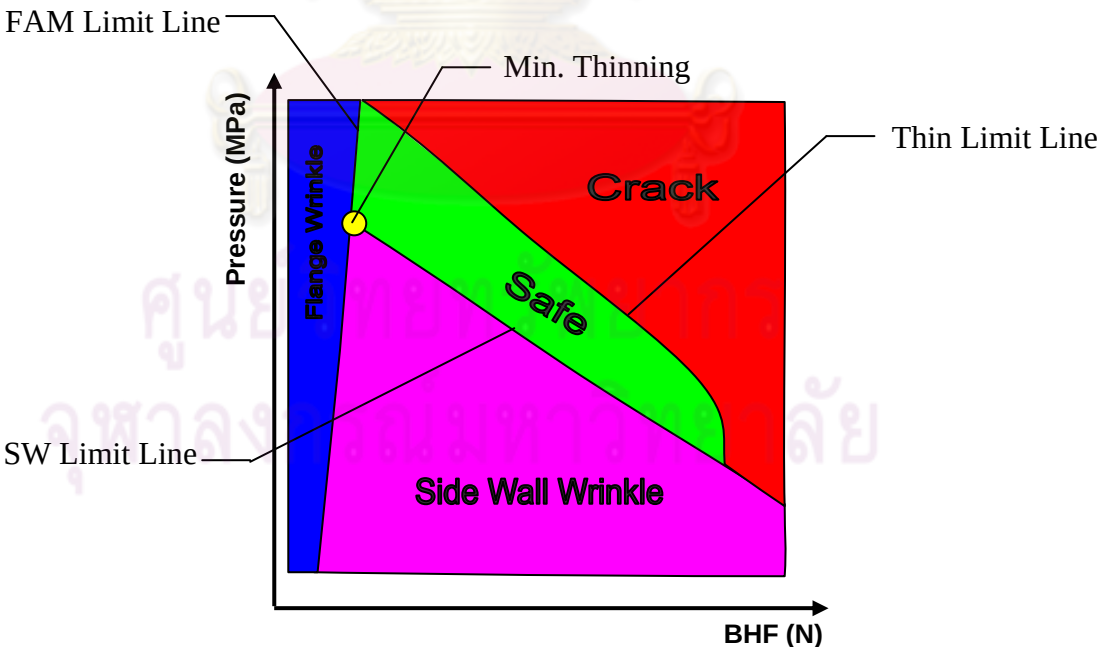

Figure 5.3 General process window of relationship between constant BHF and linear pressure affected on part quality with limit lines

To find the best quality for the center point, the general process window related with constant BHF and linear pressure and part quality with limit lines, as shown in figure 5.3 is used. In general, there are three ways to access the feasible zone; 1) access from crack boundary, 2) access from flange wrinkle and 3) access from side wall wrinkle. The parts accessed from side wall wrinkle have thinning less than the other sides. The objective to form parabolic parts with linear pressure and constant blank holder force is *minimum thinning* with *no crack* and *no wrinkles*. Therefore, the solution should be approached from side wall wrinkle boundary (SW limit line).

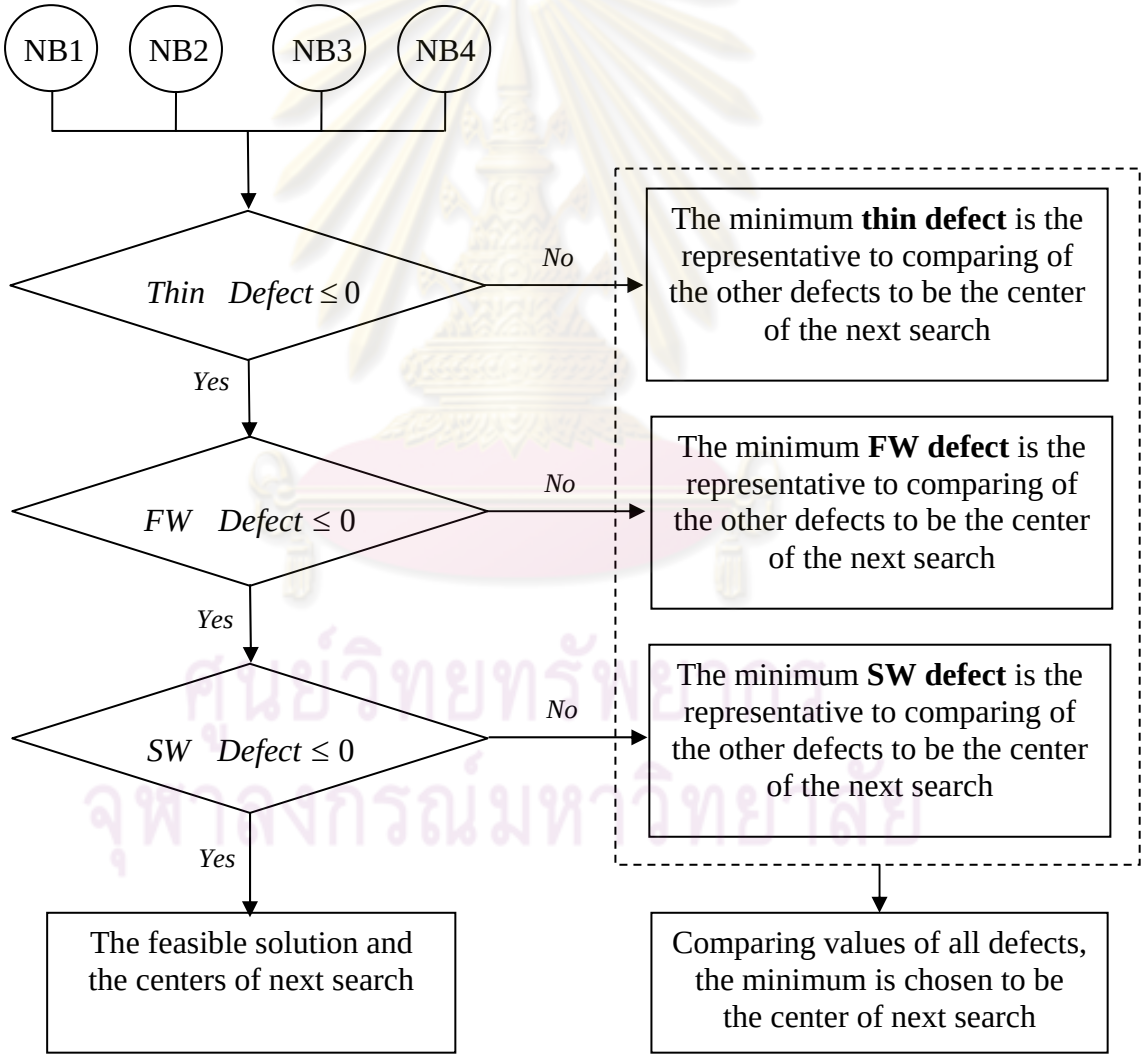

Figure 5.4 Schematic to determine the centers of the next search

The schematic to determine the center of the next search for the minimum thinning is shown in figure 5.4. The neighborhoods with cracks are considered firstly by using the thinning criterion as defined in Eq. 5.1. This is because if all neighborhoods pass the thinning criterion (to have the thin defect as zero or negative), the search will be entering the feasible region from FAM or SW limit, as suggested.

$$Thin \quad Defect = \left(\frac{Thin_i - Thin_{Lim}}{Thin_{Lim}} \right) \tag{5.1}$$

If the neighborhoods pass both the thinning criterion and FAM criterion, as defined in Eq. 5.2, the search will proceed from the SW limit as a result the parts will tend to have minimum thinning. In case of FAM is the final consideration, the search does not guarantee that the formed parts will have minimum thinning quality due to the fact that thinning values from of parts accessed from the FAM limit vary considerably.

$$FW \quad Defect = \left(\frac{FW_i - FW_{Lim}}{FW_{Lim}} \right) \tag{5.2}$$

After having passed the cracking assessment and flange wrinkle assessment, the neighborhood can still exhibit sidewall wrinkle. Hence, the SW is the final consideration. If all neighborhoods passed the thinning criterion, FAM criterion and SW criterion (defined in Eq. 5.3) the parts are obviously feasible. If the neighborhoods do not pass any of the criteria, the valued indexes (Eq. 5.1 to 5.3) of all defects are compared. The part that has minimum defect index is to be the center of the next search because it is closet the boundary of feasible region.

$$SW \quad Defect = \left(\frac{SW_i - SW_{Lim}}{SW_{Lim}} \right) \tag{5.3}$$

The 2-D interval halving method and the best quality for the center point (figure 5.4) were applied to find the minimum thinning of three parabolic parts. The solutions of Part1 were shown in table 5.1.

Table 5.1 The solutions of combination between pressure and BHF searching by 2-D interval halving of Part1

Iteration 1	P (MPa)	BHF (N)	Thinning	Dist. Thin BD	FAM	Dist. FAM BD	SW	Dist. SW BD
NB1	26.5	102500	35.69%	-10.79%	1.03166	-1.75%	0.48393	-7.82%
NB2	35.5	102500	95.04%	137.61%	1.02253	-2.62%	0.00000	-100.00%
NB3	26.5	207500	97.75%	144.37%	0.99609	-5.13%	0.00000	-100.00%
NB4	35.5	207500	100.00%	150.00%	0.00000	-100.00%	0.00000	-100.00%

Iteration 2	P (MPa)	BHF (N)	Thinning	Dist. Thin BD	FAM	Dist. FAM BD	SW	Dist. SW BD
NB1	24.25	76250	32.66%	-18.36%	1.04068	-0.89%	0.58212	10.88%
NB2	28.75	76250	34.43%	-13.93%	1.04015	-0.94%	0.48657	-7.32%
NB3	24.25	128750	36.94%	-7.65%	1.02454	-2.42%	0.49957	-4.84%
NB4	28.75	128750	42.19%	5.47%	1.02414	-2.46%	0.47707	-9.13%

Iteration 3	P (MPa)	BHF (N)	Thinning	Dist. Thin BD	FAM	Dist. FAM BD	SW	Dist. SW BD
NB1	27.625	63125	33.21%	-16.98%	1.04616	-0.37%	0.48889	-6.88%
NB2	29.875	63125	34.02%	-14.96%	1.04572	-0.41%	0.48893	-6.87%
NB3	27.625	89375	35.11%	-12.23%	1.03579	-1.35%	0.48279	-8.04%
NB4	29.875	89375	36.14%	-9.65%	1.03540	-1.39%	0.48068	-8.44%
NB5	23.125	115625	35.30%	-11.76%	1.02814	-2.08%	0.54588	3.98%
NB6	25.375	115625	36.35%	-9.14%	1.02789	-2.11%	0.48311	-7.98%
NB7	23.125	141875	37.65%	-5.89%	1.02170	-2.70%	0.5225	-0.48%
NB8	25.375	141875	40.38%	0.95%	1.02147	-2.72%	0.50979	-2.90%

In table 5.1, the feasible points are plotted in green circles on the general process window of relation between pressure and BHF. Unfeasible points are plotted in yellow circles as shown in figure 5.5. The first iteration, neighborhood 1 gives the feasible point which is split into four regions and evaluated in the next iteration. The second iteration, neighborhood 2 and 3 give the feasible points which are split into four regions and evaluated in the next iteration. The third iteration is considered to the final iteration due to the difference of pressure from second iteration and third iteration is lower than 5%. Neighborhood 1-4, 5 and 7 are the feasible points. In this part, 9 feasible points were determined after 16 neighborhoods (3 iterations) were evaluated as shown in figure 5.6.

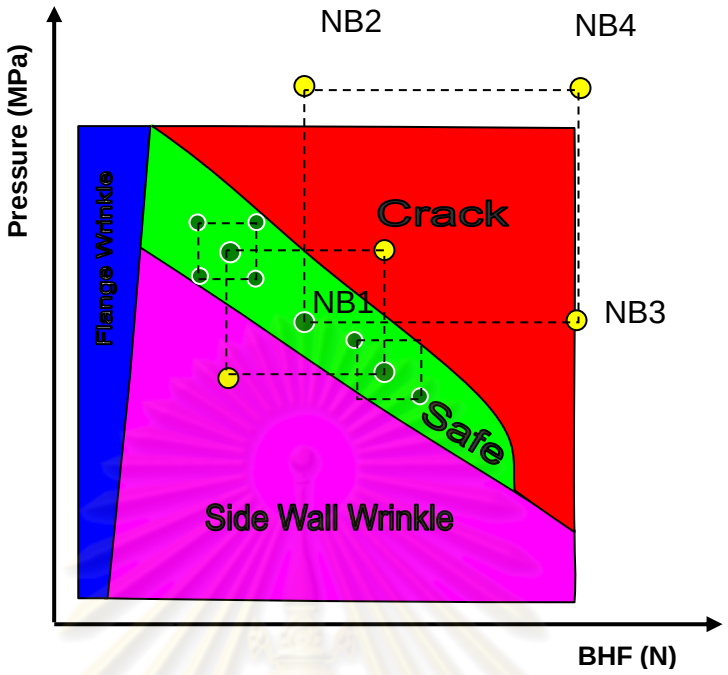

Figure 5.5 The results of 2-D interval halving method on the general process window of relation between pressure and BHF of Part1

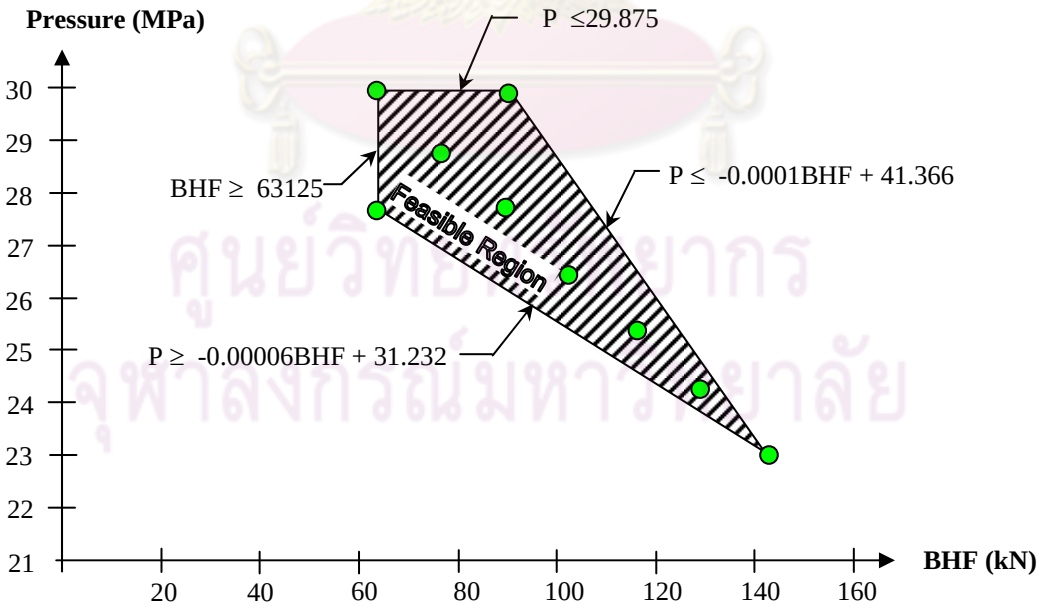

Figure 5.6 The feasible region with bound of Part1

For Part2, the 2-D interval halving method and the best quality for the center point (figure 5.4) were applied to find the minimum thinning. The solutions of Part2 were shown in table 5.2

Table 5.2 The solutions of combination between pressure and BHF searching by 2-D interval halving of Part2

Iteration 1	P (MPa)	BHF (N)	Thinning	Dist. Thin BD	FAM	Dist. FAM BD	SW	Dist. SW BD
NB1	19.5	112000	32.44%	-18.90%	1.03705	-1.23%	1.60412	205.55%
NB2	26.5	112000	40.59%	1.48%	1.03742	-1.20%	0.51716	-1.49%
NB3	19.5	224000	97.98%	144.95%	1.00370	-4.41%	0.00000	-100.00%
NB4	26.5	224000	97.15%	142.87%	1.00619	-4.17%	0.00000	-100.00%

Iteration 2	P (MPa)	BHF (N)	Thinning	Dist. Thin BD	FAM	Dist. FAM BD	SW	Dist. SW BD
NB1	24.75	84000	32.50%	-18.76%	1.04463	-0.51%	0.61328	16.82%
NB2	28.25	84000	34.35%	-14.12%	1.04587	-0.39%	0.49458	-5.79%
NB3	24.75	140000	93.52%	133.79%	1.02680	-2.21%	0.00000	-100.00%
NB4	28.25	140000	96.67%	141.68%	1.01489	-3.34%	0.00000	-100.00%

Iteration 3	P (MPa)	BHF (N)	Thinning	Dist. Thin BD	FAM	Dist. FAM BD	SW	Dist. SW BD
NB1	27.375	70000	32.51%	-18.74%	1.04972	-0.03%	0.51319	-2.25%
NB2	29.125	70000	33.76%	-15.60%	1.05050	0.05%	0.49873	-5.00%
NB3	27.375	98000	34.80%	-13.01%	1.04081	-0.88%	0.49589	-5.54%
NB4	29.125	98000	43.18%	7.96%	1.04121	-0.84%	0.49494	-5.73%

In table 5.2, the feasible points are plotted in green circles on the general process window of relation between pressure and BHF and unfeasible points are plotted in yellow circles as shown in figure 5.7. The first iteration, all neighborhoods do not give the feasible point. Hence, the minimum distance of all defects are measured and compared. In this case, neighborhood 2 is the representative of all defects because it has distance 1.48% from thin limit (it is cracked), -1.20% from FAM limit (it is not flange wrinkling) and -1.49% from SW limit (it is not side wall wrinkling). Clearly, neighborhood 2 able to be the best quality for the center point which is split into four regions and evaluated in the next iteration. The second iteration, neighborhood 2 gives

the feasible points which are split into four regions and evaluated in the next iteration. The third iteration is considered to the final iteration due to the difference of pressure from second iteration and third iteration is lower than 5%. Neighborhood 1 and 3 are the feasible points. In this part, 3 feasible points were determined after 12 neighborhoods (3 iterations) were evaluated as shown in figure 5.8.

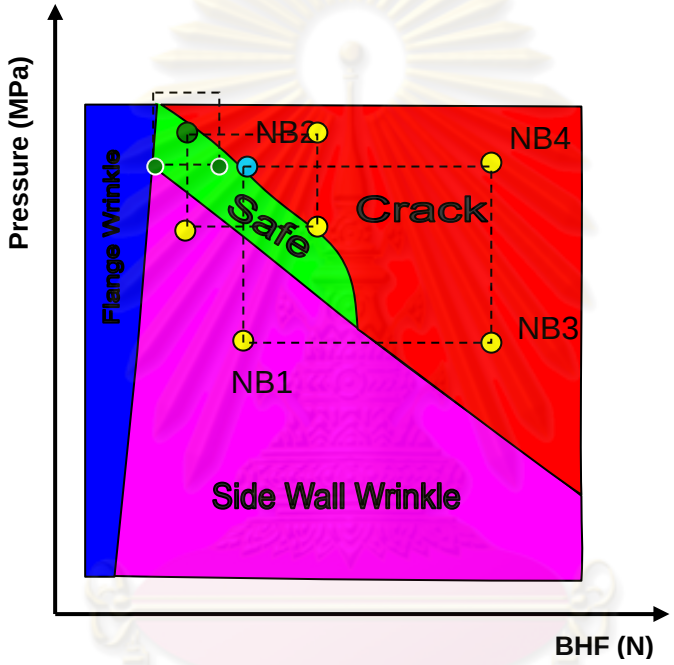

Figure 5.7 The results of 2-D interval halving method on the general process window of relation between pressure and BHF of Part2

ศูนย์วิทยทรัพยากร
จุฬาลงกรณ์มหาวิทยาลัย

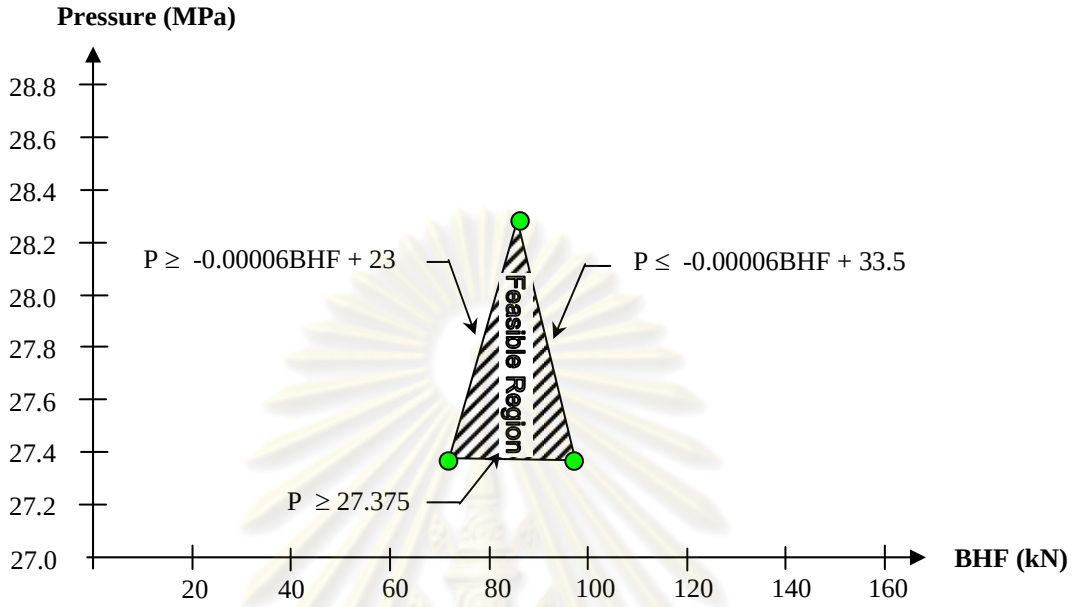

Figure 5.8 The feasible region with bound of Part2

For Part3, the 2-D interval halving method and the best quality for the center point (figure 5.4) were applied to find the minimum thinning. The solutions of Part3 were shown in table 5.3

Table 5.3 The solutions of combination between pressure and BHF searching by 2-D interval halving of Part3

Iteration 1	P (MPa)	BHF (N)	Thinning	Dist. Thin BD	FAM	Dist. FAM BD	SW	Dist. SW BD
NB1	17.25	166750	22.85%	-42.87%	1.02961	-1.94%	0.6467	23.18%
NB2	23.75	166750	24.25%	-39.37%	1.02756	-2.14%	0.526	0.19%
NB3	17.25	342250	27.42%	-31.44%	1.00623	-4.17%	0.53309	1.54%
NB4	23.75	342250	29.87%	-25.33%	1.00497	-4.29%	0.47989	-8.59%

Iteration 2	P (MPa)	BHF (N)	Thinning	Dist. Thin BD	FAM	Dist. FAM BD	SW	Dist. SW BD
NB1	22.125	298375	27.84%	-30.39%	1.00985	-3.82%	0.48131	-8.32%
NB2	25.375	298375	29.07%	-27.34%	1.00944	-3.86%	0.48194	-8.20%
NB3	22.125	386125	30.49%	-23.77%	1.00106	-4.66%	0.47924	-8.72%
NB4	25.375	386125	31.86%	-20.35%	1.00063	-4.70%	0.47261	-9.98%

Iteration 3	P (MPa)	BHF (N)	Thinning	Dist. Thin BD	FAM	Dist. FAM BD	SW	Dist. SW BD
NB1	21.3125	276437.5	26.98%	-32.54%	1.01245	-3.58%	0.49535	-5.65%
NB2	22.9375	276437.5	27.54%	-31.16%	1.01205	-3.61%	0.48538	-7.55%
NB3	21.3125	320312.5	28.32%	-29.20%	1.00777	-4.02%	0.48561	-7.50%
NB4	22.9375	320312.5	28.85%	-27.87%	1.00747	-4.05%	0.48294	-8.01%
NB5	24.5625	276437.5	28.11%	-29.73%	1.01196	-3.62%	0.48333	-7.94%
NB6	26.1875	276437.5	28.60%	-28.49%	1.01172	-3.65%	0.48153	-8.28%
NB7	24.5625	320312.5	29.49%	-26.27%	1.00710	-4.09%	0.48144	-8.30%
NB8	26.1875	320312.5	30.05%	-24.87%	1.00668	-4.13%	0.47758	-9.03%
NB9	21.3125	364187.5	29.58%	-26.05%	1.00335	-4.44%	0.48697	-7.24%
NB10	22.9375	364187.5	30.24%	-24.40%	1.00293	-4.48%	0.47864	-8.83%
NB11	21.3125	408062.5	30.67%	-23.32%	0.99937	-4.82%	0.48632	-7.37%
NB12	22.9375	408062.5	31.43%	-21.44%	0.99914	-4.84%	0.4781	-8.93%
NB13	24.5625	364187.5	30.83%	-22.92%	1.00268	-4.51%	0.47704	-9.14%
NB14	26.1875	364187.5	31.45%	-21.38%	1.00234	-4.54%	0.47246	-10.01%
NB15	24.5625	408062.5	32.15%	-19.63%	0.99890	-4.87%	0.47424	-9.67%
NB16	26.1875	408062.5	32.88%	-17.80%	0.99847	-4.91%	0.47291	-9.92%

In table 5.3, the feasible points are plotted in green circles on the general process window of relation between pressure and BHF and unfeasible points are plotted in yellow circles as shown in figure 5.9. The first iteration, neighborhood 4 gives the feasible point which is split into four regions and evaluated in the next iteration. The second iteration, all neighborhoods give the feasible points which are split into four regions and evaluated in the next iteration. The third iteration is considered to the final iteration due to the difference of pressure from second iteration and third iteration is lower than 5%. All neighborhoods are the feasible points. In this part, 21 feasible points were determined after 24 neighborhoods (3 iterations) were evaluated as shown in figure 5.10.

ศูนย์วิทยทรัพยากร
จุฬาลงกรณ์มหาวิทยาลัย

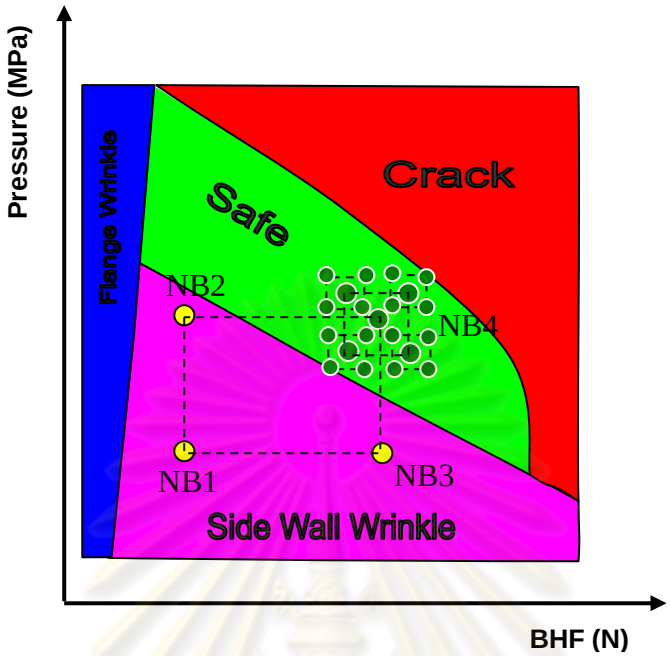

Figure 5.9 The results of 2-D interval halving method on the general process window of relation between pressure and BHF of Part3

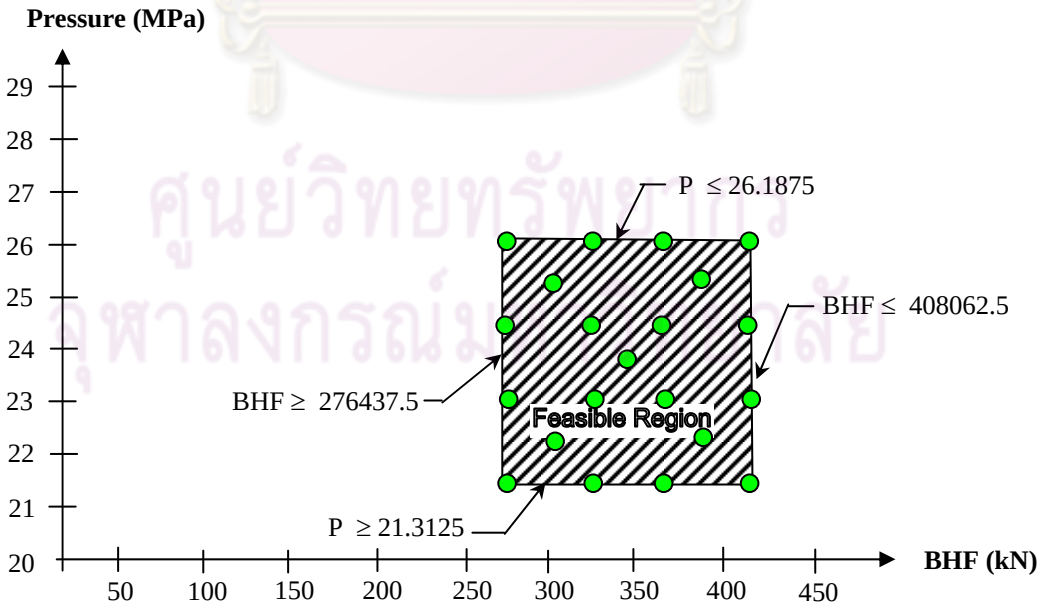

Figure 5.10 The feasible region with bound of Part3

These feasible regions of three parabolic parts are shown in figure 5.6, 5.8 and 5.10. Then, the optimization goal becomes only to determine the best process parameters within this feasible region (i.e. BHF and max. pressure) that minimize part thinning.

5.3 Response surface method (RSM)

The points from 2-D interval halving method are representatives of feasible values. To find the minimize thinning, the feasible region will be established. The feasible regions of three parts are fitted in quadratic polynomial form shown in Eq. 5.4 (Huang, Lo et al. 2006). The RSM was used to describe relationship between the process parameters (i.e. BHF and maximum pressure) and resultant part thinning percentage, Eq. 5.5.

$$y = \beta_0 + \sum_{j=1}^{k} \beta_j x_j + \sum_{j=1}^{k} \beta_{jj} x_j^2 + \sum_{i=1}^{k-1} \sum_{j=i+1}^{k} \beta_{ij} x_i x_j \qquad (5.4)$$

$$Thinning = \beta_0 + \beta_1 BHF + \beta_2 P + \beta_3 BHF \cdot P + \beta_4 BHF^2 + \beta_5 P^2 \qquad (5.5)$$

ศูนย์วิทยทรัพยากร
จุฬาลงกรณ์มหาวิทยาลัย

Using the least square polynomial approximation, the response surface over the feasible region of Part1, which has been determined through the 2-D interval halving method, is given in Eq. 5.6 to Eq. 5.10.

$$Thinning = 30.6408 - 1.39969 \times 10^{-4} BHF + 0.0322575 P + 4.88183 \times 10^{-6} BHF \cdot P + 5.02062 \times 10^{-10} BHF^2 \qquad (5.6)$$

Subjected to:

$$P \leq 29.875 \quad (5.7)$$

$$BHF \geq 63125 \quad (5.8)$$

$$P \leq -1.28571E\text{-}04BHF + 41.366 \quad (5.9)$$

$$P \geq -5.17429E\text{-}05BHF + 31.232 \quad (5.10)$$

The feasible values of BHF and pressure from 2-D interval halving method are calculated with Eq. 5.6 to compare the thinning from finite element simulation. The errors were shown in table 5.4. The error percentages were lower than 0.25%, so the Eq. 5.6 can calculate the thinning from BHF and pressure in constraints from Eq. 5.7 - 5.10.

Table 5.4 The thinning comparison of FEM and Eq. 5.6 of Part1

BHF	Pressure	Thinning (FEM)	Thinning (Eq. 5.6)	Error	%Error
102500	26.5	35.69	35.68386	0.006139	0.02%
76250	28.75	34.43	34.51647	-0.08647	-0.25%
128750	24.25	36.94	36.96649	-0.02649	-0.07%
63125	27.625	33.21	33.21004	-4.2E-05	0.00%
63125	29.875	34.02	33.97599	0.044006	0.13%
89375	27.625	35.11	35.08576	0.024238	0.07%
89375	29.875	36.14	36.14005	-4.7E-05	0.00%
141875	23.125	37.65	37.65101	-0.00101	0.00%
115625	25.375	36.35	36.31077	0.039231	0.11%

The approximated response surface of Part1 is shown in figure 5.11. Simplex method was applied to locate the optimal point, i.e. the lowest point of the surface. The optimal point is BHF of 63,125 N and maximum pressure of 27.625 MPa for the quarter model, resulting in part maximum thinning of 33.21%. In the same condition the finite element method conducts the maximum thinning as 33.21% that is the same value from Eq. 5.6 and gives FAM as 1.046 mm (no flange wrinkle), SW as 0.489 (no side wall wrinkle). The strain paths of thinnest elements (near the punch nose area) is in the biaxial stage which have the major strain (ε_1) as 0.311 and the minor strain (ε_2)

as 0.0948. Therefore, the part will be thinned before crack. The solutions were shown in figure 5.12.

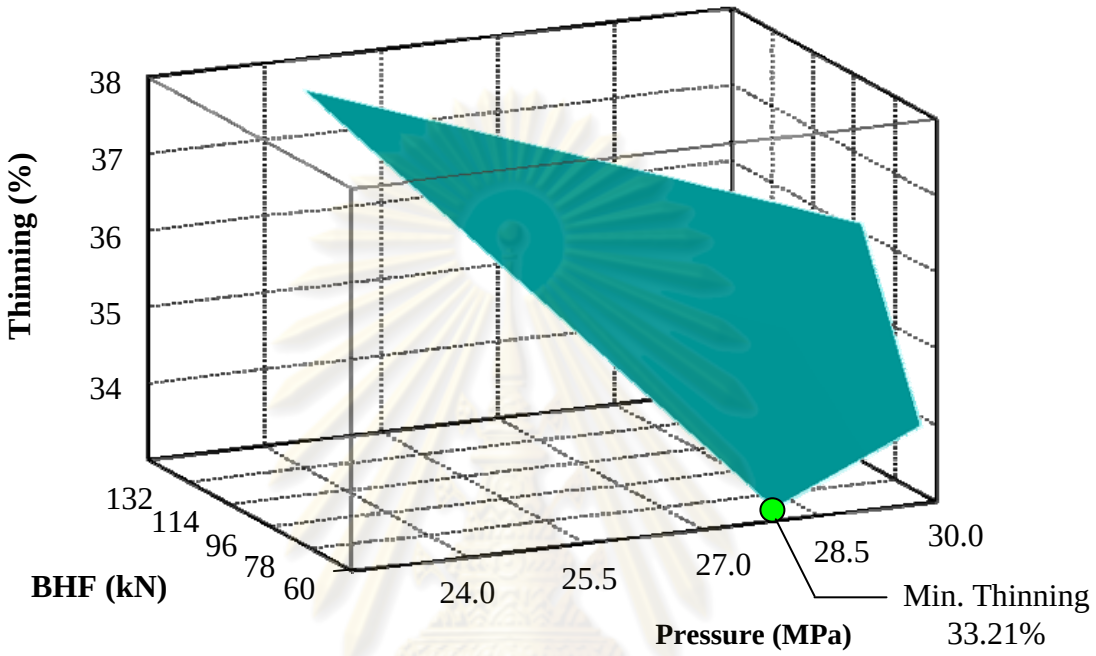

Figure 5.11 Part thinning response surface of two variables; BHF and P with constraints of Part1

The feasible points of Part2, which has been determined through the 2-D interval halving method, have 3 points that are not enough to generate the quadratic surface. However, the 3 points can create the flat triangular surface that shown in figure 5.13. The lowest point from feasible region is BHF of 70,000 N and maximum pressure of 27.375 MPa for the quarter model, resulting in part maximum thinning of 32.50%. This condition gives FAM as 1.050 mm (no flange wrinkle), SW as 0.513 (no side wall wrinkle). The strain paths of thinnest elements (near the punch nose area) is in the biaxial stage which have the major strain (ε_1) as 0.314 and the minor strain (ε_2) as 0.0804. Therefore, the part will be thinned before crack. The solutions were shown in figure 5.14.

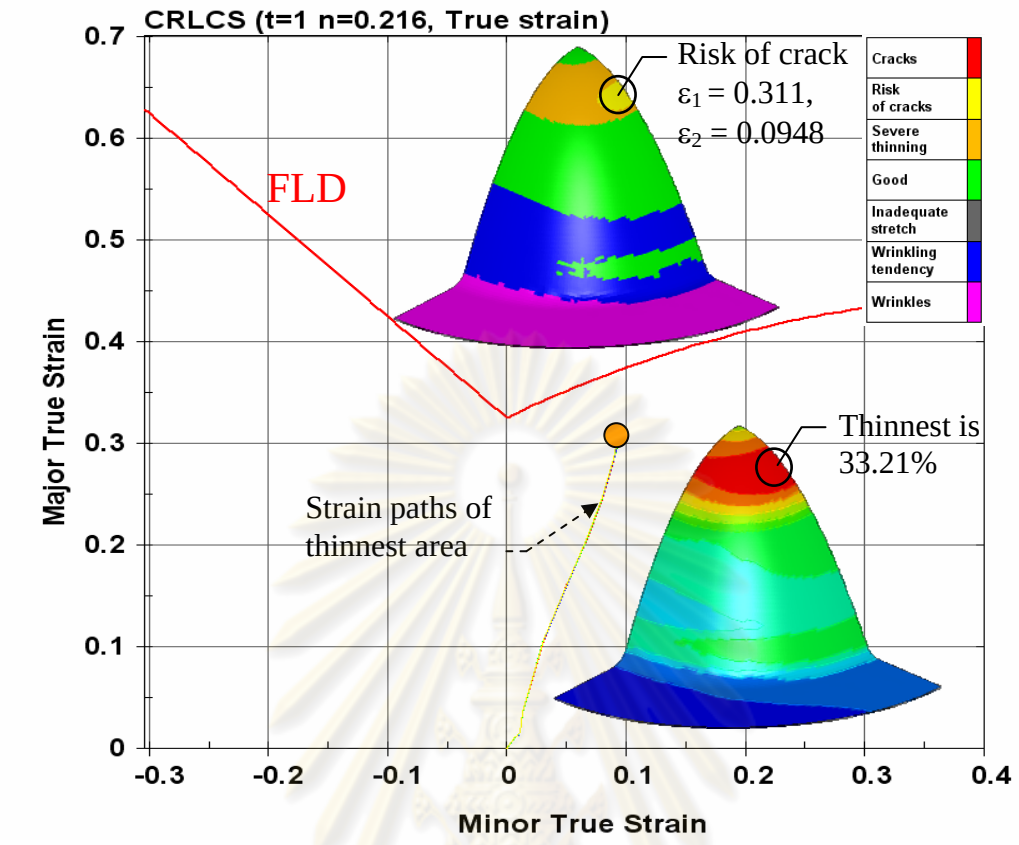

Figure 5.12 The solutions of Part1 are conducted with optimal BHF as 63,125 N (for quarter) and optimal pressure as 27.625 MPa

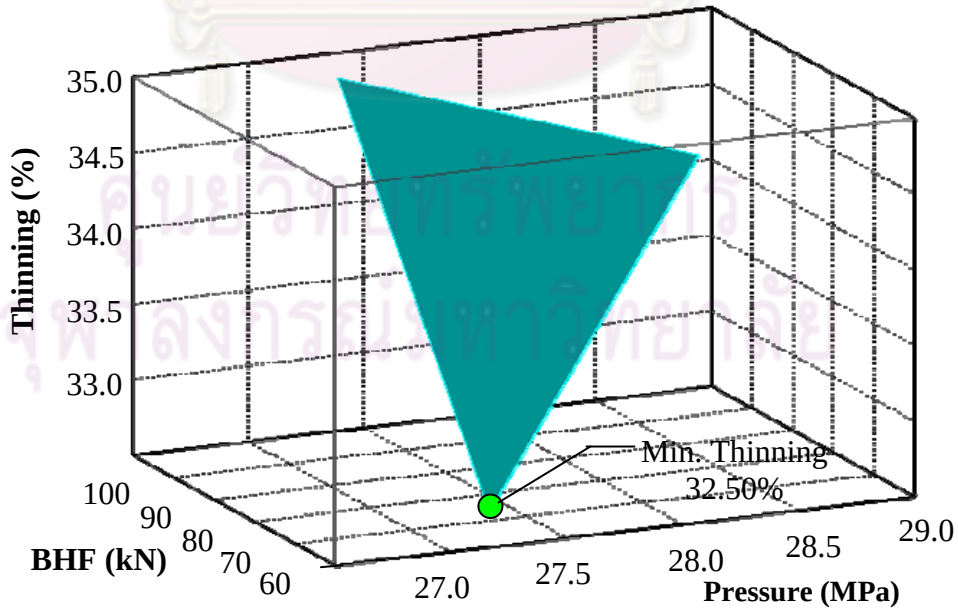

Figure 5.13 Part thinning response surface of two variables; BHF and P with constraints of Part2

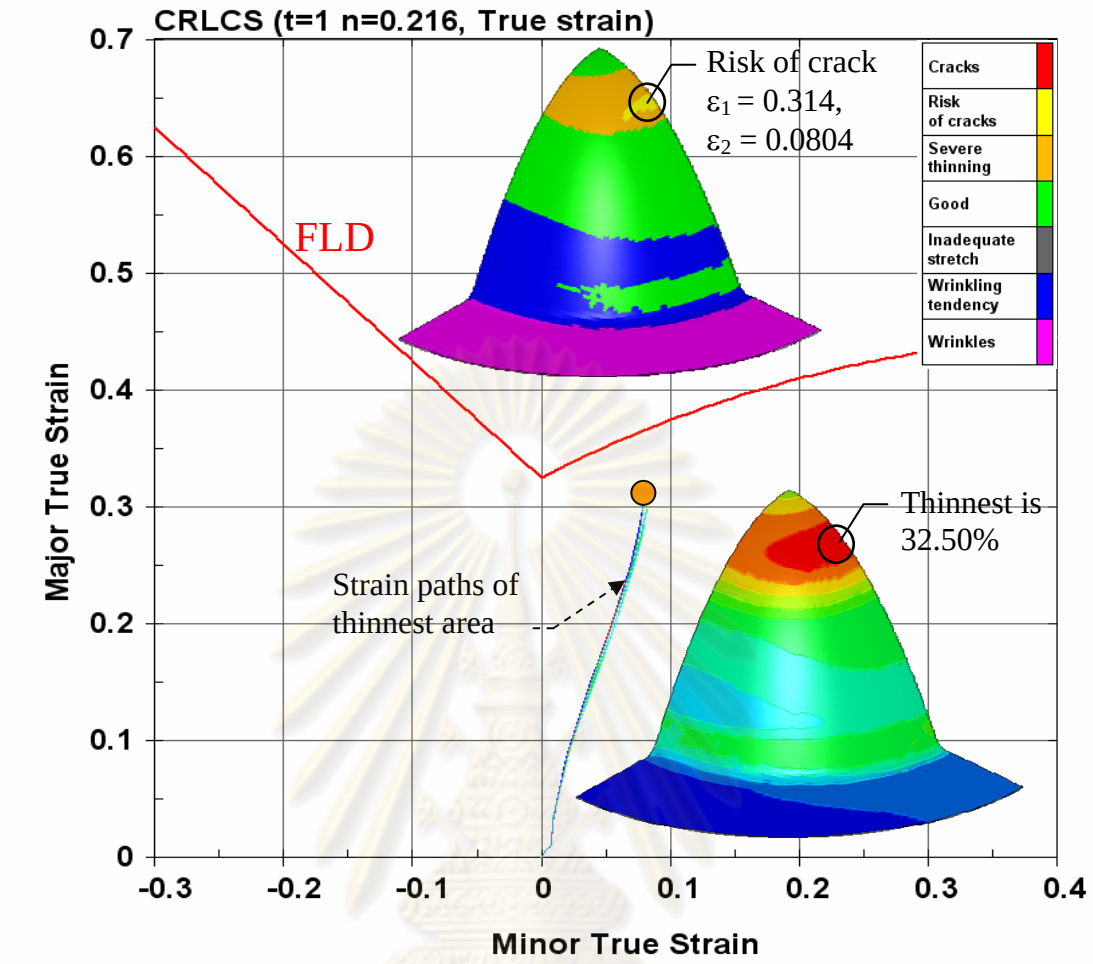

Figure 5.14 The solutions of Part2 are conducted with optimal BHF as 70,000N (for quarter) and optimal pressure as 27.375 MPa

Using the least square polynomial approximation, the response surface over the feasible region of Part3, which has been determined through the 2-D interval halving method, is given in Eq. 5.11 to Eq. 5.15.

Part3:

$$Thinning = 13.8118 + 2.10516\times10^{-5}\,BHF + 0.225859P + 8.08905\times10^{-7}\,BHF\cdot P - 1.44455\times10^{-11}\,BHF^{2} - 0.00248344\quad P^{2} \tag{5.11}$$

Subjected to:

$$P \geq 21.3125 \quad (5.12)$$

$$P \leq 26.1875 \quad (5.13)$$

$$BHF \geq 276437.5 \quad (5.14)$$

$$BHF \leq 408062.5 \quad (5.15)$$

The feasible values of BHF and pressure from 2-D interval halving method are calculated with Eq. 5.11 to compare the thinning from finite element simulation. The errors were shown in table 5.5. The error percentages were lower than 0.32%, so the Eq. 5.11 can calculate the thinning from BHF and pressure in constraints from Eq. 5.12 - 5.15.

Table 5.5 The thinning comparison of FEM and Eq. 5.11 of Part3

BHF	Pressure	Thinning (FEM)	Thinning (Eq. 5.11)	Error	%Error
342250	23.75	29.87	29.86311	0.006895	0.02%
298375	22.125	27.84	27.92849	-0.08849	-0.32%
298375	25.375	29.07	29.06357	0.006435	0.02%
386125	22.125	30.49	30.47857	0.011431	0.04%
386125	25.375	31.86	31.84433	0.01567	0.05%
276438	21.3125	26.98	26.97868	0.001316	0.00%
276438	22.9375	27.54	27.5305	0.0095	0.03%
320313	21.3125	28.32	28.2805	0.0395	0.14%
320313	22.9375	28.85	28.88999	-0.03999	-0.14%
276438	24.5625	28.11	28.0692	0.0408	0.15%
276438	26.1875	28.6	28.59478	0.005216	0.02%
320313	24.5625	29.49	29.48636	0.003639	0.01%
320313	26.1875	30.05	30.06962	-0.01962	-0.07%
364188	21.3125	29.58	29.5267	0.053299	0.18%
364188	22.9375	30.24	30.19386	0.046139	0.15%
408063	21.3125	30.67	30.71729	-0.04729	-0.15%
408063	22.9375	31.43	31.44212	-0.01212	-0.04%
364188	24.5625	30.83	30.84791	-0.01791	-0.06%
364188	26.1875	31.45	31.48883	-0.03883	-0.12%
408063	24.5625	32.15	32.15384	-0.00384	-0.01%
408063	26.1875	32.88	32.85244	0.027563	0.08%

The approximated response surface is shown in figure 5.15. Simplex method was applied to locate the optimal point, i.e. the global lowest point of the surface. The optimal point is BHF of 276,437.5 N and maximum pressure of 21.3125 MPa for the quarter model, resulting in part maximum thinning of 26.98%. In the same condition the finite element method conducts the maximum thinning as 26.98% that is the same value from Eq. 5.11 and gives FAM as 1.012 mm (no flange wrinkle), SW as 0.495 (no side wall wrinkle). The strain paths of thinnest elements (near the punch nose area) is in the biaxial stage which have the major strain (ε_1) as 0.230 and the minor strain (ε_2) as 0.0866. Therefore, the part will be thinned before crack. The solutions were shown in figure 5.16.

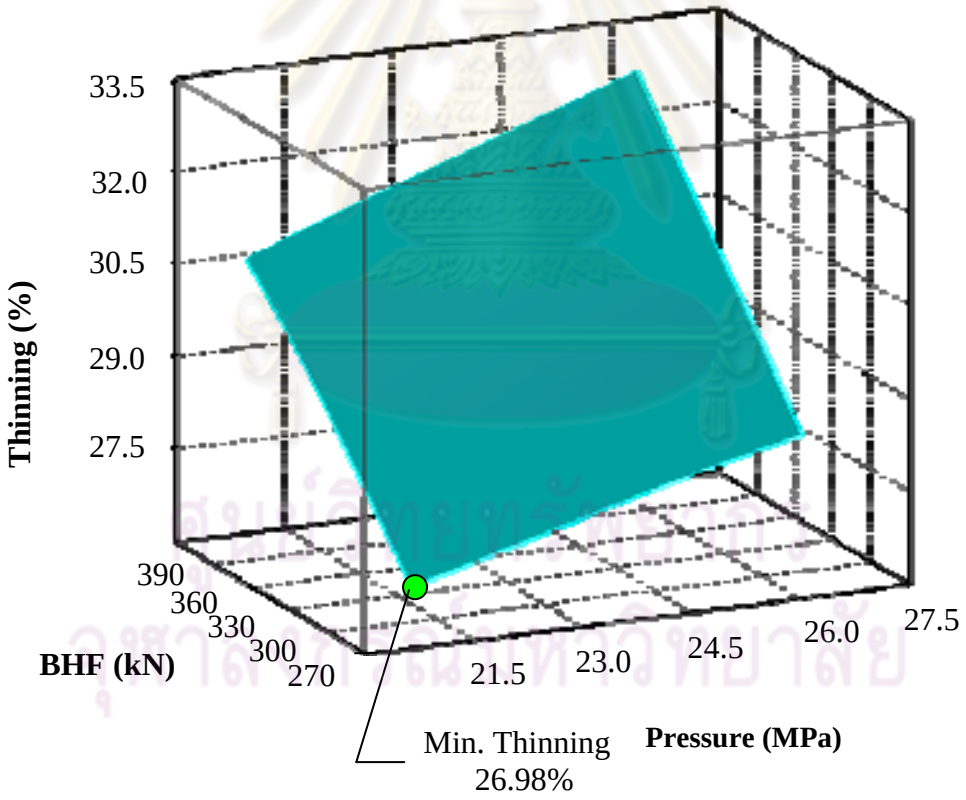

Figure 5.15 Part thinning response surface of two variables; BHF and P with constraints of Part3

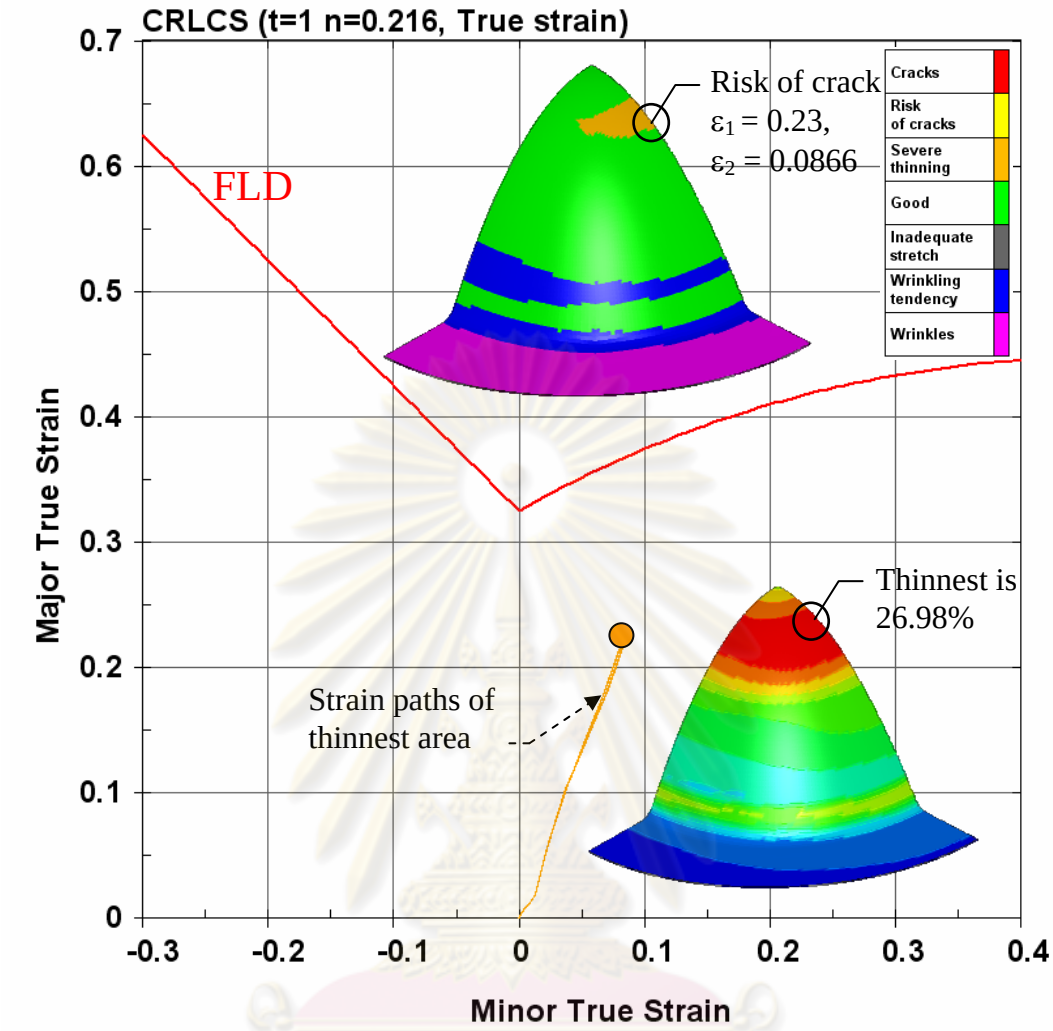

Figure 5.16 The solutions of Part3 are conducted with optimal BHF as 276,437.5 N (for quarter) and optimal pressure as 21.3125 MPa

5.4 Conclusion and discussion

The response surface method coupled with the 2-D interval halving method was applied to optimize the necessary process parameters of the constant blank holder force and linear pressure profiles for the hydromechanical deep drawing of parabolic shaped cups. The 2-D interval halving method was found to be well suited for feasible region search in a large search space such as the metal forming parameters. The response surface method was used to construct a response surface of the process

parameters in the feasible region and corresponding part quality. The constructed surface was then used to determine the optimal point using the simplex optimization method. Based on the finite element simulation results for hydromechanical deep drawing of the Part1 parabolic cup, the optimal blank holder force and maximum pressure of the quarter model were determined to be 63,125 N and 27.625 MPa, which resulted in a good part with only 33.21% thinning. The Part2 parabolic cup, the optimal blank holder force and maximum pressure of the quarter model were determined to be 70,000 kN and 27.375 MPa, which resulted in a good part with only 32.51% thinning. The Part3 parabolic cup, the optimal blank holder force and maximum pressure of the quarter model were determined to be 276,437.5 kN and 21.3125 MPa, which resulted in a good part with only 26.98% thinning. This FEA based optimization approach developed and implemented in this work is to reduce lead time and effort spent in the HMD process parameter design significantly.

ศูนย์วิทยทรัพยากร
จุฬาลงกรณ์มหาวิทยาลัย

CHAPTER VI

AUTOMATIC APPROACH TO SELECT LOADING PATH IN HYDROMECHANICAL DEEP DRAWING OF PARABOLIC PARTS USING ADAPTIVE FEA SIMULATION COUPLED WITH FUZZY LOGIC

This chapter mainly discusses the development of the adaptive simulation approach coupled with fuzzy logic. A computer program with Compaq Visual FORTRAN 6.0 was written and interfaced with LS-DYNA to implement this adaptive simulation. A fuzzy logic control algorithm coupled with adaptive finite element analysis simulation has been developed to determine pressure and blank holder force profiles simultaneously in hydromechanical deep drawing. Thinning, flange wrinkling, side wall wrinkling and draw-in velocity was used as criteria in the fuzzy logic control algorithm. The linear predictive function was used firstly to find loading curves of three parabolic cups in one hundred monitoring steps and found that the loading profiles of three parts were better fitted by an exponential equation. Therefore, the exponential prediction was applied to reduce monitoring steps in determination of loading paths of three parabolic cups. Effectiveness of the exponential prediction was later evaluated by HMD of a much bigger reflector in parabolic shape. The developed algorithm was able obtained the pressure and blank holder profiles rapidly.

ศูนย์วิทยทรัพยากร
จุฬาลงกรณ์มหาวิทยาลัย

6.1 Adaptive FEA simulation

The goal of the adaptive simulation approach is to completely eliminate the trial-and-error simulation approach and to generate feasible process parameter curves within only a few or just one simulation run.

In adaptive simulation, the process parameters for the next simulation step are to be predicted to proper values based on the forming part quality information collected

from the past and current simulation monitoring steps. In other words, during a forming process simulation run, the simulation intermediate results about forming part qualities (i.e. part wrinkles, part thinning, and etc) up to the current monitoring step is deduced through knowledge of HMD for parabolic behavior and then used it to calculate/project appropriate process parameters for the next simulation monitoring step. This is in contrast to the traditional application of FE process simulations where only the simulation results at the final step are considered and used to infer parameter adjustments for the next trial simulation run in an attempt to improve/optimize the forming process.

The adaptive simulation approach relies on ability to detect/identify an existence of defects (i.e. wrinkling and fracture) in the part being formed, and appropriate adjustments of the relevant process parameters to correct these defects during the following simulation monitoring steps.

The explicit non-linear FEA, LS-DYNA can be run as a command in the DOS operation system, so that the LS-DYNA process simulation and the related calculation programs coded with Compaq Visual FORTRAN 6.0 could be integrated in this study as a batch or a script file for DOS to fulfill the optimization process. The optimization process could then be executed by setting the related parameters in the input file and by launching the batch file. This methodology was used in by Fann and Hsiao 2003. However, they applied Visual C++ instead of Compaq Visual FORTRAN 6.0. The figure 6.1 is shown a general conceptual flow chart of the adaptive simulation interfacing with LS-DYNA.

ศูนย์วิทยทรัพยากร
จุฬาลงกรณ์มหาวิทยาลัย

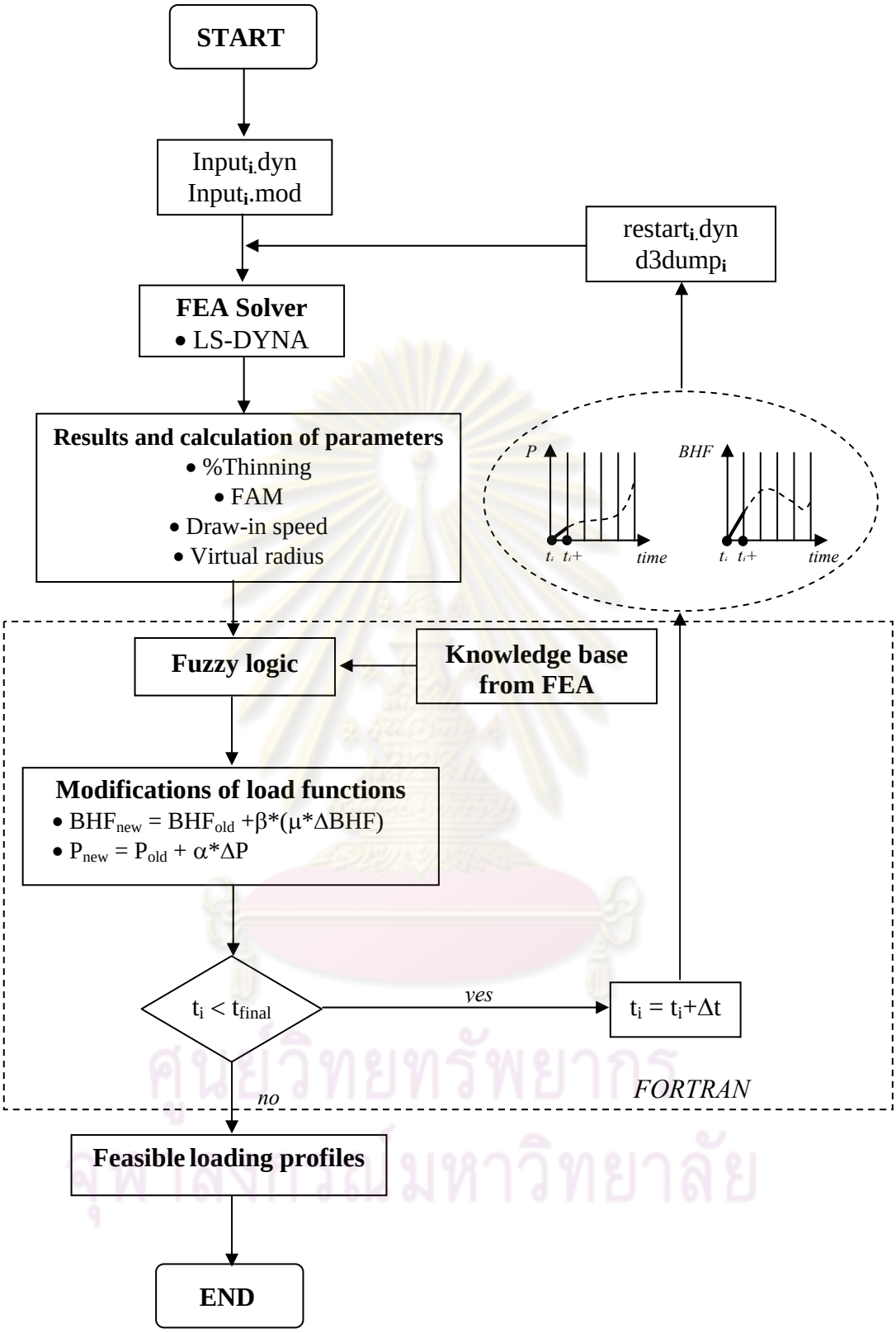

Figure 6.1 A general conceptual flow chart of the adaptive simulation interfacing with LS-DYNA

ศูนย์วิทยทรัพยากร
จุฬาลงกรณ์มหาวิทยาลัย

6.2 Fuzzy logic control

Fuzzy logic is a research area based on the principles of approximate reasoning and computational intelligence. Fuzzy models are employed in cases where a system is difficult to model exactly (but an inexact model is available), or ambiguity and imprecision is encountered in the problem formulation. It uses linguistic variables (e.g. small, medium, large), and a continuous range of truth-values in the interval [0, 1] (Klir and Yuan, 1995).

The most successful application area of fuzzy systems has definitely been the area of fuzzy control. In general, fuzzy controllers are special expert systems. Each employs a knowledge base, expressed in term of relevant fuzzy inference rules, and an appropriate inference engine to solve a given control problem. The knowledge of an experienced human operator may be used as an alternative to a precise model of the controlled process. While this knowledge is also difficult to express in precise terms, an imprecise linguistic description of the manner of control can usually be articulated by operator with relative ease. This linguistic description consists of a set of control rules that make use of fuzzy propositions. A typical form of these rules is exemplified by the rule

IF the thinning is very critical

AND the FAM is not critical

THEN the blank holder force change should be decreased.

where thinning and FAM are the observed state variables of the process, and blank holder force change is the action to be taken by the controller. The vague term *very critical*, *not critical* and *decreased* can be conveniently represented by fuzzy sets defined on the universes of this course of thinning values, FAM values and blank holder force change values, respectively. This type of linguistic rule has formed the basis for the design of a great variety of fuzzy controllers (Klir and Yuan, 1995).

A general fuzzy controller consists of four modules: a *fuzzy rule base*, a *fuzzy inference engine*, and *fuzzication/defuzzification* modules. The interconnections

among these modules and the controlled process are shown in figure 6.2. (Klir and Yuan, 1995)

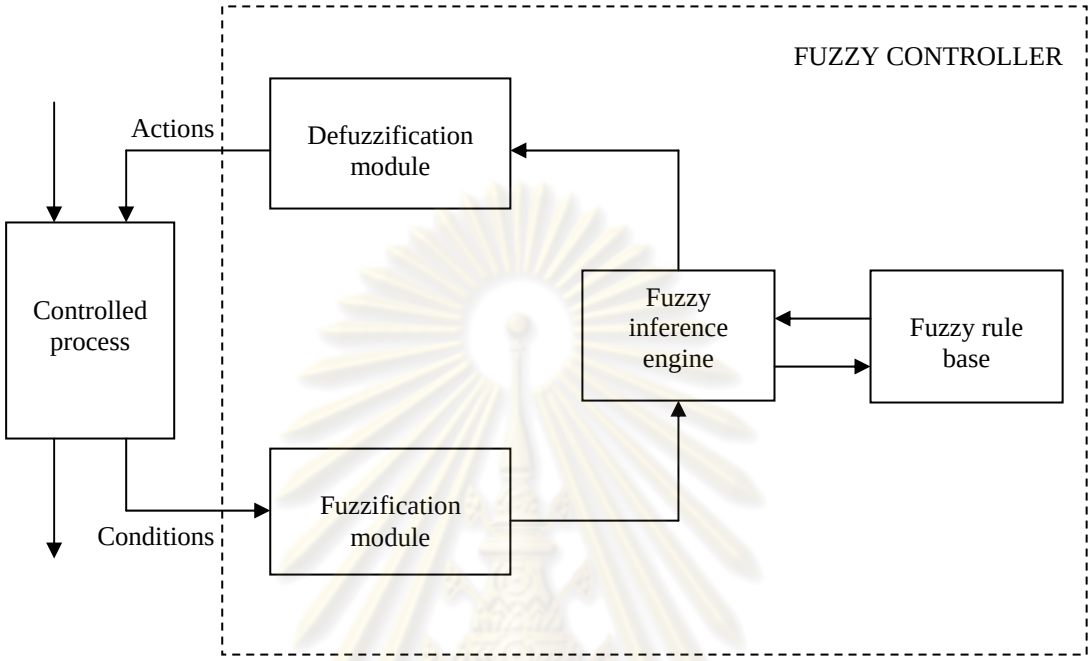

Figure 6.2 A general scheme of fuzzy controller

A fuzzy controller operates by repeating a cycle of the following four steps. First, measurements are taken of all variables that represent relevant conditions of the controlled process. Next, these measurements are converted into appropriate fuzzy sets to express measurement uncertainties. This step is called *fuzzification*. Expert knowledge can be stored in a fuzzy system's IF-THEN rules. This transfer of knowledge in the system can take place either by the manual definition of the *fuzzy rule base*. After the fuzzy rule base is defined, the system is capable of making inferences (*fuzzy inference engine*). The fuzzified measurements are then used by the inference engine to evaluate the control rules stored in the fuzzy rule base. The result of this evaluation is a fuzzy set (or several fuzzy sets) defined on the universe of possible actions. This fuzzy set is then converted, in the final step of the cycle, into a single (crisp) value (or a vector of values) that, in some sense, is the best representative of the fuzzy set (or fuzzy set). This conversion is called a

defuzzification. The defuzzified values represent actions taken by the fuzzy controller in individual control cycles.

In this work, to determine feasible counter pressure and blank holder force profiles rapidly, an adaptive FEA approach with the fuzzy control algorithm was implemented. At the beginning of each monitoring step, the input variables such as thinning, FAM, draw-in speed and bulge height, were detected in the user subroutine. Then, the degrees (0–1) of the fuzzy memberships (vCR; very critical, CR; critical, nCR; not critical) for each input variable were determined based on the input membership function. Based on the rule-based matrix, the degrees of fuzzy memberships of the output were determined. Finally, crispy outputs (α, β, μ) were calculated followed by the determination of BHF_{t+1} (blank holder force) and P_{t+1} (chamber pressure).

6.3 Fuzzy controller process

Fuzzy inference process comprises of five parts: 1) linguistic states, 2) fuzzification function, 3) fuzzy inference rules, 4) inference engine, and 5) defuzzification.

6.3.1 Fuzzy controller for the blank holder force

In the HMD process of parabolic part, thinning usually occurs around the punch nose region because of tensile stress induced by *pressure* and *blank holder force* that hold the blank material, as well as friction between the punch and blank. Therefore, the blank holder force parameter has affected directly on thinning. Moreover, the blank holder force also has an influence on the flange wrinkle, which can be checked by FAM and draw-in speed. The thinning and flange wrinkle variables progress in the opposite directions. This means that the excessive blank holder force leads to more thinning while keeping the flange wrinkle down, and on the other hand, insufficient blank holder force leads to flange wrinkle while results in less thinning.

To control the blank holder force, the thinning, flange wrinkle amplitude (FAM) and draw-in speed are variables to be considered as inputs. The coefficient (μ) to scale the initial incremental of blank holder force (ΔBHF) and weight factor (β) of the incremental of blank holder force (μ*ΔBHF) are the outputs. The schematic to control the blank holder force by fuzzy logic is shown in figure 6.3.

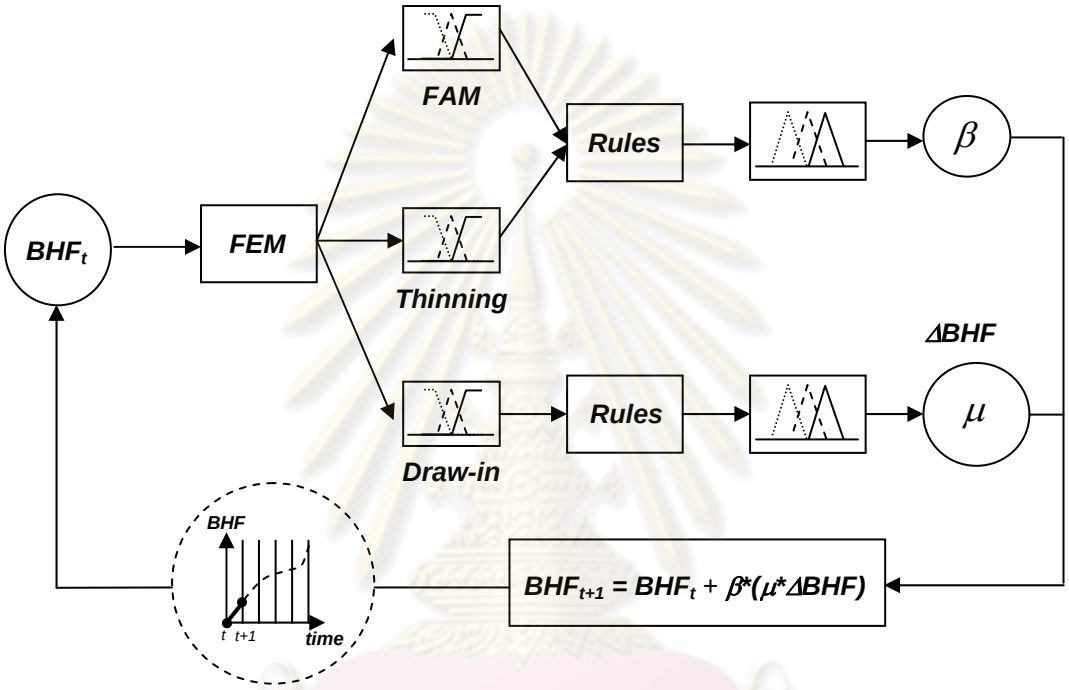

Figure 6.3 The fuzzy controlling schematic of the blank holder force

The percentage of thinning was determined by calculating ratio of the difference between initial blank thickness and current part thickness with initial blank thickness. The maximum value was saved to be used in the fuzzy control algorithm (Thinning).

The flange wrinkle was detected by distance between the binder and counter pot. The maximum value was used as an input variable in the fuzzy control algorithm (FAM).

The draw-in velocity was calculated by blank outline speed. The maximum value was used as an input variable in the fuzzy control algorithm (Draw-in).

6.3.1.1 Linguistic states

After identifying relevant input and output variables of the controller. The next step is selection meaningful linguistic states for each variable and expresses them by appropriate fuzzy sets. In this case, these fuzzy sets are fuzzy member, which represent linguistic labels as

vCR – very critical	NEG – negative (decrease)
CR – critical	ZERO – zero (hold)
nCR – not critical	POS – positive (increase)
SLO – slow	SLI – slight
FAS – fast	MOD – moderate
vFA – very fast	EXT – extreme

These linguistic states will be fuzzified with triangular-shape that are equally spread over each range in the next state.

6.3.1.2 Fuzzification function

In this step, a fuzzification function is introduced for each input variable to express the associated measurement uncertainty. The purpose of the fuzzification function is to interpret measurement of input variables, each expressed by a real number.

A membership function is a curve that defines how each point in the input space is mapped to a membership value (or degree of membership) between 0 and 1. The input membership values are used as weighting factors in the fuzzy rules to determine their influence on the fuzzy output sets of the final output conclusion. Once the functions are inferred, scaled, and combined, they are defuzzified into a crisp output, which drives the control system. Therefore, the membership function is important factor for giving accuracy of the system responses.

A triangular-shape is applied for all input and output variables. A full of triangular membership function (Trimf) is shown in figure 6.4.

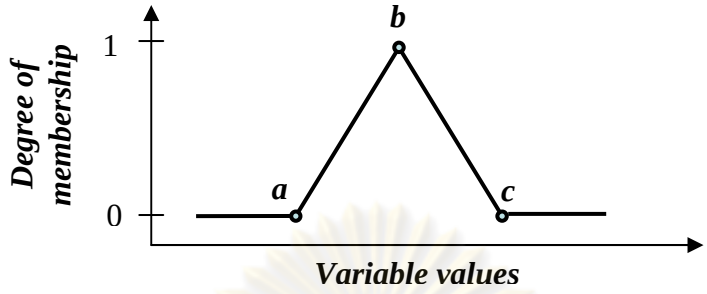

$$\text{Trimf}(x: a,b,c) = \begin{cases} 0; & x \le a \\ (x - a)/(b - a); & a < x < b \\ 1; & x = b \\ (c - x)/(c - b); & b < x < c \\ 0; & x \ge c \end{cases}$$

Figure 6.4 The full triangular membership function

The halves of triangular have two sides the right hand side and the left hand side are shown in figure 6.5.

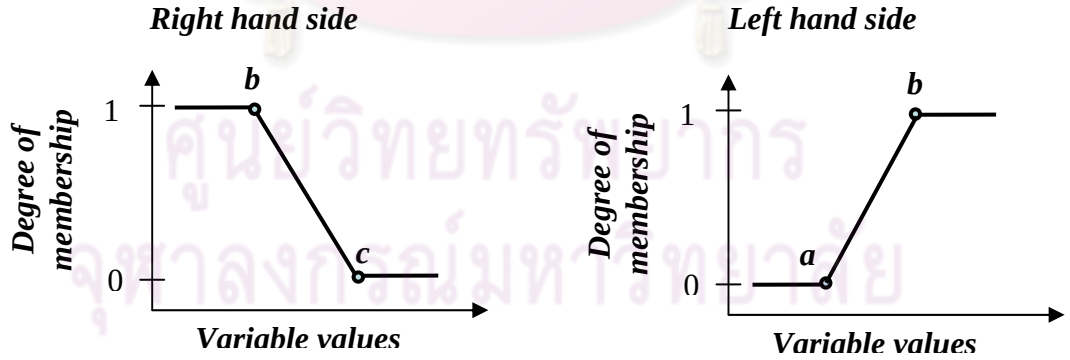

$$\text{Trimf}(x: b,c) = \begin{cases} 1; & x \le b \\ (c - x)/(c - b); & b < x < c \\ 0; & x \ge c \end{cases} \qquad \text{Trimf}(x: a,b) = \begin{cases} 0; & x \le a \\ (x - a)/(b - a); & a < x < b \\ 1; & x \ge b \end{cases}$$

Figure 6.5 The half triangular membership function

In chapter 4, we found that the typical part thinning is in the range of 20 to 40% with correct pressure and blank holder force. More than 40% thinning is likely to result in fracture, so it is very critical obviously, if the thinning is over than the 40%. The thinning less than 20% is not critical clearly due to it is the minimum value in the range. The middle value of the range as 30% is obviously critical. The very critical and not critical are defined with half triangular membership function, and the critical is defined with full triangular membership function. Figure 6.6 is the thinning membership function.

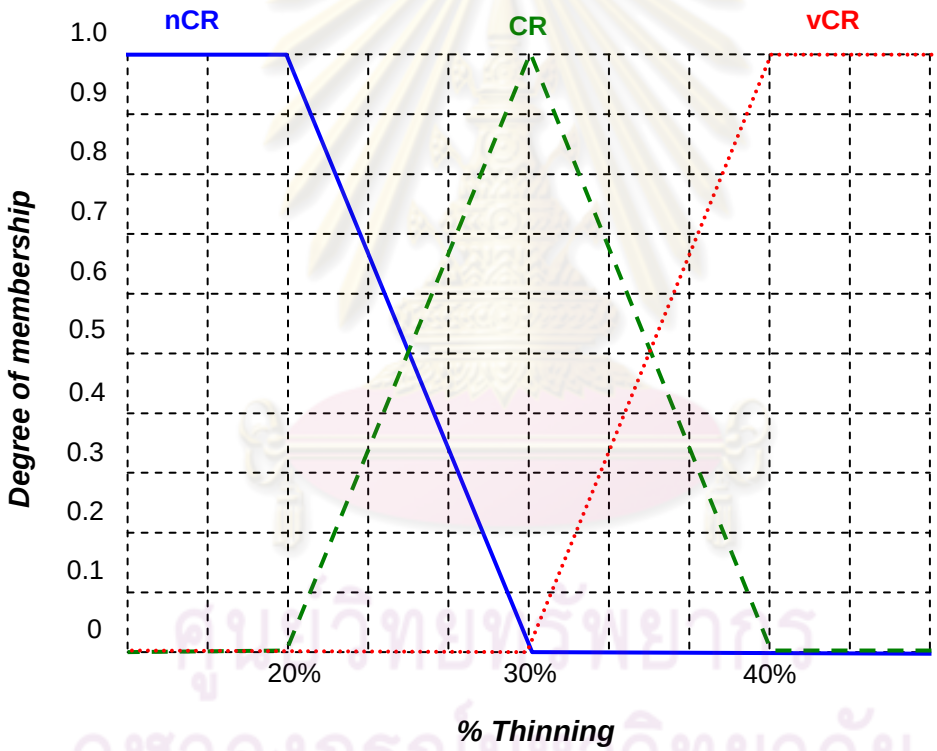

Figure 6.6 The thinning membership function

The flange wrinkle quantified by the index FAM. The FAM that becomes over its limit (1.05) is very critical surely. The initial blank thickness (1.00) is defined the minimum value of FAM membership function. For equally spread triangular-shape, the middle values as 1.025 is critical certainty. The very critical and not critical are

defined with half triangular membership function, and the critical is defined with full triangular membership function. Figure 6.7 is the FAM membership function.

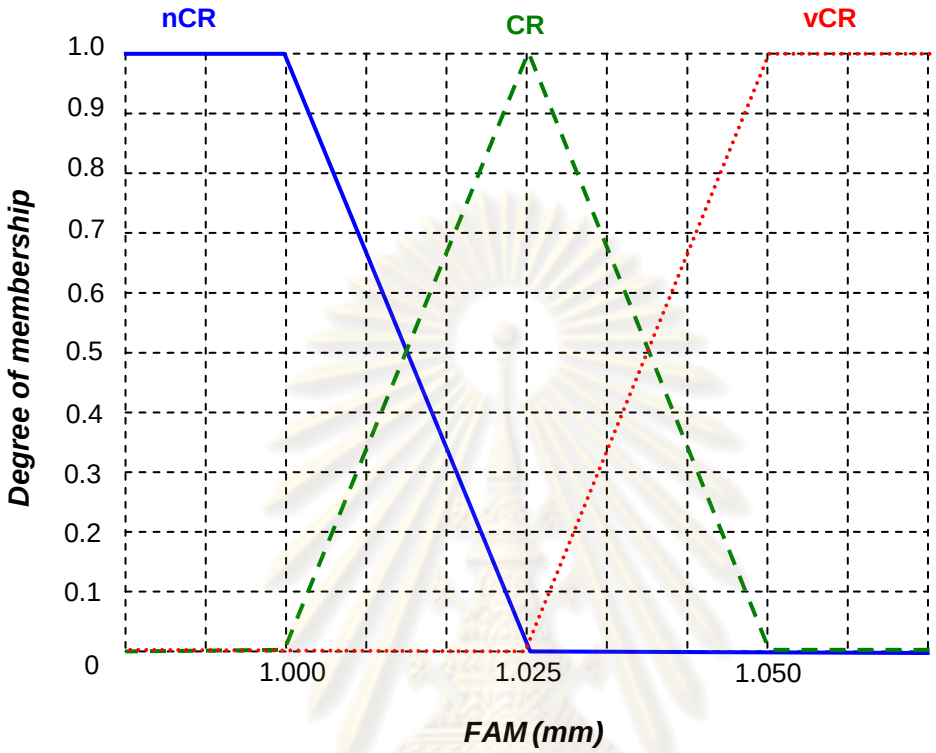

Figure 6.7 The FAM membership function

The output of weight factor (β) membership function is defined with full triangular, the center of positive value is +1, the center of zero is 0, and the center of negative value is -1 as shown in figure 6.8.

The draw-in speed versus time curve taken from a good part and wrinkled part as shown in figure 6.9. Most data in the beginning of the forming are under 500 m/s. The data in range between 500 – 1,500 m/s are found in the wrinkle stage, and maximum around 2,500 m/s is found near the end of stroke. Hence, the speed over 2,500 m/s is very fast exactly while; the speed under 500 m/s is slow. For equally spread triangular-shape, the middle values as 1,500 m/s is fast certainty. The very fast and slow are defined with half triangular membership function, and the fast is defined

with full triangular membership function. Figure 6.10 is the draw-in speed membership function.

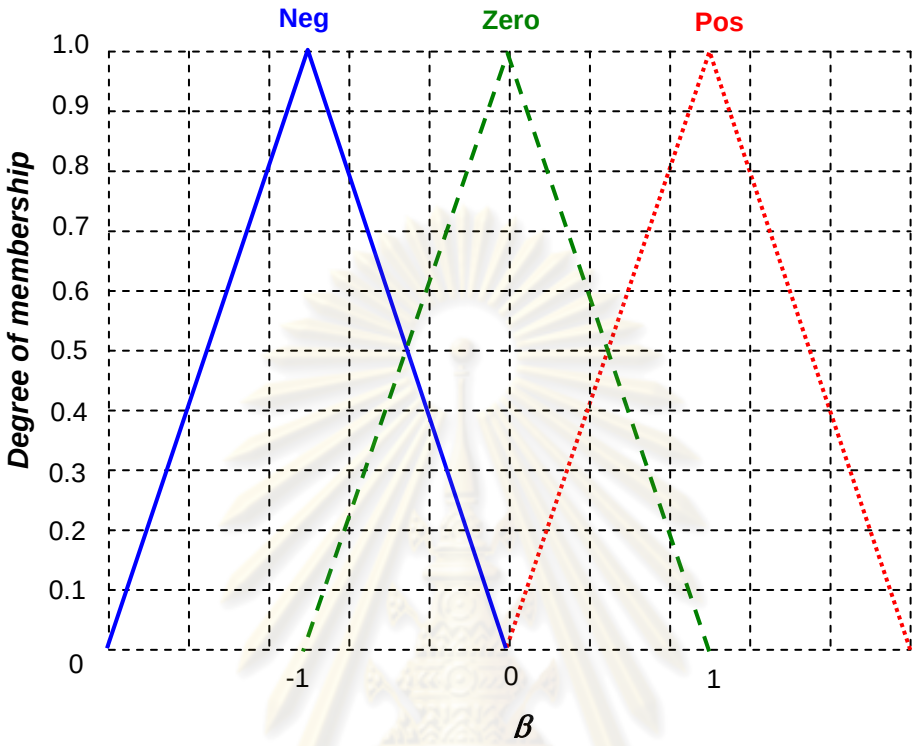

Figure 6.8 The β output membership function

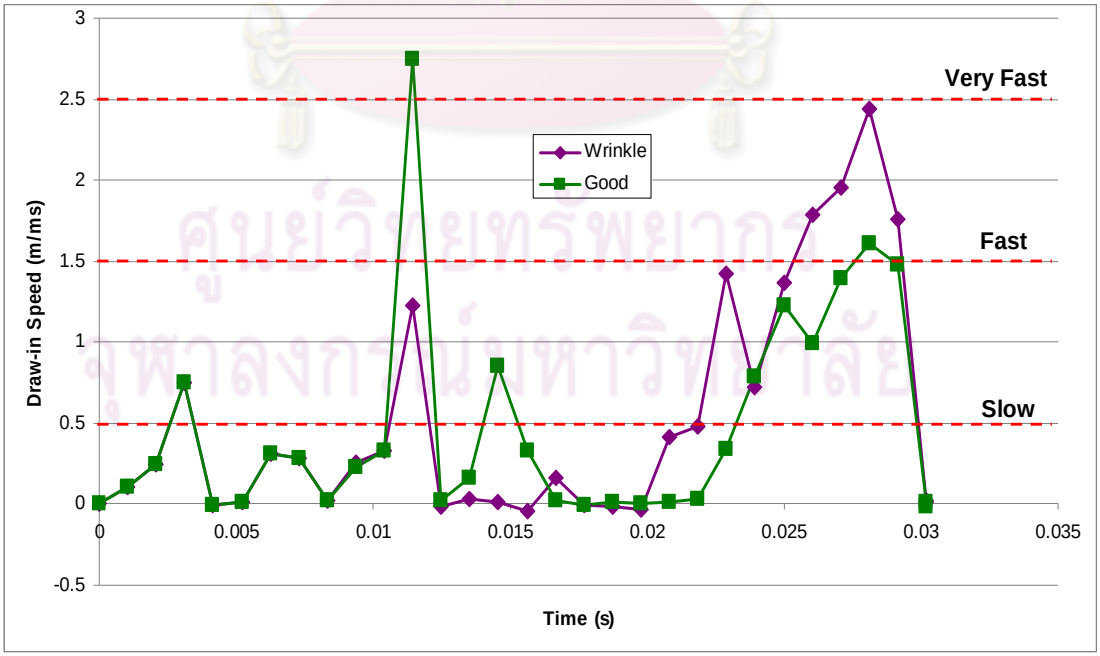

Figure 6.9 The draw-in speed depend on time

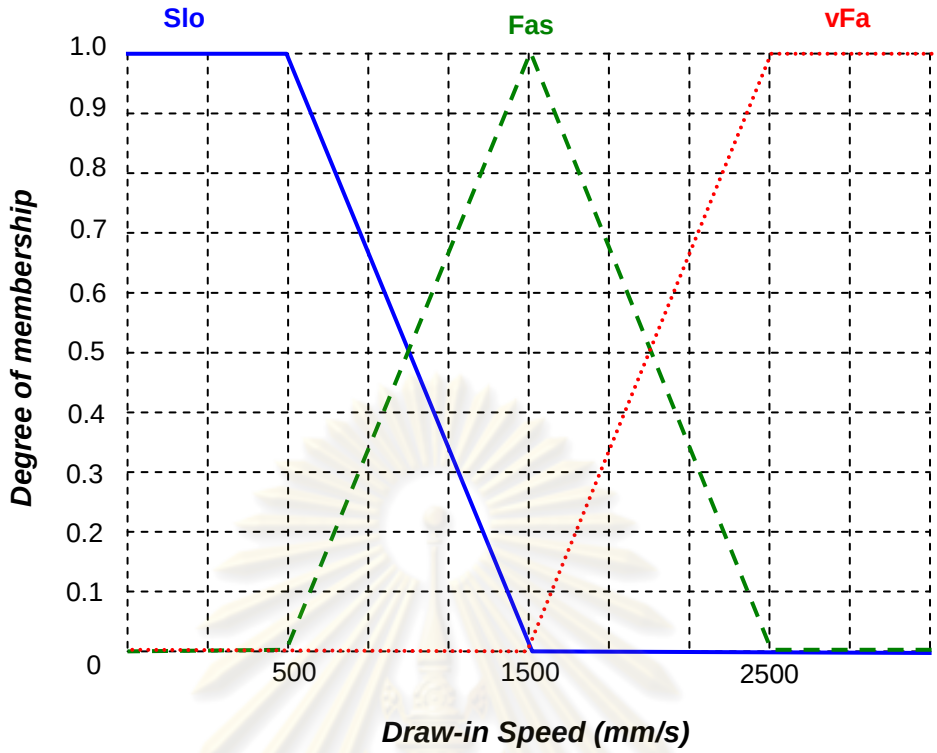

Figure 6.10 The draw-in speed membership function

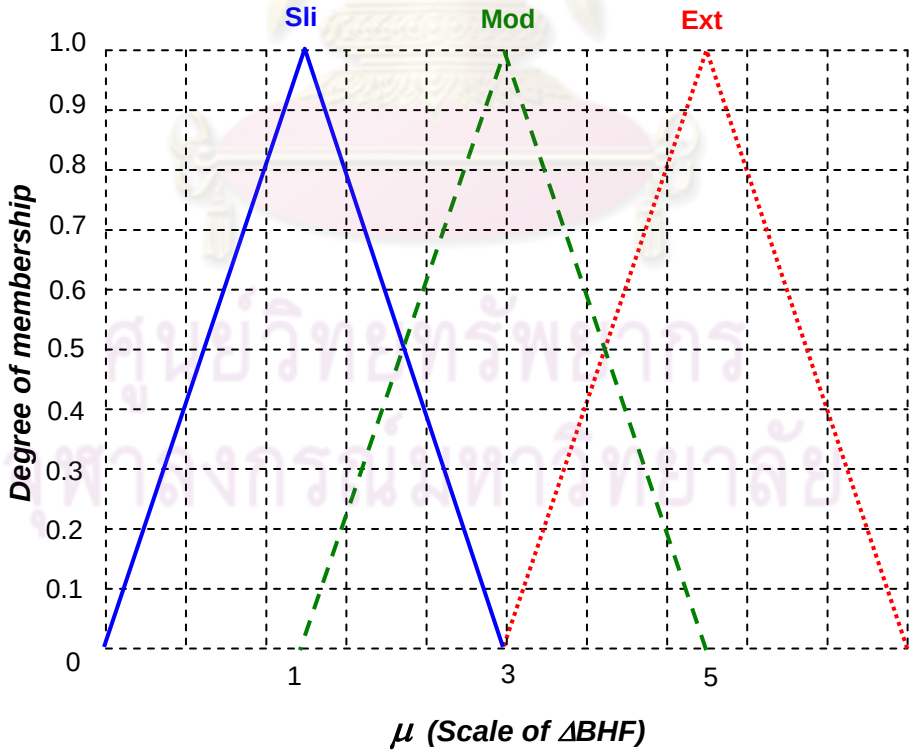

Figure 6.11 The μ membership function

The output of scaling the ΔBHF (μ) membership function is defined with full triangulars, the center of slight value is 1 (below 500 m/s), the center of fast is 3 (at 1,500 m/s is 3 times of 500 m/s), and the center of very fast value is 5 (at 2,500 m/s is 5 times of 500 m/s) as shown in figure 6.11.

6.3.1.3 Fuzzy inference rules

The fuzzy rules to be implemented are usually derived from the experience knowledge of operators or FE simulation database. In this study, the fuzzy rules are derived from FE simulations. Before incorporating the fuzzy rules into the control system, the input and the output variables of the system should be fuzzied.

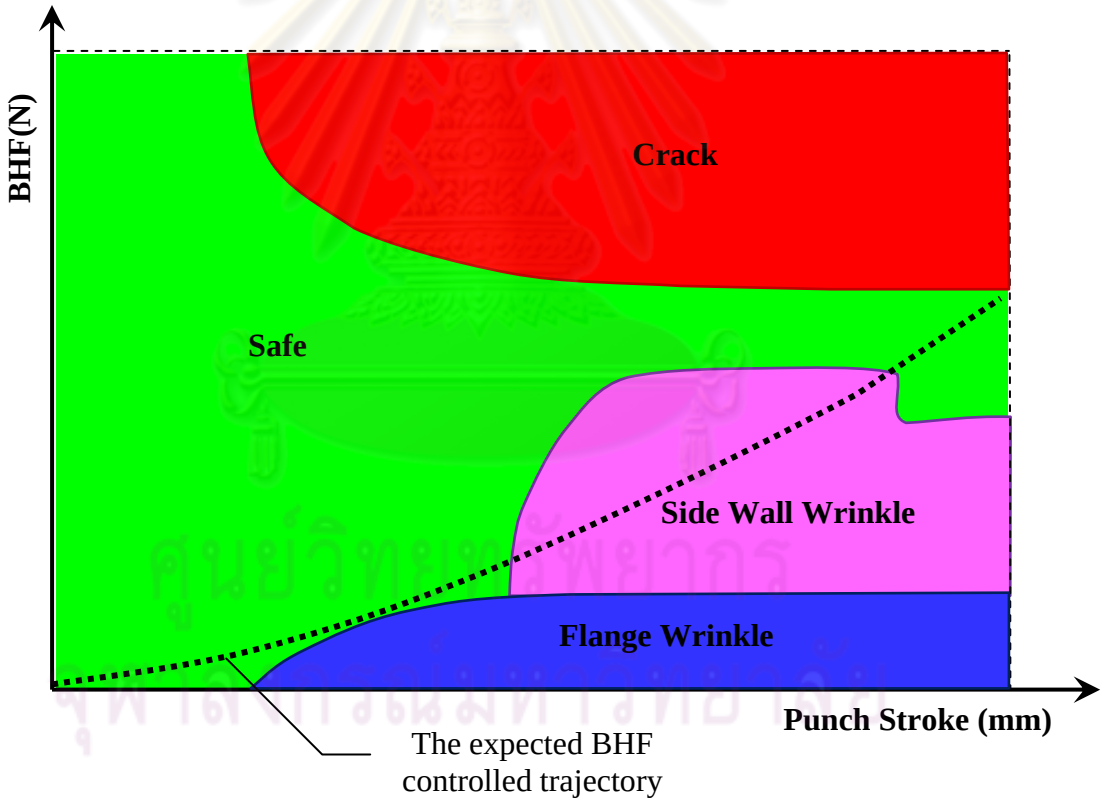

Figure 6.12 The expected BHF controlled trajectory on process window of BHF and punch stroke

The membership functions of all variables and outputs have been set thus; the goal of the control is to *minimize thinning* with *no crack* and *no wrinkles*. The blank holder force control strategy is established that at the beginning of stroke after the pre-bulge stage, the pressure and blank holder force should be low due to the thin-out stage; the blank around the punch nose is subjected to biaxial tension, which results in metal thinning. In the wrinkle stage, the blank holder force should be increased to stretch the blank by controlling the blank movement into the counter pot (draw-in speed) and to prevent the flange wrinkle that will obstruct the metal flow. The expected blank holder force trajectory should be as shown in figure 6.12.

The blank holder force rules are constructed by parabola cup simulations (in general shape or other conditions such as friction and pre-bulge, the rules will be changed). The rules to control the blank holder force are defined to be consistent of blank holder force control strategy as followings;

R1 = IF Thinning is vCR AND FAM is nCR THEN decrease the BHF

R2 = IF Thinning is vCR AND FAM is CR THEN decrease the BHF

R3 = IF Thinning is vCR AND FAM is vCR THEN hold the BHF

R4 = IF Thinning is CR AND FAM is nCR THEN hold the BHF

R5 = IF Thinning is CR AND FAM is CR THEN hold the BHF

R6 = IF Thinning is CR AND FAM is vCR THEN increase the BHF

R7 = IF Thinning is nCR AND FAM is nCR THEN hold the BHF

R8 = IF Thinning is nCR AND FAM is CR THEN increase the BHF

R9 = IF Thinning is nCR AND FAM is vCR THEN increase the BHF

The above rules are rewritten in a matrix as shown in figure 6.13.

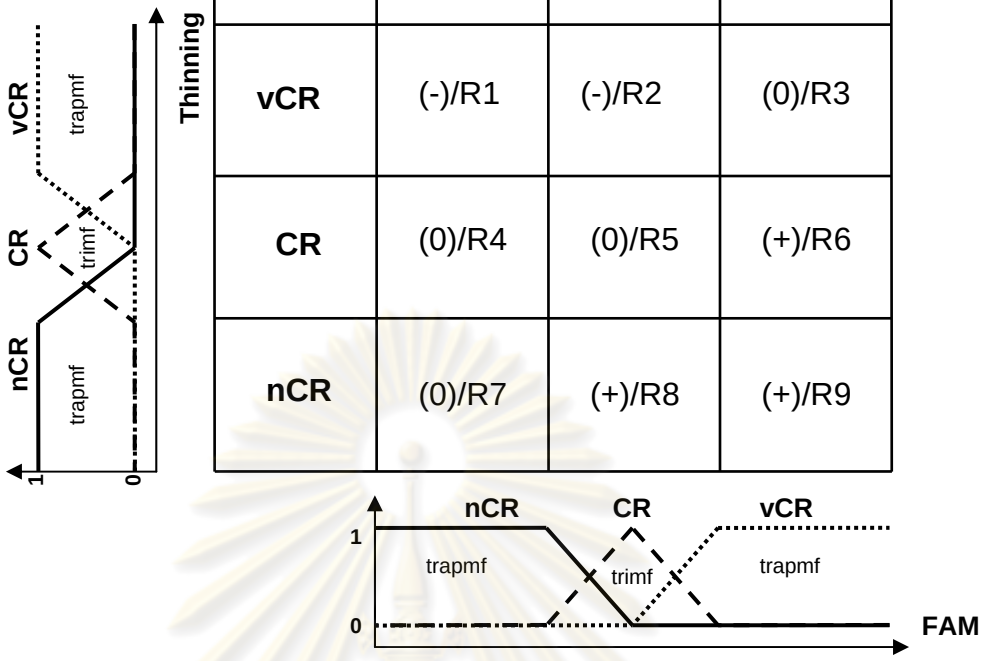

Figure 6.13 The rule matrix to control the BHF concerning thinning and FAM

From the blank holder force rules with thinning and FAM membership function, the thinning and FAM are started at nCR. It means, the blank holder is remained as pre-bulge blank holder force at the beginning and then it should be gradually increase at the end of stroke.

The rules to control the blank holder force are defined to be consistent with draw-in speed as following;

R20 = IF draw-in speed is slow THEN the ΔBHF is scaled slightly

R21 = IF draw-in speed is fast THEN the ΔBHF is scaled moderately

R22 = IF draw-in speed is very fast THEN the ΔBHF is scaled extremely

6.3.1.4 Inference engine

Measurements of input variables of fuzzy controller must be properly combined with relevant fuzzy information rules to make inferences regarding the output variables. This is the purpose of inference engine.

After the inputs are fuzzified, the next step is to obtain the degree to which each part of the antecedent is satisfied for each rule. If the antecedent of a given rule has more than one part, the fuzzy operator is applied to obtain one number that represents the result of the antecedents for that rule. This number is then applied to the output function. The input to the fuzzy operator is two or more membership values from fuzzified input variables. The output is a single truth value. AND methods are supported: *min* (minimum). Let's assume the maximum thinning is 25% and maximum FAM is 1.035 mm. The degree of fuzzy memberships for each input variable can be determined as followings;

Thinning: $vCR_{Thinning} = 0$, $CR_{Thinning} = 0.5$, $nCR_{Thinning} = 0.5$

FAM: $vCR_{FAM} = 0.4$, $CR_{FAM} = 0.6$, $nCR_{FAM} = 0$

There are nine cases (*R*1–*R*9) of situations according to the input memberships, and the fuzzy AND operation for all rules is complete. The probabilistic AND method would result in the followings;

R1 = MIN ($vCR_{Thinning}$, nCR_{FAM}) = MIN (0, 0) = 0

R2 = MIN ($vCR_{Thinning}$, CR_{FAM}) = MIN (0, 0.6) = 0

R3 = MIN ($vCR_{Thinning}$, vCR_{FAM}) = MIN (0, 0.4) = 0

R4 = MIN ($CR_{Thinning}$, nCR_{FAM}) = MIN (0.5, 0) = 0

R5 = MIN ($CR_{Thinning}$, CR_{FAM}) = MIN (0.5, 0.6) = 0.5

R6 = MIN ($CR_{Thinning}$, vCR_{FAM}) = MIN (0.5, 0.4) = 0.4

R7 = MIN ($nCR_{Thinning}$, nCR_{FAM}) = MIN (0.5, 0) = 0

R8 = MIN ($nCR_{Thinning}$, CR_{FAM}) = MIN (0.5, 0.6) = 0.5

R9 = MIN ($nCR_{Thinning}$, vCR_{FAM}) = MIN (0.5, 0.4) = 0.4

The probabilistic graphical calculation based on nine rules of BHF control is shown in figure 6.14

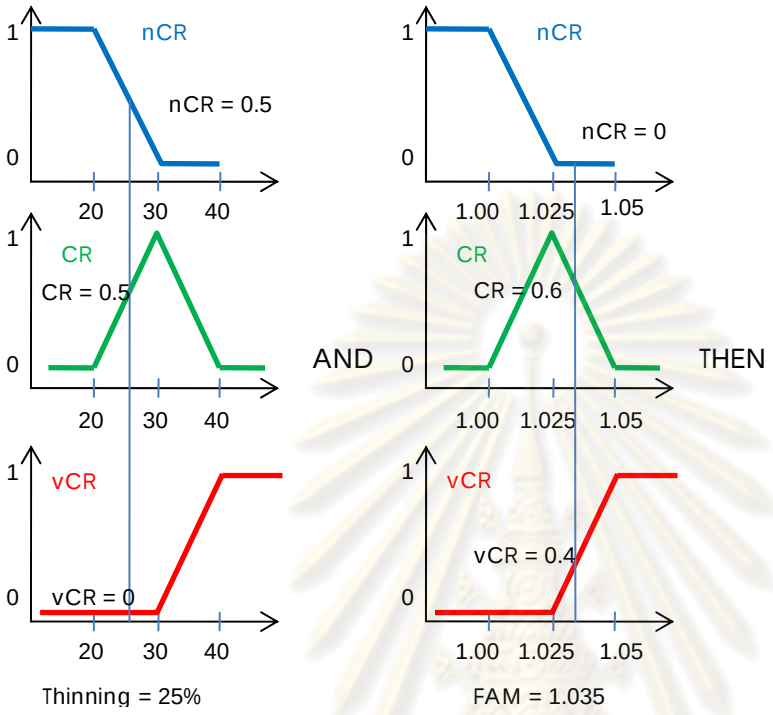

Rule matrix

BHF		FAM		
		nCR	CR	vCR
Thinning	vCR	-	-	0
	CR	0	0	+
	nCR	0	+	+

Output membership

BHF		FAM		
		nCR	CR	vCR
Thinning	vCR	0.00	0.00	0.00
	CR	0.00	0.50	0.40
	nCR	0.00	0.50	0.40

Figure 6.14 The probabilistic graphical calculation based on nine rules of BHF control

The degree of output memberships can be inferred based on the rule based matrix by root-sum-square:

$$\text{Neg} = \sqrt{\left(R_1^2 + R_2^2\right)} = \sqrt{\left(0^2 + 0^2\right)} = 0$$

$$\text{Zero} = \sqrt{\left(R_3^2 + R_4^2 + R_5^2 + R_7^2\right)} = \sqrt{\left(0^2 + 0^2 + 0.5^2 + 0^2\right)} = 0.5$$

$$\text{Pos} = \sqrt{\left(R_6^2 + R_8^2 + R_9^2\right)} = \sqrt{\left(0.4^2 + 0.5^2 + 0.4^2\right)} = 0.755$$

The implication and graphical aggregation to control the BHF is shown in figure 6.15

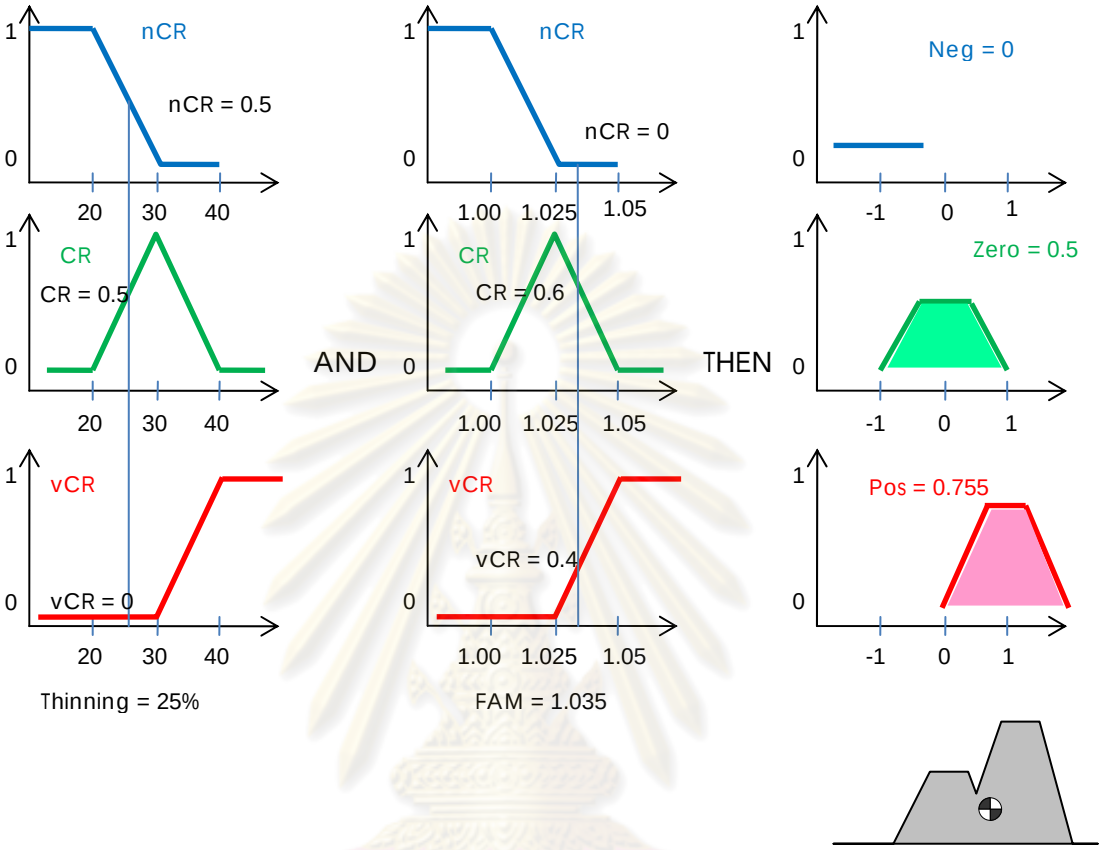

Figure 6.15 The implication and graphical aggregation to control the BHF

6.3.1.5 Defuzzification

The output of each rule is a fuzzy set. The output fuzzy sets for all rules are aggregated into a single output fuzzy set of the control system, and then the final result set is defuzzified, or resolved to a single number. Here, the center of gravity method is used for defuzzification, which computes the fuzzy centroid of the composite area.

The most frequently used defuzzifications method in the fuzzy controller is the centroid method. The defuzzified value, $d_{CA}(C)$, is defined as Eq. 6.1

$$d_{CA}(C) = \frac{\sum_{k=1}^{n} C(z_k) z_k}{\sum_{k=1}^{n} C(z_k)} \qquad (6.1)$$

where $C(z_k)$ is the result of implication output, z_k is the center value of each output.

Crispy output β can be determined from the output membership function by calculating fuzzy centroid of the area.

$$\beta = \frac{(Neg \times Center\ of\ Neg) + (Zero \times Center\ of\ Zero) + (Pos \times Center\ of\ Pos)}{(Neg + Zero + Pos)}$$

$$\beta = \frac{(0 \times (-1)) + (0.5 \times 0) + (0.755 \times 1)}{(0 + 0.5 + 0.755)} = 0.602$$

6.3.2 Fuzzy controller for the pressure

In the HMD process of parabolic part, thinning usually occurred around the punch nose region because of the tensile stress induced by *pressure* and *blank holder force* that hold the blank material, as well as friction between the punch and blank. Therefore, the pressure parameter has affected directly on thinning. Moreover, the pressure also has an influence on the side wall wrinkle, which can be checked by the bulge height (for additional stretching force). The thinning and side wall wrinkle variables progress in the opposite directions. This means that the excessive pressure leads to more thinning while keeping the side wall wrinkle down, and on the other hand, insufficient pressure lead to side wall wrinkle while results in less thinning. To control the pressure, therefore, the thinning and bulge height (SW) are variables to be considered as inputs. The coefficient (α) to scale the initial incremental of pressure (ΔP) are outputs. The schematic to control the pressure by fuzzy logic is shown in figure 6.16.

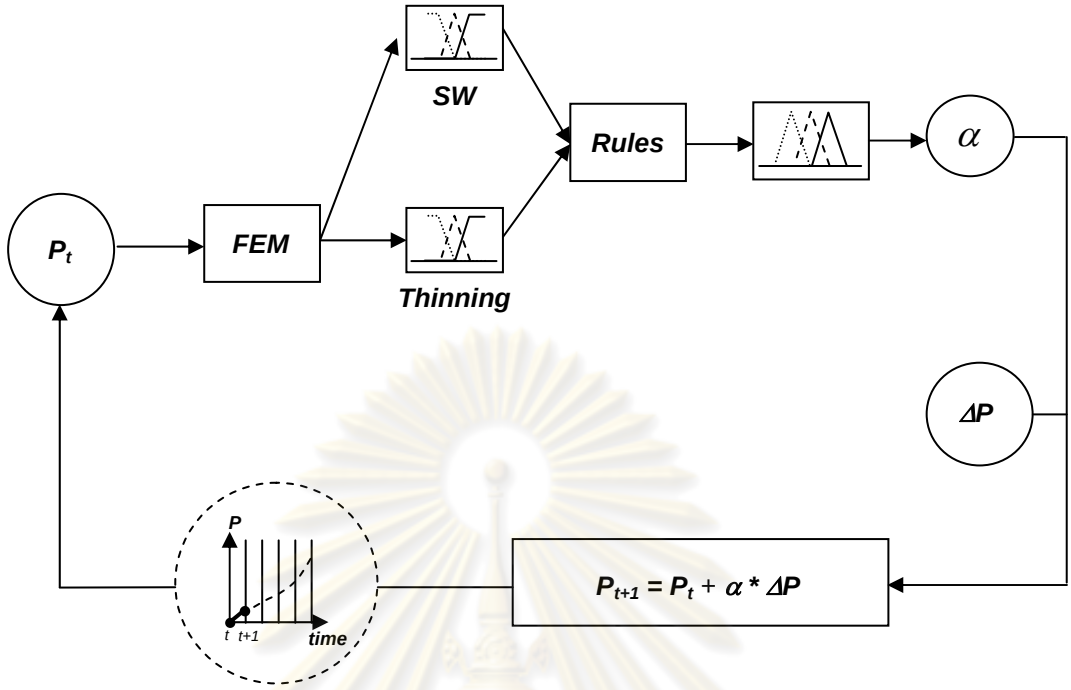

Figure 6.16 The fuzzy controlling schematic of the pressure

6.3.2.1 Linguistic states

After identifying relevant input and output variables of the controller. The next step is selection meaningful linguistic states for each variable and expresses them by appropriate fuzzy sets. In this case, these fuzzy sets are fuzzy member, which represent linguistic labels as

vCR – very critical	NEG – negative (decrease)
CR – critical	ZERO – zero (hold)
nCR – not critical	POS – positive (increase)

These linguistic states will be fuzzified with triangular-shape that are equally spread over each range in the next state.

6.3.2.2 Fuzzification function

In this step, a fuzzification function is introduced for each input variable to express the associated measurement uncertainty. The purpose of the

The side wall wrinkle is measure from bulge height (SW). The SW that over the initial dome height (initial dome height = 20) is not critical surely. After punch move down, the dome height will be descended to keep the stretching on blank the dome height will be maintained that is not below 10 mm. Due to the proper pressure and blank holder force for good parts, generated the dome height at the SW initial stage are not below the 10 mm as shown in figure 6.17. Therefore, the SW (dome height) is below 10 mm is the very critical. For equally spread triangular-shape, the middle values as 15 mm is critical certainty. The very critical and not critical are defined with half triangular membership function, and the critical is defined with full triangular membership function. Figure 6.18 is the SW membership function.

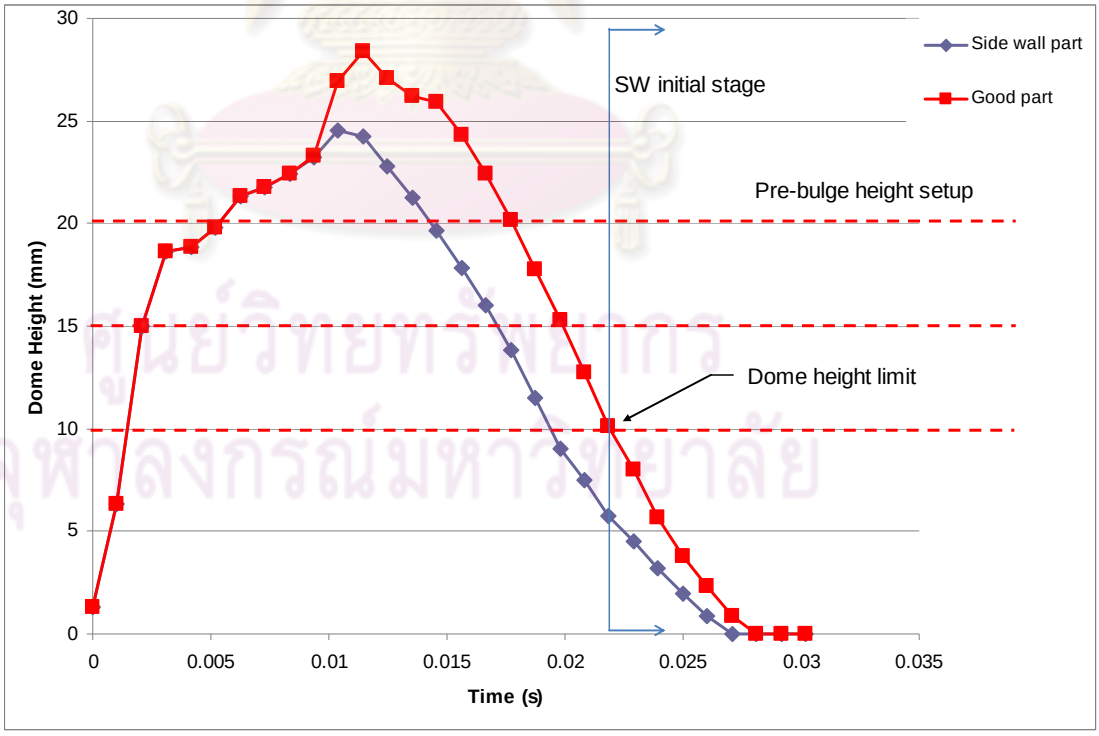

Figure 6.17 The dome height related with the side wall wrinkle

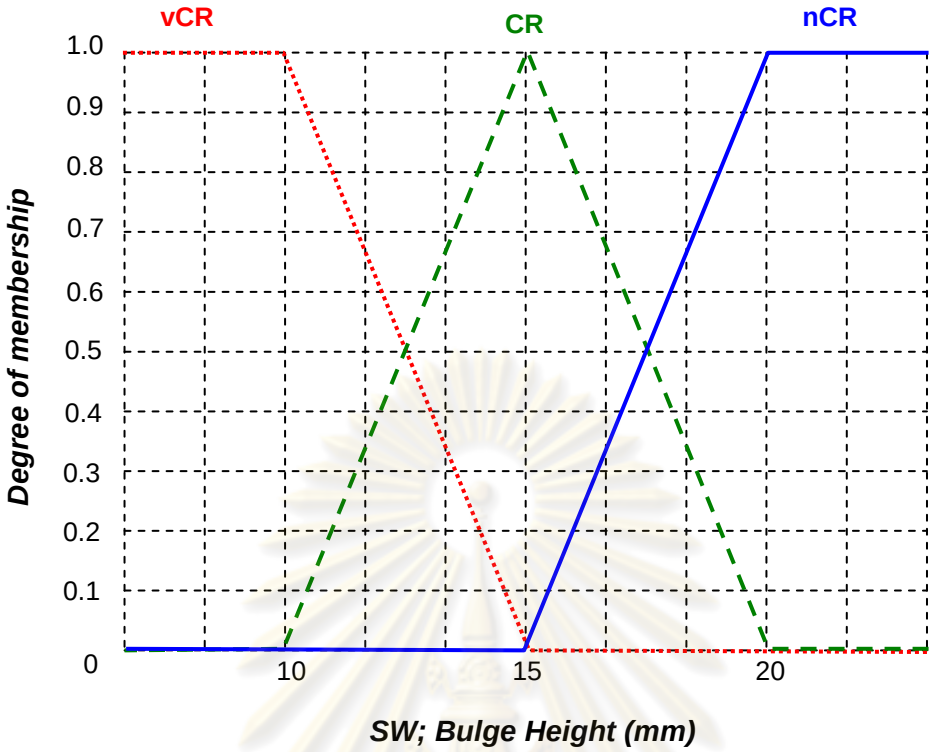

Figure 6.18 The SW membership function

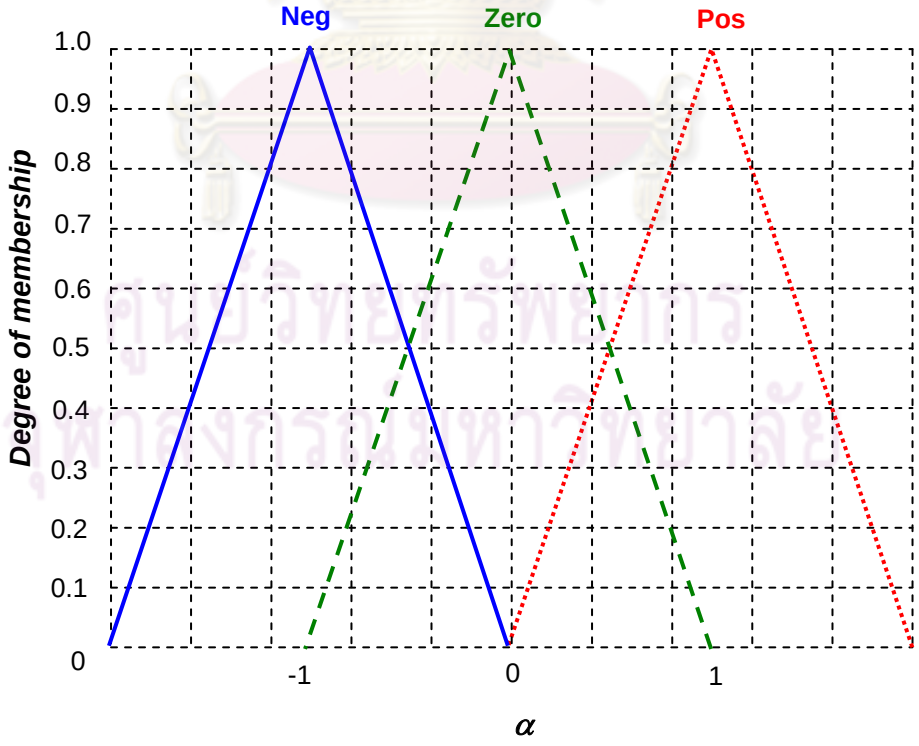

Figure 6.19 The α output membership function

The output of weight factor (α) membership function is defined with full triangular, the center of positive value is +1, the center of zero is 0, and the center of negative value is -1 as shown in figure 6.19.

6.3.2.3 Fuzzy inference rules

The fuzzy rules to be implemented are usually derived from the experience knowledge of operators or FE simulation database. In this study, the fuzzy rules are derived from FE simulations. Before incorporating the fuzzy rules into the control system, the input and the output variables of the system should be fuzzied.

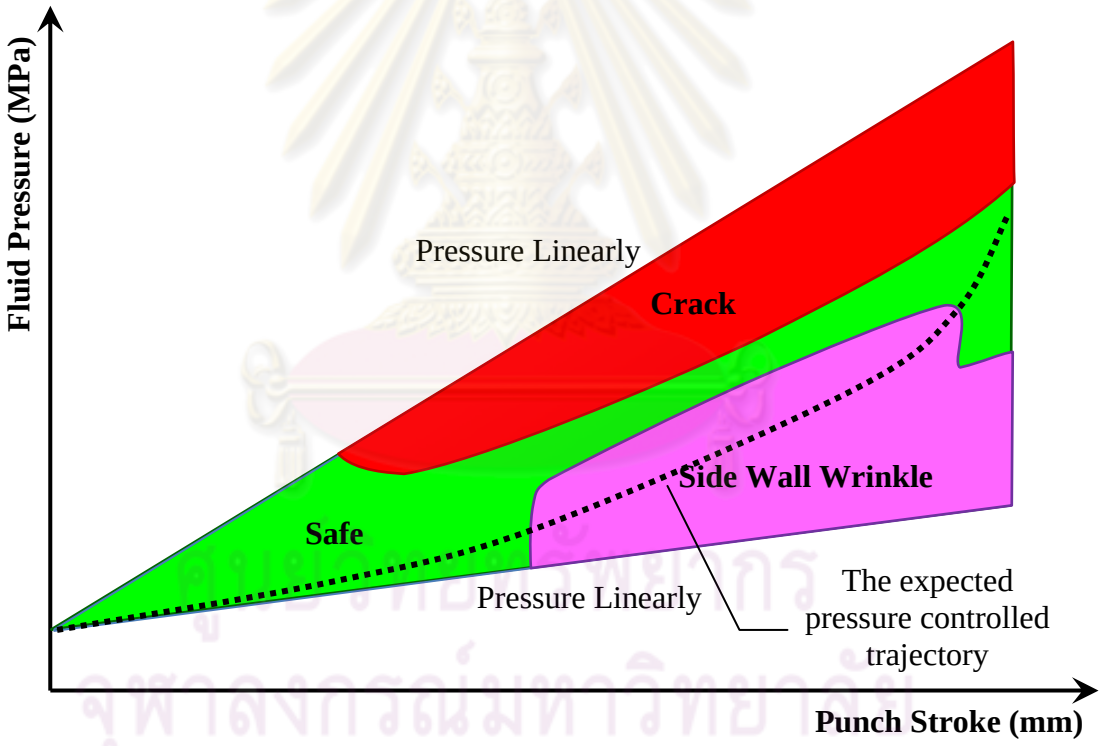

Figure 6.20 The expected pressure controlled trajectory on process window of pressure and punch stroke

The membership functions of all variables and outputs have been set thus; the goal of the control is *minimum thinning* with *no crack* and *no wrinkles*. The pressure control strategy is established that, at the beginning of stroke after the pre-bulge stage, the

pressure and blank holder force should be low due to the thin-out stage; the blank around the punch nose is subjected to biaxial tension, which results in metal thinning. In the wrinkle stage, the pressure should be increased to stretch the blank by pressurizing the bulge against the punch movement. The expected pressure trajectory should be as shown in figure 6.20.

The pressure rules are constructed by parabola cup simulations (in general shape or other conditions such as friction and pre-bulge, the rules will be changed). The rules to control the pressure are defined to be consistent of pressure control strategy as followings;

R10 = IF Thinning is vCR AND SW is vCR THEN hold the pressure

R11 = IF Thinning is vCR AND SW is CR THEN decrease the pressure

R12 = IF Thinning is vCR AND SW is nCR THEN decrease the pressure

R13 = IF Thinning is CR AND SW is vCR THEN increase the pressure

R14 = IF Thinning is CR AND SW is CR THEN hold the pressure

R15 = IF Thinning is CR AND SW is nCR THEN decrease the pressure

R16 = IF Thinning is nCR AND SW is vCR THEN increase the pressure

R17 = IF Thinning is nCR AND SW is CR THEN increase the pressure

R18 = IF Thinning is nCR AND SW is nCR THEN hold the pressure

The above rules are rewritten in matrix as shown in figure 6.21.

ศูนย์วิทยทรัพยากร
จุฬาลงกรณ์มหาวิทยาลัย

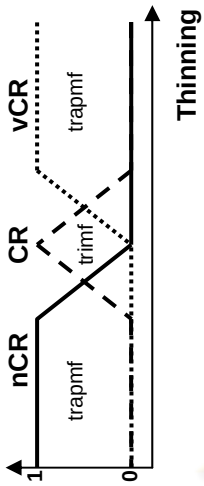

(P)	vCR	CR	nCR
vCR	(0)/R10	(-)/R11	(-)/R12
CR	(+)/R13	(0)/R14	(-)/R15
nCR	(+)/R16	(+)/R17	(0)/R18

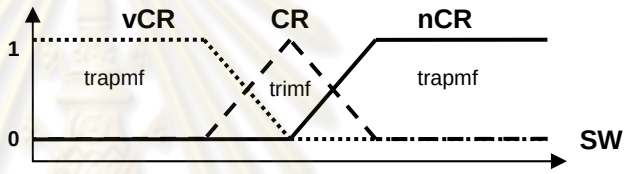

Figure 6.21 The rule matrix to control the pressure concerned with thinning and SW

6.3.2.4 Inference engine

Measurements of input variables of fuzzy controller must be properly combined with relevant fuzzy information rules to make inferences regarding the output variables. This is the purpose of inference engine.

After the inputs are fuzzified, the next step is to obtain the degree to which each part of the antecedent is satisfied for each rule. If the antecedent of a given rule has more than one part, the fuzzy operator is applied to obtain one number that represents the result of the antecedents for that rule. This number is then applied to the output function. The input to the fuzzy operator is two or more membership values from fuzzified input variables. The output is a single truth value. AND methods are supported: *min* (minimum). Let's assume the maximum thinning is 25% and maximum SW is 16 mm. The degree of fuzzy memberships for each input variable can be determined as followings;

Thinning: $vCR_{Thinning} = 0$, $CR_{Thinning} = 0.5$, $nCR_{Thinning} = 0.5$

SW: $vCR_{SW} = 0$, $CR_{SW} = 0.8$, $nCR_{SW} = 0.2$

There are nine cases (*R*10–*R*18) of situations according to the input memberships, and the fuzzy AND operation for all rules is complete. The probabilistic AND method would result in the followings;

R10 = MIN ($vCR_{Thinning}$, nCR_{SW}) = MIN (0, 0.2) = 0

R11 = MIN ($vCR_{Thinning}$, CR_{SW}) = MIN (0, 0.8) = 0

R12 = MIN ($vCR_{Thinning}$, vCR_{SW}) = MIN (0, 0) = 0

R13 = MIN ($CR_{Thinning}$, nCR_{SW}) = MIN (0.5, 0.2) = 0.2

R14 = MIN ($CR_{Thinning}$, CR_{SW}) = MIN (0.5, 0.8) = 0.5

R15 = MIN ($CR_{Thinning}$, vCR_{SW}) = MIN (0.5, 0) = 0

R16 = MIN ($nCR_{Thinning}$, nCR_{SW}) = MIN (0.5, 0.2) = 0.2

R17 = MIN ($nCR_{Thinning}$, CR_{SW}) = MIN (0.5, 0.8) = 0.5

R18 = MIN ($nCR_{Thinning}$, vCR_{SW}) = MIN (0.5, 0) = 0

The probabilistic graphical calculation based on nine rules of pressure control is shown in figure 6.22

The degree of output memberships can be inferred based on the rule based matrix by root-sum-square:

Neg = $\sqrt{\left(R_{11}^2 + R_{12}^2 + R_{15}^2\right)} = \sqrt{\left(0^2 + 0^2 + 0.2^2\right)} = 0.2$

Zero = $\sqrt{\left(R_{10}^2 + R_{14}^2 + R_{18}^2\right)} = \sqrt{\left(0^2 + 0.5^2 + 0.2^2\right)} = 0.539$

Pos = $\sqrt{\left(R_{13}^2 + R_{16}^2 + R_{17}^2\right)} = \sqrt{\left(0^2 + 0^2 + 0.5^2\right)} = 0.5$

The implication and graphical aggregation to control the BHF is shown in figure 6.23

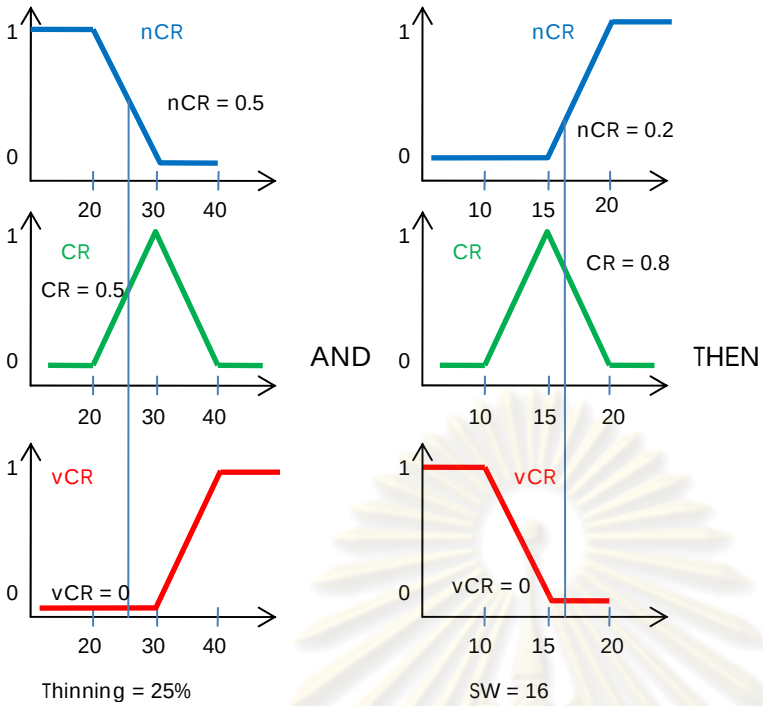

Rule matrix

P		SW (Bulge Height)		
		vCR	CR	nCR
Thinning	vCR	0	-	-
	CR	+	0	-
	nCR	+	+	0

Output membership

P		SW (Bulge Height)		
		vCR	CR	nCR
Thinning	vCR	0.00	0.00	0.00
	CR	0.00	0.50	0.20
	nCR	0.00	0.50	0.20

Figure 6.22 The probabilistic graphical calculation based on nine rules of pressure control

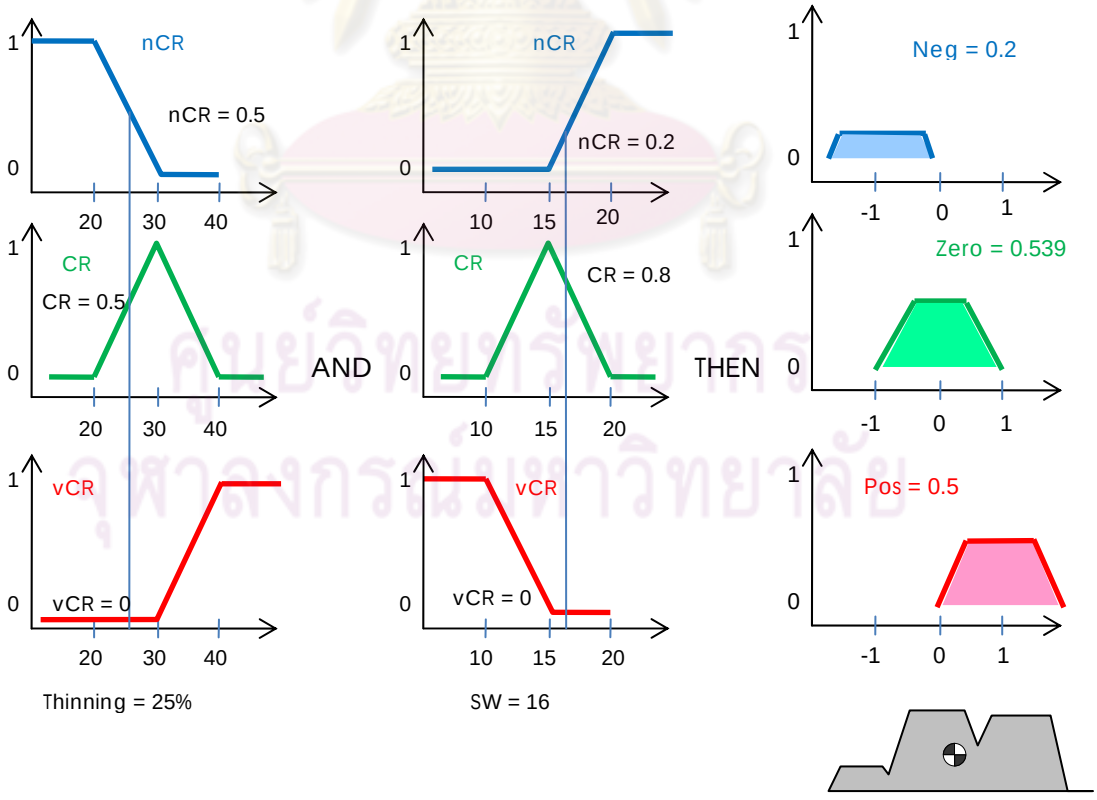

Figure 6.23 The implication and graphical aggregation to control the BHF

6.3.2.5 Defuzzification

The output of each rule is a fuzzy set. The output fuzzy sets for all rules are aggregated into a single output fuzzy set of the control system, and then the final result set is defuzzified, or resolved to a single number. Here, the center of gravity method is used for defuzzification, which computes the fuzzy centroid of the composite area.

Crispy output α can be determined from the output membership function by calculating fuzzy centroid of the area.

$$\alpha = \frac{(Neg \times Center\ of\ Neg) + (Zero \times Center\ of\ Zero) + (Pos \times Center\ of\ Pos)}{(Neg + Zero + Pos)}$$

$$\alpha = \frac{(0.2 \times (-1)) + (0.539 \times 0) + (0.5 \times 1)}{(0.2 + 0.539 + 0.5)} = 0.242$$

6.4 Calculation of ΔBHF and ΔP

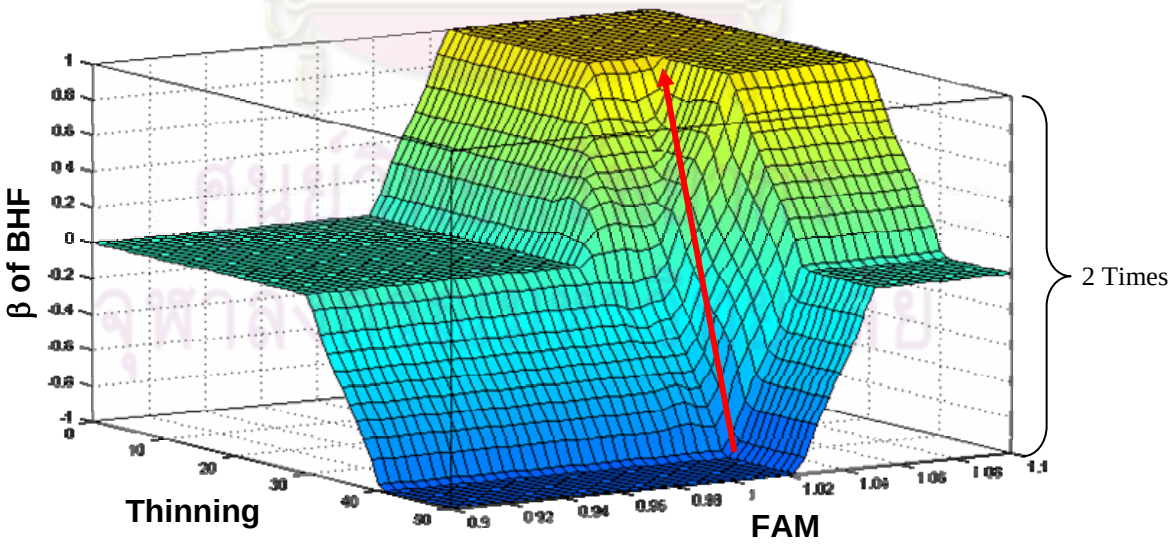

Figure 6.24 The surface of β weight factor

To calculate the ΔBHF, for modification of load function in linear form, $BHF_{New} = BHF_{Old} + (\beta*(\mu*\Delta BHF))$. The ΔBHF can calculate from maximum BHF divide by total number of monitoring steps. For Part1, the maximum BHF is around 250,000 N for quarter model. In case of 100 monitoring steps, the ΔBHF should be 2,500 N. However, the β has two sides; -1 for minimum and +1 for maximum, to guarantee that the system can capture this change, so the ΔBHF should be twice of maximum BHF divide by total number of monitoring steps. The above case ΔBHF should be 2,500 * 2 = 5,000 N. Moreover, doubling of maximum BHF will benefit the method by providing more room for a lot more shapes of profiles, as shown in figure 6.25.

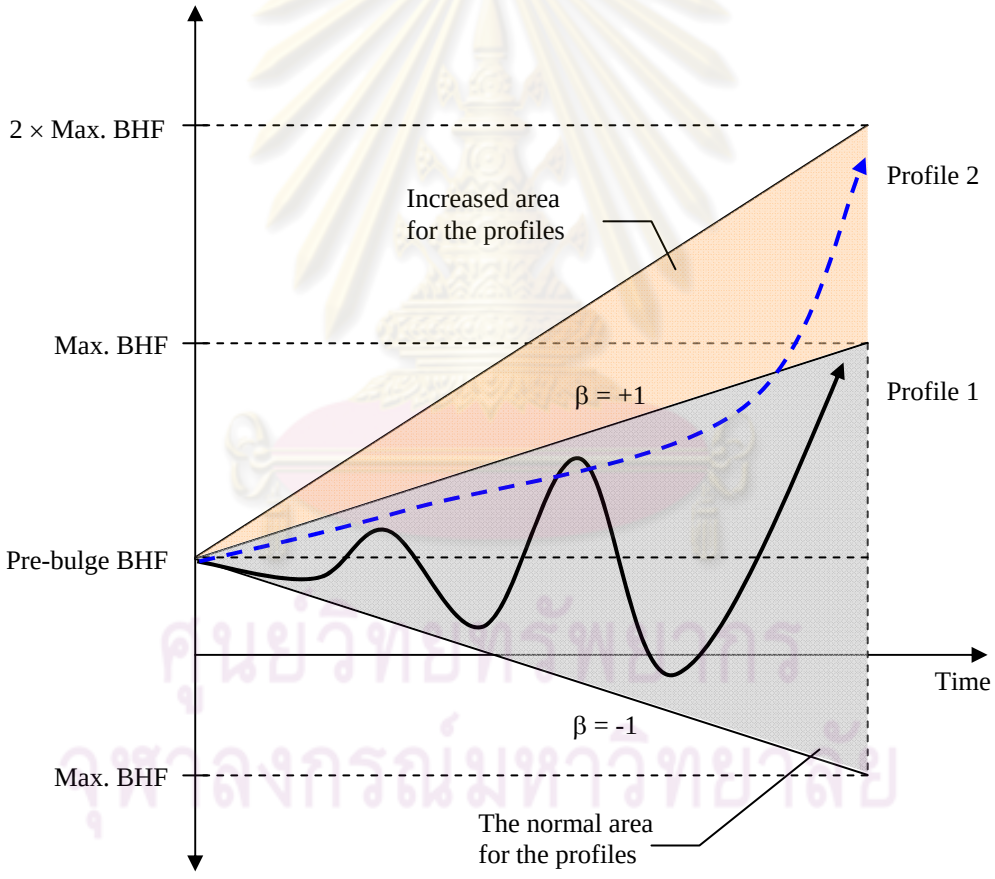

Figure 6.25 The area for generating the loading profiles

Calculation of ΔP is done similar to ΔBHF, so ΔBHF and ΔP values for Part1, Part2 and Part3 are in table. 6.1.

Table 6.1 The values of ΔBHF and ΔP

Monitoring Steps		100	50	30	20	10
Part1	ΔBHF (N)	5,000	10,000	16,667	25,000	50,000
	ΔP (MPa)	0.8	1.6	2.67	4	8
Part2	ΔBHF (N)	5,600	11,200	18,667	28,000	56,000
	ΔP (MPa)	0.6	1.2	2	3	6
Part3	ΔBHF (N)	8,500	17,000	28,333	42,500	85,000
	ΔP (MPa)	0.5	1	1.67	2.5	5

6.5 Modification of load functions in linear form

In general for unknown profiles, the linear load function is typically used with good predictive capability. In this work, the blank holder force is determined by Eq. 6.2 and the pressure is determined by Eq. 6.3.

$$BHF_{New} = BHF_{Old} + (\beta*(\mu*\Delta BHF)) \quad (6.2)$$

$$P_{New} = P_{Old} + \alpha*\Delta P \quad (6.3)$$

where BHF_{New} is the updated BHF for next step, BHF_{Old} is the previous BHF, β is the weight factor from thinning and FAM, μ is the weight factor from draw-in speed and ΔBHF is the incremental of blank holder force. P_{New} is the updated pressure for next step, P_{Old} is the previous pressure, α is the weight factor from thinning and dome height (SW) and ΔP is the incremental of pressure.

The adaptive simulation with fuzzy control algorithm was implemented in the user subroutine. The fuzzy control algorithm was called at the end of each monitoring step. The calculated loads (pressure and blank holder force) in Eq. 6.2 and Eq. 6.3 were applied as boundary conditions during the next monitoring step. To reduce calculation time, the loading profiles will be determined after the pre-bulge stage. This section is aimed to apply the automatic approach for determining the loading paths with modification of load functions in a linear form and to examine the effect of number of monitoring steps on loading paths.

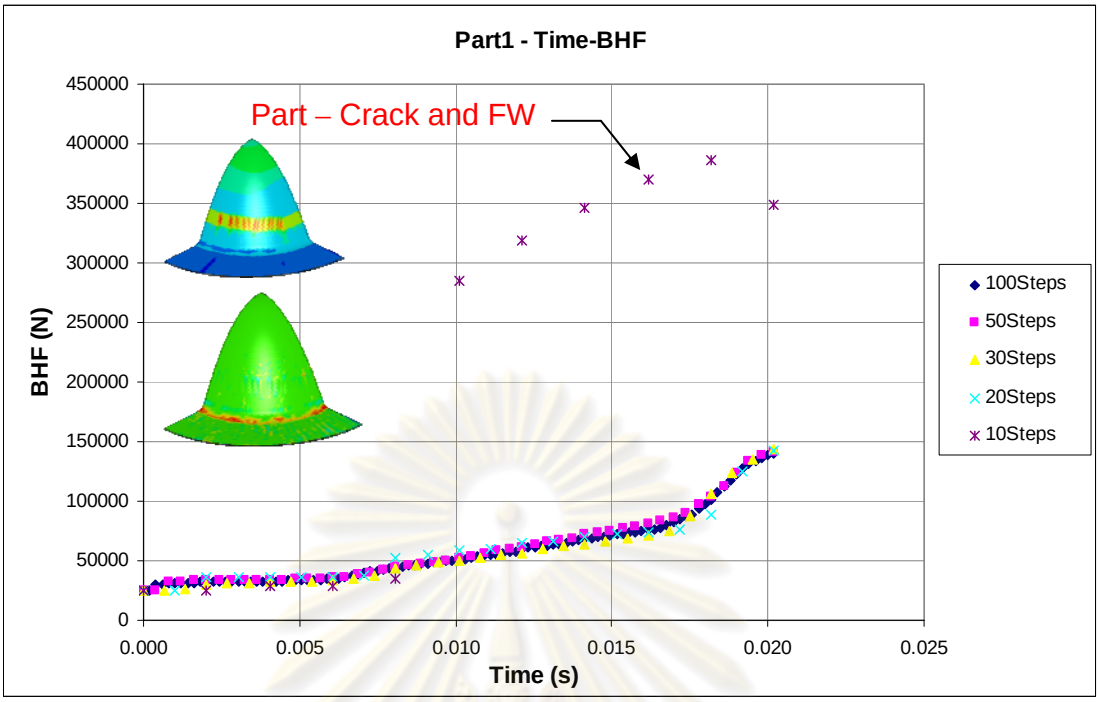

Figure 6.26 BHF profiles varying by number of monitoring steps of Part1

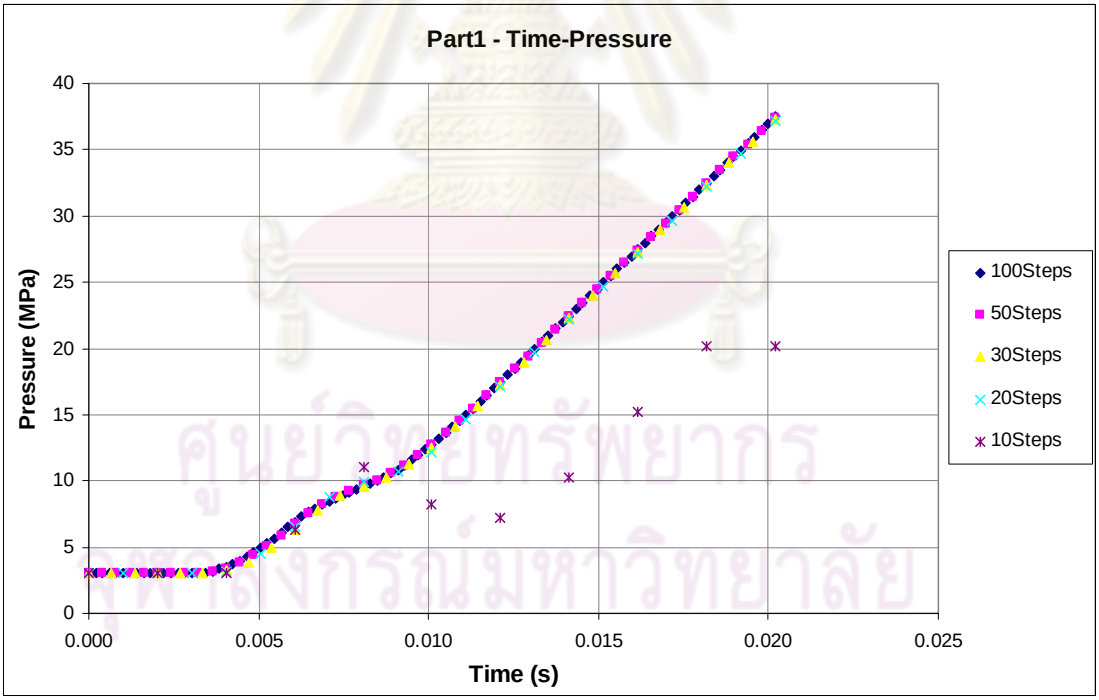

Figure 6.27 Pressure profiles varying by number of monitoring steps of Part1

The loading paths of Part1 in each monitoring steps are shown in figure 6.26 – 6.27. The blank holder force and pressure profiles at 20, 30, 50 and 100 monitoring steps

are consistent while, the 10 monitoring steps are different. The results of thinning, FAM and SW are shown in table 6.2

Table 6.2 Results of Part1 by adaptive simulation with fuzzy logic control

Monitoring Steps		**100**	**50**	**30**	**20**	**10**
Part1	Thinning	29.42950	29.27400	29.54390	29.64840	88.98560
	FAM	1.03142	1.03063	1.03148	1.03116	1.03350
	SW	0.48399	0.48326	0.48521	0.48412	-

The forming results obtained from using loading paths from the adaptive simulation and fuzzy logic control algorithm are good (no crack, no wrinkle) except for when using10 monitoring steps that the loading paths given the cracked part. Figure 6.28 shows the thinning distribution on Part1 using 100 monitoring steps; the maximum thinning is 29.43, the part is not cracked. For the FAM and SW values, they are below their limits; the part has no wrinkles. To make sure that the wrinkles do not appear on the part, the zebra line visualization technique was used and found that all lines are straight. The maximum thinning from the adaptive simulation and fuzzy logic control algorithm is less than the maximum thinning as a result from the optimal constant BHF and linear pressure from process window (34.43%). In addition, the adaptive simulation method used only one simulation.

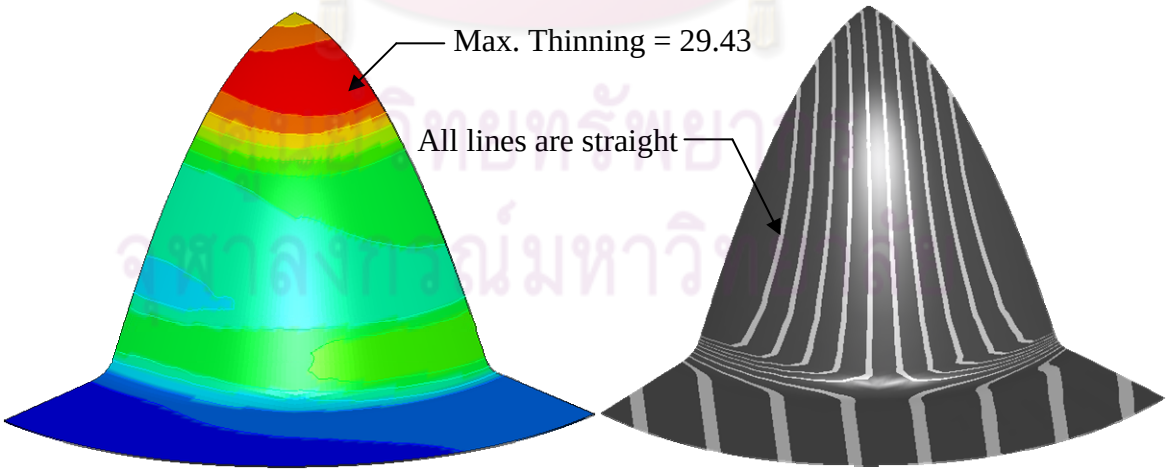

Figure 6.28 The thinning distribution and zebra lines on the Part1 using 100 monitoring steps

Thickness distribution on curvilinear of Part1 from loading paths of the adaptive simulation and fuzzy logic control algorithm is shown in figure 6.29. The minimum thickness is around 60 mm from the top of dome (punch nose). The second minimum thickness is around 160 mm (near counter pot radius).

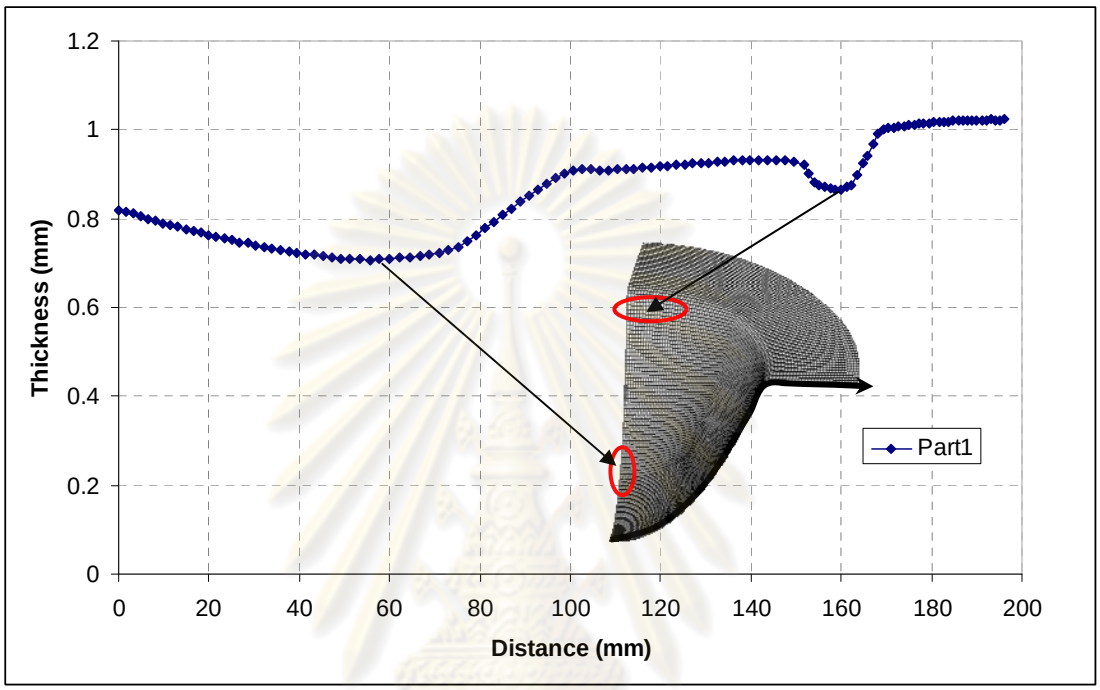

Figure 6.29 The thickness distribution on curvilinear of the Part1

The loading paths of Part2 in each monitoring steps are shown in Figure 6.30 – 6.31. The blank holder force and pressure profiles at 20, 30, 50 and 100 monitoring steps are consistent, while the 10 monitoring steps are different. The results of thinning, FAM and SW are shown in table 6.3

Table 6.3 Results of Part2 by adaptive simulation with fuzzy logic control

Monitoring Steps		**100**	**50**	**30**	**20**	**10**
Part2	Thinning	27.65640	27.62810	27.16310	26.72190	29.02310
	FAM	1.01811	1.01840	1.01477	1.01831	1.02112
	SW	0.48351	0.48264	0.48098	0.48064	0.55315

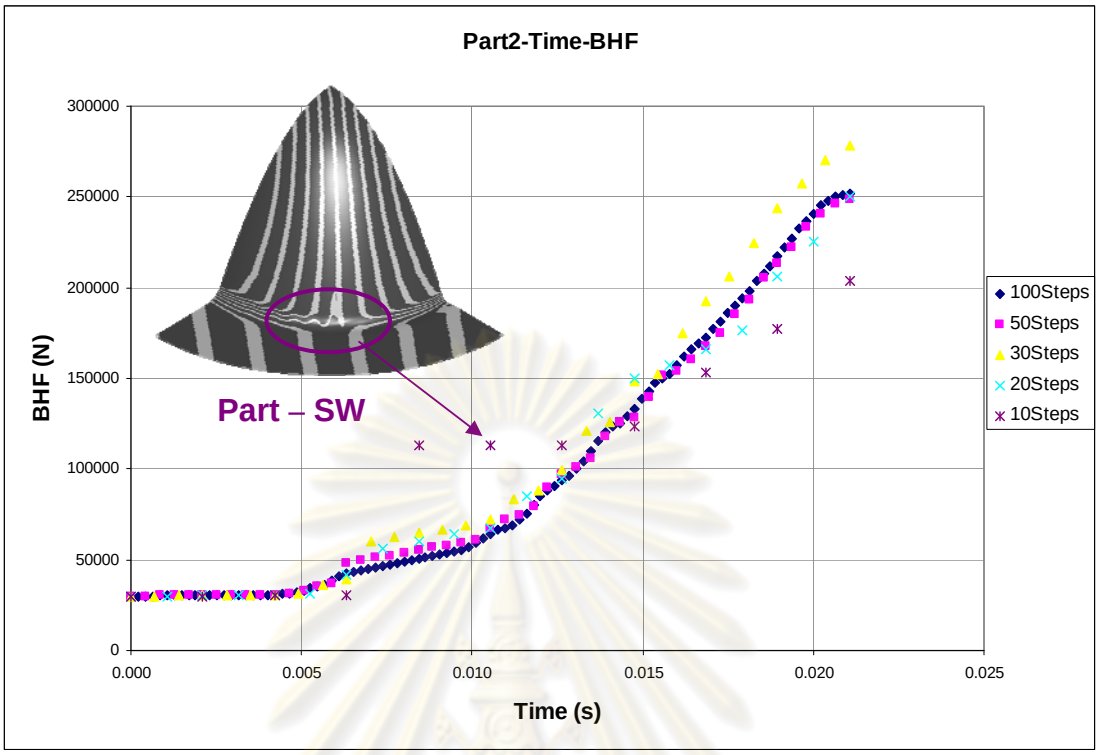

Figure 6.30 BHF profiles varying by number of monitoring steps of Part2

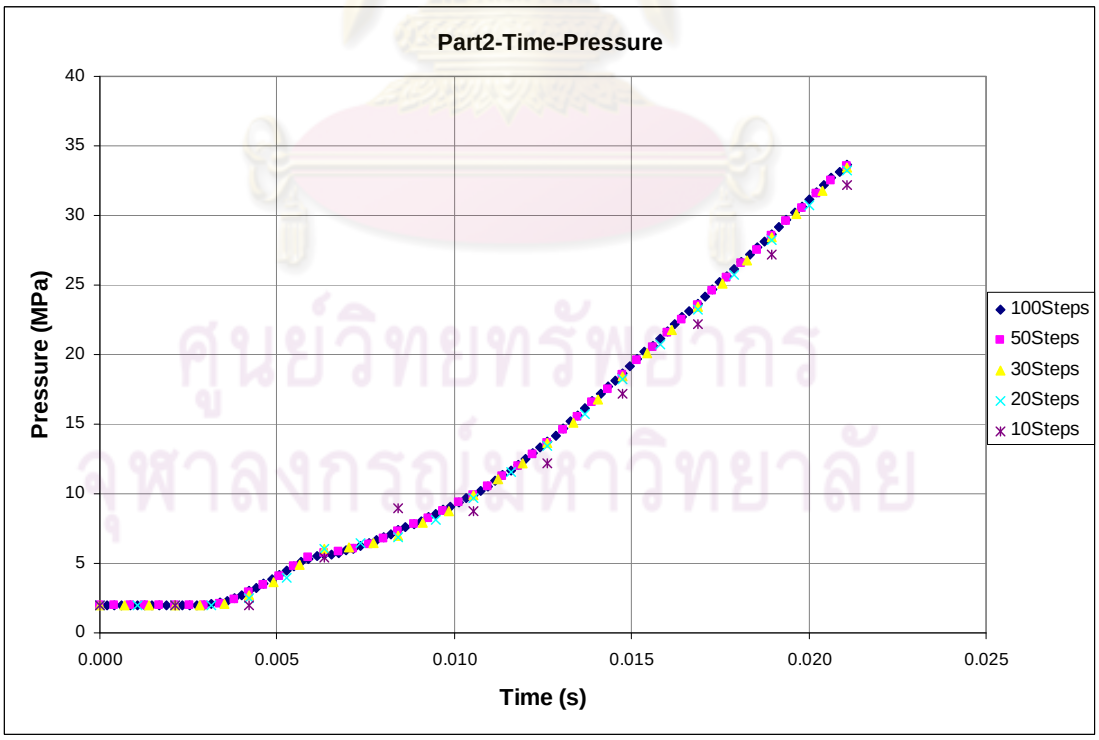

Figure 6.31 Pressure profiles varying by number of monitoring steps of Part2

The forming results obtained from using loading paths from the adaptive simulation and fuzzy logic control algorithm are good (no crack, no wrinkle) except for when using10 monitoring steps that the loading paths given the cracked part. Figure 6.32 shows the thinning distribution on Part2 using 100 monitoring steps; the maximum thinning is 27.66, the part is not cracked. For the FAM and SW values, they are below their limits; the part has no wrinkles. To make sure that the wrinkles do not appear on the part, the zebra line visualization technique was used and found that all lines are straight. The maximum thinning from the adaptive simulation and fuzzy logic control algorithm is less than the maximum thinning as a result from the optimal constant BHF and linear pressure from process window (33.84%). In addition, the adaptive simulation method used only one simulation.

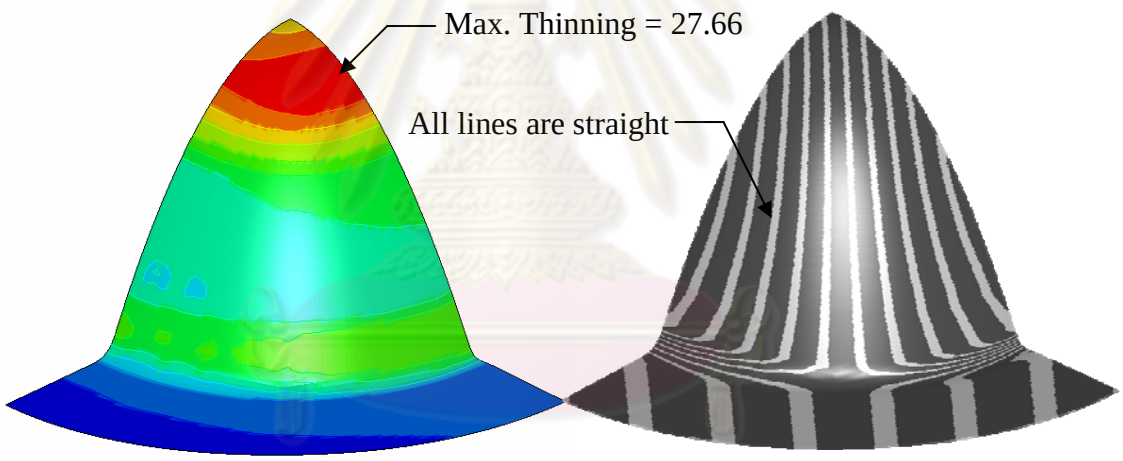

Figure 6.32 The thinning distribution and zebra lines on the Part2 at 100 monitoring steps

ศูนย์วิทยทรัพยากร
จุฬาลงกรณ์มหาวิทยาลัย

Thickness distribution on curvilinear of Part2 from loading paths of the adaptive simulation and fuzzy logic control algorithm is shown in figure 6.33. The minimum thickness is around 40 mm from the top of dome (punch nose). The second minimum thickness is around 160 mm (near counter pot radius).

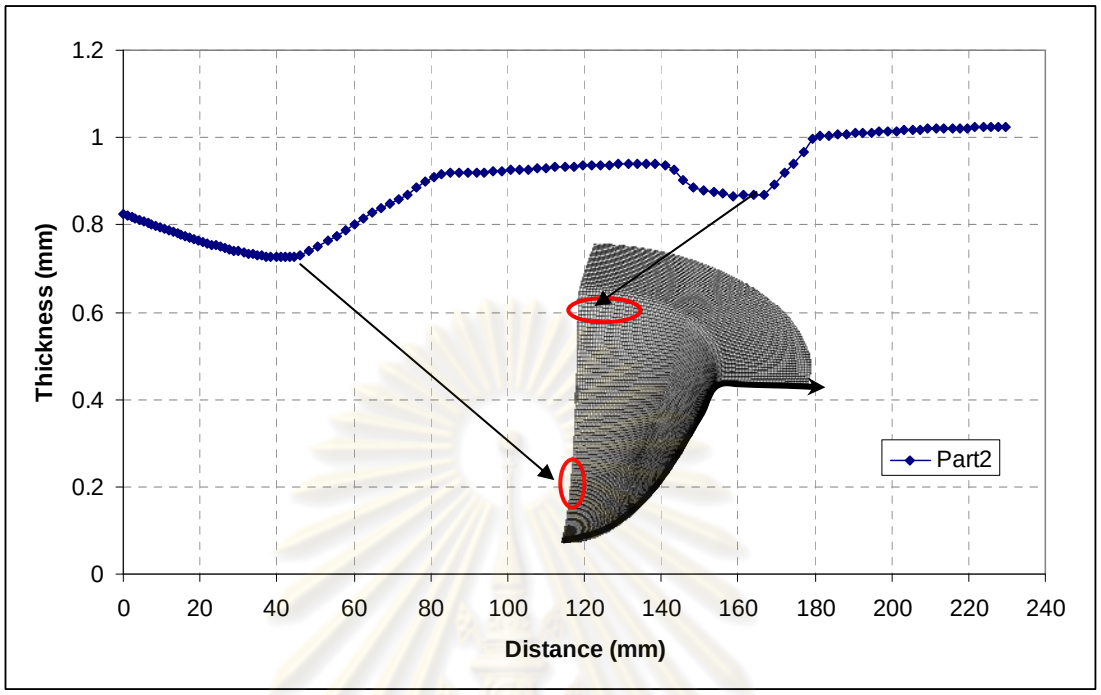

Figure 6.33 The thickness distribution on curvilinear of the Part2

The loading paths of Part3 in each monitoring steps are shown in figure 6.26 – 6.27. The blank holder force and pressure profiles at 20, 30, 50 and 100 monitoring steps are consistent while, the 10 monitoring steps are different. The results of thinning, FAM and SW are shown in table 6.4

Table 6.4 Results of Part3 by adaptive simulation with fuzzy logic control

Monitoring Steps		**100**	**50**	**30**	**20**	**10**
Part3	Thinning	27.0553	27.1418	25.9573	24.44050	25.07240
	FAM	1.01789	1.01773	1.01425	1.00923	1.01495
	SW	0.47471	0.47490	0.47035	0.47059	0.76415

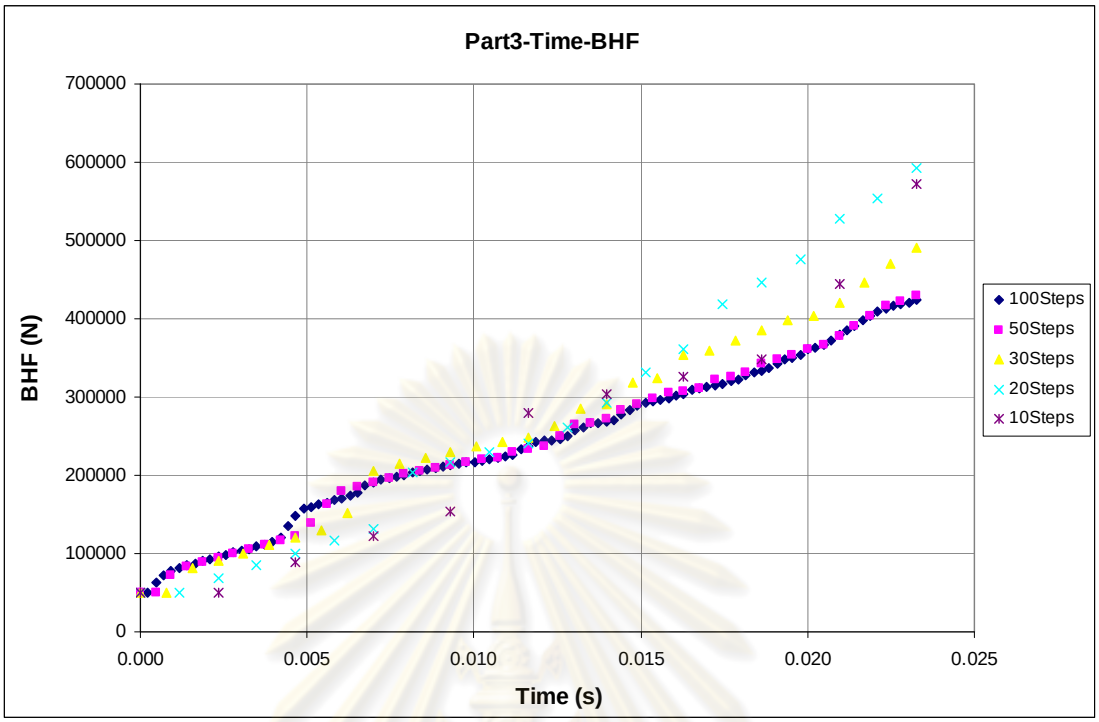

Figure 6.34 BHF profiles varying by number of monitoring steps of Part3

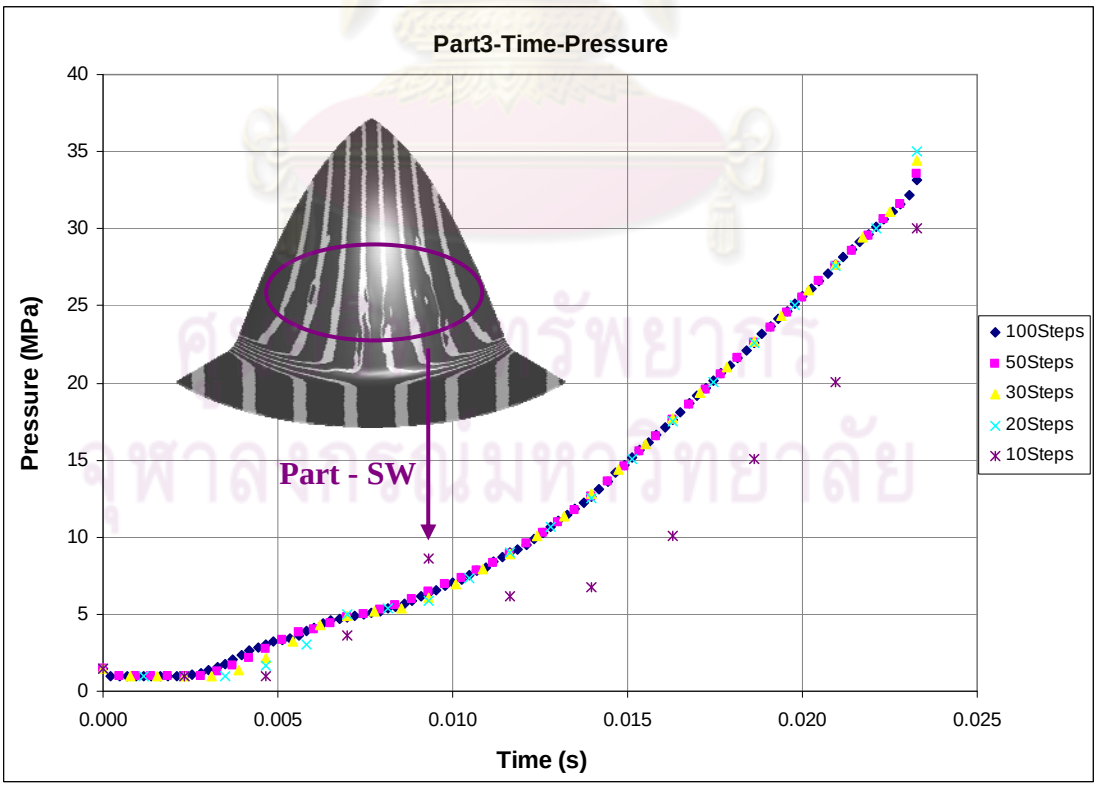

Figure 6.35 Pressure profiles varying by number of monitoring steps of Part3

The forming results obtained from using loading paths from the adaptive simulation and fuzzy logic control algorithm are good (no crack, no wrinkle) except for when using10 monitoring steps that the loading paths given the cracked part. Figure 6.36 shows the thinning distribution on Part3 using 100 monitoring steps; the maximum thinning is 27.06, the part is not cracked. For the FAM and SW values, they are below their limits; the part has no wrinkles. To make sure that the wrinkles do not appear on the part, the zebra line visualization technique was used and found that all lines are straight. The maximum thinning from the adaptive simulation and fuzzy logic control algorithm is less than the maximum thinning as a result from the optimal constant BHF and linear pressure from process window (25.64%). In addition, the adaptive simulation method used only one simulation.

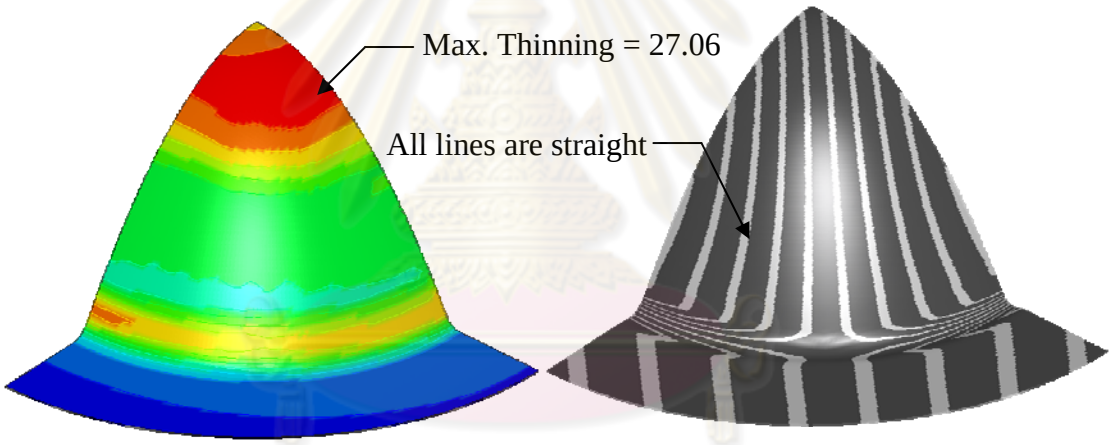

Figure 6.36 The thinning distribution and zebra lines on the Part3 at 100 monitoring steps

Thickness distribution on curvilinear of Part3 from loading paths of the adaptive simulation and fuzzy logic control algorithm is shown in figure 6.37. The minimum thickness is around 50 mm from the top of dome (punch nose). The second minimum thickness is around 210 mm (near counter pot radius).

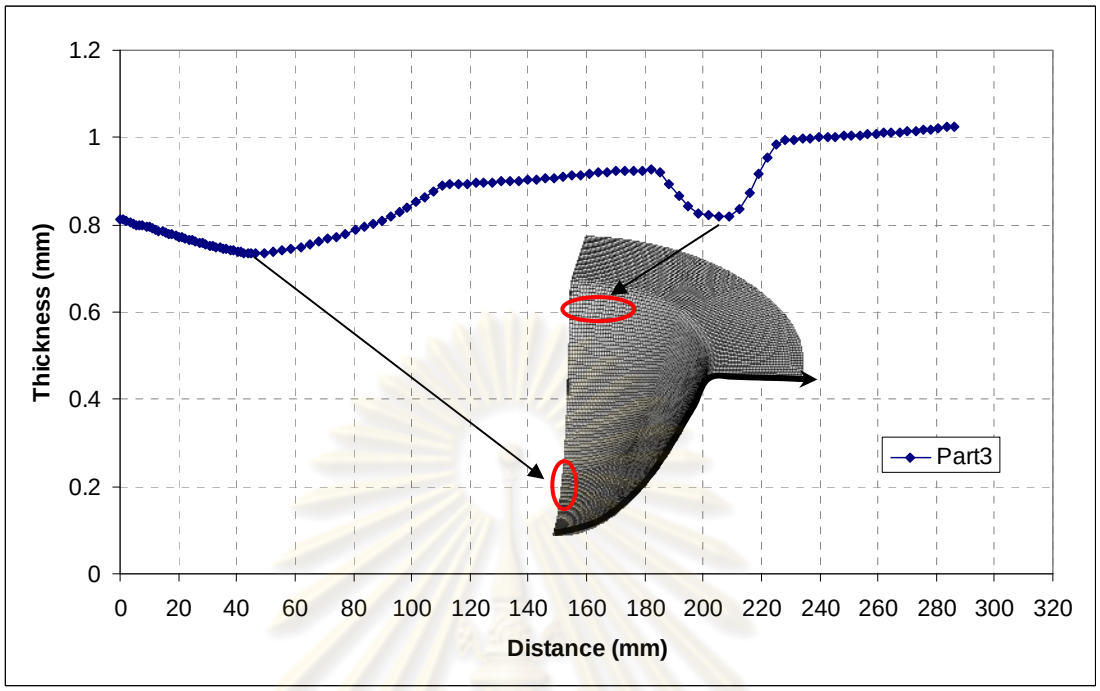

Figure 6.37 The thickness distribution on curvilinear of the Part3

The loading profiles obtained from the three parabolic parts can be summarized in figure 6.38 – 6.39. It can be seen that the BHF profiles of all parts can be well fitted in exponential curves. The BHF profile of Part1 is fitted in Eq. 6.4 that has $R^2 = 0.9597$, Part2 is fitted in Eq. 6.5 that has $R^2 = 0.9717$ and Part3 is fitted in Eq. 6.6 that has $R^2 = 0.9064$.

$$y = 24779e^{74.814x} \quad (6.4)$$

$$y = 21056e^{119.87x} \quad (6.5)$$

$$y = 92281e^{72.49x} \quad (6.6)$$

The pressure profiles of all parts can also be well fitted in exponential curves. The pressure profile of Part 1 is fitted in Eq. 6.7 that has $R^2 = 0.971$, Part 2 is fitted in Eq. 6.8 that has $R^2 = 0.9759$ and Part 3 is fitted in Eq. 6.9 that has $R^2 = 0.9559$.

ศูนย์วิทยทรัพยากร
จุฬาลงกรณ์มหาวิทยาลัย

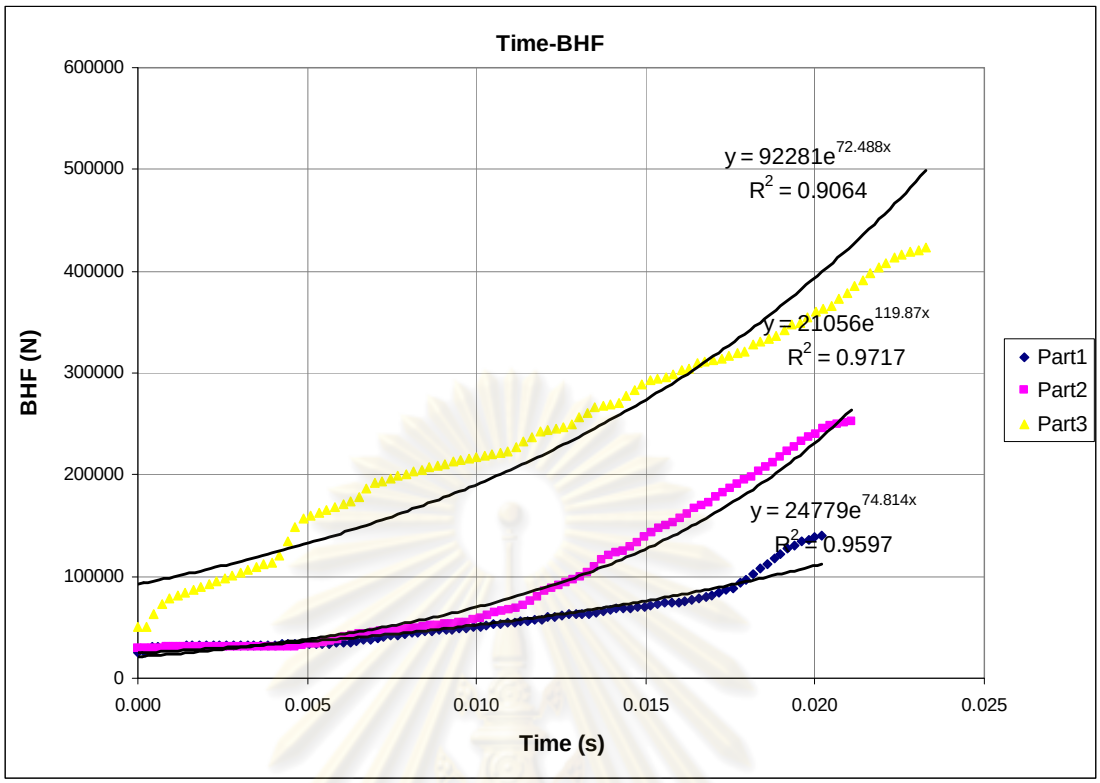

Figure 6.38 BHF profiles using 100 monitoring steps of three parabolic parts

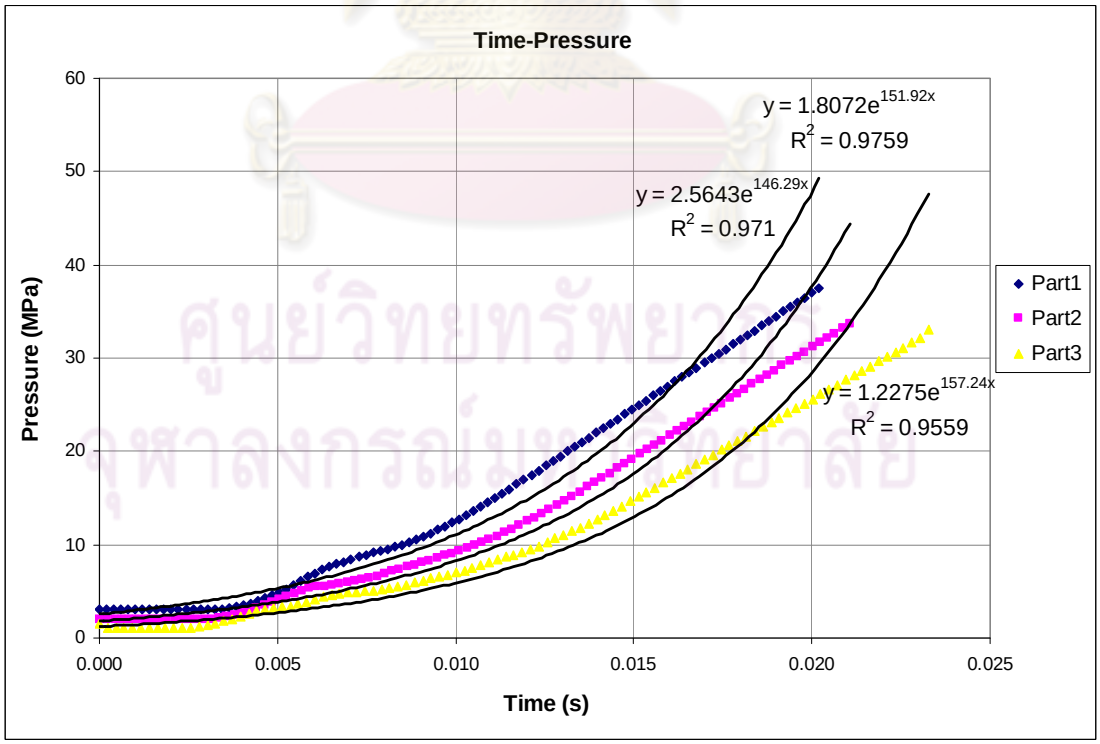

Figure 6.39 Pressure profiles using 100 monitoring steps of three parabolic parts

$$y = 2.5643e^{146.29x} \quad (6.7)$$

$$y = 1.8072e^{151.92x} \quad (6.8)$$

$$y = 1.2275e^{157.24x} \quad (6.9)$$

Thickness distribution on curvilinear of three parabolic shapes from loading paths of the adaptive simulation and fuzzy logic control algorithm is shown in figure 6.40. The first chance of crack happens on the part near the punch nose. It occurs at the thin-out stage after pre-bulge, this stage does not need as much of pressure and blank holder force. The second chance of crack appears on the part near the counter pot radius. It occurs before the end of stroke due to more pressure and blank holder force. Before the end of stroke, more pressure and blank holder force are needed to keep the blank stretched, to prevent the side wall wrinkle from happening around 100 mm distance following curvilinear starting at the top of dome.

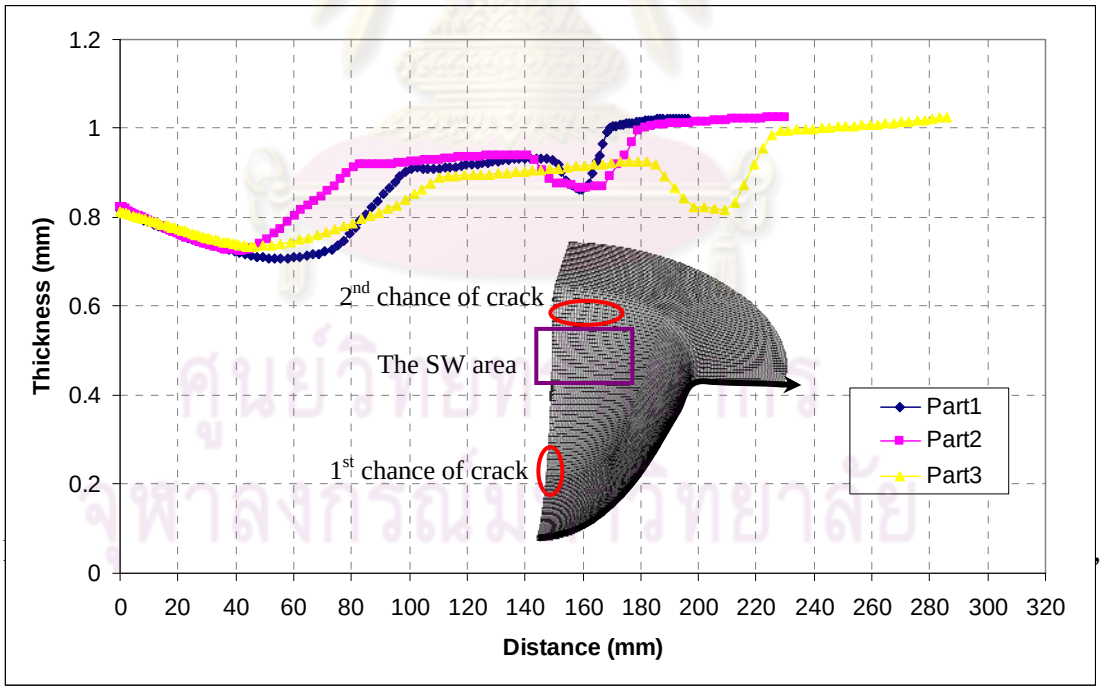

Figure 6.40 The thickness distribution on curvilinear of three parabolic parts

The automatic approach with adaptive simulation coupled with fuzzy logic control algorithm can determine the BHF and pressure profiles in one simulation, while the determination of optimal constant BHF and linear pressure requires more number of simulations. The minimum thinning from loading paths of adaptive simulation coupled with fuzzy logic control algorithm is almost less than the loading paths of optimal constant BHF and linear pressure. The monitoring step does not affect the convergence of solutions except when using 10 steps or below. It was also formed that to form parabolic shapes with HMD, the exponential curves is proper for the part because it needs the lower BHF and pressure at the beginning of stroke (thin-out stage) and gradually increases at the middle of stroke (wrinkle stage) and rapidly increases at the end of stroke (re-strike). Consequently, the loading paths of three parabolic parts are fitted in exponential equations. To determine the loading paths in 10 monitoring steps is challenging. The known curve (exponential) is used to enable 10 monitoring steps and results in much less computational time.

6.6 Modification of load function in exponential form

From previous section, the modification of load function in linear form can determine the BHF and pressure profiles, when using more than 10 monitoring steps. The BHF and pressure curves are fitted in exponential equations. Consequently, to reduce the monitoring steps required the exponential form was applied instead of the linear form as the Eq. 6.10 and 6.11.

$$BHF_{New} = BHF_{Old} * e^{(\beta+\mu)} \quad (6.10)$$

$$P_{New} = P_{Old} * e^{\alpha} \quad (6.11)$$

Eq. 6.10 is the modification of BHF function in exponential form and Eq. 6.11 is the modification of pressure function in exponential form. These equations do not have the ΔBHF and ΔP term. However, the output membership function will be changed to consistent of the result from modification of load function in linear form. BHF

equations of three parts (Eq. 6.4 – 6.6) show the exponent values as 74.81x, 119.87x and 72.49x where x is the simulation time. In final stroke, the power of exponent is around 1.5, 2.5 and 1.7. From figure 6.38, the minimum requirement of all parts is around 1.7 (100 steps), so the center of slightly values of β and μ should be added not less than 0.17 in 10 steps (1.7/10). The slightly value of β is 0.15, the moderate value is 0.2 and the extremely value is 0.25. Therefore, the proper slightly of μ (draw-in speed) should be 0.02(2%). To remain the scale of blank holder force in linear form as 1, 3 and 5 times, so the moderate value of μ is 0.06 (6%) and the extremely value of μ is 0.10 (10%). The β output membership function of modification of load function in exponential form is shown in figure 6.41 and the μ output membership function of modification of load function in exponential form is shown in figure 6.42

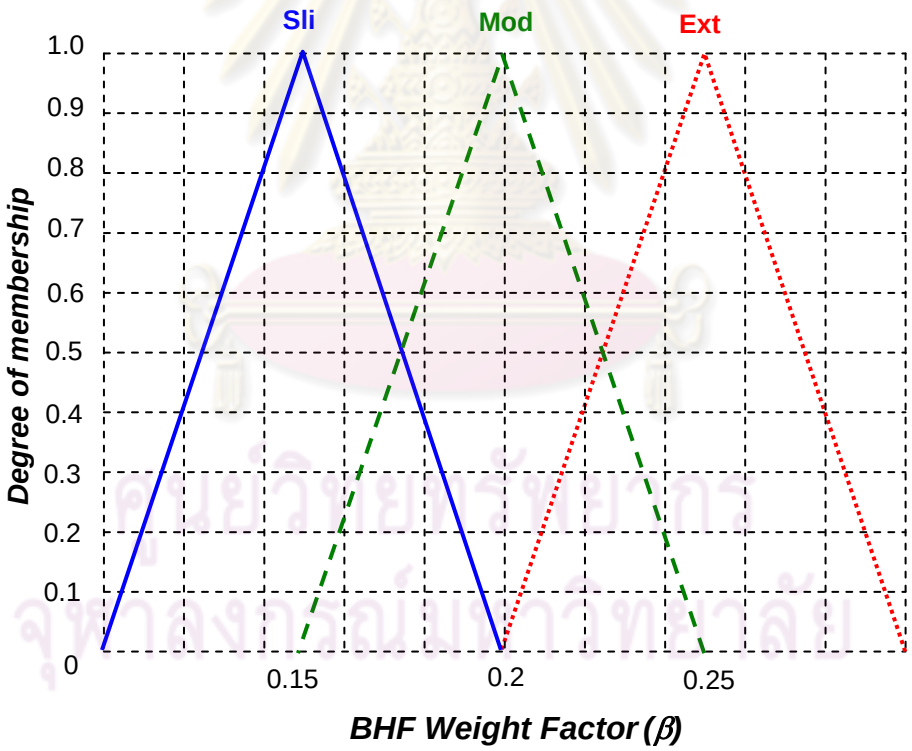

Figure 6.41 The β output membership function of load function in exponential form

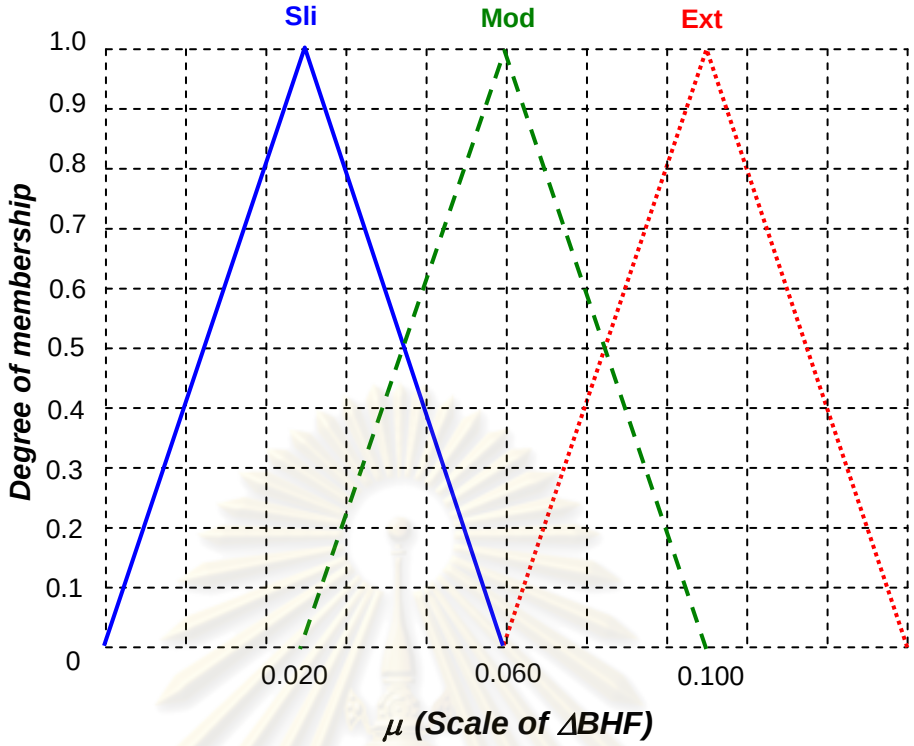

Figure 6.42 The μ output membership function of load function in exponential form

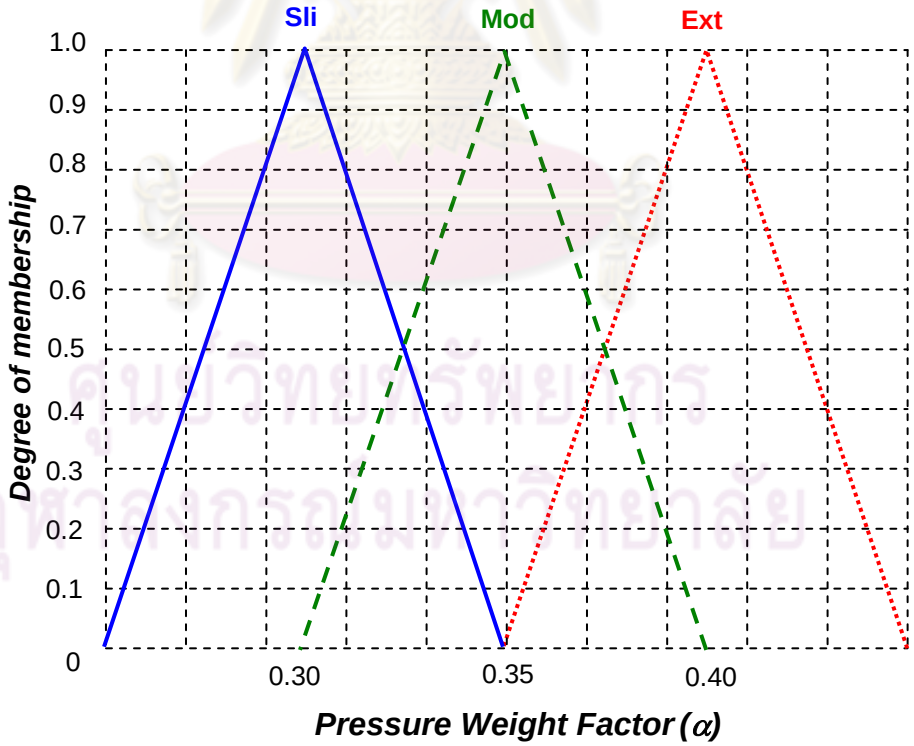

Figure 6.43 The α output membership function of load function in exponential form

Pressure equations of three parts (Eq. 6.7 – 6.9) show the exponent values as 146.29x, 151.92x and 157.24x where x is the time. In final stroke, the power of exponent is around 3.0, 3.2 and 3.7. To translate them into the output membership function in 10 monitoring steps, divided them with 10 so, the slightly value is around 0.30, the moderate value is about 0.35 and the extremely value is around 0.40. The α output membership function of modification of load function in exponential form is shown in figure 6.43.

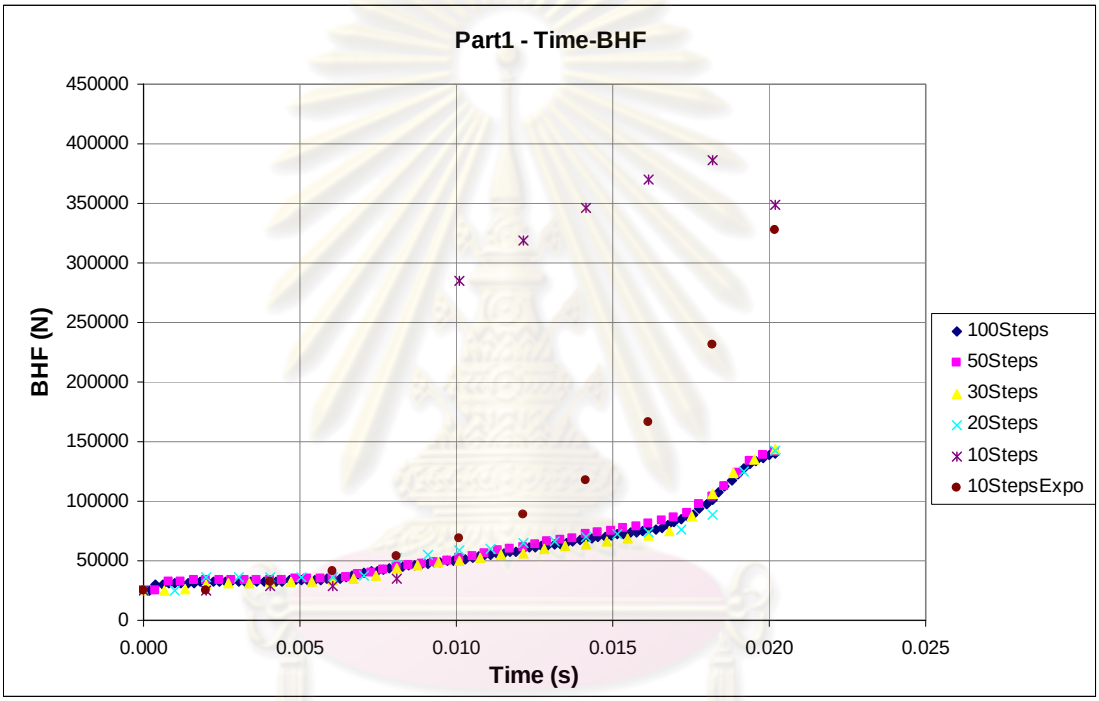

Figure 6.44 BHF profiles varying by monitoring steps of Part1 with 10 monitoring steps of load function in exponential form

The loading paths of Part1 in every monitoring step of modification of load function in linear form and 10 monitoring step with modification of load function in exponential form are shown in figure 6.44 – 6.45. The BHF and pressure profiles from modification of load function in exponential form are consistent with profiles from modification of load function in linear form in 20, 30, 50 and 100 monitoring steps. The results obtained from loading paths of modification load function in exponential form are good (no crack, no wrinkle). Figure 6.46 shows the thinning distribution on Part1 at 10 monitoring step with modification load function in

exponential form; the maximum thinning is 29.76, it means the part is not cracked. The FAM is 1.008 and SW is 0.46971, they are below their limits; it means the part has no wrinkles. To make sure that the wrinkles do not appear on the part, the zebra lines are used and found that all lines are straight. The adaptive simulation and fuzzy logic control algorithm with modification load function in exponential form is near the maximum thinning of modification load function in linear form as 29.43. For parabolic parts with HMD, the modification load function in exponential form can determine the loading paths with less a number of monitoring steps than the modification load function in linear form.

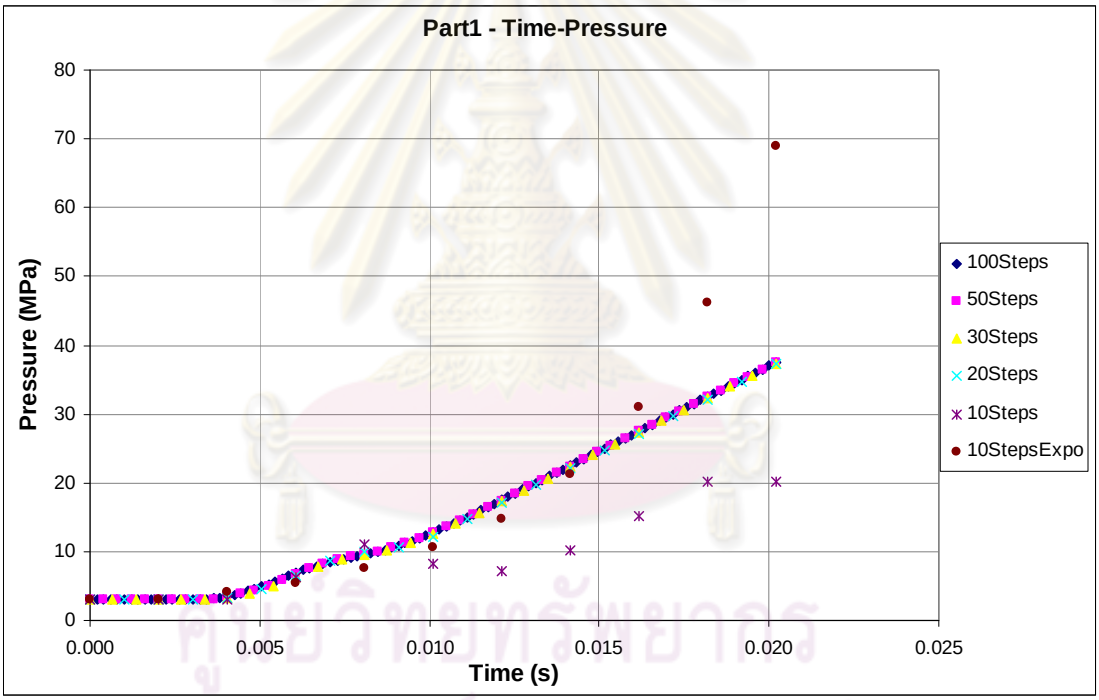

Figure 6.45 Pressure profiles varying by monitoring steps of Part1 with 10 monitoring steps of load function in exponential form

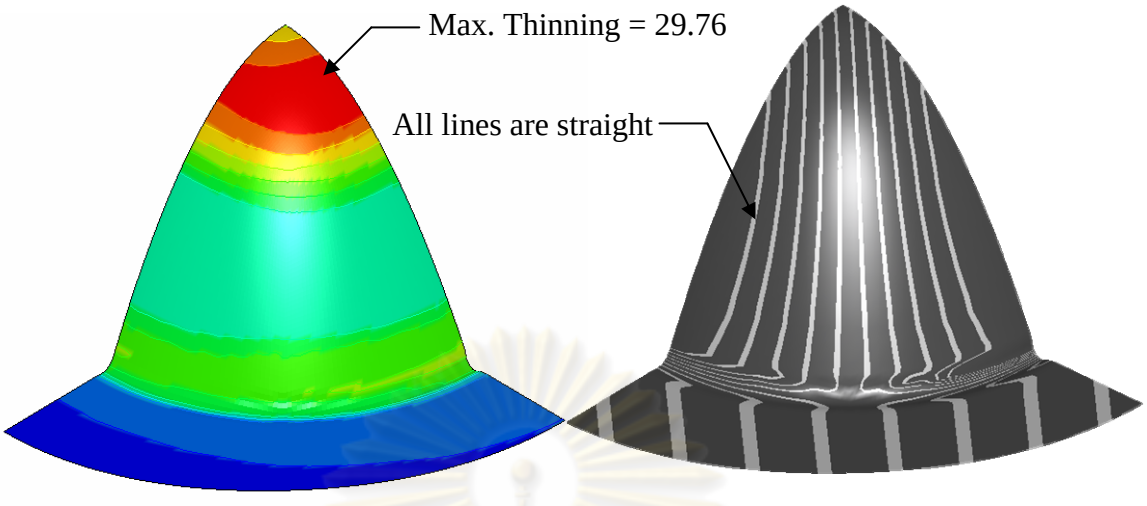

Figure 6.46 The thinning distribution and zebra lines on the Part1 at 10 monitoring steps of load function in exponential form

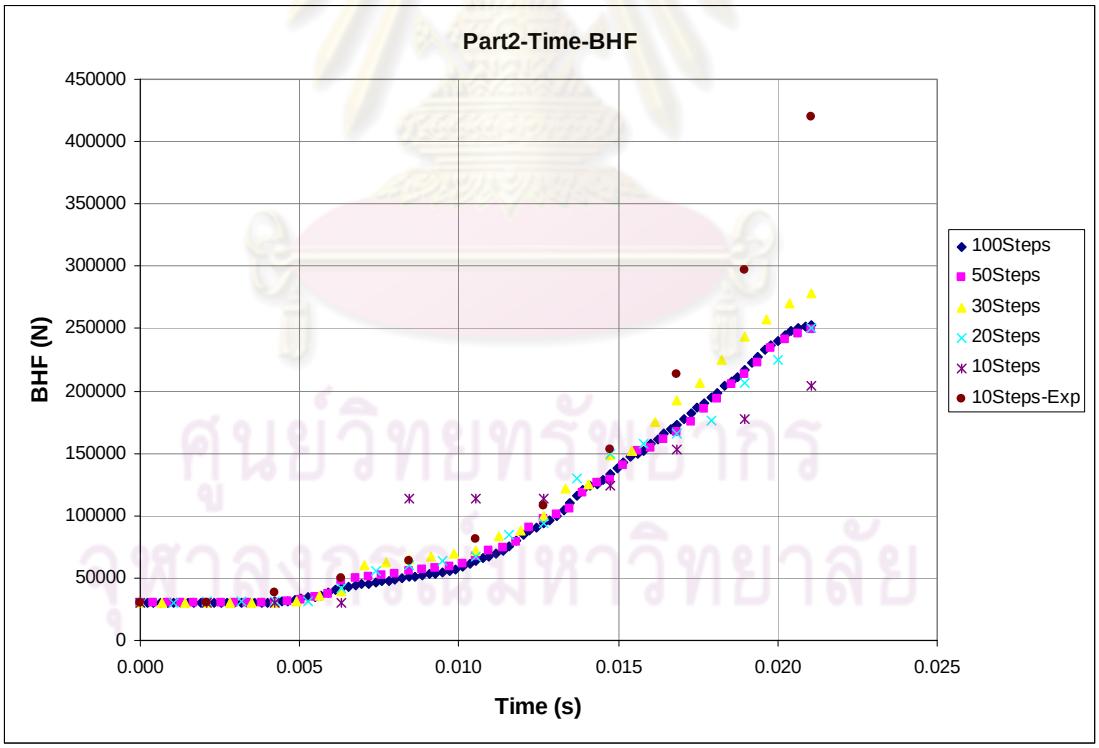

Figure 6.47 BHF profiles varying by monitoring steps of Part2 with 10 monitoring steps of load function in exponential form

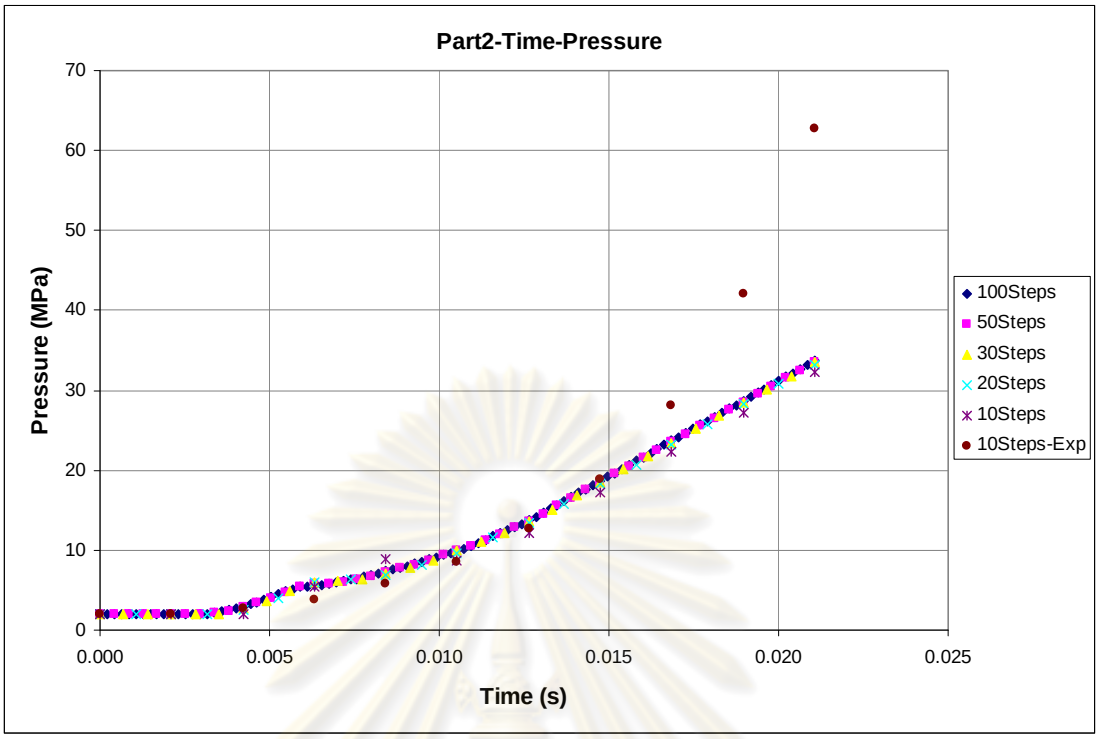

Figure 6.48 Pressure profiles varying by monitoring steps of Part2 with 10 monitoring steps of load function in exponential form

The loading paths of Part2 in every monitoring step with modification of load function in linear form and 10 monitoring step with modification of load function in exponential form are shown in figure 6.47 – 6.48. The BHF and pressure profiles from modification of load function in exponential form are consistent with profiles from modification of load function in linear form in 20, 30, 50 and 100 monitoring steps. The results obtained from loading paths with modification of load function in exponential form are good (no crack, no wrinkle). Figure 6.49 shows the thinning distribution on Part2 at 10 monitoring step with modification of load function in exponential form; the maximum thinning is 27.10, it means the part is not cracked. The FAM is 1.007 and SW is 0.48418, they are below their limits; it means the part has no wrinkles. To make sure that the wrinkles do not appear on the part, the zebra lines are used and found that all lines are straight. The adaptive simulation and fuzzy logic control algorithm with modification of load function in exponential form is near the maximum thinning of modification of load function in linear form as 27.66. For parabolic parts with HMD, the modification of load function in exponential form can

determine the loading paths with less a number of monitoring steps than the modification of load function in linear form.

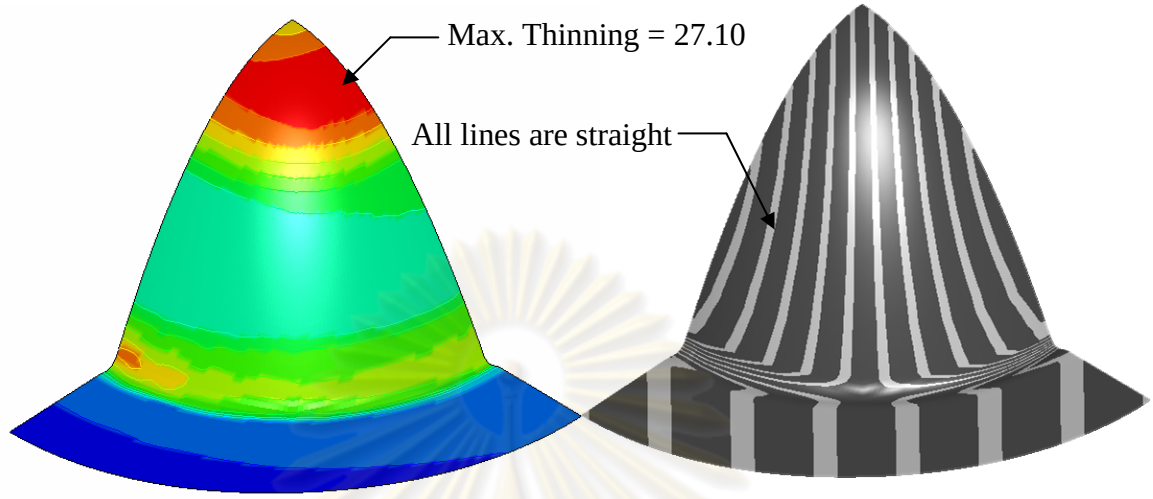

Figure 6.49 The thinning distribution and zebra lines on the Part2 at 10 monitoring steps of load function in exponential form

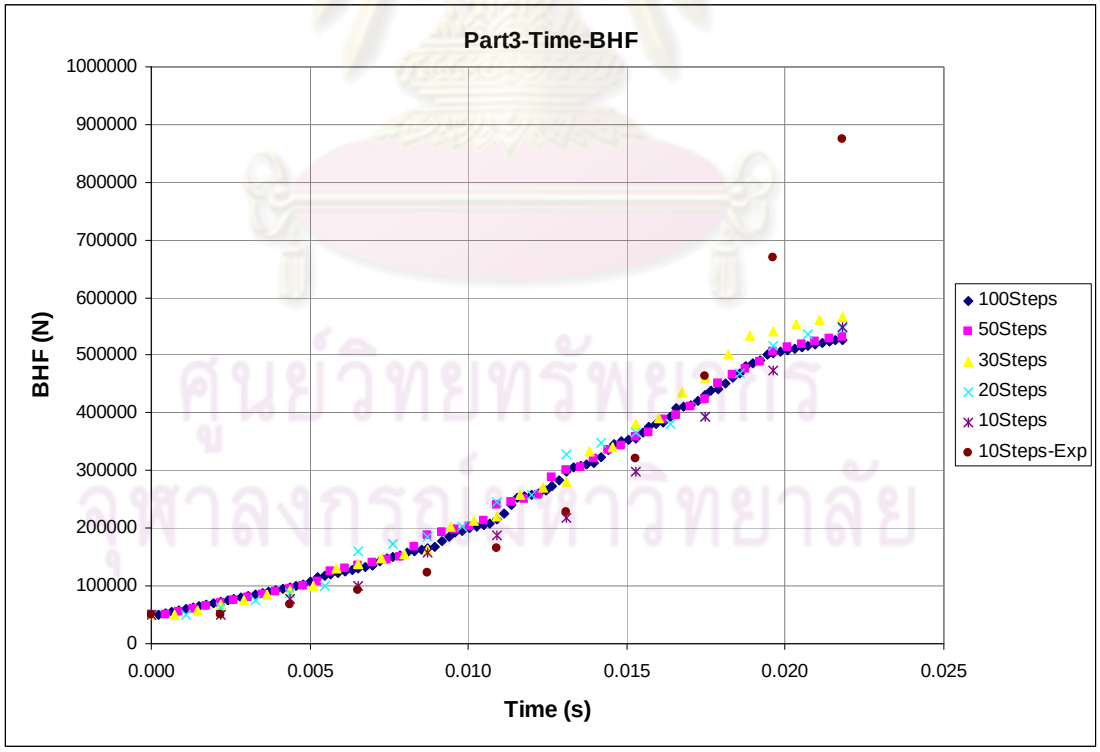

Figure 6.50 BHF profiles varying by monitoring steps of Part3 with 10 monitoring steps of load function in exponential form

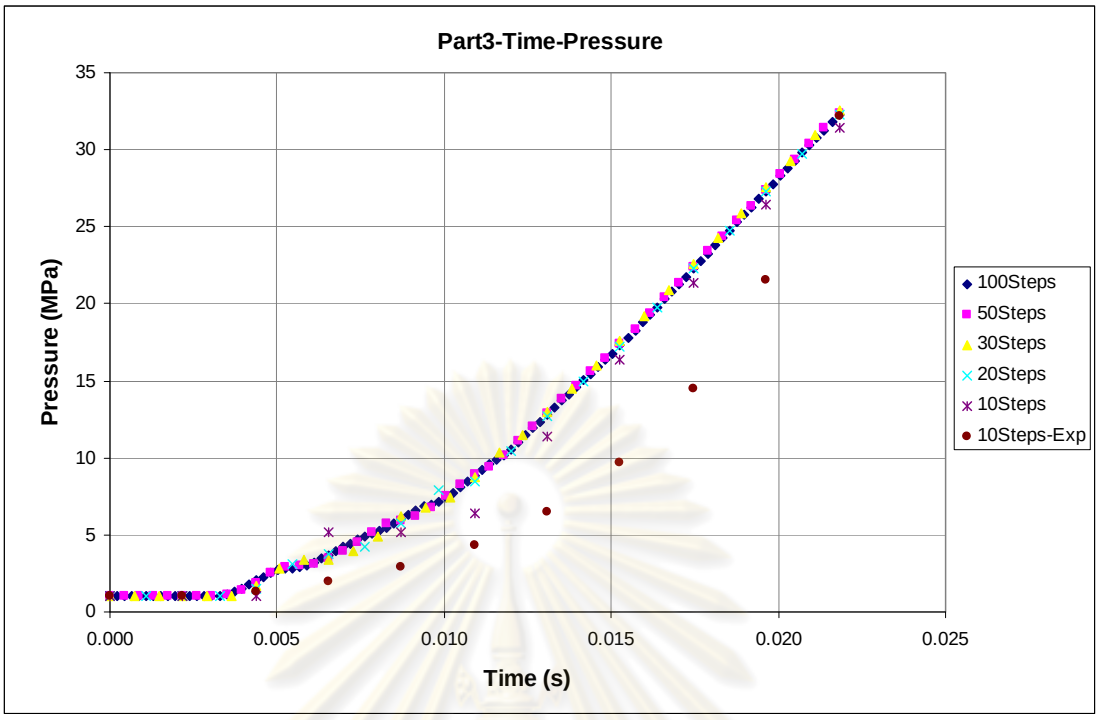

Figure 6.51 Pressure profiles varying by monitoring steps of Part3 with 10 monitoring steps of load function in exponential form

The loading paths of Part3 in every monitoring step with modification of load function in linear form and 10 monitoring step with modification of load function in exponential form are shown in figure 6.50 – 6.51. The BHF and pressure profiles from modification of load function in exponential form are consistent with profiles from modification of load function in linear form in 20, 30, 50 and 100 monitoring steps. The results obtained from loading paths with modification of load function in exponential form are good (no crack, no wrinkle). Figure 6.52 shows the thinning distribution on Part3 at 10 monitoring step with modification of load function in exponential form; the maximum thinning is 30.52, it means the part is not cracked. The FAM is 1.007 and SW is 0.49936, they are below their limits; it means the part has no wrinkles. To make sure that the wrinkles do not appear on the part, the zebra lines are used and found that all lines are straight. The adaptive simulation and fuzzy logic control algorithm with modification of load function in exponential form is near the maximum thinning of modification of load function in linear form as 27.06. For

parabolic parts with HMD, the modification of load function in exponential form can determine the loading paths with less a number of monitoring steps than the modification of load function in linear form. The maximum thinning happens on the counter pot radius instead of the punch nose because of the higher values of blank holder force and pressure at the end of stroke.

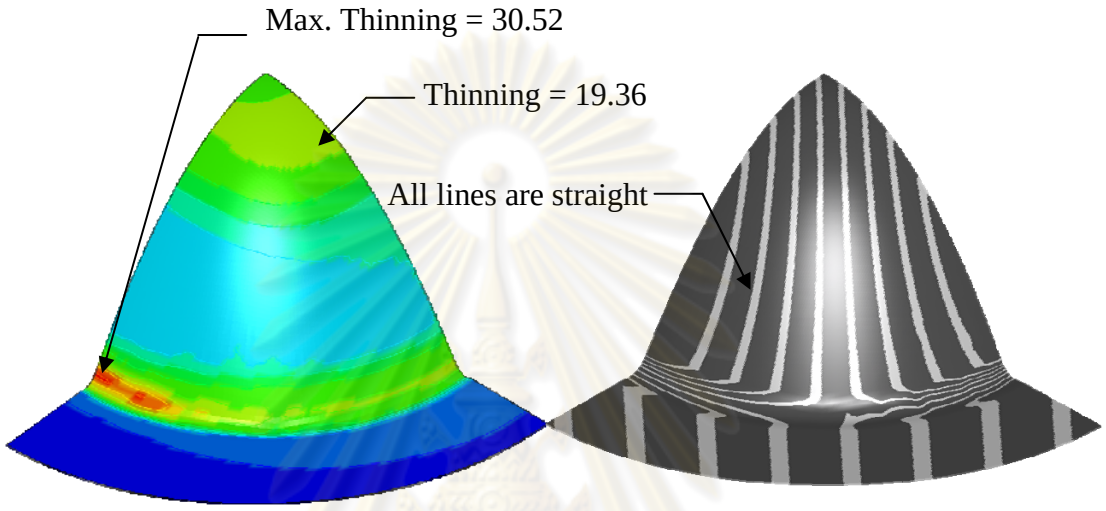

Figure 6.52 The thinning distribution and zebra lines on the Part3 at 10 monitoring steps of load function in exponential form

The modification of load function in exponential form is proper for forming parabolic parts with HMD. In 10 steps monitoring, it can converge the solutions while, the linear cannot. However, at the end of stroke, the modification of load function in exponential form gives the BHF and pressure profiles higher than the modification of load function in linear form (over need for re-strike) as a result some part has another thinning near the counter pot radius. Therefore, the modification of load function in exponential form is not proper for deeply parabolic shape. The physical meaning of exponential is the percentage of incremental from initial values. Consequently, the initial of BHF and pressure are very important. In case of the solutions are not proper, the initial BHF and pressure should be adjusted firstly. If it cannot be fixed, the input

and output membership functions should be adjusted. Or to improve the accuracy of responses, the output membership functions should be also changed.

6.7 Validation of modification of load function in exponential form on other parabolic cup

To prove the modification of load function in exponential form, a new parabolic part was selected to determine the loading paths. This part is shown in figure 6.53 - 6.54. Figure 6.54 shows Part51 compared of with the three parabolic parts. The Part51 is bigger and deeper than the other. The input and output membership function of this part is similar to that of three parts.

Determination of loading paths of Part51 using 10 monitoring step with modification of load function in exponential form is shown in figure 6.55 – 6.56. The results obtained from loading paths in modification of load function in exponential form are good (no crack, no wrinkle). Figure 6.57 shows the thinning distribution on Part51 at 10 monitoring step with modification of load function in exponential form; the maximum thinning is 37.80, the part is not cracked. The maximum thinning happens near the counter pot radius. The FAM is 0.990 and SW is 0.52399, they are below their limits; the part has no wrinkles. To make sure that the wrinkles do not appear on the part, the zebra lines are used and found that all lines are straight.

ศูนย์วิทยทรัพยากร
จุฬาลงกรณ์มหาวิทยาลัย

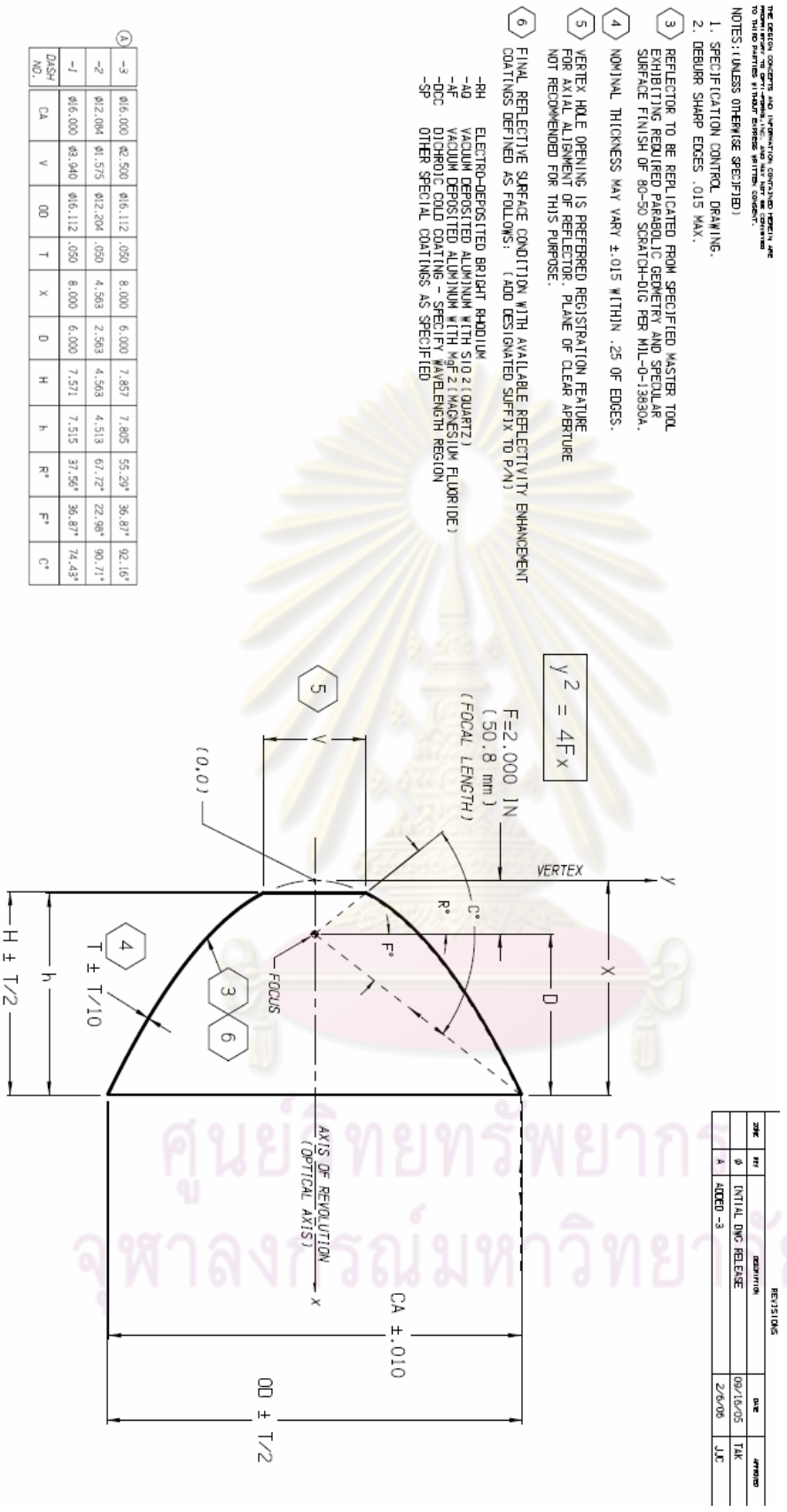

DASH NO.	CA	V	OD	T	X	D	H	h	R°	F°	C°
-3	Ø16.000	Ø2.500	Ø16.112	.050	8.000	6.000	7.857	7.805	55.29°	36.87°	92.16°
-2	Ø12.084	Ø1.575	Ø12.204	.050	4.563	2.563	4.563	4.513	67.72°	22.98°	90.71°
-J	Ø16.000	Ø3.040	Ø16.112	.050	8.000	6.000	7.571	7.515	37.56°	36.87°	74.43°

Figure 6.53 The new parabolic part (Part51)

	Focus (mm)	Width (mm)	Height (mm)	Blank Dia. ϕ (mm)
Part #51	**51.0**	**417.1**	**203.2**	**760.00**

Figure 6.54 The new parabolic part

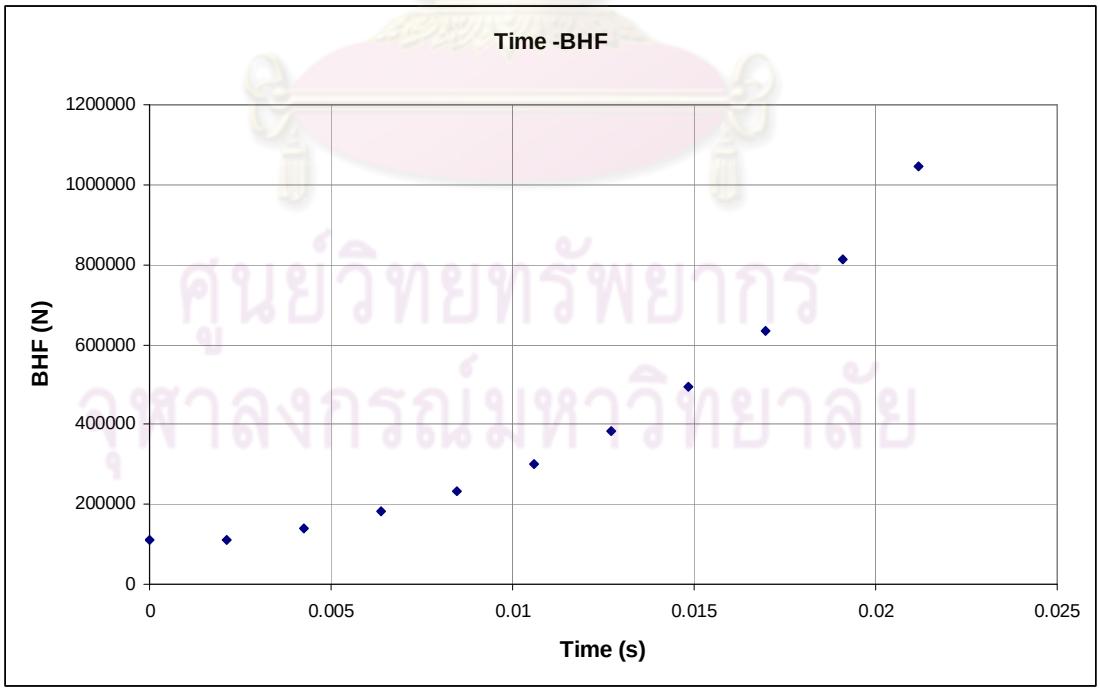

Figure 6.55 BHF profiles of Part51 with 10 monitoring steps using load function in exponential form

ศูนย์วิทยทรัพยากร
จุฬาลงกรณ์มหาวิทยาลัย

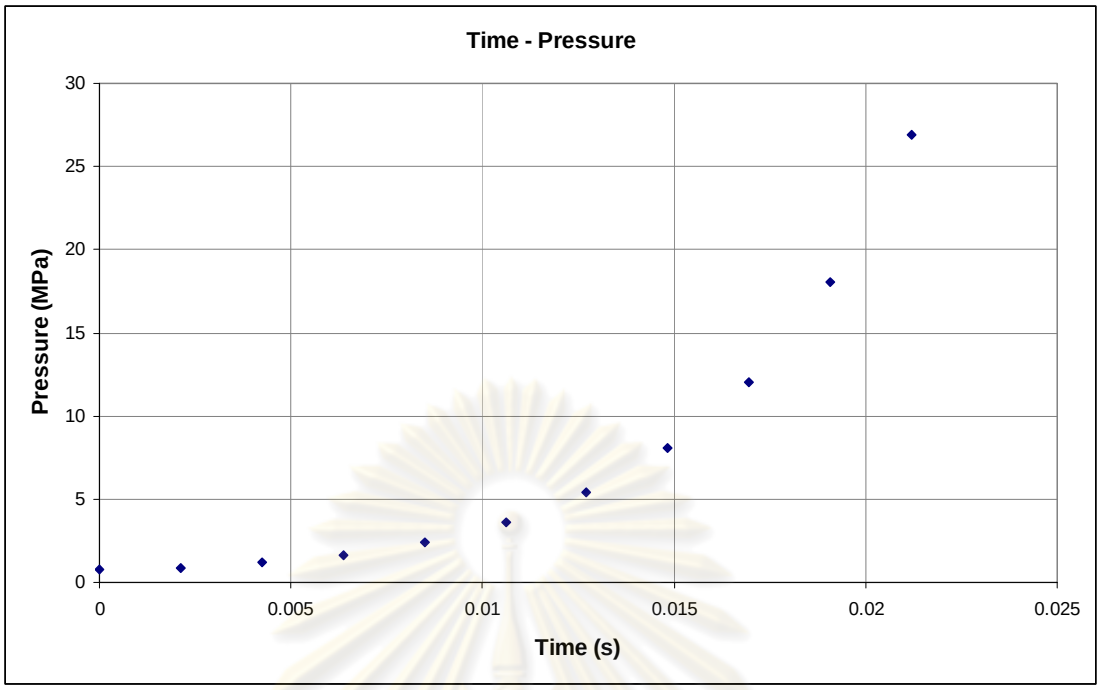

Figure 6.56 Pressure profiles of Part51 with 10 monitoring steps of load function in exponential form

The maximum thinning happens on the counter pot radius instead of the punch nose because of the higher values of blank holder force and pressure at the end of stroke.

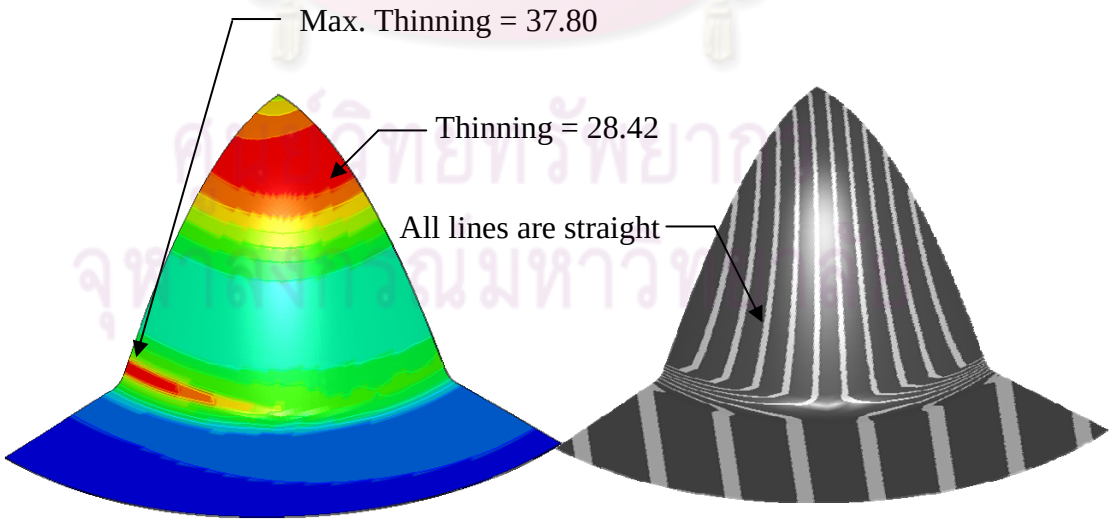

Figure 6.57 The thinning distribution and zebra lines on the Part51 using 10 monitoring steps of load function in exponential form

At the end of stroke, the modification of load function in exponential form will give rise to the blank holder force and pressure values that are over the need as a result the parabolic part near the counter pot radius is in risk of crack while, the maximum thinning should be occur at the punch nose. To correct this problem, the limits of blank holder force and pressure have been defined. In Part51, the limit of blank holder force as 600,000 N and pressure as 30 MPa. The new BHF profile and pressure profile were shown in figure 6.58 and figure 6.59 respectively.

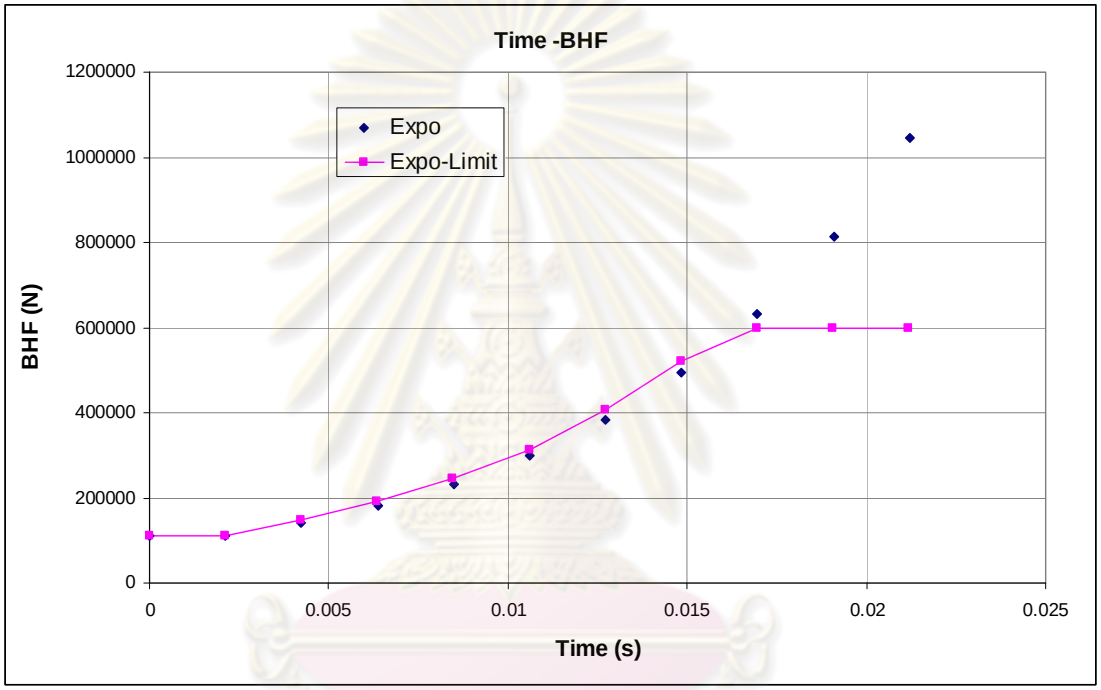

Figure 6.58 BHF profiles of Part51 with 10 monitoring steps of load function in exponential form with limit

The BHF gradually increase following the exponential curve when it has been reached to the limit around 0.017 s it remains in 600,000 N until the end of stroke while the pressure profile does not reach to limit at 30 MPa.

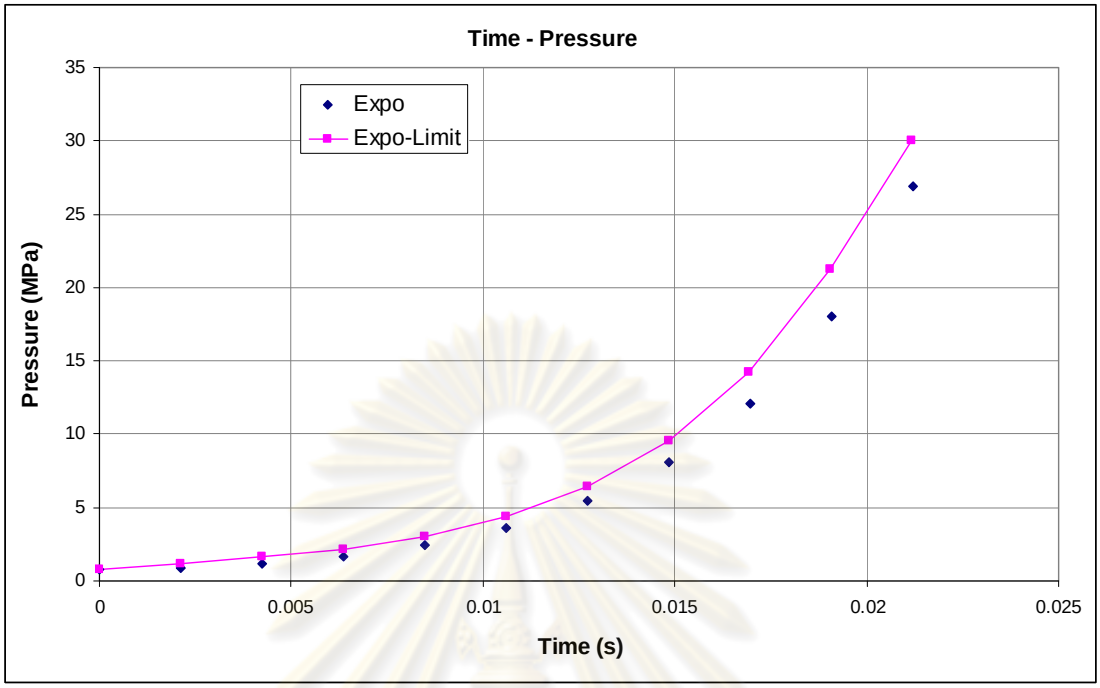

Figure 6.59 Pressure profiles of Part51 with 10 monitoring steps of load function in exponential form with limit

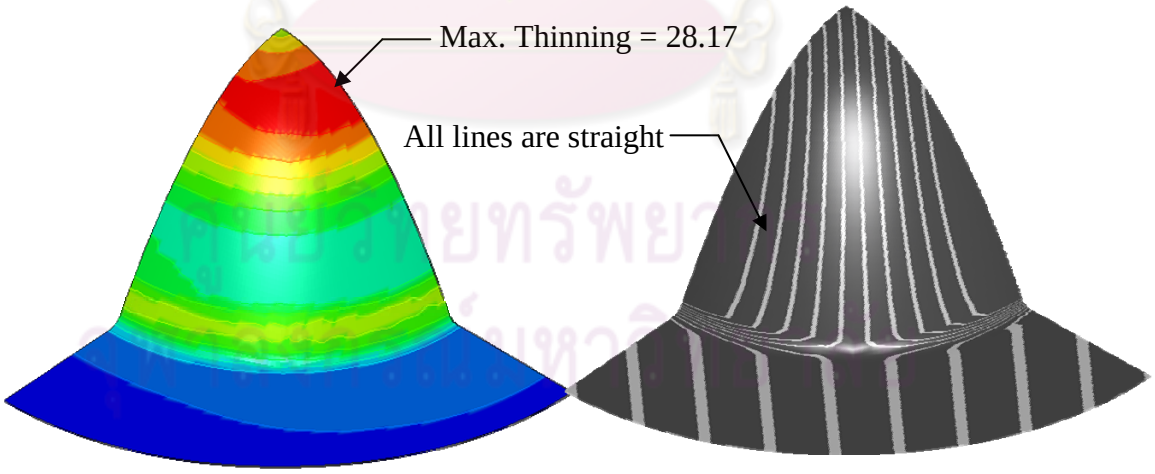

Figure 6.60 The thinning distribution and zebra lines on the Part51 using 10 monitoring steps of load function in exponential form with limit

The results obtained from loading paths with modification of load function in exponential form with limit are good (no crack, no wrinkle). Figure 6.60 shows the thinning distribution on Part51 at 10 monitoring step; the maximum thinning is 28.17, it means the part is not cracked. The FAM is 1.007 and SW is 0.48272, they are below their limits; it means the part it means the part has no wrinkles. To make sure that the wrinkles do not appear on the part, the zebra lines are used and found that all lines are straight. The maximum thinning occurs at the punch nose that moves to counter pot radius. It is the correct position to form the parabolic part.

6.8 Effect of membership function shape of thinning, FAM and SW

The membership function is an important factor to the accuracy of the system responses. However, to get the best function in each parameter is very difficult and needs a lot of data. The membership functions in this algorithm were created from simple shape (triangular) and symmetry. This section is aimed to investigate effects of membership function shape on the part quality obtained. The modification of load function in a linear form of 100 steps was used. Part1 is the part of interest to be examined because it can be validated by experiments.

6.8.1 Thinning membership function

To examine the effect of thinning membership function, it is required to skew the function to the left and to the right. The thinning membership function skewed to the left is shown in figure 6.61 and the thinning membership function skewed to the right is shown in figure 6.62

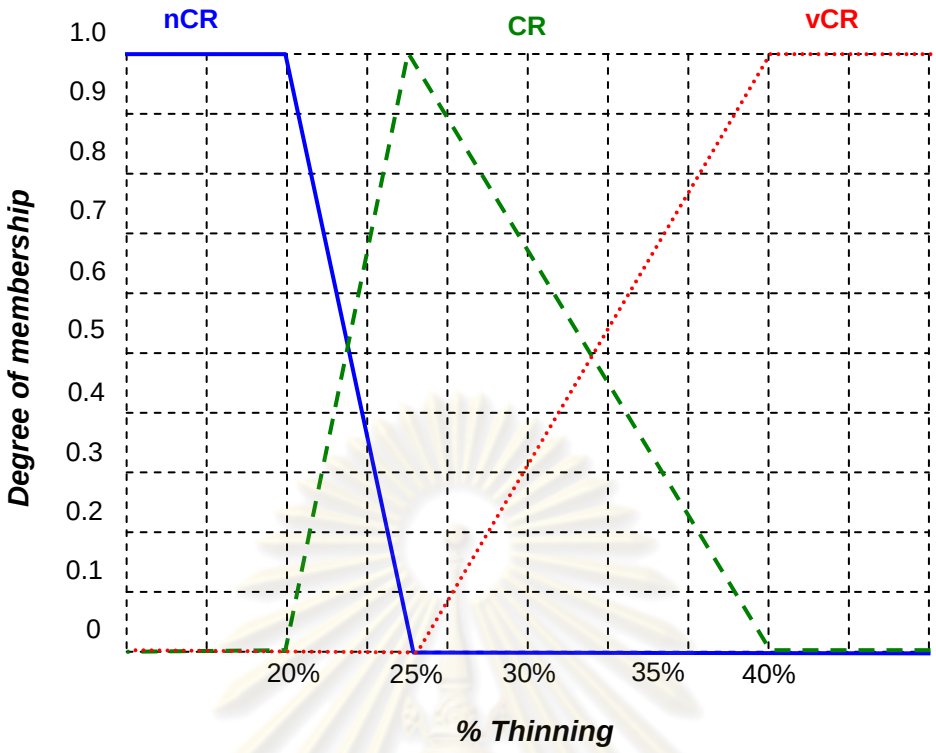

Figure 6.61 The thinning membership function skewed to the left

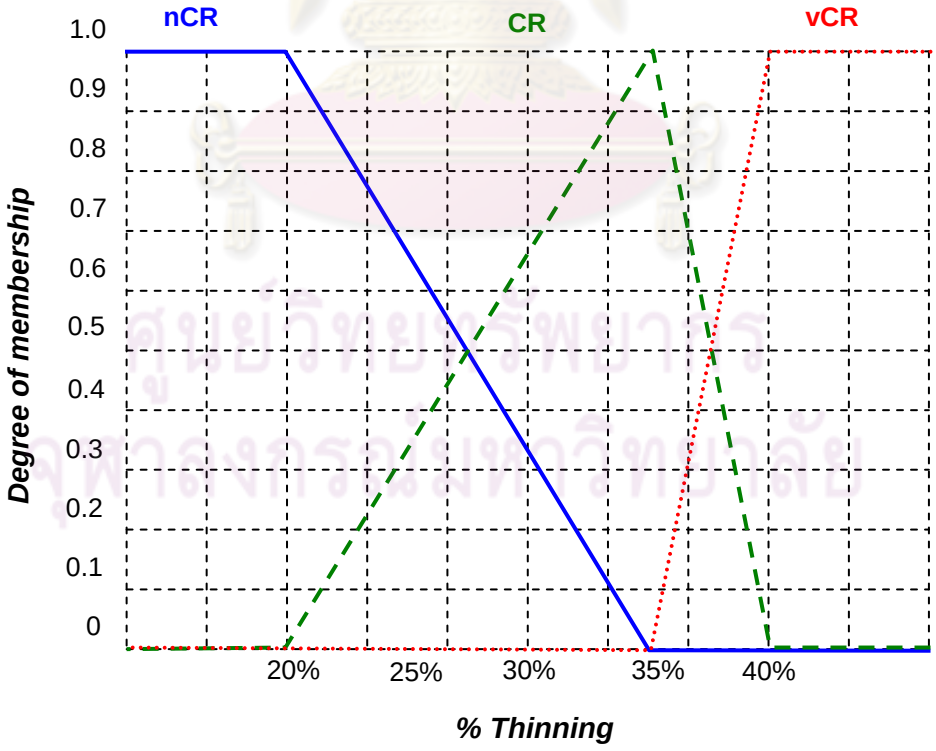

Figure 6.62 The thinning membership function skewed to the right

The loading paths of Part1 obtained with the thinning membership function skewed to the left, centered and skewed to the right are shown in figure 6.63 – 6.64. The blank holder force profile obtained from thinning membership function skewed to the right is higher than the centered one. The BHF profile obtained from the thinning membership function skewed to the left is lower than the centered one. The pressure profiles obtained from the thinning membership functions that are centered and skewed to the right are similar.

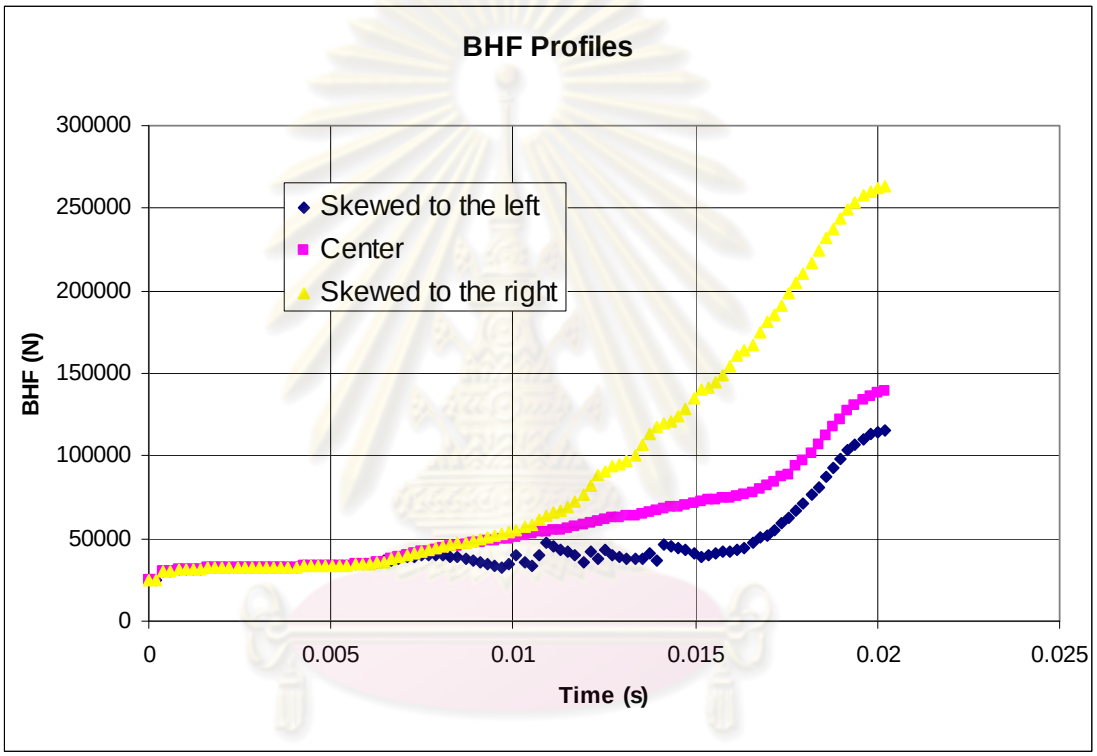

Figure 6.63 BHF profiles of Part1 obtained from different thinning membership function shapes

The resultant thinning, FAM and SW are shown in table 6.5. The side wall wrinkle occurs on the part from loading paths with thinning membership function skewed to the left due to the lower blank holder force and pressure profiles. While, the part from loading paths with thinning membership function skewed to the right is a good. Therefore, it can be seen that the thinning membership function affects both BHF and pressure profiles obtained. If it is skewed to the left the BHF and pressure will be lower, the part tends to have the side wall wrinkle and thinning lower than the others.

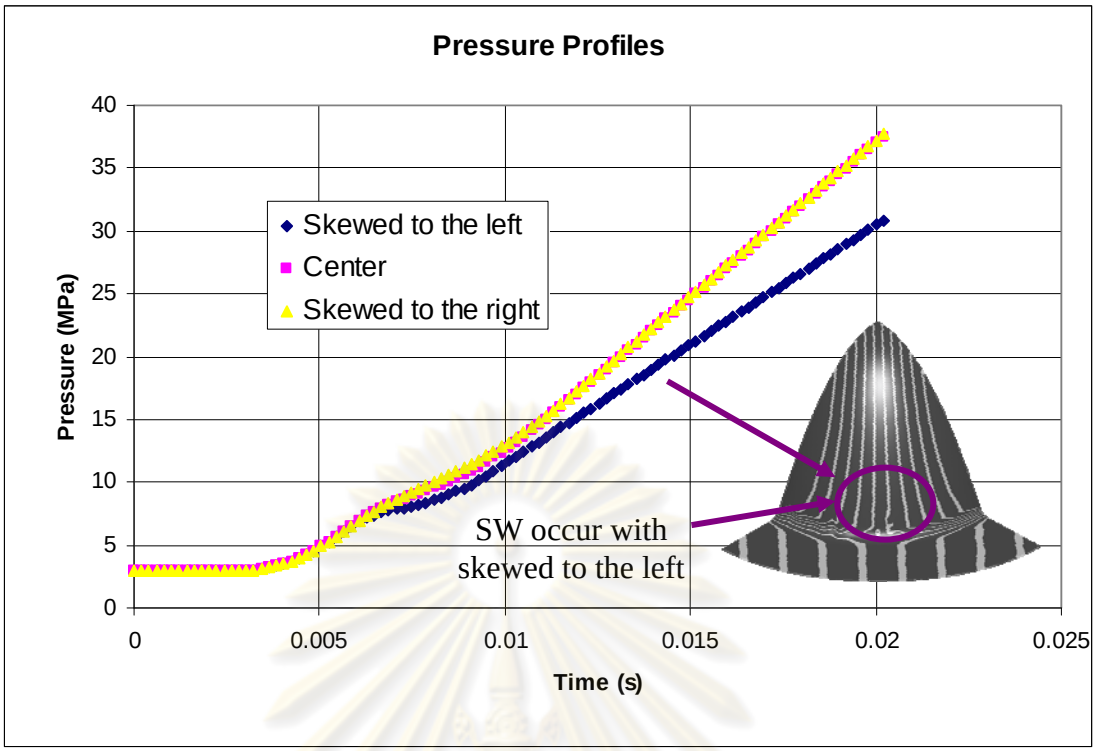

Figure 6.64 Pressure profiles of Part1 obtained from different thinning membership function shapes

Table 6.5 Results of Part1 obtained from different thinning membership function shapes

Thinning membership function		Skewed to the left	Center	Skewed to the right
Part1	Thinning	28.49220	29.42950	29.67700
	FAM	1.03936	1.03142	1.01079
	SW	0.63346	0.48399	0.47634

6.8.2 FAM membership function

To examine the sensitivity of thinning membership function, it is required to skew to the left and the right. The FAM membership function skewed to the left is shown in figure 6.65 and the FAM membership function skewed to the right is shown in figure 6.66.

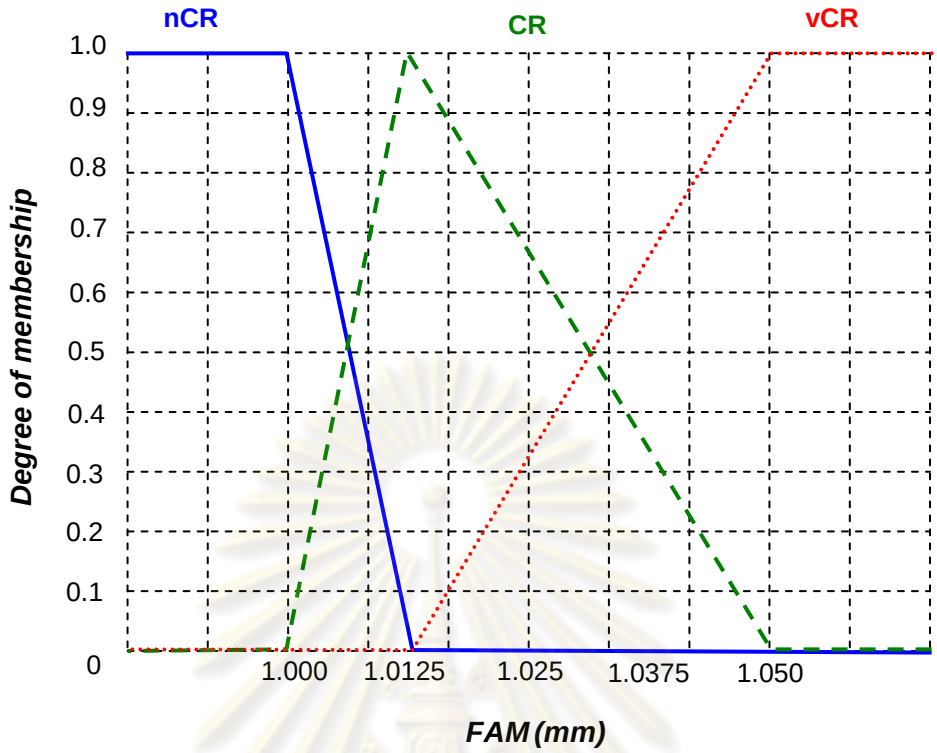

Figure 6.65 The FAM membership function skewed to the left

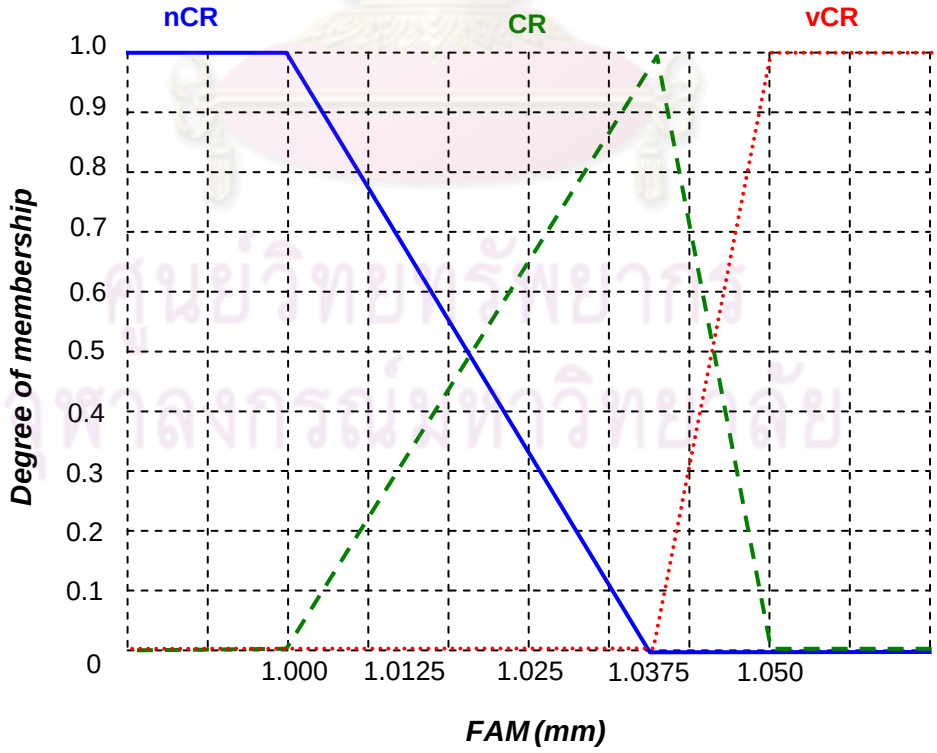

Figure 6.66 The FAM membership function skewed to the right

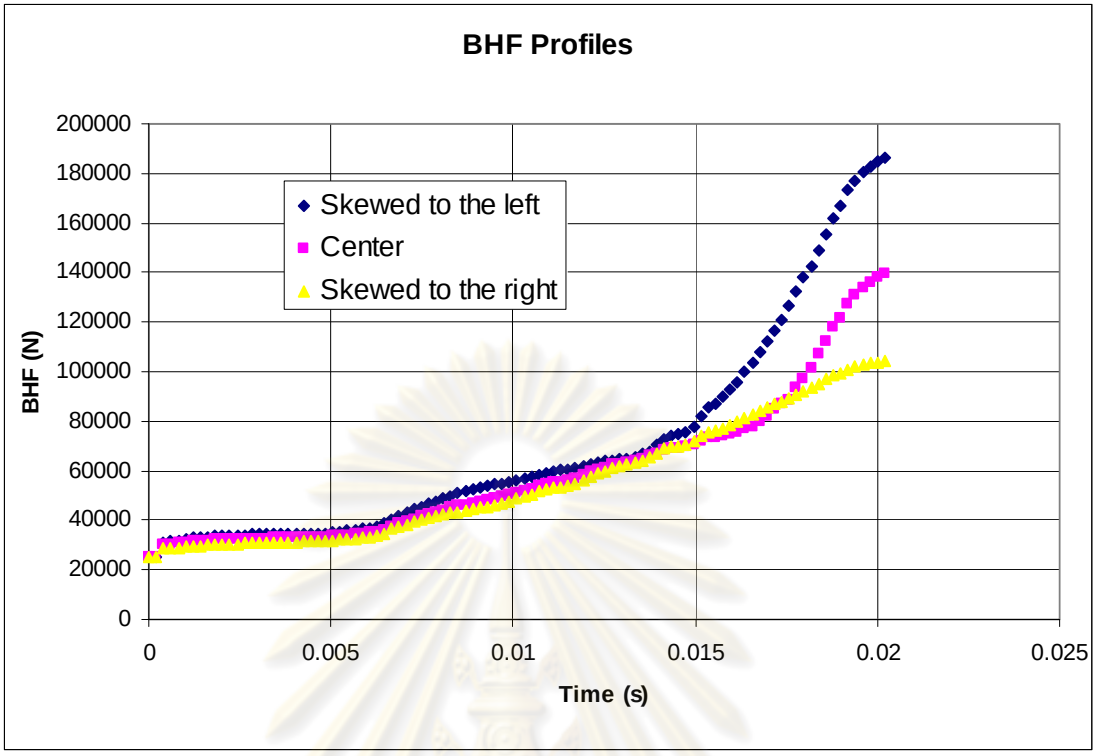

Figure 6.67 BHF profiles of Part1 obtained from different FAM membership function shapes

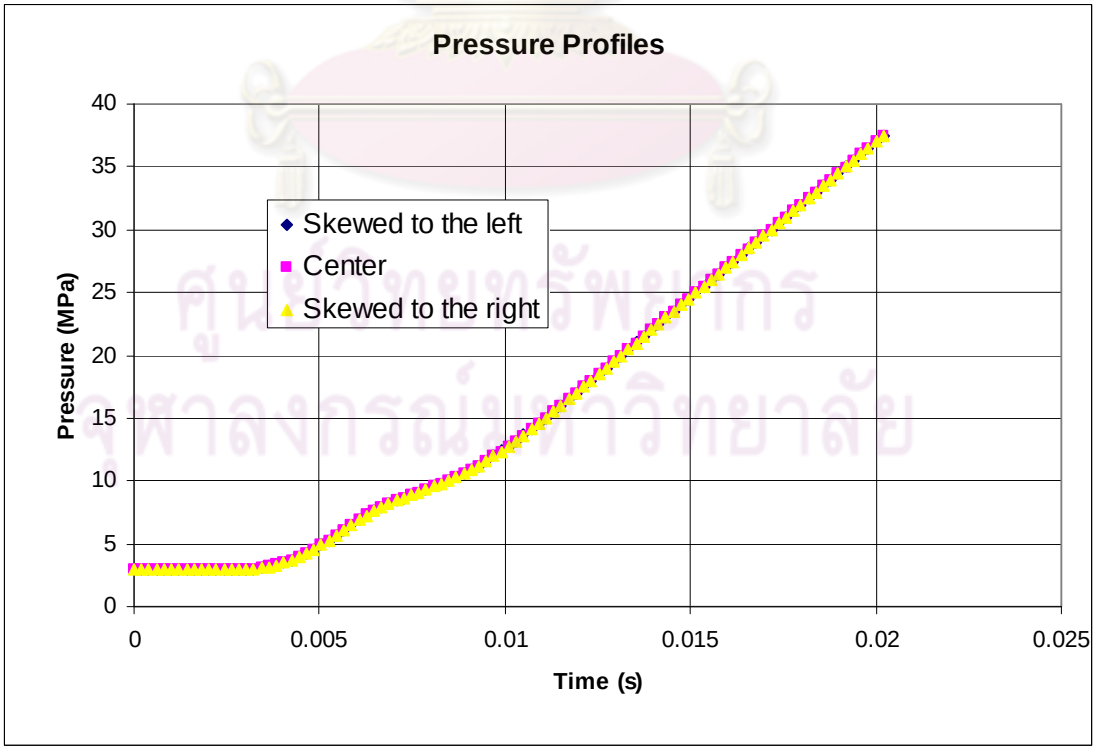

Figure 6.68 Pressure profiles of Part1 obtained from different FAM membership function shapes

The loading paths of Part1 obtained with the FAM membership function skewed to the left, centered and skewed to the right are shown in figure 6.67 – 6.68. The blank holder force profile obtained from FAM membership function skewed to the left is higher than the centered one. The BHF profile obtained from the FAM membership function skewed to the right is lower than the centered one. The pressure profiles obtained from the FAM membership functions shapes investigated are identical.

The resultant thinning, FAM and SW are shown in table 6.6. The part from loading paths with FAM membership function skewed to the left and the right are good parts. Therefore, the FAM membership function does affect the blank holder force profile in the wrinkle stage, but it does not affect the pressure profile.

Table 6.6 Results of Part1 obtained from different FAM membership function shapes

FAM membership function		Skew to the left	Center	Skew to the right
	Thinning	29.59520	29.42950	29.27690
Part1	FAM	1.02320	1.03142	1.03675
	SW	0.48264	0.48399	0.48474

6.8.3 SW membership function

To examine the sensitivity of thinning membership function, it is required to skew to the left and the right. The SW membership function skewed to the left is shown in figure 6.69 and the SW membership function skewed to the right is shown in figure 6.70

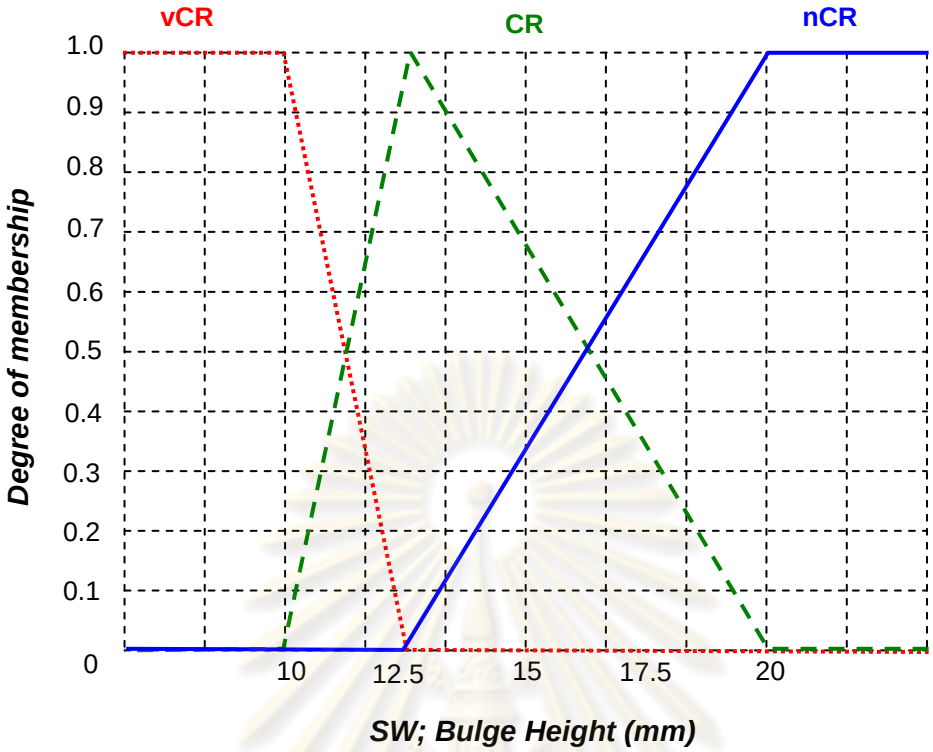

Figure 6.69 The SW membership function skewed to the left

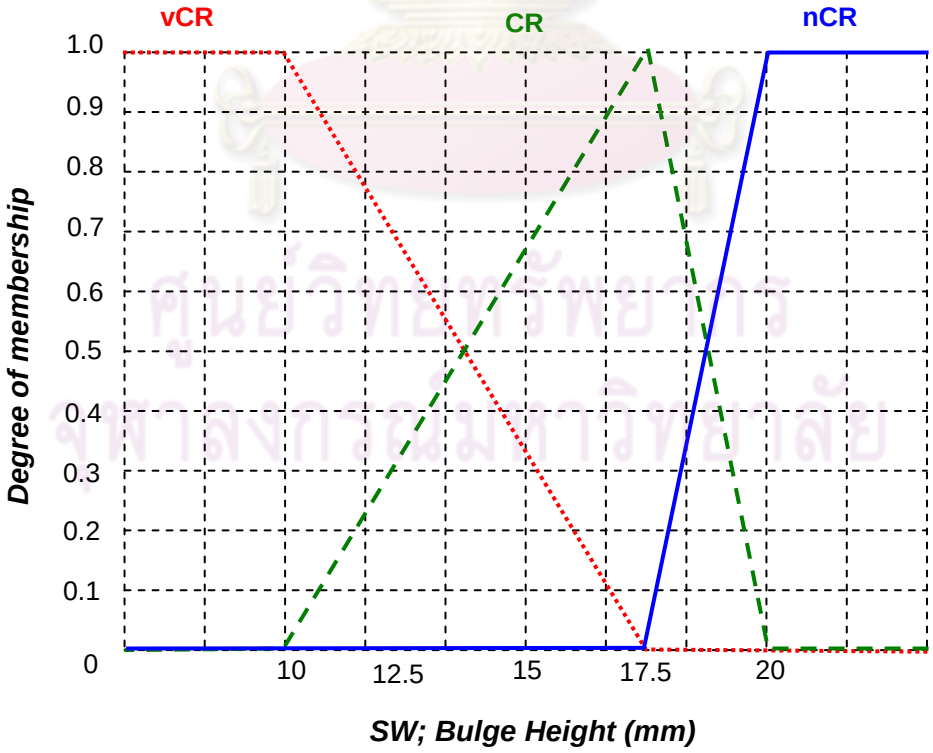

Figure 6.70 The SW membership function skewed to the right

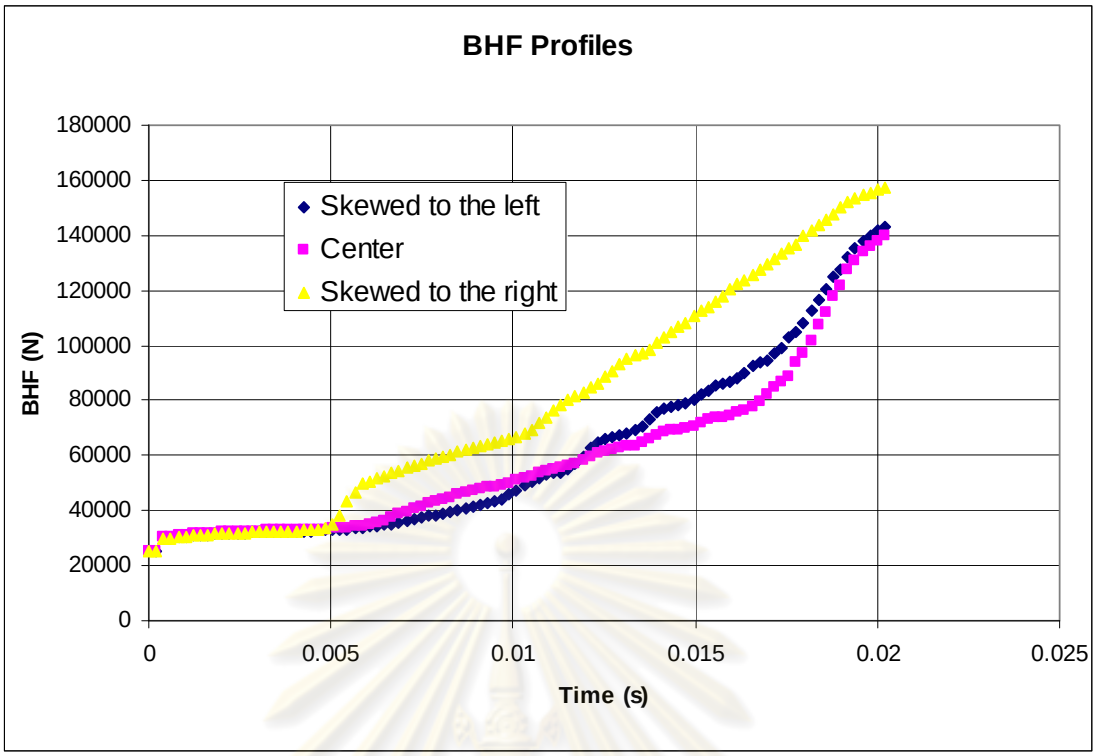

Figure 6.71 BHF profiles of Part1 obtained from different SW membership function shapes

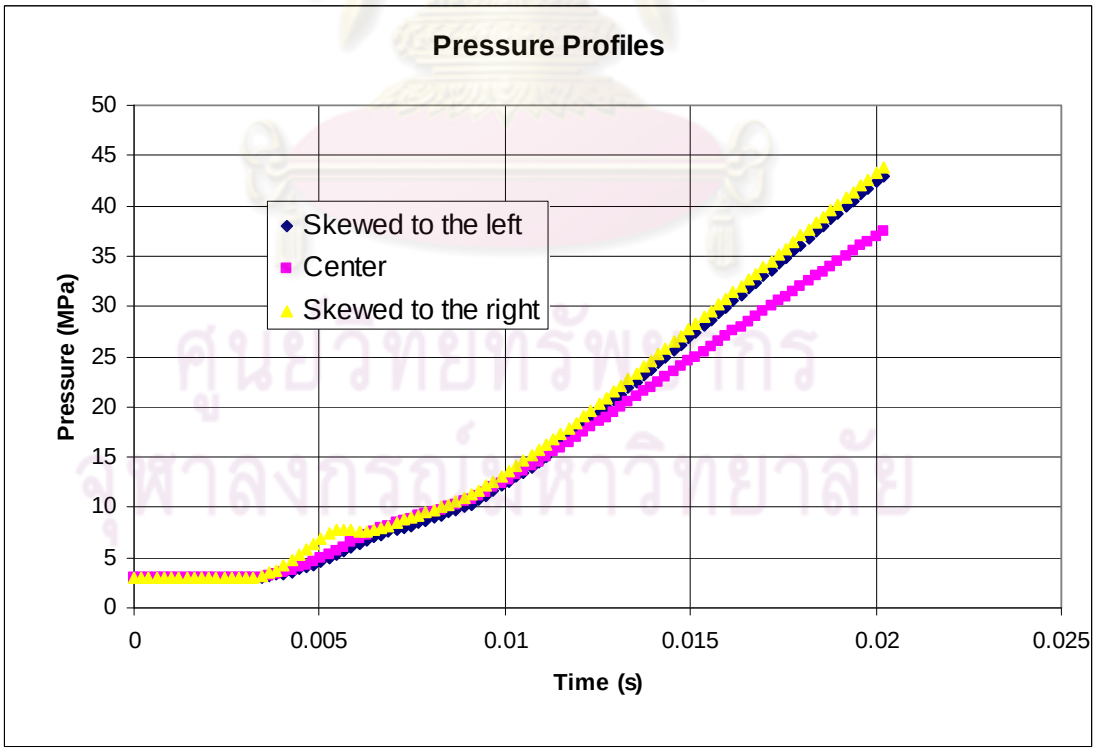

Figure 6.72 Pressure profiles of Part1 obtained from different SW membership function shapes

The loading paths of Part1 obtained with the SW membership function skewed to the left, centered and skewed to the right are shown in figure 6.71 – 6.72. The blank holder force profile obtained from SW membership function skewed to the left is higher than the centered one. The BHF profile obtained from the SW membership function skewed to the right is similar to the centered one. The pressure profiles obtained from the SW membership functions shapes investigated are identical.

The resultant thinning, FAM and SW are shown in table 6.7. The part from loading paths with SW membership function skewed to the left and the right are good parts. Therefore, the SW membership function shapes affected slightly on the blank holder force and pressure profile. If the membership function shape is skewed to both the left and the right, the BHF and pressure will be higher than the centered one.

Table 6.7 Results of Part1 obtained from different SW membership function shapes

SW membership function		Skew to the left	Center	Skew to the right
	Thinning	28.92660	29.42950	28.66960
Part1	FAM	1.03164	1.03142	1.02567
	SW	0.4819	0.48399	0.47542

6.9 Conclusion and discussion

The automatic approach with adaptive simulation coupled with fuzzy logic control can determine the loading paths (blank holder force and pressure profiles) of parabolic parts in hydromechanical deep drawing. The fuzzy control algorithm was implemented in the user subroutine. The fuzzy control algorithm was called at the end of each monitoring step. The linear and exponential predictive load functions (blank holder force and pressure) were applied to predict the proper parameter in the next monitoring step. The two general process windows of relationship 1) between blank holder force and punch stroke 2) between pressure and punch stroke with corresponding part quality were used to define the expected loading paths in the fuzzy

logic control algorithm. Tuning of the fuzzy logic control system could be done by changing the rule based matrix, the value of input/output membership functions, and the value of ΔBHF, ΔP. *Tuning of the rule-based matrix helped to improve convergence* whereas *changing the value of the membership function, ΔBHF and ΔP improved accuracy of the system responses*. The linear load curve function was first implemented. It was found beneficial in cases when the optimum load curve shape was not known a priory. However, it was discovered that for all the parabolic parts in this study have load curves that resemble exponential form. Then, an exponential load curve was implemented in the predictive load curve function. A much less number of simulation monitoring steps was needed to find a feasible process parameter load curves using this exponential load curve function. The main contribution here is the finding of modification of load function in exponential form to predict the next loading paths (blank holder and pressure) of forming parabolic cups with hydromechanical deep drawing process. The effects of thinning, FAM and SW membership function shapes are examimed.

The exponential curve is proper for the parabolic part. Typically, good BHF curve and pressure curve start with a lower values at the beginning of stroke (thin-out stage) and gradually increase at the middle of stroke (wrinkle stage) and rapidly increase at the end of stroke (re-strike). However, it is not good for the deeply parabolic shapes due to the load values at the end are higher enough. To correct this problem, the limit of blank holder force and pressure are defined thus, the risk of crack area near the counter pot radius is reduced.

The goal of the parameter adjustment module is essentially to select loading path that would result in “best” part quality possible. It should be noted that global optimum part quality cannot be obtained through using adaptive simulation coupled with fuzzy logic approach as it only utilizes the simulation results on part formability from past up until current simulation monitoring step to project the “best” future loading path in the following monitoring step. No global optimization is attempted in this adaptive simulation coupled with fuzzy logic approach.

CHAPTER VII

EXPERIMENTAL VALIDATIONS OF SIMULATION RESULTS

This chapter explains all the experimental validations conducted to evaluate the Finite Element Analysis (FEA) in sheet metal forming modeling of various parts and processes. First, a shape conical cup and a hemispherical dome cup were studied, where a deep drawing process and a sheet hydroforming process were used to form the parts, respectively. Then, as a main targeted part and process of this study, a parabolic cup hydromechanical deep drawing (HMD) experiments were conducted using the process parameters determined through the methodologies developed in chapter 5 and 6. This essentially concludes and validates the FEA based techniques for practical applications in the physical HMD process.

7.1 Comparison between FEA modeling and forming experiment of simple part using classical deep drawing process and sheet hydroforming process

7.1.1 Conical cup forming with deep drawing process (hard tooling)

ศูนย์วิทยทรัพยากร
จุฬาลงกรณ์มหาวิทยาลัย

7.1.1.1 FE Modeling of conical cup

The drawing of a conical cup was investigated in order to validate the finite element method and an experimental. A shape and dimension of tool components were illustrated in figure 7.1

An FE quarter model of the blank and tool components was used in the analysis to take advantage of the symmetry and to reduce calculation time as shown in figure 7.2. The Belytchko-Tsay thin-shell elements were used for blank and the tool components

were defined as rigid bodies, using rigid elements with four-node thin shell (material type 20).

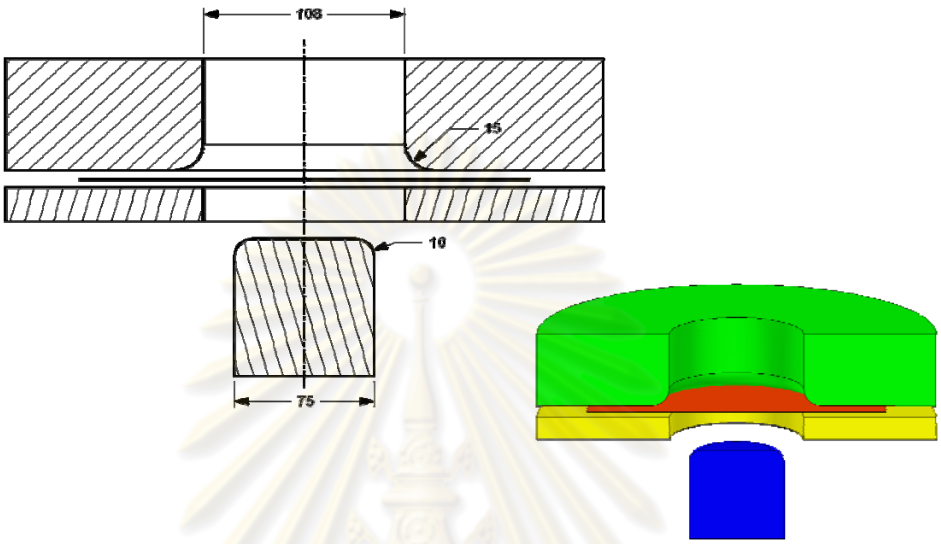

Figure 7.1 The shape and dimension of conical cup tool components

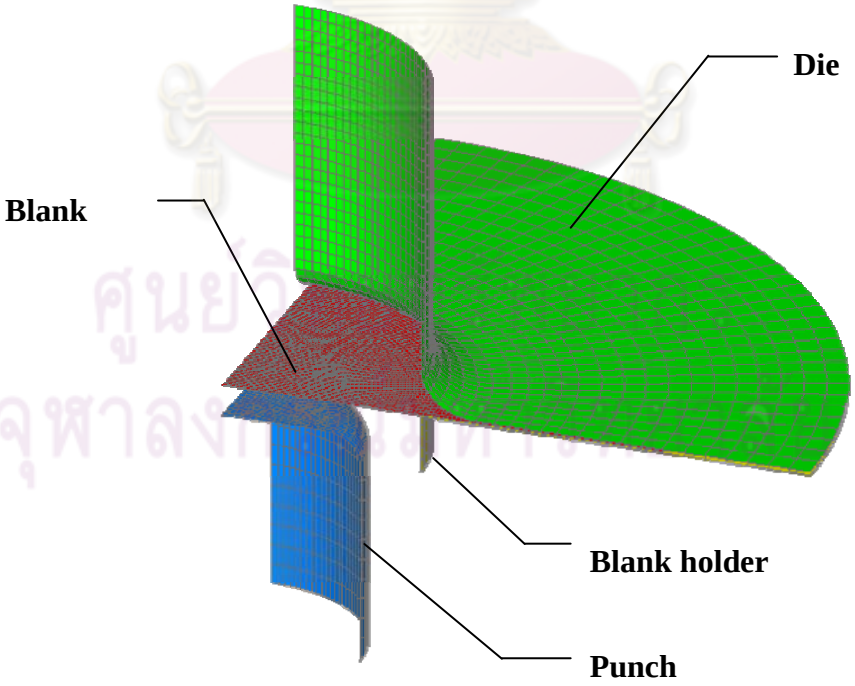

Figure 7.2 Quarter finite element model of conical cup drawing

Contact model between the blank and the tool components assumed Coulomb friction assumption. The friction coefficient was defined as 0.12.

Time scaling was used to secure a reasonable calculation time, the scaling factor being taken as 1,000.

Balat-Lian's three-parameter model was defined for the blank material model and 5 integration points through the thickness was also used for blank. The SPCC is indicated in BCC structure, so the M value of 6 was selected. The material properties are shown in table 5.1.

7.1.1.2 Conical cup experiment

The conical cup tooling components are shown in figure 7.3 and the formed cups are shown in figure 7.4. Necking was found on the top corner of the part and mild wrinkle were found in the flange area.

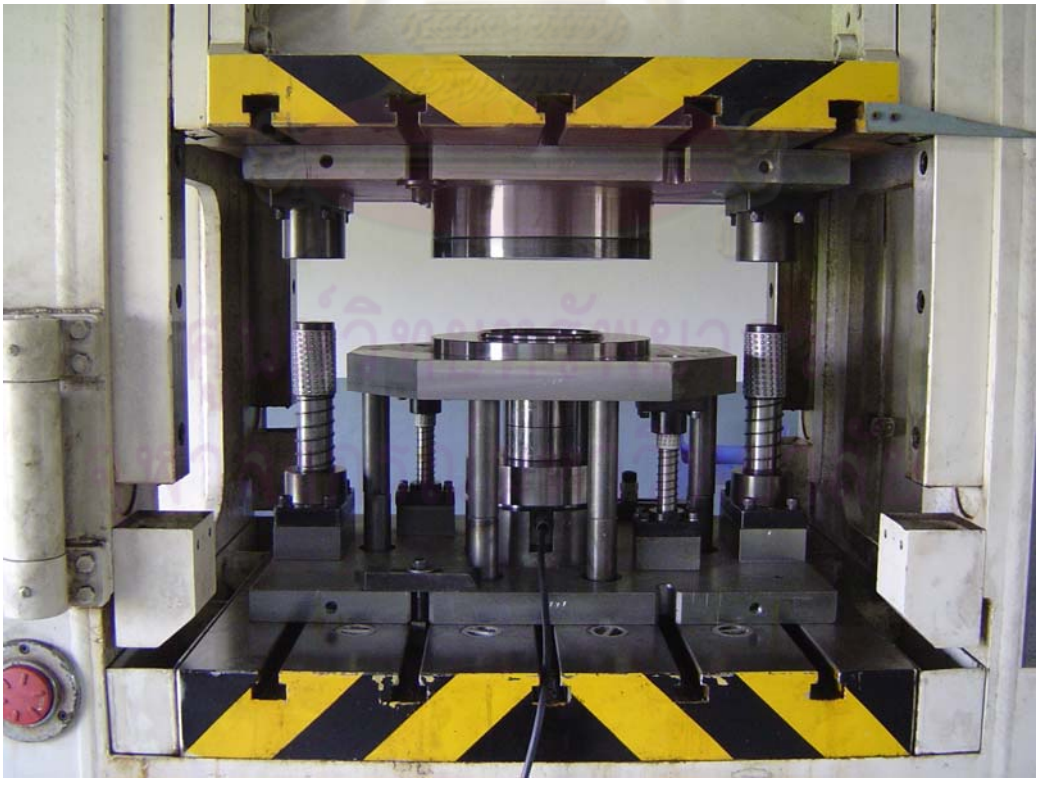

Figure 7.3 Tooling components of conical cup drawing

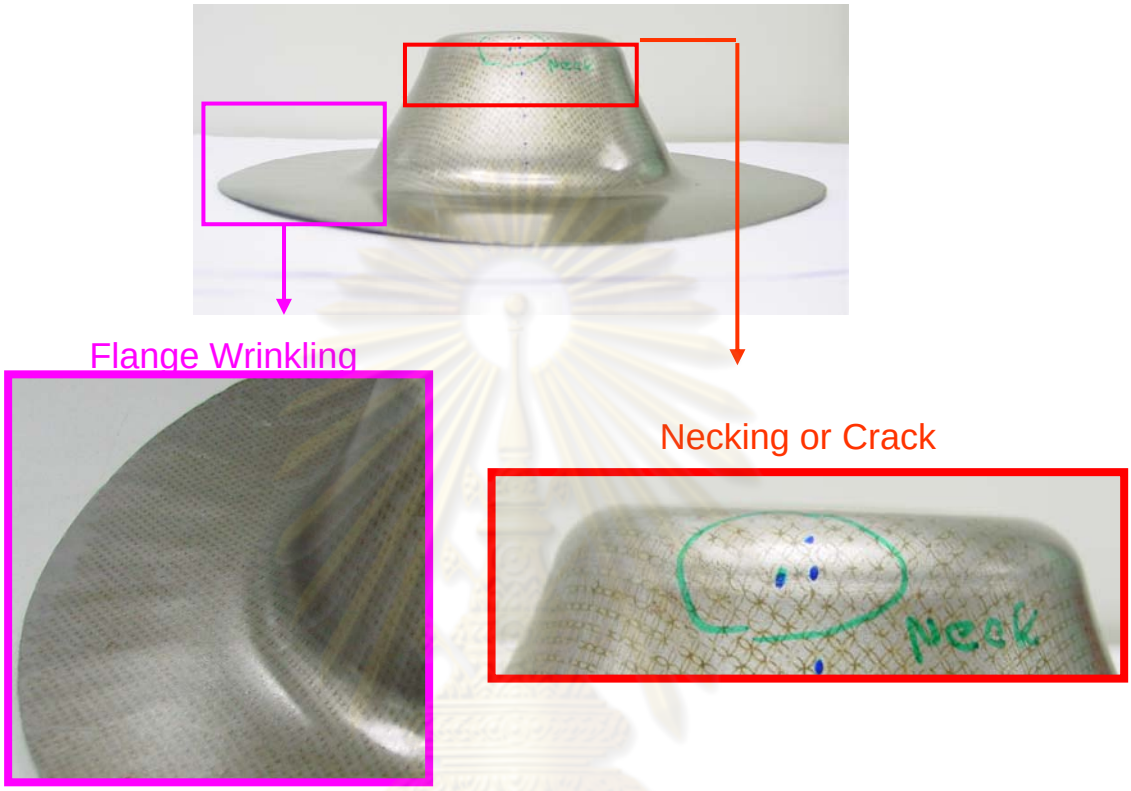

Figure 7.4 Conical cup obtained from experiments

Figure 7.5 shows the result of FEA compared with the experimental result. The periphery from FEA is very close in both dimensions and shape to the experimental periphery. The necking position in FEA is in the same position as in the experimental cup (at the top of the punch radius) and similar flange wrinkles can be seem in the same location of both FEA and experiment. The limited height of cup is 51.6 mm in both the experiment and FEA. Moreover, the FEA can also predict a buckle in a side wall of the cup.

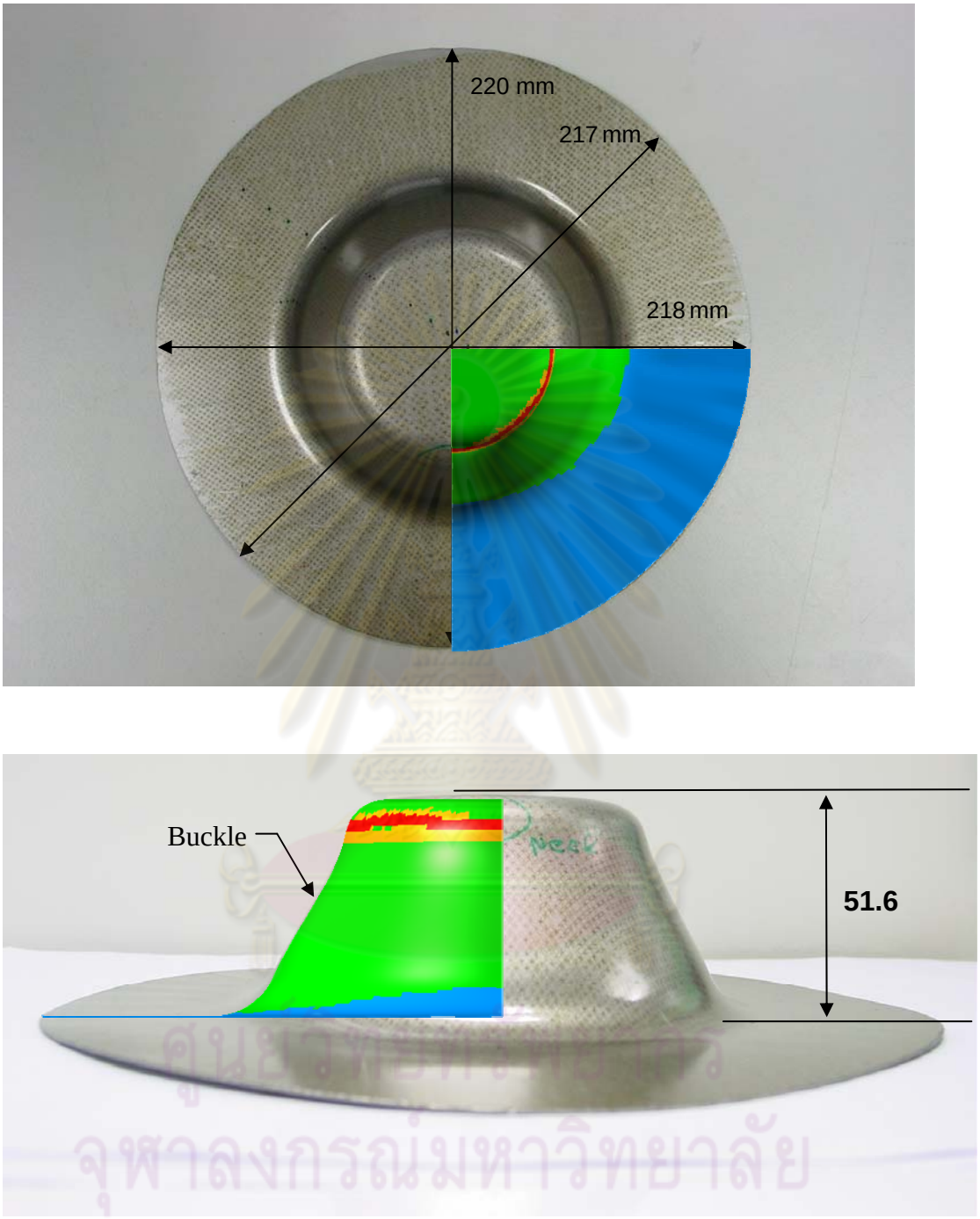

Figure 7.5 Comparison of the results from FEA and experiment

The major and minor strains were measured from the formed cup using a circle grid analysis technique. The behavior of major and minor strains predicted by FEA was consistent with the experimental results as shown in figure 7.6.

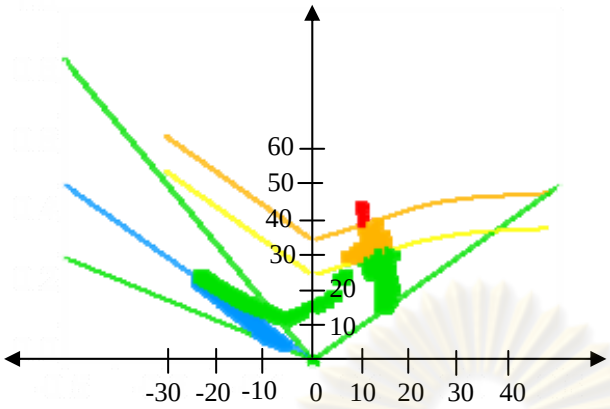

FEA

Experiment

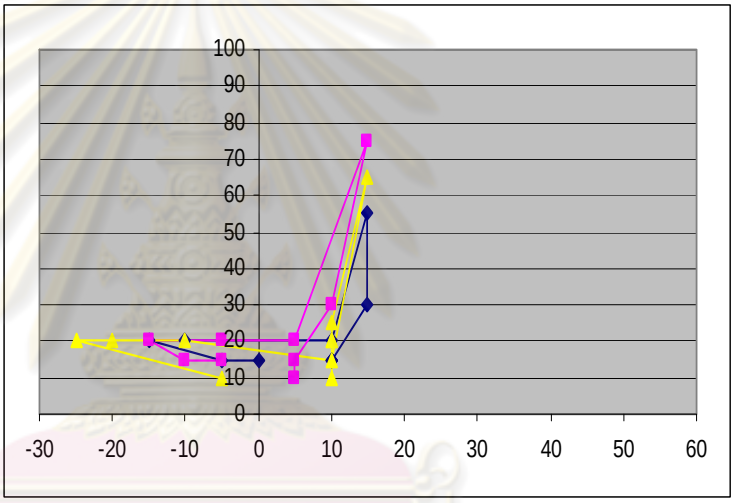

Figure 7.6 Comparison of major and minor strains from the FEA and experiment of conical cup drawing

7.1.2 Simple sheet hydroformed part and effect of process parameters using FEA modeling

This experiment was conducted at BT Engineering Company. Different forming results of the hemispherical cup formed with a solid punch and pressurized fluid are apparent in the position of tearing as shown in figure 7.7. The fluid makes the part crack at the highest position of the dome. However, due to punch-blank interface friction, the solid punch forms the part with a much lower positioned crack, figure 7.7.

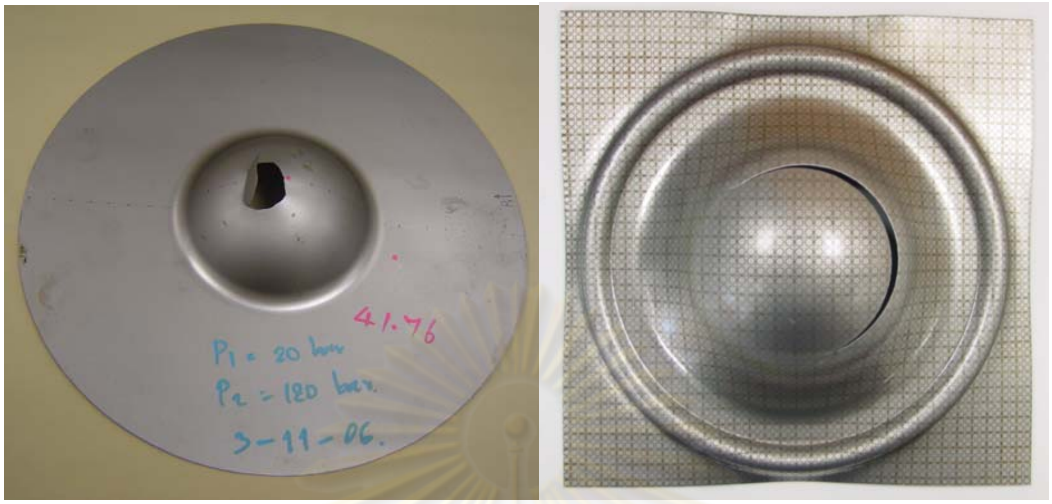

Figure 7.7 Comparison of hemispherical cups formed using fluid punch (left) and solid punch (right)

7.1.2.1 Verification between FE modeling and experiment of simple bulge

The FE quarter model of the blank and tool components were used in the analysis to take advantage of the symmetry and to reduce calculation time as shown in figure 7.8. The Belytchko-Tsay thin-shell elements were used for blank and the tool components were defined as rigid bodies, using a rigid element with four-node thin shell (material type 20).

Contact model between the blank and the tool components assumed Coulomb friction assumption. The friction coefficient was defined as 0.12.

Time scaling was used to secure a reasonable calculation time, the scaling factor being taken as 1,000.

The pressure curve was applied with linearly increasing from 0 to 12 MPa as shown in figure 7.8.

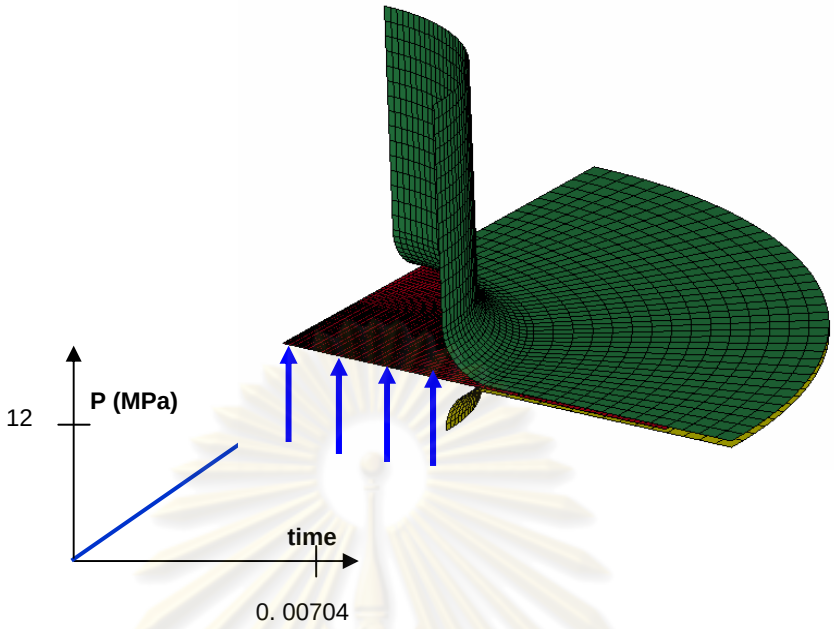

Figure 7.8 FE model and pressure curve to simulate the hemispherical dome

The limited dome height from simulation was 42.12 mm and the experiment was 41.76 mm as shown in figure 7.9.

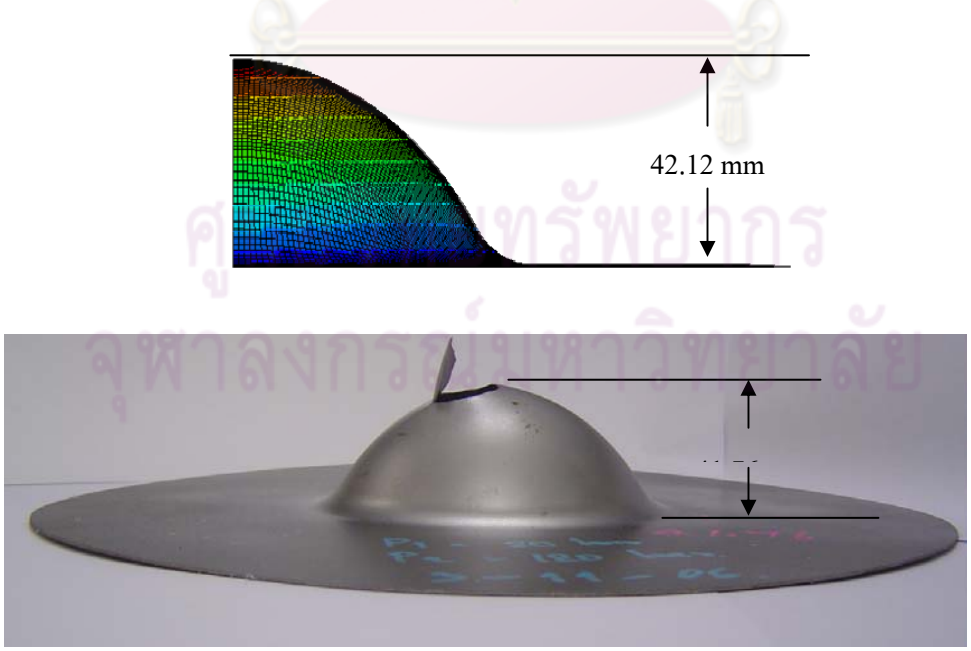

Figure 7.9 The limited dome height from simulation and experiment

The comparison of thickness distribution along a curvilinear between the experiment and simulation is shown in figure 7.10. The pattern of curve from simulation is in a good agreement with the experiment and the minimum thickness is on the top of the dome.

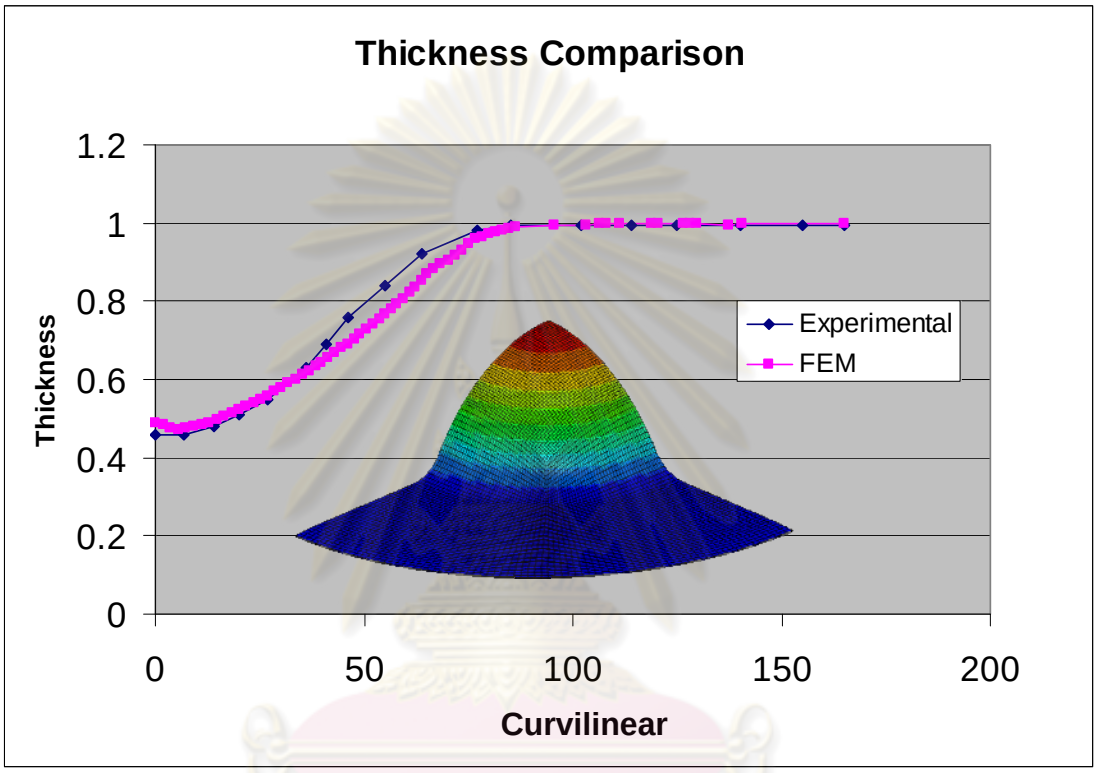

Figure 7.10 Thickness distributions from simulation and experiment along curvilinear of the part

7.2 Comparison between FEA modeling and HMD experiment of parabolic part

Due to the limitation of maximum clamping force of the press machine (200 Ton), only Part1 can be formed. Part2 and Part3 require much larger clamping forces. A die set was designed as shown in figure 7.11

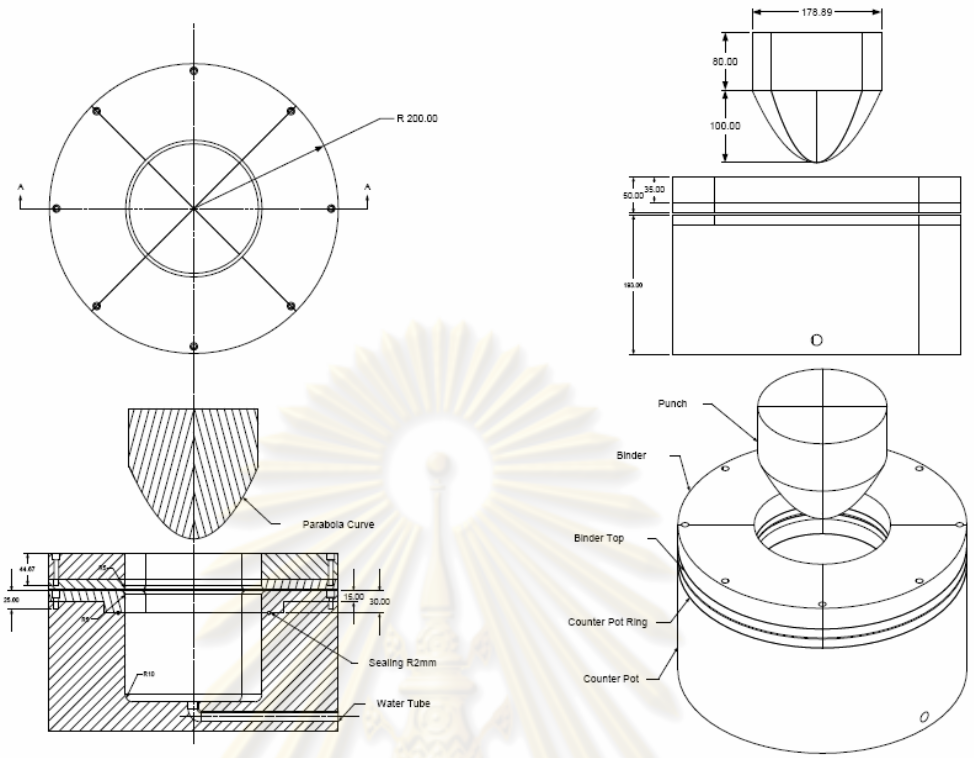

Figure 7.11 Die set drawing of Part1

The die set of Part1 was installed in the press machine as shown in figure 7.12. Then a blank was put on the die set centered by two guides as shown in figure 7.13

Figure 7.12 Die installed in press machine

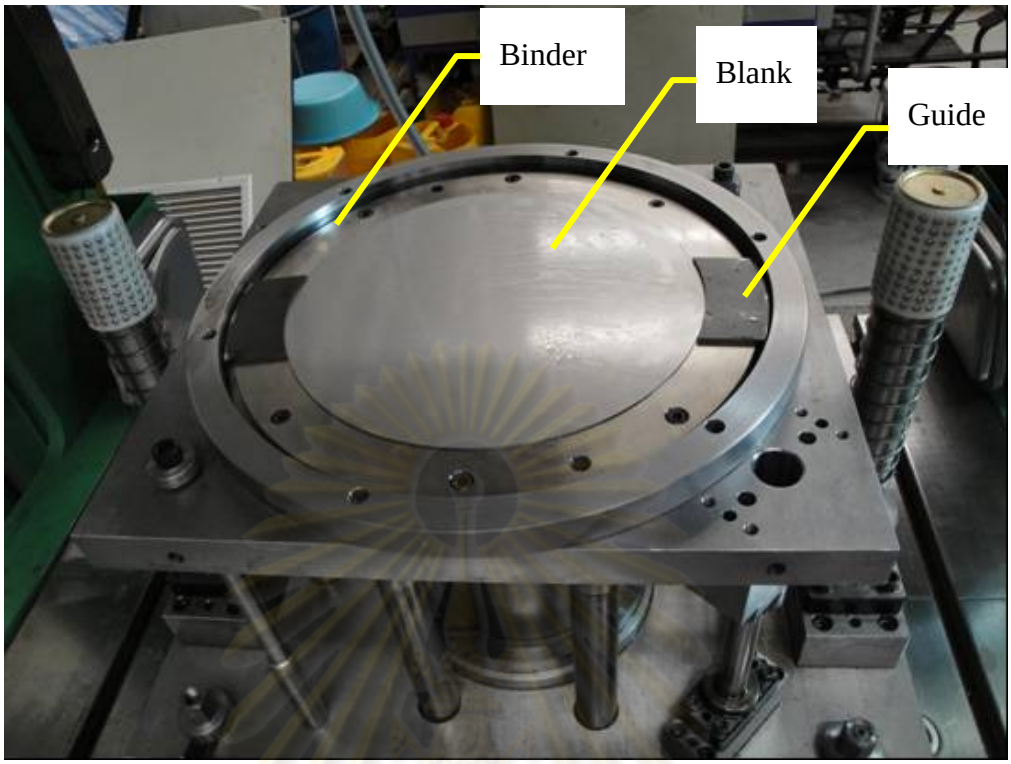

Figure 7.13 Blank position

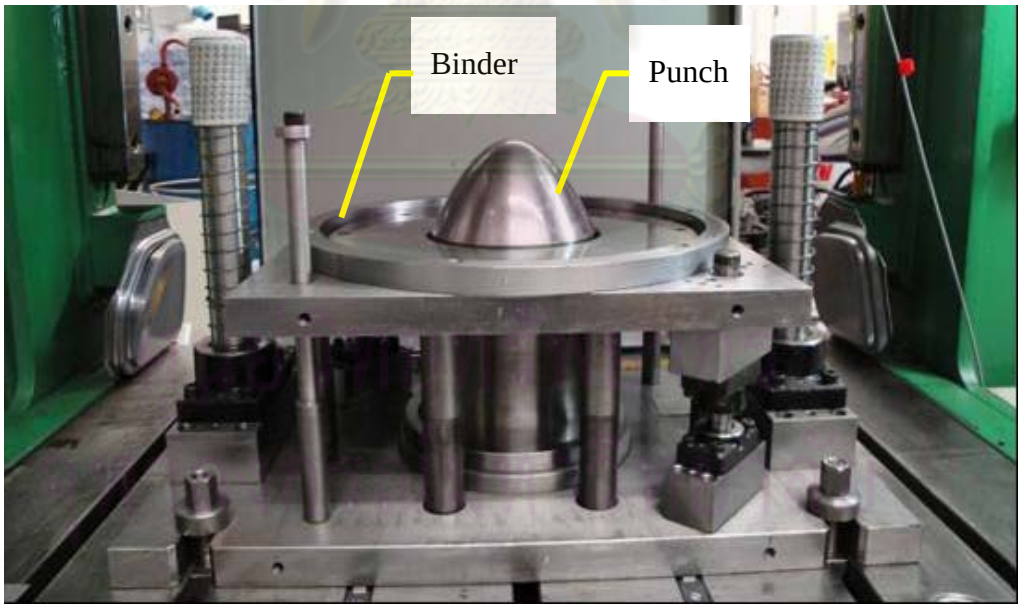

Figure 7.14 Final stroke and ram up

At final stroke, the punch will be over the binder surface by 105 mm as shown in figure 7.14. After the die set has been installed, movement of the press with die set is checked for readiness.

7.2.1 Tryout the process capability

- Constant BHF with no pressure

This condition was tested firstly to check how the die set can form the part. The figure 7.15 shows the top view of part and figure 7.16 shows the front view of part. The part cracked at 65 mm of height and draw-in 2 mm. This process condition is to resemble normal deep drawing process.

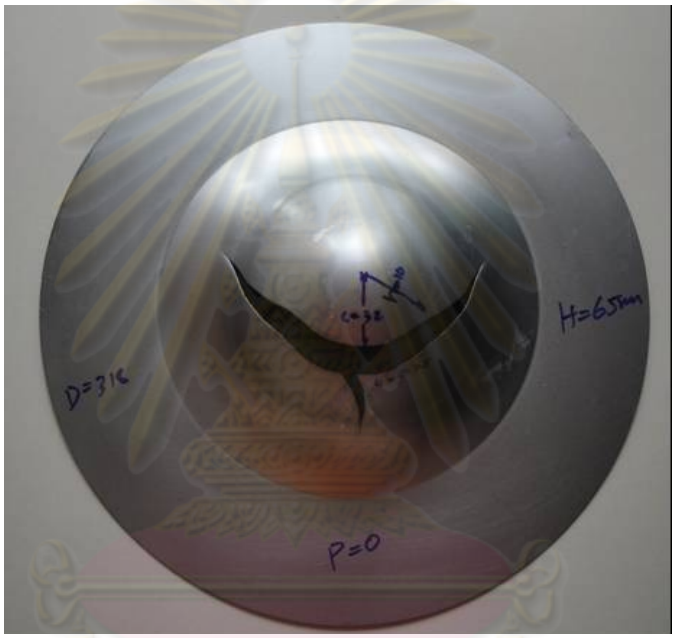

Figure 7.15 Top view of part with no pressure condition

Figure 7.16 Front view of part with no pressure condition

- Pre-bulge forming

This condition was tested to see if the pressure intensifier controller can form the pre-bulge correctly. Figure 7.17 shows the pre-bulged part at 16 mm of height with pressure of 2 MPa. Therefore, the system can generate the pre-bulge. However, due to some hydraulic related problems, the pre-bulge pressure could not be readily controlled and precisely.

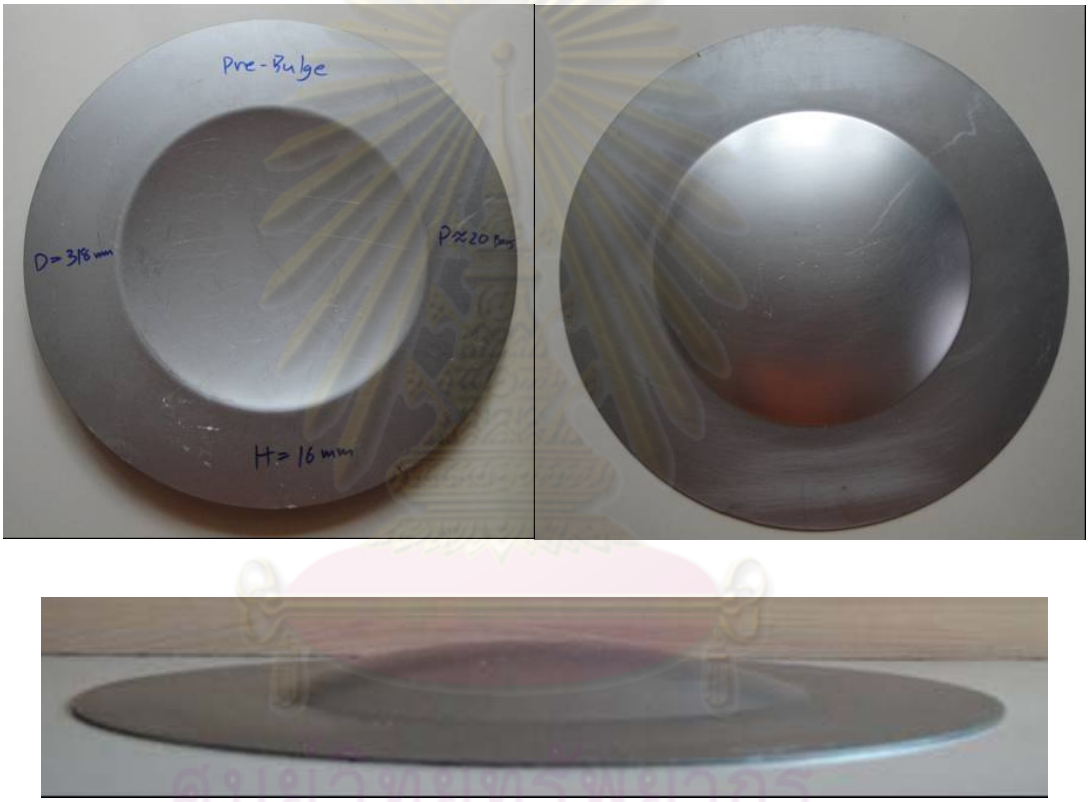

Figure 7.17 Pre-bulge stage of part

- Constant BHF with constant pressure

This condition was tested to check the side wall wrinkle on the part with no crack. It should be noted here that this condition is not the optimum nor feasible solution from the methodologies developed. The profile of blank holder force and pressure are shown in figure 7.18. The pressure was applied as 4, 6 and 8 MPa. The results are shown in figure 7.19 – 7.24.

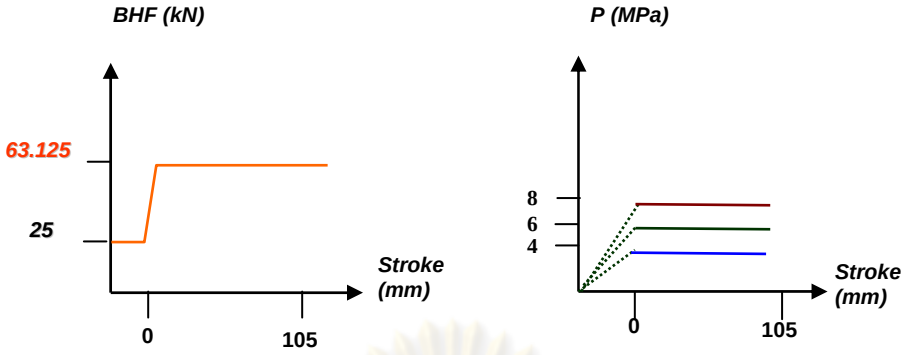

Figure 7.18 Loading profiles of constant BHF and pressure

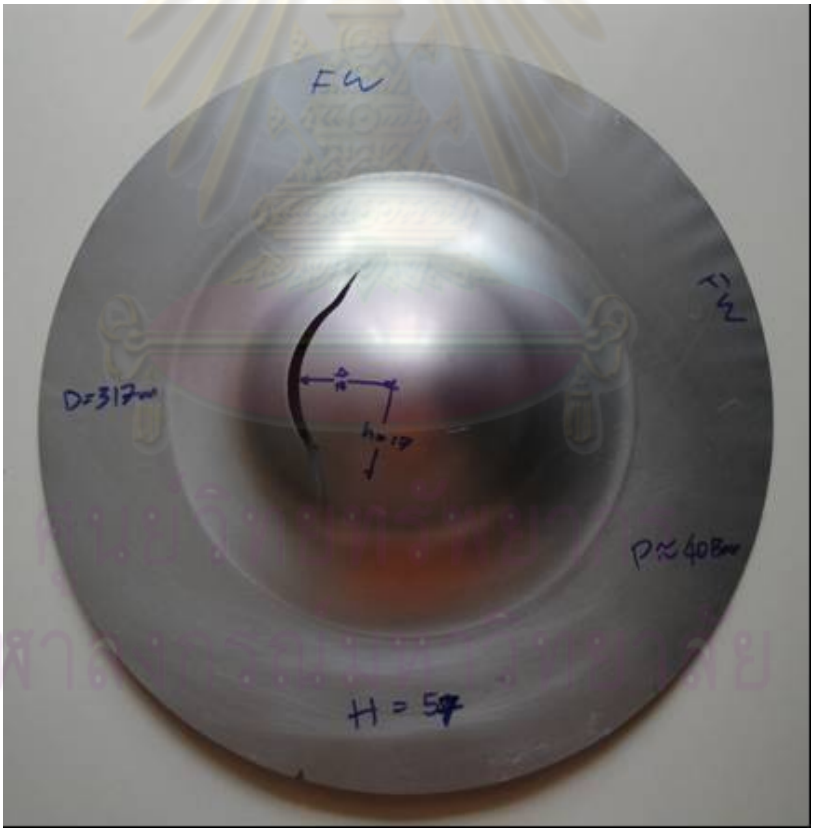

Figure 7.19 Top view of part with constant BHF of 63,125 N (full as 25.25 tons) and constant pressure of 4 MPa

Figure7.20 Front view of part with constant BHF of 63,125 N (full as 25.25 tons) and constant pressure of 4 MPa

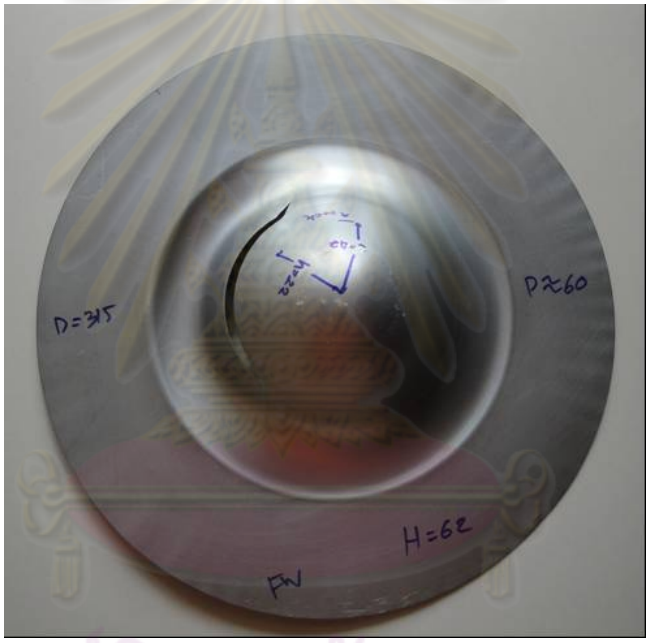

Figure7.21 Top view of part with constant BHF of 63,125 N (full as 25.25 tons) and constant pressure of 6 MPa

Figure7.22 Front view of part with constant BHF of 63,125 N (full as 25.25 tons) and constant pressure of 6 MPa

Figure7.23 Top and bottom view of part with constant BHF of 63,125 N (full as 25.25 tons) and constant pressure of 8 MPa

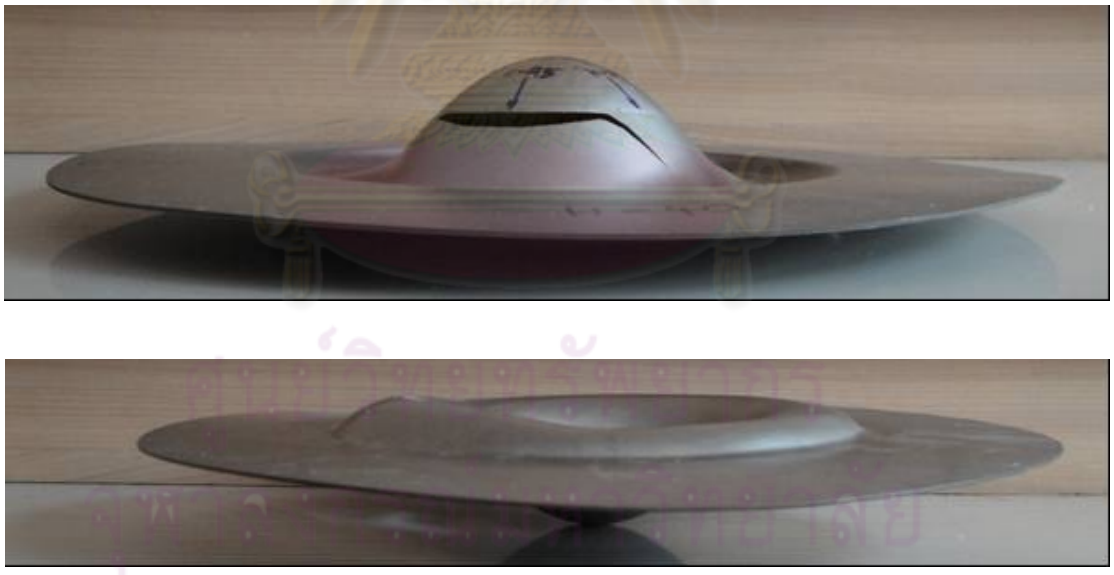

Figure7.24 Front and back view of part with constant BHF of 63,125 N (full as 25.25 tons) and constant pressure of 8 MPa

For all experiment results, the part cannot form successfully. From the expected results of the FEA, the parts should have the side wall wrinkle but in stead the crack happened on the parts at around 40-60 mm of height.

More simulations were later conducted to investigate the causes of discrepancies by focusing on friction coefficient used on the punch-blank interface. The simulation was set up with P = 27.625 MPa, BHF = 63.125 KN (25.25 Ton Full), μ_s between binder and blank = 0.06 and μ_s between counter pot and blank = 0.06

Table 7.1 Effect of friction coefficient between punch and blank

Punch – Friction Coeff	**Pictures (Thinning) and Height**	**Remark**
0.05	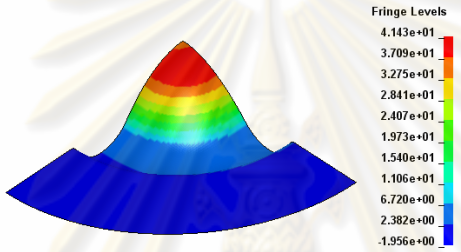 Time = 0.0176968	
0.10	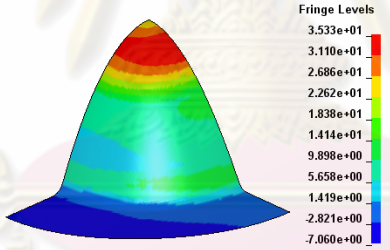 Good	Element cracked; 17972
0.12	Good	This is defined value
0.15	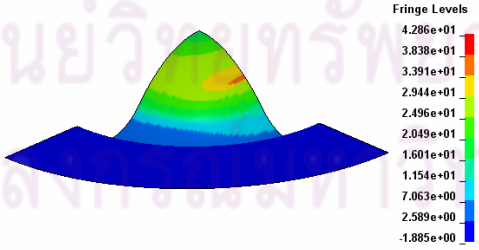 Time = 0.0176968	Cracked height = 26.71351 Pressure = 7.572356 Curvilinear = 40.622 Part height = 16.328
0.20	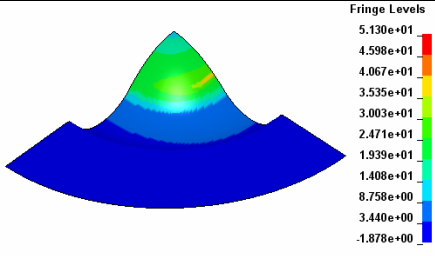 Time = 0.0156148	Cracked height = 12.66036 Pressure = 6.335525 Curvilinear = 38.1334 Part height = 14.676

0.25	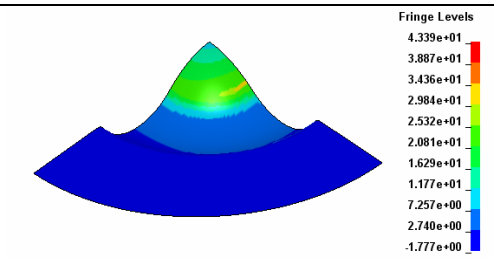 Time = 0.0145736	Cracked height = 5.632999 Pressure = 5.71699 Curvilinear = 35.2015 Part height = 12.807
0.30	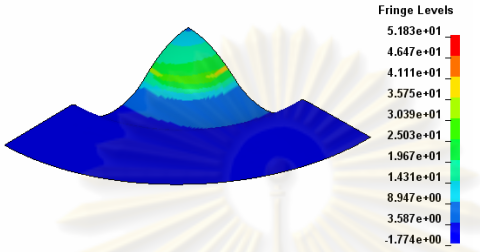 Time = 0.0145736	Cracked height = 5.632999 Pressure = 5.71699 Curvilinear = 34.8358 Part height = 12.594
0.35	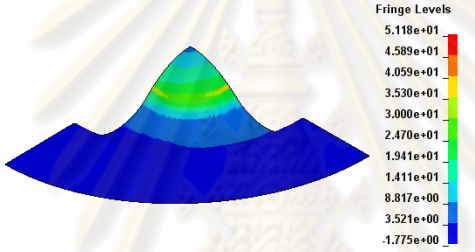 Time = 0.0145736	Cracked height = 5.632999 Pressure = 5.71699 Curvilinear = 34.836 Part height = 12.594
0.40	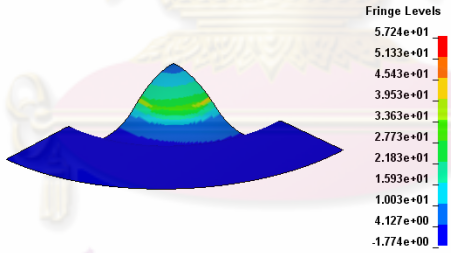 Time = 0.0145736	Cracked height = 5.632999 Pressure = 5.71699 Curvilinear = 35.912 Part height = 13.271

From table 7.1, it can be concluded that the friction coefficient between punch and blank is a sensitive parameter to a successful forming. If this value is higher than 0.15, the part will be cracked before reaching the final stroke. Therefore, during the previous experiments the punch surface with oil lubricant must have head friction coefficient of a value over 0.15. To reduce and maintain friction coefficient, a PE lubricant was applied to punch, binder and counter pot. As a result, the friction coefficients of punch, binder and counter pot were the same of a much lower value.

The experiments were conducted again and the friction coefficients used in all the later simulations was changed as 0.06.

7.2.2 Experimental validation

7.2.2.1 Constant BHF with no pressure

The constant BHF with no pressure condition was performed to investigate the difficulty to form this part in conventional tooling, i.e. deep drawing process. The simulation and experiment results are shown in figure 7.25 - 7.26.

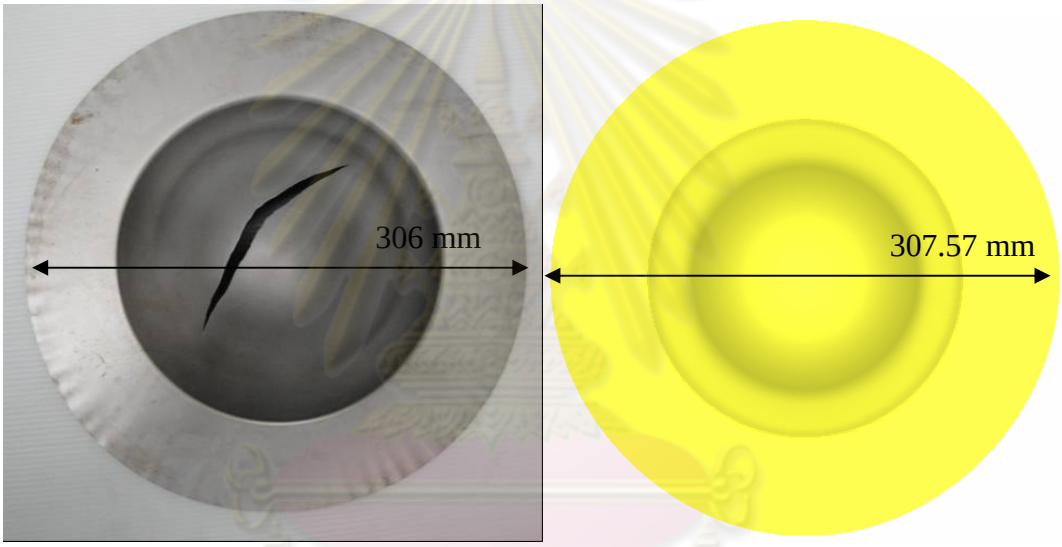

Figure7.25 Top view of part with constant BHF of 63,125 N (full as 25.25 tons) and no pressure

ศูนย์วิทยทรัพยากร
จุฬาลงกรณ์มหาวิทยาลัย

The experiment result has a diameter of 306 mm and simulation result has 307.57 mm. The part is cracked at 88.5 mm of height from experiment while the simulation is cracked at 89.8 mm of height. The experiment and simulation show the buckle on the part. Overall, the simulation show very good agreements with the experimental results.

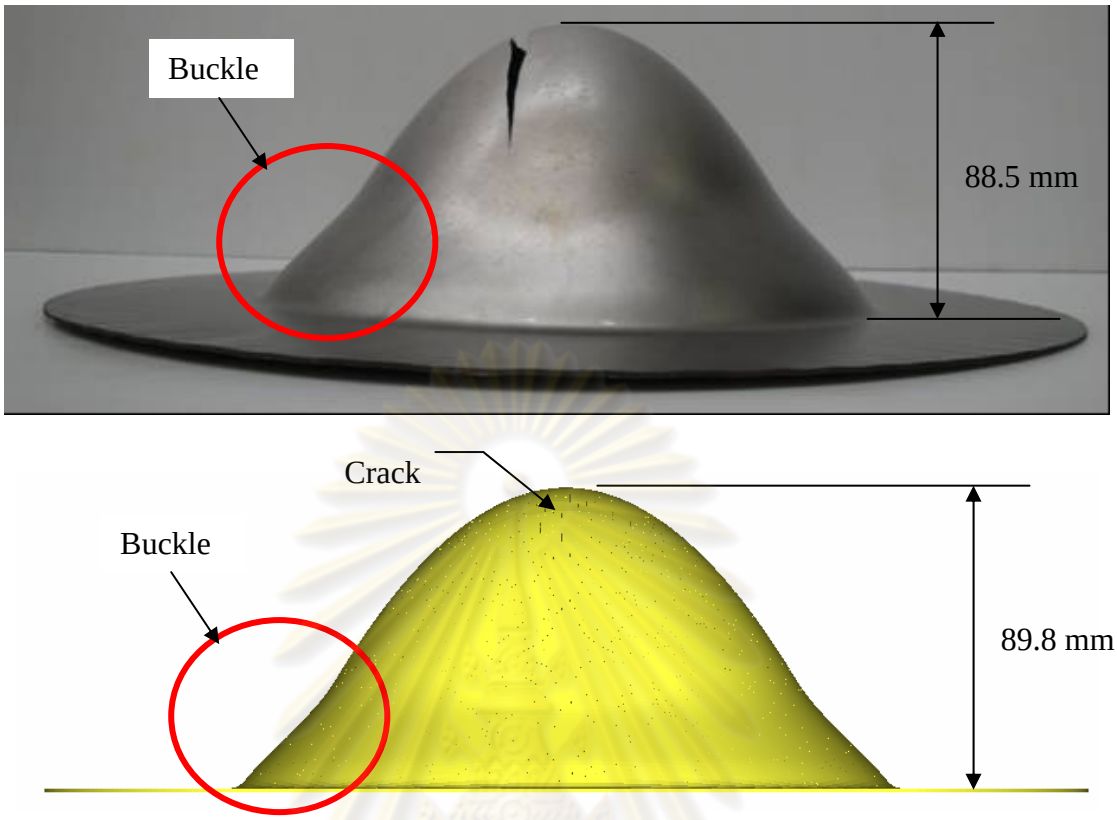

Figure7.26 Front view of part with constant BHF of 63,125 N (full as 25.25 tons) and no pressure

7.2.2.2 Constant BHF with constant pressure

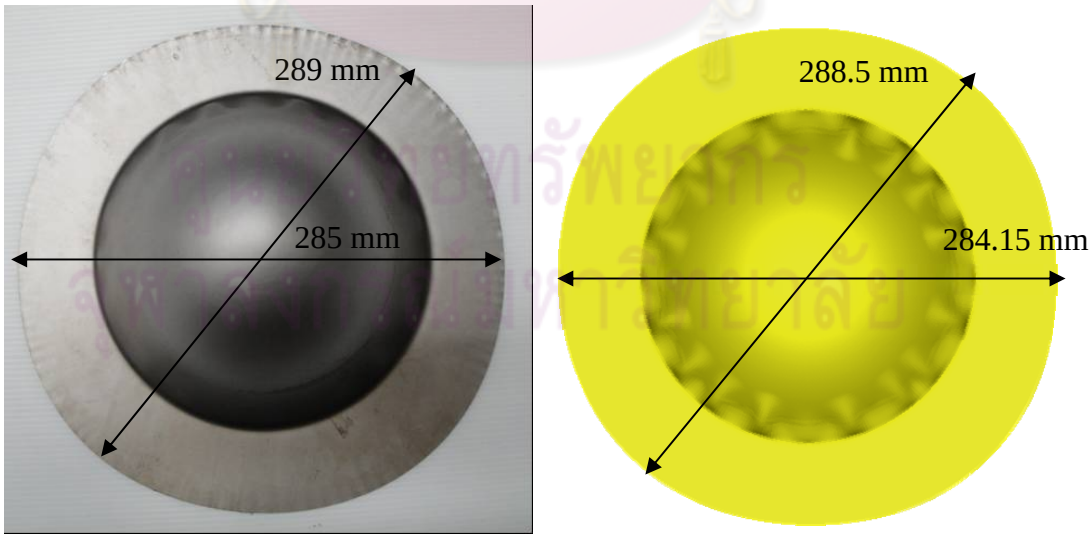

Figure7.27 Top view of part with constant BHF of 63,125 N (full as 25.25 tons) and constant pressure of 3 MPa

The constant BHF as 63,125 N for quarter model with constant pressure as 3 MPa (pre-bulge pressure) condition was performed to investigate the importance of pressure available that helps delay the crack but the side wall should still occur on the part. The simulation and experiment results are shown in figure 7.27 - 7.30.

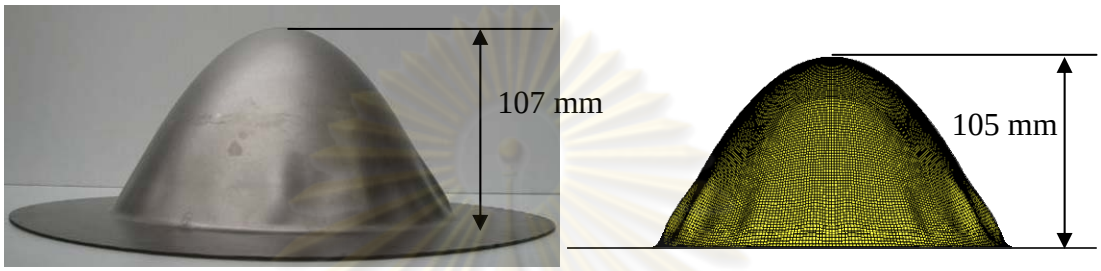

Figure7.28 Front view of part with constant BHF of 63,125 N (full as 25.25 tons) and constant pressure of 3 MPa

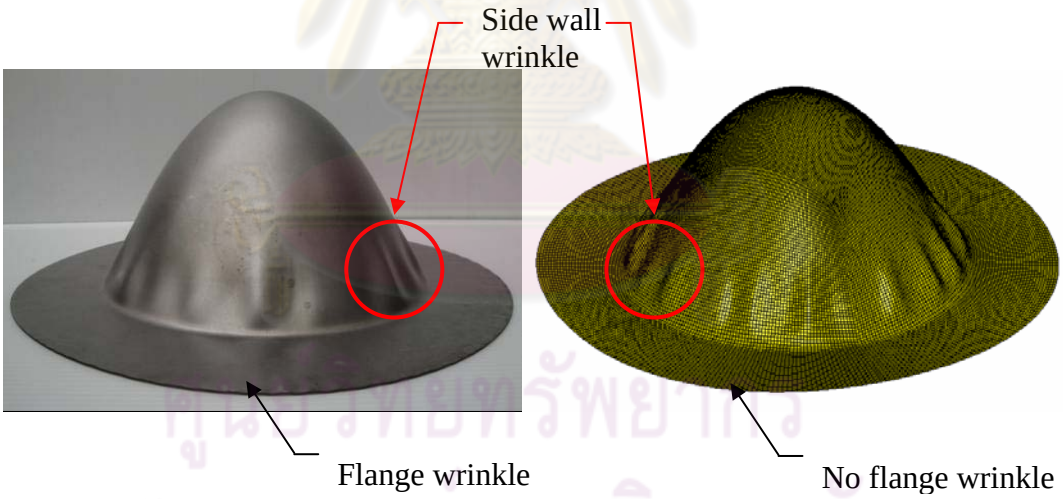

Figure7.29 Parabolic part with constant BHF of 63,125 N (full as 25.25 tons) and constant pressure of 3 MPa

The experiment result shows the effect of sheet anisotropy shape; shorter diameter has 285 mm and longer diameter in 45° of shorter diameter has 289 mm while the simulation result has shorter diameter as 284.15 mm and longer diameter as 288.5 mm. The part can reach to the final stroke at 105 mm for simulation but for experiment the part has 107 mm of height. Both experiment and simulation show the

side wall wrinkle on the part. Small flange wrinkle can be observed in a experiment while the simulation cannot.

Figure7.30 Parabolic part with constant BHF of 63,125 N (full as 25.25 tons) and constant pressure of 3 MPa in half-section view

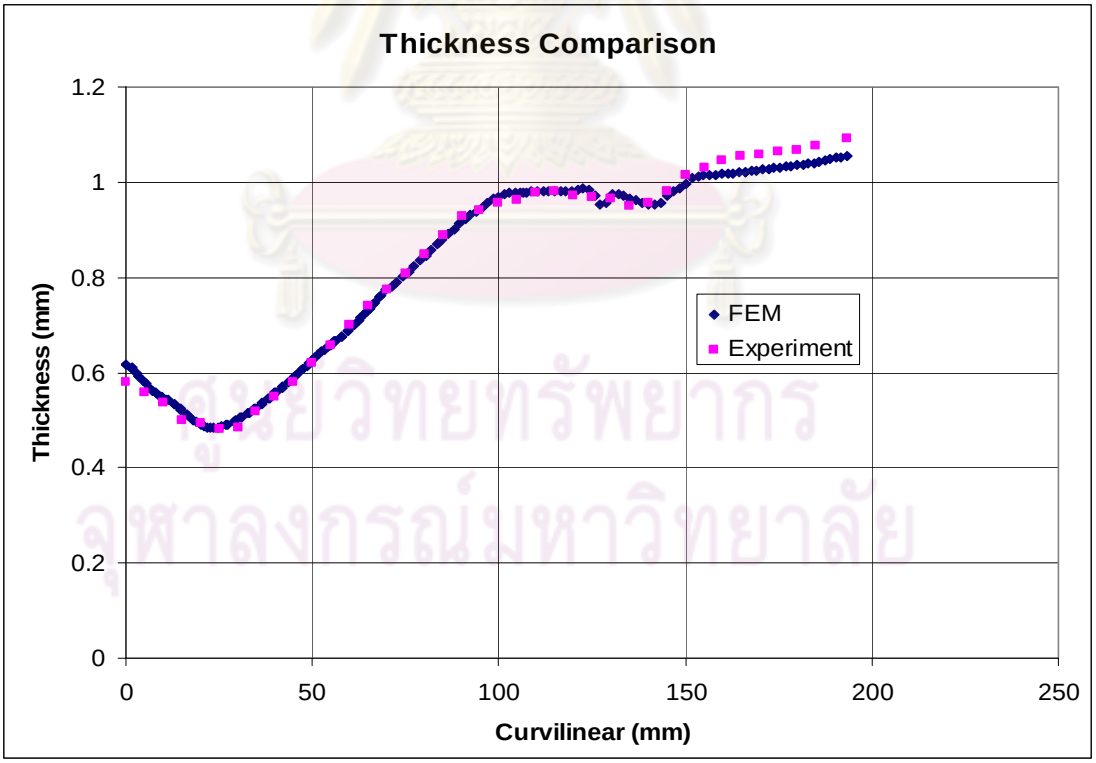

Figure7.31 Thickness distributions from simulation and experiment along curvilinear of the part with constant BHF of 63,125 N (full as 25.25 tons) and constant pressure of 3 MPa

The comparison of thickness distribution along a curvilinear between the experiment and simulation is shown in figure 7.31. The pattern of curve from simulation is very similar to the experiment. The minimum thickness is on the punch nose at 25 mm along curvilinear.

7.2.2.3 Verify optimal constant BHF and linear pressure curve

The constant BHF of 63,125 N for quarter model and a linear pressure curve of maximum value 27.625 MPa condition was performed to validate the predicted optimum loading paths. Unfortunately, during the process, the ram was moved up automatically due to the ram force was not enough for the process. The hydraulic has been leaked so it could not hold the force as setting (120 ton). It could only form part at 66 mm of height. The simulation and experiment results are shown in figure 7.32-7.34

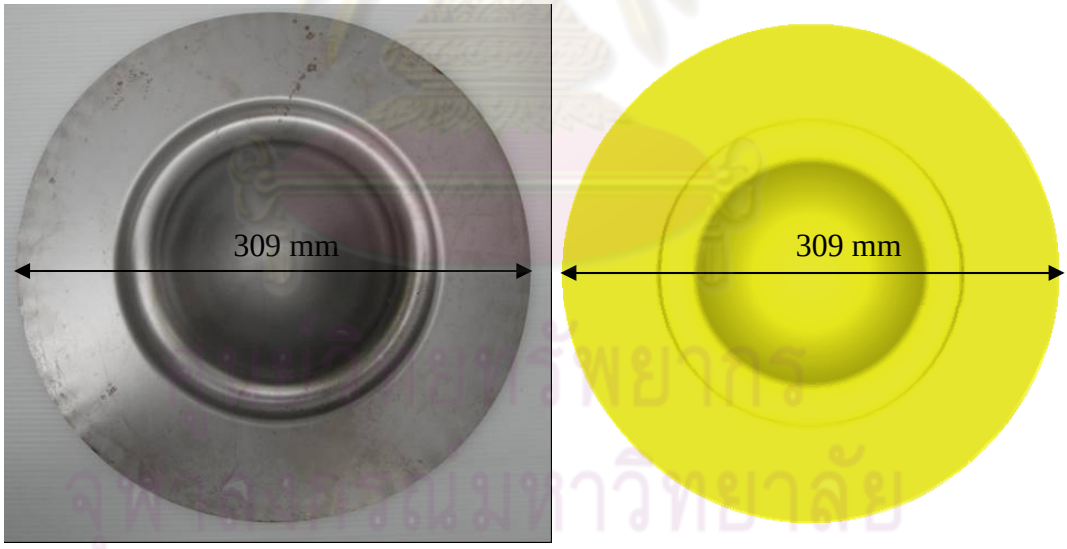

Figure7.32 Top view of part with constant BHF of 63,125 N (full as 25.25 tons) and linear pressure of 27.625 MPa at height of 66 mm

The experiment result shows the diameter as 309 mm that equal to the simulation results. The part can reach to the final stroke at 61.74 mm for simulation but for

experiment the part stop at 66 mm of height. The experiment and simulation showed a promising forming quality of a good part, i.e. no crack, no side wall wrinkle.

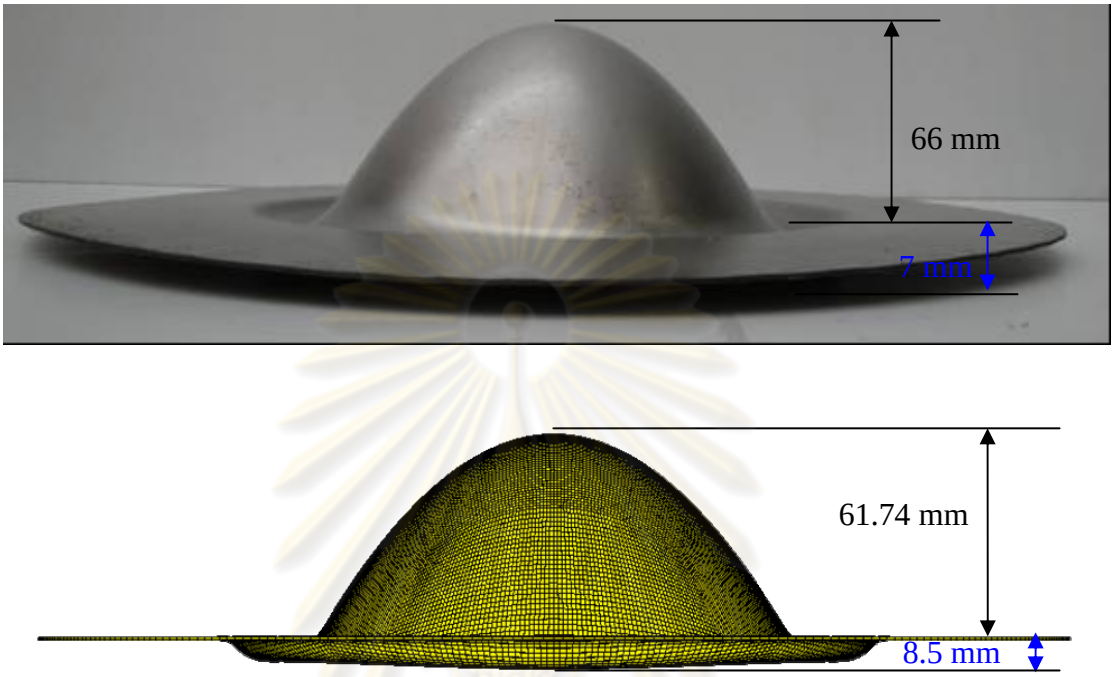

Figure7.33 Front view of part with constant BHF of 63,125 N (full as 25.25 tons) and linear pressure of 27.625 MPa at height of 66 mm

Figure7.34 Parabolic part with constant BHF of 63,125 N (full as 25.25 tons) and linear pressure of 27.625 MPa in half-section view at height of 66 mm

The comparison of thickness distribution along a curvilinear between the experiment and simulation was shown in figure 7.35. The pattern of curve from simulation was similar the experiment and the minimum thickness was on the punch nose at 30 mm along curvilinear.

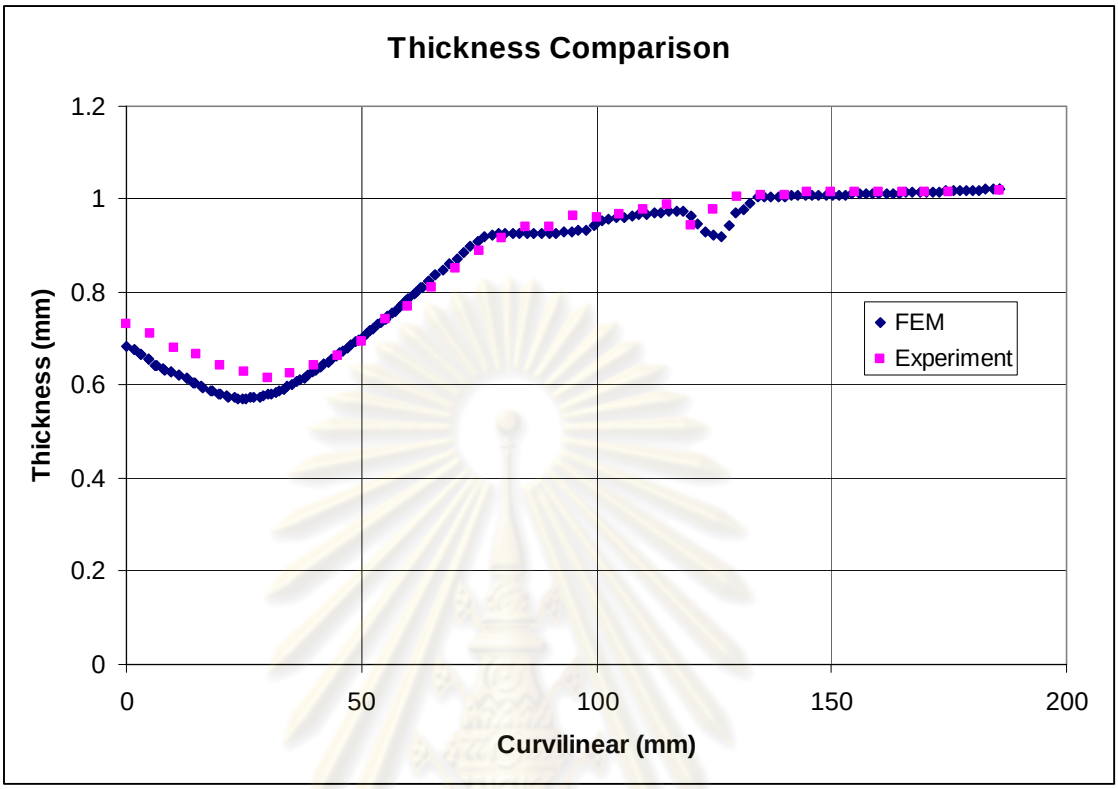

Figure7.35 Thickness distributions from simulation and experiment along curvilinear of the part with constant BHF of 63,125 N (full as 25.25 tons) and linear pressure of 27.625 MPa at height of 66 mm

ศูนย์วิทยทรัพยากร
จุฬาลงกรณ์มหาวิทยาลัย

CHAPTER VIII

CONCLUSION AND FUTURE RESEARCH

8.1 Conclusion

This research work was intended to develop methodologies for design of process parameters in hydromechanical deep drawing (HMD) process for parabolic parts. The specific goals of this study were to develop a) methodologies for design and optimize constant blank holder force and linear pressure for hydromechanical deep drawing process of the parabolic cups and b) methodologies for design feasible loading paths of blank holder force and pressure in hydromechanical deep drawing process of the parabolic cups.

First, investigation of these two proper process parameters was conducted. Numerous simulations were required for this work. The general process windows of the two parameters, constant blank holder force and linear pressure, were obtained from this work. The determined process windows facilitated through understanding of hydromechanical deep drawing process.

It was found from the process window that only certain profiles of the pressure and blank holder force form successfully, i.e. proper constant blank holder force combine with linearly increasing pressure. The types of part defects, i.e. crack, flange wrinkle and side wall wrinkle, resulted from improper level and profile of the two process parameters were clearly demonstrated and quantified. This gained process in sight led to the implementation of the two methodologies to design pressure and blank holder force necessary to hydromechanical deep drawing from the chosen parabolic parts.

a) Optimization-based simulation was developed to reduce a number of simulations necessary to optimize the process parameters. 2-D interval halving search and response surface method (RSM) were applied to optimize constant blank holder force

and linear pressure. The general process window showing constant blank holder force, linear pressure and corresponding on part quality was used to formulate the search algorithms using the 2-D interval halving technique. The main contribution here is procedures to setup and formulate a normal trial-and-error analysis of parabolic cup forming with hydromechanical deep drawing process simulation into an optimization-based simulation run to optimize the constant blank holder force and linear pressure. This optimization-based simulation approach is very versatile in that it takes most process relevant mathematical expressions into the formulations. However, this approach still required somewhat large number of simulations. Also, it seemed that a very experienced user in both optimization and hydromechanical deep drawing processes is required to use this approach.

b) Automatic adaptive simulation coupled with fuzzy logic control approach for rapid deformation of loading paths (blank holder force and pressure) was developed. A fuzzy control algorithm program (in FORTRAN) was coded and integrated into the internal solver of LS-DYNA. Both linear and exponential forms of predictive load curves (or load function) were applied in the adaptive algorithm. The two general process windows of 1) blank holder force and punch stroke 2) pressure and punch stroke were utilized to define the expected trajectory in the fuzzy logic control system. Tuning of the fuzzy logic control system could be done by changing the rule based matrix, the value of input/output membership functions, and the value of ΔBHF, ΔP. *Tuning of the rule-based matrix helped to improve convergence* whereas *changing the value of the membership function, ΔBHF and ΔP improved accuracy of the system responses*. The linear load curve function was first implemented. It was found beneficial in cases when the optimum load curve shape was not known a priory. However, it was discovered that for all the parabolic parts in this study have load curves that resemble exponential form. Then, an exponential load curve was implemented in the predictive load curve function. A much less number of simulation monitoring steps was needed to find a feasible process parameter load curves using this exponential load curve function. The main contribution here is the finding of modification of load function in exponential form to predict the next loading paths

(blank holder and pressure) of forming parabolic cups with hydromechanical deep drawing process.

The exponential curve is proper for the parabolic part. Typically, good BHF curve and pressure curve start with a lower values at the beginning of stroke (thin-out stage) and gradually increase at the middle of stroke (wrinkle stage) and rapidly increase at the end of stroke (re-strike). However, it is not good for the deeply parabolic shapes due to the load values at the end are higher enough. To correct this problem, the limit of blank holder force and pressure are defined thus, the risk of crack area near the counter pot radius is reduced.

Ideally, all hydroformed parts demand maximum part thickness and wrinkle-free quality. In practice, these high requirements are relaxed depending on the intended part functionality and the hydroformability of part itself. The goal of the parameter adjustment module is essentially to select loading path that would result in “best” part quality possible. It should be noted that global optimum part quality cannot be obtained through using adaptive simulation coupled with fuzzy logic approach as it only utilizes the simulation results on part formability from past up until current simulation monitoring step to project the “best” future loading path in the following monitoring step. No global optimization is attempted in this adaptive simulation coupled with fuzzy logic approach.

The two advanced finite element methods developed in this study for loading path determination of parabolic cups certainly have shortcomings as they always come with benefits. Pros and cons of two methods are essentially the trade-off between lead-time and final part quality obtained. Some experiments were performed to validate the results from finite element method.

8.2 Future Research

Though these advanced finite element methods developed in this study have advantages, there are many tasks that can be implemented to improve the methods. Among these tasks, the most important ones are as follows:

1) Improve of optimization-based approach: Large simulation runs is the disadvantage of this approach. Improvements of the search method should be further developed to reduce the simulation runs necessary.

2) Examine the sensitivity of the rule-based matrix, the value of the membership functions, ΔBHF and ΔP in the automatic adaptive simulation coupled with fuzzy logic control approach.

3) Collect the loading paths and experiences gained from usages of these finite element methods and store them in a form of knowledgebase for future use.

4) Apply the automatic adaptive simulation coupled with fuzzy logic control approach program to more hydromechanical deep drawing part geometries as to continuously improve the process parameter adjustment schemes.

5) Improve the experiment of hydromechanical deep drawing process i.e. the capability of press machine, the pressure control system and the water filling system to conduct experiments conveniently.

6) Adjust the other process parameters i.e. friction coefficient between punch and blank, friction coefficient between binder and blank, friction coefficient between counter pot and blank, pre-bulge height from experiments to close to the simulation data.

7) Improve defect criteria: The onset of wrinkle is difficult to detect. More accurate criteria but still easy to implement should improve the methodologies.

ศูนย์วิทยทรัพยากร
จุฬาลงกรณ์มหาวิทยาลัย

REFERENCES

Abedrabbo, N. 2002. Experimental and numerical investigations of stamp hydroforming and ironing of wrinkling in sheet metal forming. Master thesis. Michigan State University.

Abedrabbo, N., Zampaloni, M., Pourboghrat, F. 2005. Wrinkling control in aluminum sheet hydroforming. **International Journal of Mechanical Sciences**. 47(3): 333-358.

Ahmetoglu, M., Hua, J., Kulukuru, S., Altan, T. 2004. Hydroforming of sheet metal using a viscous pressure medium. **Journal of Materials Processing Technology.** 146(1): 97-107.

Altan, T., Palaniswamy, H., Aue-u-lan, Y. 2004. **Advanced in hydroforming for manufacturing automotive parts**. Engineering Research Center for Net Shape Manufacturing (ERC/NSM). The Ohio State University.

Amino, H., Nakamura K, Nakagawa T. 1990. Counter-pressure deep drawing and its application in the forming and automobile parts. **Journal of Material Processing Technology**. 23: 243-265.

Aust, M. 2001. Modified hydromechanical deep-drawing. Proceedings of the International Conference on Hydroforming of Tubes, Extrusions and Sheets. Edited by K Siegert. 2: 215-234

Aydemir, A., de Vree, J.H.P., Brekelmans, W.A.M., Geers, M.G.D., Sillekens, W.H., Werkhoven, R.J. 2005. An adaptive simulation approach designed for tube hydroforming processes. **Journal of Materials Processing Technology**. 159(3): 303-310.

Bathe, K.J. 1996. **Finite Element Procedures**. New York :Prentice Hall,

Cao, J., Boyce, M.C. 1994. Design and Control of Forming Parameters using Finite Element Analysis. **Computational Material Modeling**. 42: 265-285.

Cao, J., Jalkh, P., Boyce, M.C., Hardt, D.E. 1994. Improvement of forming height and stability of aluminum parts using active binder control. **IDDRG'94**. 1-13.

Choi, H., Koc, M., Ni, J. 2007. Determination of optimal loading profiles in warm hydroforming of lightweight materials. **Journal of Materials Processing Technology**. 190(1-3): 230-242.

Chung, J.S., Hwang, S.M. 1997. Application of a Genetic Algorithm to the Optimal Design of the Die Shape in Extrusion. **Journal of Materials Processing Technology**. 72(1): 69-77

Dechaumphai, P. 1999. **Finite Element Method in Engineering**. Second Edition. Bangkok: Chulalongkorn University Press,

Doege, E., Sommer, N. 1983. Optimierung der niederhalterkraft beim tiefziehen rechteckiger teile (Optimization of the Blank-holder Force during Deep Drawing of Rectangular Parts). **Stahl und Eisen**. 103(3): 139-142

El-Sebaie, M.G., Mellor, M.G. 1973. Pressure assisted deep drawing: **Ann. CIRP**. 22(1): 71-72.

Fann, K.J., Hsiao, P.Y. 2003. Optimization of loading conditions for tube hydroforming. **Journal of Materials Processing Technology**. 140(1-3): 520-524.

Feng, J.P., Luo, Z.J. 2000. A Method for the Optimal Control of Forging Process Variables using the Finite Element Method and Control Theory. **Journal of Materials Processing Technology**. 108(1): 40-44.

Fourment, L., Vieilledent, D., Chung, S.H., Chenot, J.L., Spence, P.J. 2001. Direct Differentiation and Adjoint State Methods for Shape Optimization of Non-steady Forming Process. **Simulation of Materials Processing: Theory, Methods and Applications**. Ken-ichiro Mori Editor. 133-138

Fung, Y.C. 1965. **Foundations of Solid Mechanics**. International Edition. Prentice-Hall,

Ghouati, O., Lenoir, H., Gelin, J.C. 2000. Optimal Design of Forming Process Using the Finite Element Methods. **Advanced Engineering Materials**. 7: 438-442

Grandhi, R., Kumar, A., Chaudhary, A., Malas, J.C. 1993. State-space Representation and Optimal Control of Non-linear Material Deformation using the Finite Element Method. **International Journal for Numerical Methods in Engineering**. 36: 1967~1986.

Hosford, W.F., Caddell, R.M. 1993. **Metal Forming Mechanics and Metallurgy**. Second Edition. New Jersey: PRT Prentice Hall,

Hsu, T.C. and Hsieh, S.J. 1996. Theoretical and Experimental Analysis of Failure for the Hemisphere Punch Hydroforming Processes. **Journal of Manufacturing Science and Engineering**. 118: 434-438.

Hsu, C.W., Ulsoy, A.G., Demeri, M.Y. 2002. Development of process control in sheet metal forming. **Journal of Materials Processing Technology**. 127: 361-368.

Huang, Y., Lo, Z.Y., Du, R. 2006. Minimization of the thickness variation in multi-step sheet metal stamping. **Journal of Materials Processing Technology**. 177(1-3): 84-86.

Jiratheranat, S. 2004. Advanced methods for finite element simulation for part and process design in tube hydroforming. Ph.D dissertation. The Ohio State University.

Jo, H.H., Lee, S.K., Ko, D.C., Kim, B.M. 2001. A Study on the Optimal Tool Shape Design in a Hot Forming Process. **Journal of Materials Processing Technology**. 111(1-3): 127-131

Keeler, S.P., Backofen, W.A. 1963. Plastic instability and fracture in sheet stretched in rigid punches. **Transaction of the ASM**. 56: 25-48.

Kim, J., Son, B.M., Kang, B.S., Hwang S.M., Park, H.J. 2004. Comparison stamping and hydro mechanical forming process for an automobile fuel tank using finite element method. **Journal of Material Processing Technology.** 153/154: 550-557.

Kleiber, M., Knabel, J., Rojek, J. 2002. Reliability assessment in metal forming operations. **Computer Methods in Applied Mechanics and Engineering**. 191(39-40): 4511-4532.

Klir, J.G., Yuan, B. 1995. **Fuzzy sets and fuzzy logic theory and applications**. New Jersey: Prentice-Hall Inc,

Khandeparkar, T. and Liewald, M. 2007. "Hydromechanical deep drawing of cups with stepped geometries". **Journal of Materials Processing Technology**.

Kobayashi, S., Oh, S.I., Altan, T. 1989. **Metal forming and the finite-element method**. New York: Oxford University Press,

Koç M. 2008. **Hydroforming for advanced manufacturing**. Edited by Muammer Koç. New York, USA: Woodhead Publishing Limited and CRC Press LLC,

Kumar, D.R. 2002. Formability analysis of extra-deep drawing steel. **Journal of Materials Processing Technology**. 130-131: 31-41.

Kusiak, J. 1996. A Technique of Tool-shape Optimization in Large Scale Problems of Metal Forming. **Journal of Materials Processing Technology**. 57(1-2): 79-84

Lang, L.H., Danckert, J., Nielsen, K.B. 2004. Investigation into the effect of pre-bulging during hydromechanical deep drawing with uniform pressure onto the blank. **International Journal of Machine Tools & Manufacture**, 44(6): 649-657.

Lang, L.H., Danckert, J., Nielsen, K.B., Zhou, X. 2005. Investigation into the forming of a complex cup locally constrained by a round die based on an innovative hydromechanical deep drawing method. **Journal of Materials Processing Technology**. 167(2-3): 191-200.

Lang, L.H., Li, T., An, D., Chi, C., Nielsen, K.B., Danckert, J. 2009. Investigation into hydromechanical deep drawing of aluminum alloy - Complicated components in aircraft manufacturing. **Materials Science and Engineering A**. 499: 320–324

Lee, K.J., Kumai, S., Arai, T., Aizawa, T. 2007. Interfacial microstructure and strength of steel/aluminum alloy lap joint fabricated by magnetic pressure seam welding. **Materials Science and Engineering**: A. 471(1-2): 95-101.

Lin, J., Zhao, S.D., Zhang, Z.Y., Wang, Z.W. 2009. Deep drawing using a novel hydromechanical tooling. International **Journal of Machine Tools & Manufacture.** 49: 73-80.

Lo, S.W., Hsu, T.C. and Wilson, W.R.D. 1993. An Analysis of the Hemispherical-Punch Hydroforming Process. **Journal of Materials Processing Technology**. 37: 225-239.

Marciniak, Z., Kuczynski, K. 1967. Limit strains in the processes of stretch-forming sheet metal. **International Journal of Mechanical Science**. 9(9): 609-620.

Myers, R.H., Montgomery, D.C. 2002. **Response surface methodology process and product optimization using designed experiments**. Second Edition. New York, USA: John Wiley and Sons Inc,

Obermeyer, E.J., Majlessi, S.A. 1998. A review of recent advances in the application of blank holder force towards improving the forming limits of sheet metal parts. **Journal of Materials Processing Technology**. 75(1-3): 222-234.

Qin, Y., Balendra, R. 2004. Design considerations for hydromechanical deep drawing of sheet components with concave features. **Journal of Materials Processing Technology**. 145(2): 163-170.

Ray, P., Mac Donald, B.J. 2004. Determination of the optimal load path for tube hydroforming processes using a fuzzy load control algorithm and finite element analysis. **Finite Elements in Analysis and Design**. 41(2): 173-192.

Roux, W.J., Stander, N., Haftka, R.T. 1998. Response surface approximations for structural optimization. **Int J Numer Meth Eng**. 42: 517-534.

Schmoeckel, D., Hielscher, C., Huber, R. 1999. Metal forming of tubes and sheets with liquid and other flexible media. **Annals of CIRP**. 48(2): 1-20

Sharma, A.K., Rout, D.K. 2009. Finite element analysis of sheet Hydromechanical forming of circular cup. **Journal of Materials Processing Technology**. 209: 1445-1453.

Sheng, Z.Q., Jirathearanat, S., Altan, T. 2004. Adaptive FEM simulation for prediction of variable blank holder force in conical cup drawing. **International Journal of Machine Tools & Manufacture**. 44(5): 487-494.

Siebel, E., Beisswanger, H. 1955. **Deep Drawing**. Munich: Carl Hanser,

Siegert, K., HaÈussermann, M., LoÈsch, B., Rieger, R. 2000. Developments in hydroforming. **Journal of Materials Processing Technology**. 98(2): 251-258.

Silva, M.B., Baptista, R.M.S.O., Martins, P.A.F. 2004, Stamping of automotive components: a numerical and experimental investigation. **Journal of Materials Processing Technology**. 155-156: 1489-1496.

Singh, S.K., Dixit, A., Kumar, D.R. 2007. Optimization of the design parameters of modified die in hydro-mechanical deep drawing using LS-DYNA. **International Journal of Advanced Manufacturing Technology**. 38(1-2): 32-37.

Tekkaya, A.E. 2000. State-of-the-art of simulation of sheet metal forming. **Journal of Materials Processing Technology**. 103: 14-22.

Thomas, W.J. 1998. Product, Tool, and Process Design Methodology for Deep Drawing and Stamping of Sheet Metal. Ph.D dissertation. The Ohio State University.

Wang, L., Lee, T.C. 2005. Controlled strain path forming process with space variant blank holder force using RSM method. **Journal of Materials Processing Technology**. 167(2-3): 447-455.

Wang, X., Cao, J. 2000. On the prediction of side-wall wrinkling in sheet metal forming process. **International Journal of Mechanical Sciences**. 42: 2369-2394.

Yang, J.B., Jeon, B.H., Oh, S.I. 2001. Design sensitivity analysis and optimization of the hydroforming process. **Journal of Materials Processing Technology**. 113(1-3): 666-672.

Yossifon S, Tirosh J, Kochavi E. 1984. On suppression of plastic buckling in hydroforming processes. **International Journal of Mechanical Science**.26: 389-402.

Zampaloni, M., Abedrabbo, N., Pourboghrat, F. 2003. Experimental and numerical study of stamp hydroforming of sheet metals. **International Journal of Mechanical Sciences**. 45(11): 1815-1848.

Zhang, S.H., and Danckert, J. 1998. Development of hydro mechanical deep drawing. **Journal of Material Processing Technology**. 83: 14-25.

Zhang, S.H., Jensen, M.R., Nielsen, K.B., Danckert, J., Lang, L.H., Kang, D.C. 2003. Effect of anisotropy and prebulging on hydromechanical deep drawing of mild steel cups. **Journal of Materials Processing Technology**. 142(2): 544-550.

ศูนย์วิทยทรัพยากร
จุฬาลงกรณ์มหาวิทยาลัย

Zhang, S.H., Lang, L.H., Kang, D.C., Danckert, J., Nielsen, K.B. 2000. Hydromechanical deep-drawing of aluminum parabolic workpieces-experiments and numerical simulation. **International Journal of Machine Tools & Manufacture**. 40(10): 1479-1492.

Zhang, S.H., Nielsen, K.B., Danckert, J., Kang, D.C., Lang, L.H. 2000. Finite element analysis of the hydromechanical deep-drawing process of tapered rectangular boxes. **Journal of Materials Processing Technology**. 102(1-3): 1-8.

Zhang, S.H., Wang, Z.R., Xu Y., Wang, Z.T., Zhou, L.X. 2004. Recent developments in sheet hydroforming. **Journal of Materials Processing Technology**. 151(1-3): 237-241.

Zhong, Z.H. 1993. **Finite Element Procedures for Contact-Impact Problems**. Oxford: Oxford University Press,

Zienkiewicz, O.C., Taylor, R.L. 1991. **Finite Element Method**. volume 1: The basis. Fourth Edition. Singapore: McGraw-Hill Press,

ศูนย์วิทยทรัพยากร
จุฬาลงกรณ์มหาวิทยาลัย

VITA

Mr.Thanasan Intarakumthornchai was born on June 10th, 1975 in Suphanburi province, Thailand. He graduated from King Mongkut's Institute of Technology Thonburi, Thailand in academic year 1996 with a bachelor's degree in Production Engineering. He earned a Master's degree in Industrial Engineering from Chulalongkorn University, Thailand in academic year 2000. After his graduation, he worked at National Metal and Materials Technology Center (MTEC) for 5 years and decided to study for a Doctor of Philosophy in Industrial Engineering at Chulalongkorn University, Thailand.

ศูนย์วิทยทรัพยากร
จุฬาลงกรณ์มหาวิทยาลัย